Two-Photon Dyes for Biological Application

A thesis submitted to the board of the faculty of mathematical, physical & life sciences in partial fulfilment of the requirements for the degree of

Doctor of Philosophy at the University of Oxford

by

Philip M. Bennett

Under the supervision of Prof. H. L. Anderson FRS

at the Chemistry Research Laboratory and Magdalen College

Trinity Term 2013

Contents

Acknowledgments

"Nothing in this world can take the place of persistence. Talent will not; nothing is more common than unsuccessful people with talent. Genius will not; unrewarded genius is almost a proverb. Education will not; the world is full of educated derelicts. Persistence and determination alone are omnipotent. The slogan 'press on' has solved and always will solve the problems of the human race"

- Calvin Coolidge

First and foremost, my thanks go to Professor Anderson, who not only gave me the opportunity to research in his group, but also for creating a group full of such kind, supportive and unique people. For their support and advice over the past four years I am forever indebted to many people, but Ismael, Jan, Hazel, Johannes and James R. deserve a huge thank you for their help, patience, and positivity. For making lab life bearable and for all the fun outside of work I must thank Sals, Jan, Mitsuhiko, Marta, Andrea, Phoom, Patrik, Julien, Levon, Sophie, Arjen, Michelle, Joanna, James W., Igor, Dima, Georg, and Jon.

Additionally, I need to thank all those with whom I collaborated during my DPhil. Specifically, thank you to Sebastian, Cesar, and Esther for their help with the PDT project and Eduardo for his help with synthesis for the two-photon uncaging project. The hard work and dedication of Karolina were instrumental in the development of the two-photon uncaging project, and she deserves a special thank you.

Finally, I must thank my parents and family for their undying support (emotionally and financially!), Jim for being the best friend anyone could ask for, and Masha, without whom I would never have believed this day could come.

Acronyms and Abbreviations

δ_a	Two-photon absorption cross-section
δ_C	Carbon chemical shift
δ_D	Dipolar term
δ_H	Hydrogen chemical shift
δ_u	Two-photon uncaging cross-section
ε	One-photon absorption cross-section
ε_u	One-photon uncaging cross-section
ϕ_u	Quantum yield of uncaging
ϕ_f	Quantum yield of fluorescence
5-ALA	5-Aminolevulinic acid
9-MC	9-Methylcarbazole
A	Acceptor
ACPD	1-Amino-1,3-dicarboxycyclopentane
Alloc	Allyloxycarbonyl
AMD	Age-related macular degeneration
AMPA	(2-Amino-3-(3-hydroxy-5-methyl-isoxazol-4-yl)propanoic acid
AO	Amino-oxy
ATP	Adenosine triphosphate
BAX	Bcl-2 gene-associated X protein
bFGF	Basic fibroblast growth factor
Bhc	Bromohydroxycoumarin
Boc	Di-*tert*-butyldicarbonate
br	broad singlet
BSA	Bovine serum albumen
C	Caged compound
d	doublet
D	Donor
DAPI	4',6-Diamidino-2-phenylindole
dba	Dibenzylideneacetone
DCC	Dicylcohexylcarbodiimide
DCM	Dichloromethane
DDQ	2,3-Dichloro-5,6 dicyanoanthroquinone
DHPG	3,5-Dihydroxyphenylglycine
DiCHAP	Dicyclohexylammonium phosphate
DIPA	Diisopropylamine
DIPEA	Diisopropylethylamine
DMAP	Dimethylaminopyridine
DMEM	Dulbecco's modified eagle's medium
DMF	Dimethylformamide
DMSO	Dimethylsulfoxide
DNA	Deoxyribonucleic Acid
ECM	Extracellular Matrix
EDC	*N*-ethylcarbodiimide
E_{OX}	Oxidation potential
EPSC	Excitatory post-synaptic current
E_{RED}	Reduction potential
ESI	Electrospray Ionisation
Et	Ethyl group (CH_2Me)
FBS	Foetal bovine serum

Fc	Ferrocene
FDA	Food and drug administration
$\Delta G_{(-)eT}$	Free energy of (back) electron transfer
g	gerade (symmetrical)
GABA	γ-Aminobutyric acid
GM	Göppert-Mayer unit
HBTU	*O*-benzotriazol-1-yl tetramethyluronium
HeLa	Human epithelial cervical carcinoma cells
HEp2	Human epithelial type 2
HFIP	Hexafluoroisopropanol
HOMO	Highest occupied molecular orbital
Hp	Haematoporphyrin
HpD	Haematoporphyrin derivative
HPLC	High performance liquid chromatography
hυ	Light quantum
ICT	Intramolecular charge transfer
IR	Infrared
J	NMR coupling constant
$k_{(-)eT}$	Rate of (back) electron transfer
LD_{50}	Light dose required to reduce cell viability by 50%
LED	Light emitting diode
LG	Leaving Group
LUMO	Lowest unoccupied molecular orbital
m	*meta*
m	multiplet
MALDI	Matrix-assisted laser desorption ionisation
Me	Methyl group (CH_3)
MeCN	Acetonitrile
MeOH	Methanol
MS	Mass spectrometry
MTS	3-(4,5-dimethylthiazol-2-yl)-5-(3-carboxymethoxyphenyl) -2-(4-sulfophenyl)-2H-tetrazolium
NA	Numerical aperture
NBS	*N*-bromosuccinimide
Nd:YAG	Neodynium-doped yttrium aluminium garnet laser, $Nd:Y_3Al_5O_{12}$
NMDA	*N*-methyl-D-aspartic acid
NMM	*N*-Methylmorpholine
NMR	Nuclear magnetic resonance
o	*ortho*
OAc	Acetate
OPA	One-photon absorption
p	*para*
PBS	Phosphate-buffered saline
PDT	Photodynamic therapy
PeT	Photoinduced electron transfer
pH(D)	Hydrogen (or Deuterium) ion concentration
Ph	Phenyl group
PpIX	Proto-porphyrin IX
ppm	parts per million
PyBOP	(Benzotriazol-1-yloxy)tripyrrolidinophosph-onium hexafluorophosphate

R	Alkyl or organic group
RP	Reverse phase
rt	room temperature
S_0	Ground singlet state molecular energy level
S_1	Lowest excited singlet state molecular energy level
s	singlet
SASRIN	Super acid-sensitive resin
SK-OV-3	Human ovarian epithelial adenocarcinoma cell line
t	triplet
TBAF	Tetra-*N*-butylammonium fluoride
TBDMS	*Tert*-butyldimethylsilyl
TEA	Triethylamine
TFA	Trifluoroacetic acid
THF	Tetrahydrofuran
THS	Trihexylsilyl
TIPS	Triisopropylsilyl
Ti:sapphire	Titanium-sapphire laser: $Ti:Al_2O_3$.
TLC	Thin-layer chromatography
TMS	Trimethylsilyl
TNBS	2,4,6-Trinitrobenzenesulfonic
TNFα	Tumour necrosis factor α acid
TPA	Two-photon absorption
TPEF	Two-photon excited fluorescence
TPP	Tetraphenylporphyrin
TP-PDT	Two-photon photodynamic therapy
u	ungerade (antisymmetric)
UV	Ultraviolet
VEGFA (C)	Vascular endothelial growth factor A (or C)

Abstract

Two photon absorption (TPA) is the near simultaneous absorption of two photons of light to achieve an electronically excited state. It has led to huge advances in microscopy and microfabrication due to its quadratic dependence on the local light intensity. This thesis describes the design, synthesis and application of dyes with strong TPA properties, and as such is divided into three chapters. The first introduces the theory and measurement of TPA as well as structure-property relationships known to maximise the efficiency of TPA. The subsequent chapters present explorations of the application of these dyes in biological applications; namely two-photon uncaging and two-photon photodynamic therapy. A recurring theme in my research is the discussion and evaluation of strategies for improving the compatibility of organic macromolecules with biological systems.

Uncaging is the use of photolysis to achieve a rapid increase in the local concentration of a physiologically active species *via* a photoremovable protecting groups. Photoremovable protecting groups are covalently attached to the physiologically active species, thus rendering it inactive. At the desired time and location, a light dose releases the molecule in its active form. There are many compounds known to uncage following photoexcitation, but there are few examples of caging groups which exhibit both strong two-photon absorption properties and highly efficient uncaging. Chapter 2 discusses the rational design of such groups through the development of a new mechanism for uncaging, in which a photoinduced electron transfer (PeT) between a two-photon-excited electron donor and an electron acceptor/release group drives the uncaging event.

Photodynamic therapy (PDT) is a treatment for neoplastic disorders such as cancer in which localised cell death is induced through photoexcitation of a sensitiser. Following light absorption, the photosensitiser enters a relatively long-lived excited state which reacts with cellular oxygen to produce its highly cytotoxic singlet form. The main challenges of the field are to achieve deep penetration of light into tissue and to reduce coincident damage to unaffected tissue by light scattering during irradiation. In 2008, the Anderson group reported the development of PDT photosensitisers with highly efficient two-photon absorption as well as high singlet oxygen quantum yields. Chapter 3 discusses strategies for improving the pharmacokinetics and defining the sub-cellular localisation of these photosensitisers.

Chapter 1: Introduction

This chapter introduces the concepts of nonlinear optics and specifically TPA. The models describing TPA for centrosymmetric chromophores are explained, as well as the techniques used to measure TPA cross-sections. The structure-property relationships which result in efficient TPA in quadrupolar chromophores are discussed, followed by the advantages of TPA techniques over their one-photon counterparts.

1.1 Nonlinear Optics

Nonlinear optics describes the optical response of a nonlinear medium during irradiation with high intensity light.[1]

When a photon interacts with a chromophore, its electric field induces polarisation in the molecule. At low intensity, this polarisation is simply proportional to the electric field strength, however at high intensity, the Taylor expansion of this model must be considered. The polarisation induced by high intensity light can be related to its electric field strength by **Equation 1**.

$$P = \alpha E + \beta E^2 + \gamma E^3 + \cdots \qquad \textbf{Equation 1}$$

where P is the induced polarisation, E is the electric field strength and α, β, and γ are the molecule polarisability, first hyperpolarisability, and second hyperpolarisability respectively.[2]

The nonlinearity of a bulk optical medium can be estimated by taking the ensemble average of all the molecules in the medium. This average can be expressed using **Equation 2**.

$$P = \varepsilon_0\left(\chi^{(1)}E + \chi^{(2)}E^2 + \chi^{(3)}E^3 + \cdots\right) \qquad \textbf{Equation 2}$$

where ε_0 is the permittivity of free space and $\chi^{(n)}$ is the bulk n^{th} order susceptibility constant of the medium (per unit volume). In a centrosymmetric environment, even orders in **Equations 1 & 2** are zero or, alternatively, only molecules without inversion symmetry aligned in a non-centrosymmetric arrangement have non-zero $\chi^{(n)}$ where n is even.

Nonlinear optical effects were predicted during the 1930s but could not be observed until the invention of the laser due to the requirement of a high intensity light source. In the 1960s, effects such as multi-photon absorption, stimulated Raman scattering, as well as second and third harmonic generation were observed. Research performed since has elucidated many structure-property relationships, which has meant that today research can focus on the development of dyes and dye systems for practical applications.

1.2 Two-Photon Absorption

The prediction of the simultaneous absorption of multiple photons is credited to Maria Göppert-Mayer, an American theoretical physicist.[3] In 1931, she developed a new quantum mechanical treatment of light, which extended Dirac's description of the absorption and emission of single photons to the simultaneous absorption of two photons.[4] The phenomenon

was first observed thirty years later *via* the detection of fluorescence induced by two-photon excitation of Eu^{3+} in a doped crystal.[5]

Two-photon absorption is a nonlinear process, the efficiency of which is proportional to the imaginary part of γ in **Equation 1**.[6,7] Degenerate TPA, the process by which the dyes discussed in this thesis operate, is defined as the population of an excited electronic (and vibrational) state by the simultaneous absorption of two photons with energy equal to half that required for the corresponding one-photon process. The first photon interacts with the molecule to form a 'virtual' excited state, which cannot be described classically.[8] This state only exists for the time in which the photon's radiation field interacts with the molecule (<5 femtoseconds), so the second photon must arrive before the virtual state decays.[9] Though the excited states may differ for one- and two-photon excitation, subsequent photochemical processes are generally identical. This is because non-radiative decay leads to the lowest excited state of the same multiplicity in both cases, and conversion of S_n to S_1 is generally faster than S_1 to S_0.[10]

The efficiency of TPA is dependent on both the spatial and temporal distribution of photons.[11] High spatial photon density can be achieved inexpensively by focussing a laser beam. High temporal density is more difficult to achieve with current technology since it requires expensive, ultrafast pulsed light sources. As beam intensity decreases quadratically with distance above and below the diffraction-limited focal plane, TPA reduces according to the fourth power of distance along the beam-path from the focal point.[12] As a result, excitation is effectively restricted to the focal volume of the beam.

TPA is quantified by the two photon absorption cross-section, δ_a, measured in Göppert-Mayer (GM) units where 1 GM is equivalent to 10^{-50} cm^4 s $photons^{-1}$ $molecule^{-1}$. For centrosymmetric molecules, a simplified form of δ_a is given by the three 'essential' states model, summarised in **Equation 3**.[13]

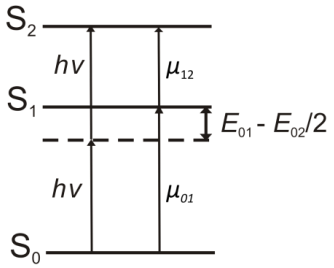

$$\delta_a \propto \frac{\mu_{01}^2 \mu_{12}^2}{\left(E_{01} - \frac{E_{02}}{2}\right)}$$ **Equation 3**

Where μ is the transition dipole moment and E is the transition energy. The subscripts 0, 1, and 2 refer to the S_0, one-photon allowed S_1 and two-photon allowed S_2 states respectively.

The three states have alternating symmetry, both the S_0 and S_2 states are *gerade* (symmetric with respect to their centres of inversion), while the intermediate state is *ungerade* (antisymmetric).[14] Therefore, the transitions $S_0 \leftrightarrow S_1$ and $S_1 \leftrightarrow S_2$ are one-photon electric dipole allowed whereas only $S_0 \leftrightarrow S_2$ is two-photon allowed. This indicates that one-photon absorption (OPA) and TPA have opposite symmetry requirements.[15] For two-photon absorption, the frequency v is out of resonance with the $S_0 \leftrightarrow S_1$ and $S_1 \leftrightarrow S_2$ transitions and it is from this energy mismatch that the virtual state, which is a superposition of S_0 and S_1, arises. The transient contribution of S_1 with *ungerade* symmetry allows the second photon to induce an electric-dipole transition to the final *gerade* state.

For linear centrosymmetric molecules, such as those described herein, the S_0, S_1 and S_2 states of the essential states model are labelled $1A_g$, $1B_{1u}$ and $2A_g$ respectively (**Figure 1**).

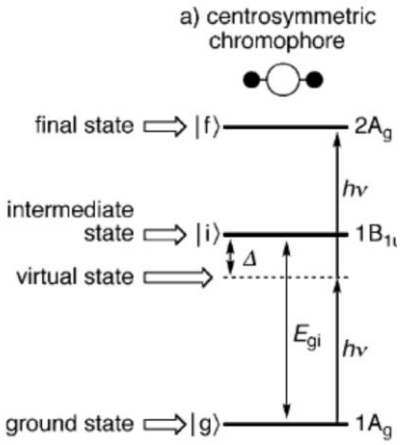

Figure 1: *An energy level diagram of the essential states model for a centrosymmetric chromophore, representing the general case for the lowest two-photon transition of a linear centrosymmetric system. Reproduced, with permission, from reference 16.*

1.3 The Design of Two-Photon Chromophores

In the process of designing molecules with large two-photon cross-sections, theory can provide some important guidelines. For example, the magnitudes of μ_{01} and μ_{12} (**Equation 3**) are proportional to the one-photon oscillator strengths and so can be predicted from the linear absorption spectrum of the chromophore. In centrosymmetric chromophores, if there is a one-

photon transition in close proximity to the two-photon absorption wavelength, δ_a is enhanced when Δ is small (**Figure 1**).

In addition, molecules which posses a permanent dipole exhibit enhanced δ_a. This is a consequence of the large change in dipole moment ($\Delta\mu$) which occurs upon the transition from a donor-centred ground state to an acceptor-centred excited state. [17] Therefore, an important aim in designing molecules with high TPA cross-sections is maximising intramolecular charge transfer (ICT) upon excitation. The contribution to the two-photon absorption cross-section from the change in dipole moment is referred to as the dipolar term (δ_D) and is modelled by only considering the ground and two-photon excited states (**Equation 4**).[7,14]

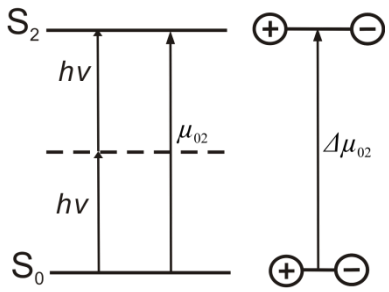

$$\delta_D \propto \frac{\mu_{02}(\Delta\mu_{02})^2}{E_{02}^2}$$ **Equation 4**

The transition moments are also dependent on the distance over which the charge is displaced, so large π-conjugated systems commonly exhibit efficient TPA. However, the magnitude of the cross-section does not scale directly with chromophore length as the coherence of the wavefunction is not maintained beyond what is known as the 'conjugation length'. This means that electrons become confined to segments of the chain, the length of which is difficult to predict but co-planarity in the chromophore can increase their size.[16] Dipolar enhancement can be achieved centrosymmetrically as well. By arranging two dipoles in a D-π-A-π-D or A-π-D-π-A configuration (where π represents a π-conjugated bridge), a so-called quadrupolar arrangement is achieved. These compounds are essentially two dipoles arranged symmetrically and are therefore inherently more efficient at TPA than dipolar constructions.[16]

Electronic transitions cannot be represented by simple changes in occupancy of elementary molecular orbitals.[18] However, calculation methods have been developed which allow for the electronic configurations which contribute to the excited states to be represented as 'electron'

or ‘hole’ distributions. **Figure 2** shows these distributions for a centrosymmetric D-π-A-π-D system of D_{2h} symmetry.

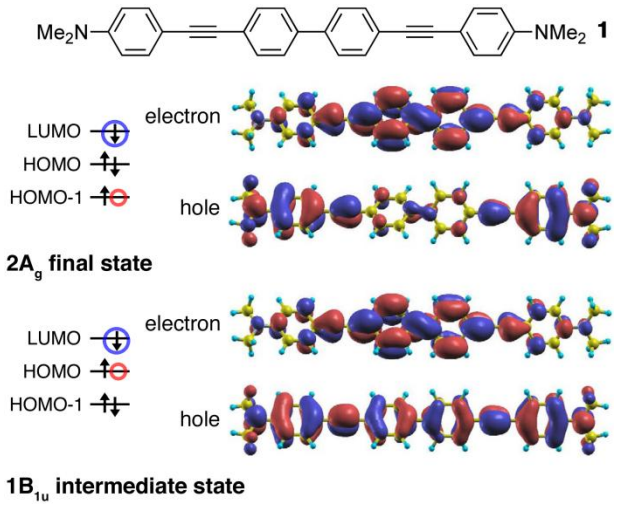

Figure 2: *The intermediate and final states of the lowest two-photon absorption for **1**. The HOMO -1, HOMO and LUMO occupancies are shown alongside the natural transition state orbitals for the electron and hole distributions of these states. Reproduced, with permission, from reference 16.*

These give an excellent graphical representation of the change in electron distribution upon two-photon excitation in a quadrupolar molecule. In the intermediate $1B_{1u}$ state for compound **1**, the ‘hole’ distribution is spread evenly over the entire molecule, while the electron is mostly localised at its centre. This demonstrates the net displacement of charge from the electron-rich donors towards the core upon transition from the $1A_g$ to $1B_{1u}$ states. In the final $2A_g$ state, the electron distribution changes very little, while the ‘hole’ distribution becomes localised on the donor moieties, further enhancing the quadrupolar polarisation.

For the purposes of this thesis, only centrosymmetric quadrupolar systems will be discussed. There are two thorough reviews which discuss the TPA of dipolar and octupolar molecules in addition to quadrupolar systems.[16,19]

1.4 Measuring Two-Photon Absorption Cross-Sections

The measurement of TPA cross-sections is difficult to perform reliably as the apparent cross-section can be dependent on the technique used to measure it.[20] Therefore, when comparing the two-photon absorption cross-sections of known molecules, it is important to consider how the measurement was made.

The methods fall in to two categories: either a change induced by TPA is measured (for example transmittance),[21] or, the energy transferred to the material by TPA is measured (for

example changes in temperature,[22] fluorescence,[23] or acoustic signals[24]). Two techniques have emerged which are considered to be reliable; these are the open aperture z-scan technique and two-photon luminescence methods.[2]

The open aperture z-scan technique involves moving the sample along the path of a focussed laser beam and measuring the change in light intensity at the detector as a function of its position along the beam. Under a two-photon regime, the transmittance exhibits a quadratic dependence on the distance from the focal point of the laser, while OPA remains constant along the beam path. Therefore this technique is only sensitive to two-photon excitation.[3] Two effects other than true simultaneous TPA can contribute to the measured cross-section. Firstly, some light may not reach the detector due to self-defocusing and nonlinear scattering, which result in extra contributions to the nonlinear absorption. Secondly, a build up of excited-state populations can lead to nonlinear transmission through excited state absorption. This contribution can be minimised by the use of wavelengths where OPA is negligible, very short laser pulses, or low pulse repetition rates (<1 KHz).

The z-scan technique provides an experimentally simple method of TPA cross-section determination, however, the problems are difficult to avoid and lead to enhanced TPA cross-sections. Another common method of measuring TPA efficiency is two-photon-excited fluorescence (TPEF) spectroscopy.[2,25] The sample, at an optical density of around 0.1 to minimise self-absorption,[26] is excited by a pulsed laser at half the nonlinear absorption wavelength. Emission is measured at wavelengths where the fluorescence intensity exhibits a quadratic dependence on the laser intensity, to eliminate any contributions from one-photon fluorescence. The TPA cross-section is determined by comparing the TPEF spectrum with that of a known standard (commonly fluorescein), measured under identical conditions. The assumption used in this technique is that the fluorescence quantum yield is independent of the excitation process, which is not necessarily the case as one- and two-photon absorption may have different non-radiative decay pathways.[7] However, it is generally accepted that this effect, if it exists, is negligible.

Although this technique implies that only chromophores which exhibit significant fluorescence can be measured, it is also possible to determine the two-photon absorption cross-section by detecting the formation of singlet oxygen as a result of absorption.[26]

In the following sections, the technique used to measure the TPA cross-section was TPEF unless otherwise stated.

1.5 Molecular Design Principles for Maximising Two-Photon Absorption

1.5.1 Stilbene Derivatives

One of the earliest studies performed into the structure-property relationships of two-photon chromophores resulted from the discovery that increasing the degree of ICT upon excitation in centrosymmetric molecules significantly increases their TPA cross-section.[27] A series of molecules based on a stilbene platform were synthesised to determine the effect of minor structural changes on ICT (**Figure 3, Series 1**). Since this seminal study, maximising the TPA cross-section of centrosymmetric stilbene derivatives has been thoroughly explored; literature highlights of which are shown in **Figure 3**.

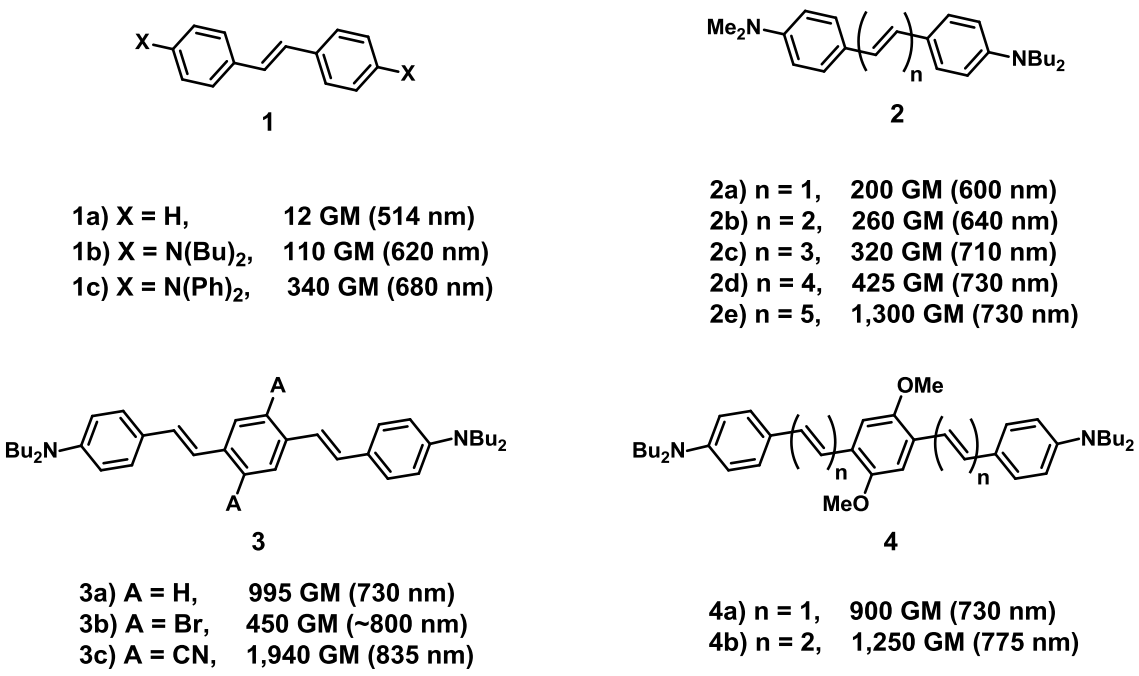

Figure 3: *Four series of two-photon chromophores derived from stilbene, illustrating the effects of structural changes on the TPA cross-section. These data were reproduced from reference 19.*

From **Figure 3**, several general structure-property relationships can be established. Regarding the π-bridge between the donor and acceptor moieties, comparing **Series 2a-e** and **3a** suggests that while extending conjugation by the addition of double bonds improves the TPA cross-section, it is more effective to increase conjugation by addition of a phenyl group. The introduction of a benzene ring offers the opportunity to increase the conjugation length while maintaining overall rigidity and stability.

Other trends that can be identified are related to the nature and position of donors and acceptors. Between compounds **1b** and **c**, the alkyl-substituted aniline donors have been exchanged for phenyl-substituted analogues, which results in a three-fold TPA cross-section increase. This is likely a consequence of the increased π electron count and the stronger electron donor capability of the aryl-amino groups. Although not presented here, the use of oxygen-based donors tends to be less effective, due to their weaker donor capability.[28]

A method of significantly increasing the TPA cross-section without making large structural additions to the chromophore is to add a donor or acceptor to the π-bridge. **Series 3** demonstrates the power of this technique. The addition of two strong acceptor groups (cyano) to the central phenyl ring nearly doubles the TPA cross-section, and shifts the TPA maximum to a longer wavelength. Conversely, adding a donor at the central phenyl ring appears to have little impact on the cross-section (**4a**). This is due to the fact that the ICT upon excitation in a D-π-D-π-D system is lower compared to a D-π-A-π-D system.

1.5.2 Exploring the Effect of the Core and Linking Bonds

The basic structure-property relationships described above can be used to synthesise compounds with TPA cross-sections that are considered high (10^3 GM). However, increasing the conjugation length in the ways described in **Section 1.5.1** generally leads to a decrease in molecular rigidity and thus poor quantum yields of fluorescence. This reduces the suitability of the chromophores to applications such as biological imaging and TPEF, which are common for such dyes. Consequently, there was a desire to develop chromophores exhibiting strong TPA while maintaining a high fluorescence quantum yield.

The most significant work towards this goal was performed by the group of Dr Blanchard-Desce.[29,30,31] Their initial publications focused on fluorene, dihydrophenanthrene and dithienothiophene derivatives (**Figure 4**).

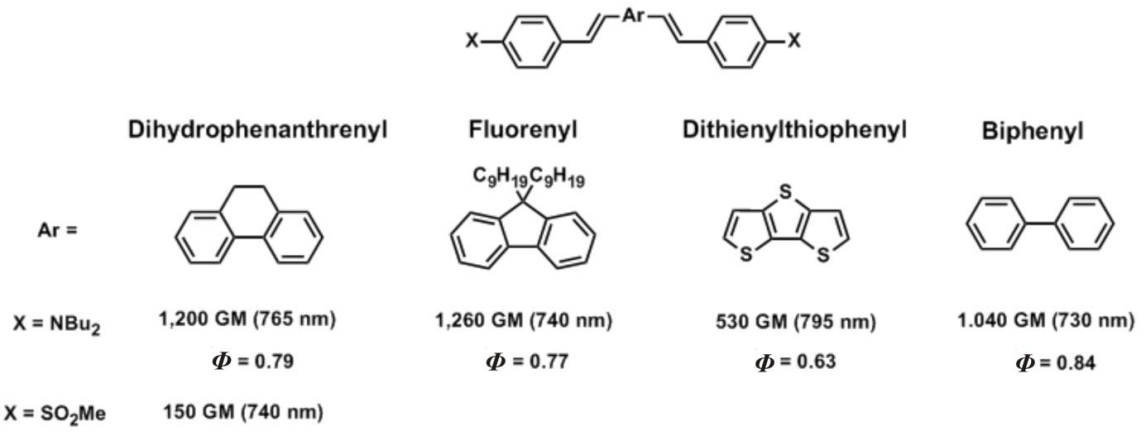

Figure 4: *The effect of changing the core structure on the TPA cross-section and fluorescence quantum yield.*

These results demonstrated that a more rigid π-bridge can increase the TPA cross-section while maintaining a high fluorescence quantum yield. This is due to the fact that electronic coupling, and therefore ICT, is optimised when a π system adopts a planar geometry. For comparison, compound **2e** in **Figure 3** (consisting of five alkene bonds connecting two alkyl-substituted aniline donors) exhibits a TPA cross-section of 1,300 GM and a fluorescence quantum yield of 0.12, while a molecule with only one pair of alkene bonds and a fluorene or dihydrophenanthrene core results in a similar TPA cross-section and a fluorescence quantum yield of around 0.8 **(Figure 4)**.

This study also indicates that replacing the tertiary amine donor group with a relative electron acceptor (SO_2Me) resulted in an almost ten-fold decrease in the TPA cross-section, suggesting that a D-π-D arrangement is favoured over A-π-A.

A later study looked at the extension of π-conjugation by addition of rigid or semi-rigid linkers between donors and fluorene or biphenyl cores.[32] The fundamental structure-property relationship that this sought to establish was the relative efficiency of alkyne versus alkene links (**Figure 5**).

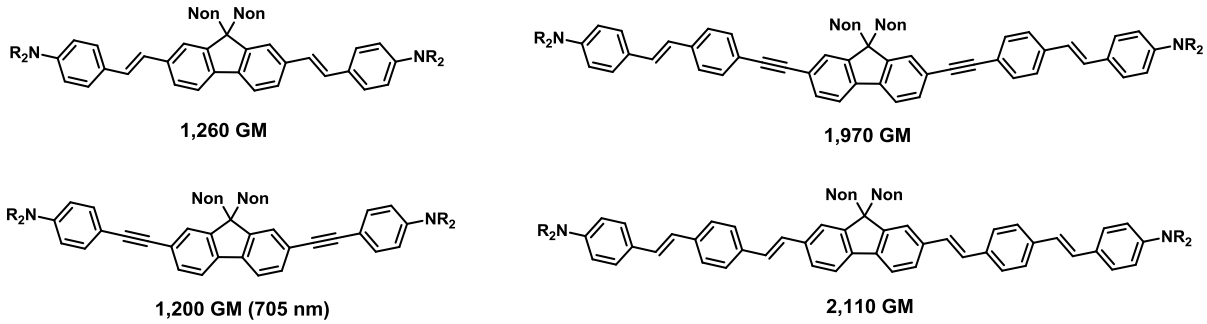

Figure 5: *Two pairs of fluorene-based chromophores demonstrating the effect of bond order on the TPA cross-section.*

From the data in **Figure 5** the difference between alkene and alkyne bonds is only 5-10%, which is similar to the expected experimental error. The rationale for the increased efficiency of TPA with double bonds versus triple bonds is that the π-π and π^*-π^* mismatch at the sp^1-sp^2 connection in triple bonds affects ICT detrimentally. Conversely, triple bonds are more electron-withdrawing and so the core becomes a better electron acceptor when compared to an alkene system. From the results presented here, it appears that these two effects cancel out.

1.5.3 The Two-Photon Absorption of Porphyrin Derivatives

Porphyrins represent a special class of two-photon chromophore. The structure-property relationships discussed thus far have established that extending π-conjugation over a rigid, planar molecule is crucial for maximising the TPA cross-section. Considering this, porphyrins provide the ideal framework for the design of new two-photon chromophores, and it is therefore not surprising that chromophores based on porphyrin cores have resulted in some of the highest cross-sections observed.[33]

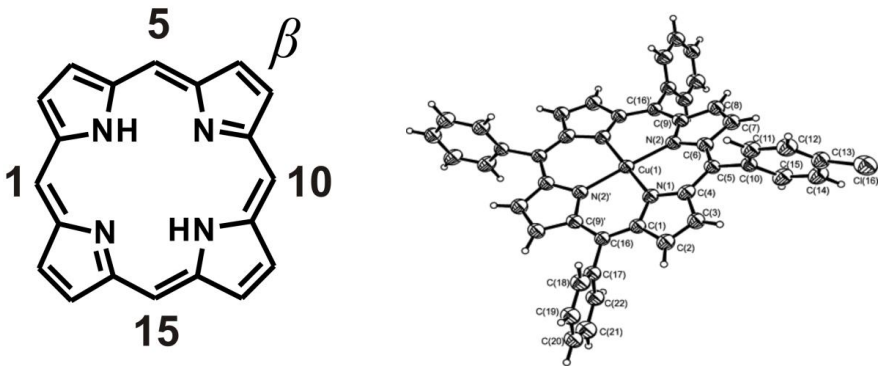

Figure 6: *The structure of the basic porphyrin core (left) showing two of the eight 'β' and the 1,5,10 and 15 'meso' positions. The crystal structure of Cu*

(II) tetraphenylporphyrin (right), showing the planarity of the core.[34] *Note that the phenyl groups bound at the meso positions are twisted out-of-plane, and so are not in conjugation with the core.*

The porphyrin core has a fully conjugated, planar structure (**Figure 6**). In addition, there is a huge amount of chemistry that can be performed at the β and/or meso positions, which has led to the synthesis of a vast number systems characterised by high TPA probability (**Figure 7**).

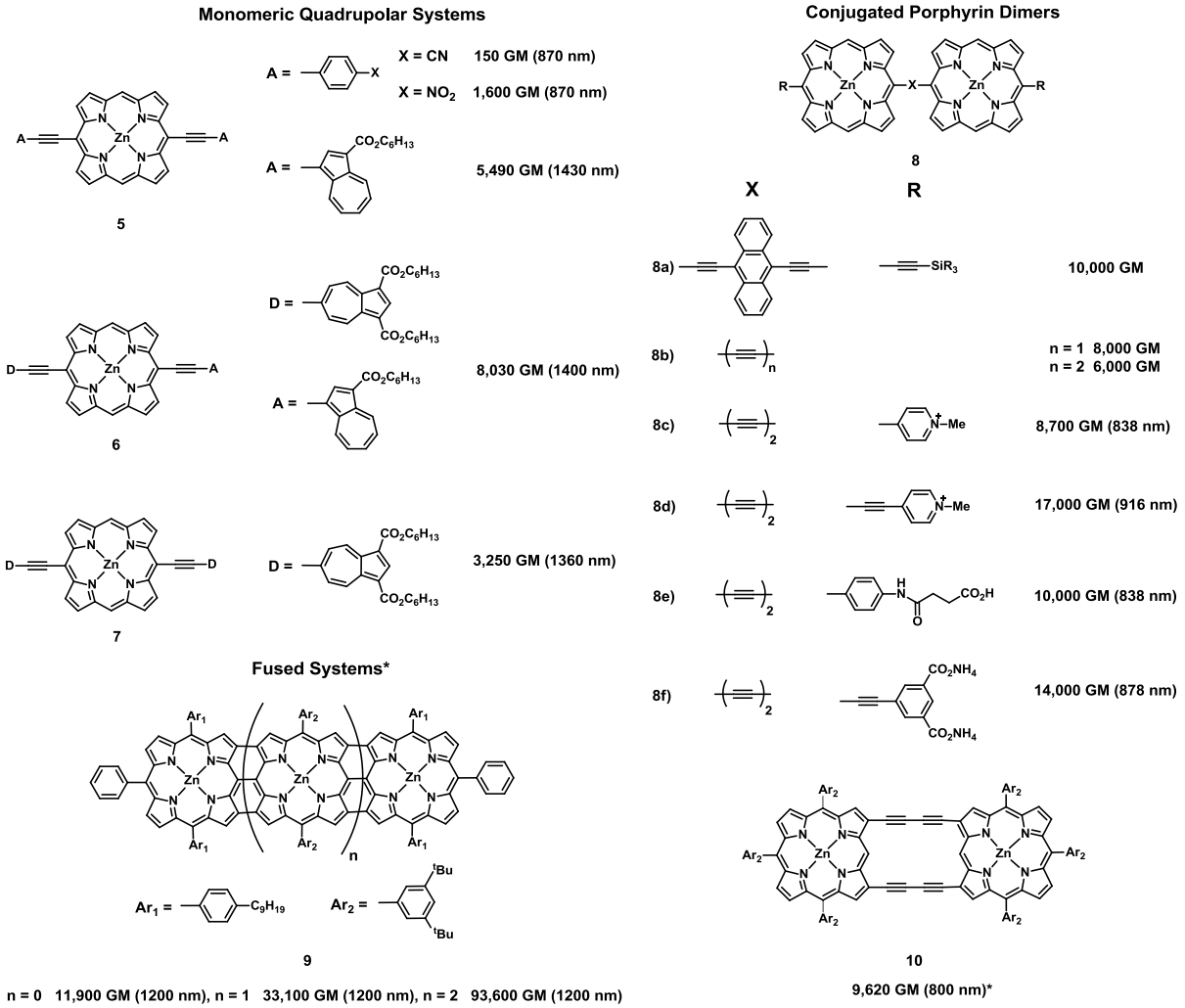

Figure 7: *Literature highlights of porphyrin derivatives with high TPA cross-sections. Adapted from references 13,35,36,37.*denotes values obtained by the z-scan technique.*

These compounds highlight the effect on the TPA efficiency of simply conjugating another porphyrin unit to the system. The highest monomer-based value shown is around 8,000 GM (compound **6**), which is similar to the TPA cross-section of the most basic conjugated dimer (compound **8b**, **n = 1**).

The data presented in **Figure 7** emphasise the importance of planarity. For the dimers conjugated by a single ethynyl link (**Series 8**), rotation is possible, so the two porphyrin cores are not necessarily co-planar. When fixed in position however, there is a dramatic increase in

the TPA cross-section. For example, the meso-linked butadiyne system (**8b**, **n = 2**) has a TPA cross-section around two-thirds that of the analogous system in which the two porphyrins units are link by ethynyl groups at two adjacent β positions (**10**). The clearest example of this phenomenon is in the fused systems (**9**). The fused dimer (**9**, **n = 0**) has a TPA cross-section of nearly 12,000 GM, while a fused tetramer is closer to 100,000 GM. This is because in fused systems both conjugation and planarity are optimised. It should be noted that these values are likely to be exaggerated as they were measured by the z-scan technique in the region of an OPA band.

Porphyrin derivatives are used widely in two-photon related applications.[38,39,40] Not only is their synthesis well-developed and versatile, but they also exhibit strong fluorescence and are generally bio-compatible (see **Chapter 3**).

1.6 The Advantages and Applications of Two-Photon Absorption

There are two main differences between OPA and TPA: the excitation characteristics and the wavelength range at which absorption is achieved. It is these two differences that give TPA its advantages over OPA and form the basis of its main applications.

When irradiated with a collimated monochromatic beam of light through an objective lens, molecular excitation occurs at the focal point of the beam. If one photon is used to achieve this, the excitation density is directly proportional to the local light intensity, whereas if two-photon excitation is employed, the excitation density is proportional to the square of the local light intensity. Therefore, excitation density decreases more rapidly when moving away from the focus and the focus itself is smaller, increasing excitation resolution (**Figure 8a**).

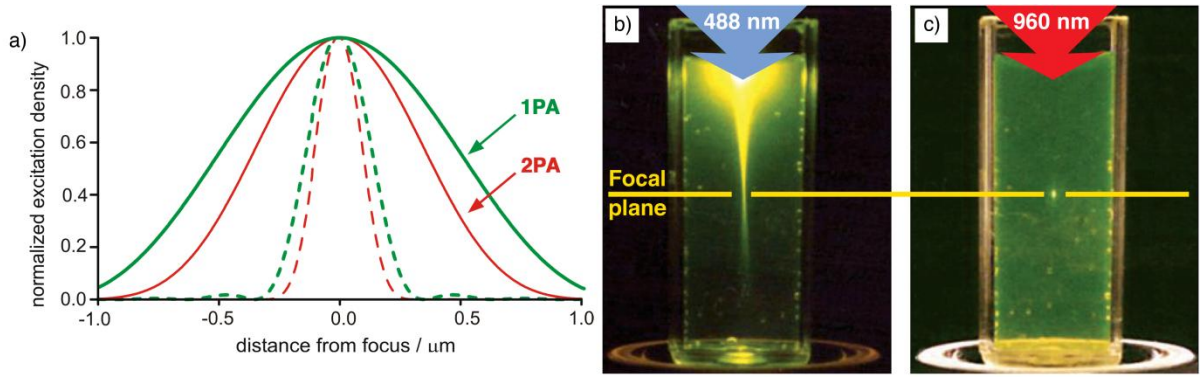

Figure 8: *(a) Excitation density as a function of radial (solid) and axial (dashed) distance from focus for OPA (green) and TPA (red) (b) one-photon and (c) two-photon excited fluorescence demonstrating the difference in the size of the excitation volume in each case. Reproduced, with permission, from reference 16.*

The focal volume is defined as the ellipsoid whose diameter is directly proportional to the wavelength of light and inversely proportional to the numerical aperture of the lens.[41] The excitation volume is the volume at which excitation is at least 50% that at the focus. At distances from the focus outside this volume, the excitation density fluctuates periodically, with its average obeying the inverse square law. At a distance of 10 μm the density is a factor of 10^4 lower for one-photon excitation and 10^8 for two-photon excitation.[16] **Figure 8b & c** demonstrates the effect of this phenomenon. The cuvette contains a solution of a two-photon fluorescent dye irradiated by two lasers; in **Figure 8b** laser is exciting *via* OPA while **Figure 8c** shows excitation *via* TPA. Because of the dramatic reduction in excitation density with distance from the focal volume, TPEF is essentially restricted to the focal volume, while one-photon fluorescence is observed along the entire beam path.

That a small, well-defined volume within a sample can be accessed exclusively is a huge advantage of TPA. When comparing OPA at 400 nm and TPA at 800 nm, the resolution of TPA is in fact lower than OPA as the size of the focal volume is proportional to the wavelength of light (and so doubles between 400 and 800 nm), while the reduction in focal volume between OPA and TPA is less than a factor of two.[16] It is the sharper contrast in excitation intensity between OPA and TPA which makes TPA more attractive for applications in which a high degree of spatial resolution is required. An example of this is microfabrication, in which a contrast in solubility is achieved using photoinitiated polymerisation or depolymerisation.[42,43] When one-photon excitation is employed, a significant amount of polymerisation is induced above and below the focal point of the laser beam. The restricted excitation demonstrated by two-photon absorption however, allows sub-micron resolution to be achieved in fabrication (**Figure 9**).[44]

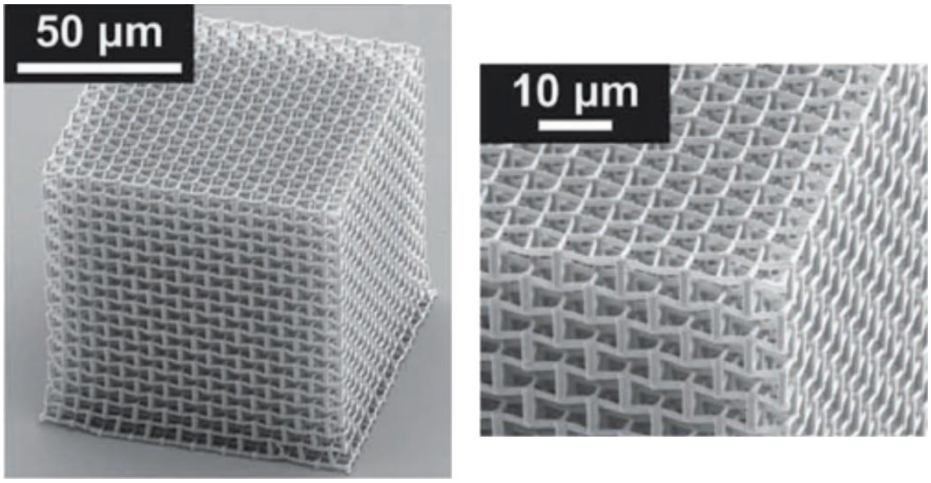

Figure 9: *Scanning electron microscopy (SEM) images of a three-dimensional micro-structured material fabricated using two-photon induced polymerisation. Reproduced, with permission, from reference 45.*

The second advantage of TPA over OPA is related to the typical excitation wavelength. One of the main limitations for the application of optical techniques to living systems is the achievable depth of light penetration through tissue.[45] For a two-photon sensitive chromophore, a one-photon transition in the UVA region (320 – 400 nm) will have a corresponding two-photon transition in the near-IR/IR (700-1300 nm). The ability to excite in the near-IR region has led to the application of two-photon techniques widely in the biosciences. In highly scattering media such as animal tissue, longer wavelength light experiences reduced scattering, and the light which is scattered does not lead to TPA as the photon flux is too low. Moreover the use of longer wavelength, lower energy light results reduced cellular photodamage.[46]

This thesis is concerned with the application of quadrupolar two-photon chromophores to biological systems. The following chapters discuss the design, synthesis and application of two-photon chromophores to the fields of two-photon uncaging and two-photon photodynamic therapy.

Chapter 2: Biologically compatible two-photon labile protecting groups

This chapter describes the design and synthesis of two-photon labile protecting groups which operate via *a photoinduced electron transfer between an excited photosensitiser/electron donor and an acceptor/release group. Initially, the design and synthesis of a suitable photosensitiser is discussed, followed by the evaluation of several potential acceptor/release groups. Intermolecular PeT uncaging is performed to test the principle and to develop an experimental protocol. The photosensitiser/donor and acceptor/release group are then incorporated into a unimolecular system.*

2.1 Introduction to Photo-Removable Protecting Groups and Historical Overview

The continuing desire to probe and understand cellular and sub-cellular processes requires ever-more sophisticated investigative tools. An increasingly important prerequisite of these tools is their ability to selectively target the region of interest within the cell. Photo-removable protecting groups (or caging groups) utilise photolysis to achieve a rapid increase in the local concentration of a physiologically active species.[47] They have found application in many areas of bioscience, and have led to a greater understanding of the cell as they provide an excellent framework for the controlled and targeted release of physiologically active compounds in living systems.[48,49] In their caged form, the compounds are inactive. Upon irradiation, photoexcitation leads to fragmentation which liberates the active species. The variety of biomolecules which have been caged is enormous; nearly every signalling molecule, from protons[50] to enzymes,[51] to proteins,[52] neurotransmitters,[53] nucleotides,[54] and mRNA,[55] has been successfully protected with photolabile groups.

Photolysis is an ideal trigger for the targeted release of molecules in biological systems.[48,56] Unlike conventional deprotection methods in organic synthesis, photolysis is rapid, and orthogonal to the majority of cellular processes. Thus it provides a high degree of temporal control over the release of the biological compound. Furthermore, the use of focused laser light provides fine spatial control; a very important attribute for investigation on the sub-cellular level. Uncaging *via* two-photon excitation further improves spatial control, as excitation is restricted to the focal volume of the laser. In addition, the use of longer wavelengths leads to deeper penetration and reduced scattering in biological media (see **Section 1.6**).[16]

The process of uncaging can be divided into two steps: an initial light absorption step, followed by bond scission. [57] When evaluating caging groups it is important to quantify how well the group absorbs light as well as how efficiently excitation is used in subsequent photochemical reactions. The ability of a molecule to absorb light is quantified by its absorption coefficient; (either its extinction coefficient (ε) for one-photon absorption or its TPA cross-section (δ_a)). The uncaging efficiency is quantified by the uncaging quantum yield (ϕ_u), the number of uncaging events per absorbed photon. Thus an important parameter for caging groups is the product of these two values, $\varepsilon.\phi_u$ or $\delta_a.\phi_u$, known as the one- or two-photon uncaging cross-sections (ε_u or δ_u) respectively.

The first example of the photolytic release of biological compounds was demonstrated by Barltrop and Schofield, while working at the University of Oxford in 1967.[58] Their brief communication reported a benzyloxycarbonyl system which was shown to release glycine upon irradiation with ultraviolet light (254 nm). In the late seventies, Kaplan and co-workers first adopted the phrase 'caged molecule' to describe a physiologically active species protected by a photo-removable group, and developed a protected form of adenosine triphosphate (ATP).[59] This was the first example of an *ortho*-nitrobenzyl-caged system, a group which is still the most common and widely used today. Uncaging was demonstrated by the activation of a Na:K pump in human erythrocytes when, and only when, caged-ATP was delivered in combination with a light dose. Their use of the term 'caging' distinguishes the idea of rendering a compound with a physiological function inactive from the previously established concept of protecting functional groups with photolabile protecting groups for organic synthesis.[60]

In 1982, as isolated studies began to develop into a coherent field of research, Lester and Nerbonne proposed a list of criteria for the design of photosensitive molecules suitable for pharmacological studies.[61] Many of these principles are still relevant today, and are presented in adapted form below:

1. The compound must be soluble in aqueous solutions of high ionic strength (>1 mM).
2. The photochemical reaction must proceed in this medium with high quantum efficiency (ϕ_u ~0.1)
3. Both the precursor and the photoproduct should have simple, well-characterised equilibrium effects on the physiological system.
4. The photochemical reaction should proceed at wavelengths that cause no significant damage to cellular components.
5. Under a two-photon regime, an uncaging cross-section (δ_u) above 1 GM is desired.

Between the late 1970s and end of the 1990s, several uncaging groups were established (**Figure 10**). These groups all demonstrated, to varying degrees, fast and efficient uncaging, while the availability of cheap precursors meant they could be easily derivatised with a variety of biomolecules.[62]

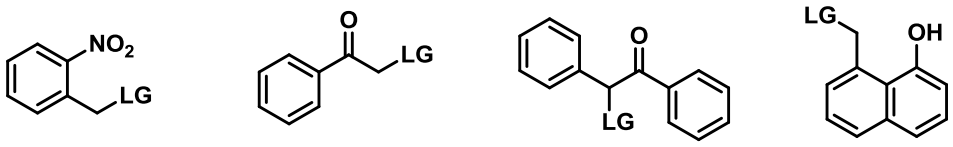

Figure 10: *From left to right the ortho-nitrobenzyl, phenacyl, benzoin and methylnaphthol caging groups. LG represents the position of the caged species.*

Despite generally exhibiting favourable photochemical characteristics (ϕ_u >0.1), there are some clear inadequacies in their molecular design when considering their application to the biosciences. Firstly, the groups presented in **Figure 10** all exhibit poor water-solubility and secondly, as relatively small π systems, their absorption maxima fall in the UV region. Both of these points limit their biological compatibility; their solubility limits the concentration of the caged species that can be introduced into the biological system, and the low excitation wavelength can cause significant photodamage to the surrounding cellular environment. Although structural modifications have been made to the first generation of caging groups to improve their aqueous solubility and increase their excitation wavelength, it was not until the advent of two-photon uncaging that a significant number of new caging groups were developed.

The first thorough demonstration of two-photon uncaging by Furuta *et al* in 1999 initially evaluated *ortho*-nitrobenzyl cages under a TPA regime and, as expected, found them to have low two-photon uncaging cross-sections (~0.01 GM).[63] In addition, they evaluated a recently-developed class of caging group, based on a coumarin core (**Figure 11**).

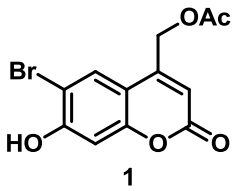

1

Figure 11: *Bromohydroxycoumarin (Bhc) caged acetate.*

The coumarin derivatives exhibited a significant two-photon uncaging cross-section, with the highest value of 2 GM at 740 nm reported for compound **1**. Following this demonstration, there was a steady flow of publications reporting new two-photon caging groups. Some of these were purely novel, while others attempted to improve the photochemical characteristics of existing cages by extending conjugation. These approaches have produced mixed results, the highlights of which are summarised in **Table 1**.

Table 1: *Two-photon uncaging literature highlights, modified, in part, from reference 64. Unless stated in italics, the link between LG and the caging group is an ester bond.*

Entry	Caging Group	Substituent(s)	δ_u /GM
1	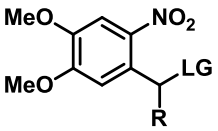	**R** = Br, **LG** = Coumarin[65] **R** = Me, **LG** = Glutamate[66] **R** = Me, **LG** = OAc[67]	0.68 (740 nm) 0.17 (720 nm) 0.03 (740 nm)
2	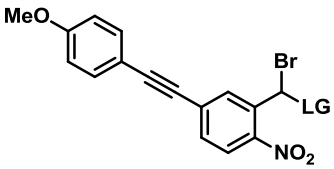	**LG** = Carboxylate[68]	0.05 (750 nm)
3	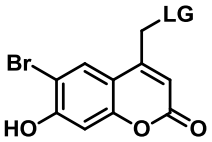	**LG** = OAc[8] **LG** = *Carbamate*-Glutamate[8] **LG** = cAMP[69]	1.99 (740 nm) 0.89 (740 nm) 2.28 (740 nm)
4	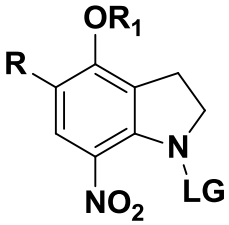	**R** = **H, R$_1$ = Me** (MNI) **R** = **NO$_2$, R$_1$ = Me** (MDNI) **R** = **H, R$_1$ = CH$_2$COOH** (CDI) **R** = **NO$_2$, R$_1$ = CH$_2$COOH** (CDNI) **R** = **H, R$_1$ = CH(CH$_2$OPO$_3$H$_2$)** (DPNI)	**MNI**-Glutamate[70] **MDNI**-Glutamate[14] **CDNI**-Glutamate[71] **CNI**-GABA[72] **CDNI**-GABA[16] **DPNI**-GABA[73]	0.06 (720 nm) 0.06 (720 nm) 0.24 (720 nm)* 0.06 (720 nm)* 0.24 (720 nm)* 0.06 (720 nm)*
5	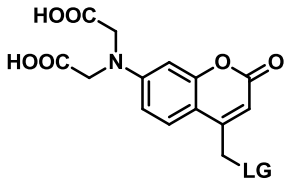	**LG** = *Carbamate*-Capsaicin[74] **LG** = cGMP[75]	2.47 (740 nm) 1.24 (740 nm)
6	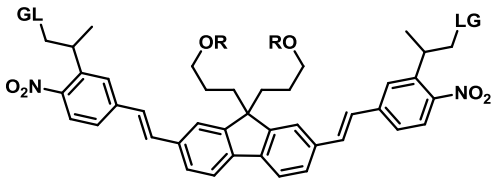	**LG** = Glutamate[76]	5 (800 nm)
7	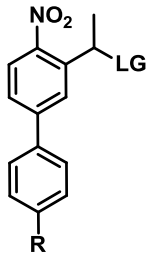	**R** = OMe, **LG** = Glutamate[77] **R** = N(*N*,*N*-di-CH$_2$COCO^{t}Bu), **LG** = GABA[76] **R** = N(*N*,*N*-di-diglyme), **LG** = GABA[76]	0.37 (800 nm) 3.7 (800 nm) 11 (800 nm)

**these data were estimated from the uncaging of different compounds from similar caging groups.*

Table 1 illustrates two features of two-photon uncaging research which present opportunities to significantly advance the field. Firstly, there are no clear structure-property relationships for maximising δ_u. It is difficult to predict how a structural modification will affect the uncaging quantum yield of a known uncaging group, and for novel groups there is no way of estimating the quantum yield prior to synthesis. As a result, the achievement of significant increases in δ_u can be somewhat serendipitous. Secondly, although the structural factors which maximise TPA cross-sections are known,[16] there is only one example (**Table 1, Entry 6**) of a caging group with a TPA cross-section above 100 GM.[76]

2.2 Project Aim

There is a clear need to develop a new strategy for the synthesis of two-photon uncaging groups which utilises our knowledge for maximising TPA cross-sections to approach the problem from a more rational standpoint.

An interesting prospect for the rational design of two-photon caging groups is uncaging *via* a two-photon photoinduced electron transfer (PeT). Here the two steps of uncaging are decoupled; absorption and bond scission occur in different parts of the system and are linked by the PeT. Such an arrangement allows for the optimisation of absorption and bond scission independently. A schematic representation of this idea is illustrated in **Figure 12**.

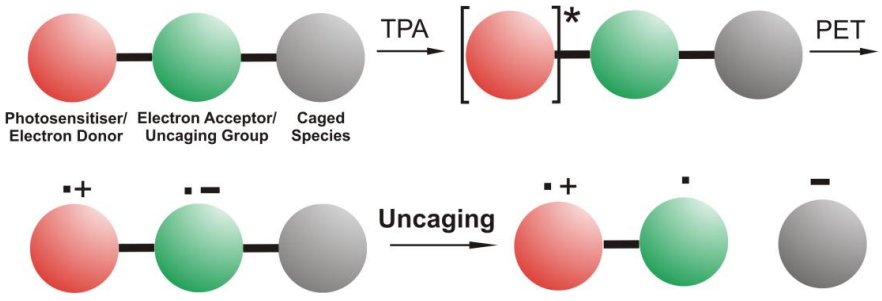

Figure 12: *A schematic representation of PeT uncaging in which a photosensitiser/electron donor (red) is excited by light absorption and transfers an electron to an electron acceptor/uncaging group (green) forming a charge-separated pair. Subsequently the caged species (grey) is released.*

The strategy first involves the photoexcitation of the sensitiser/donor, leading to the formation of a singlet excited state. In polar solvents, quenching of the photosensitiser excited state by electron-transfer to the redox partner can occur efficiently to form the charge separated state.[78] This charge-separated state rearranges to release the caged species. Quenching of the products can occur by various mechanisms, depending on the nature of the groups.

My research focuses on the development of a two-photon photolabile protecting group which operates *via* a two-photon photoinduced electron transfer from a photoexcited donor to an electron acceptor/uncaging group.

2.3 Photoinduced Electron Transfer

Early theoretical models of PeT were put forward by Rudolph Marcus.[79,80,81] His theory predicted a quadratic dependence of the rate of electron transfer (k_{eT}) on the free energy of electron transfer (ΔG_{eT}) rather than linear. Thus the rate of electron transfer will increase with increasing free energy of electron transfer up to a certain energy (the energy where ΔG_{eT} is equal to the nuclear reorganisation energy). Beyond this energy, the rate of electron transfer then decreases as ΔG_{eT} increases. This is the so-called Marcus inverted region. The first experimental evidence for Marcus' theory was reported by Miller and Closs, who investigated PeT in rigid donor-acceptor systems.[82,83,84] Later investigations into intermolecular PeT by Gould and Francis also showed agreement with the theory.[85,86]

The suitability of a donor-acceptor pair for an electron transfer system can be assessed using the Rehm-Weller equation (**Equation 5**), which states that electron transfer is energetically favourable if the excited state of the donor (E_{00}) is of sufficient energy to both oxidise the donor to its radical cation (E_{OX}) and reduce the acceptor to its radical anion (E_{RED}). It is important to remember that, even when electron transfer is energetically favourable, uncaging is in competition with back electron transfer to the lowest energy state (k_{-eT} in **Figure 13**).[87]

$$\Delta G_{eT} = (E_{OX} - E_{RED}) - E_{00} \qquad \textbf{Equation 5}$$

This equation is represented graphically in **Figure 13**.

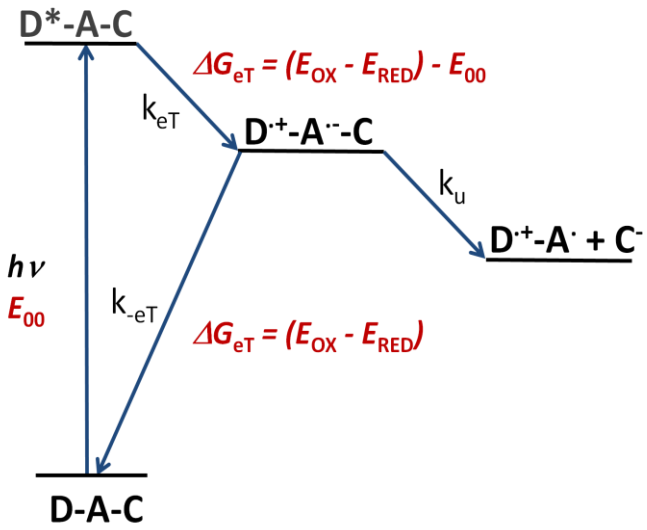

Figure 13: *An energy level diagram for uncaging* via *PeT. The photosensitiser/electron donor is represented by D, the acceptor/uncaging group by A and the caged species by C.*

The values in **Equation 5** can all be determined experimentally. The excited state energy (E_{00}) is defined as the energy of transition between the lowest vibrational level of the ground and excited states, and manifests as the point of overlap between the absorption and emission spectra, while the oxidation potential of the donor (E_{OX}) and reduction potential of the acceptor (E_{RED}) can be measured electrochemically.

2.4 Uncaging *via* PeT

Falvey *et al* were the first to introduce the concept of removing protecting groups by means of a PeT.[88,89] After initially proving the principle with an intermolecular PeT using *N*,*N*-dimethylaniline as a photosensitiser (in which they were able to uncage a large variety of carboxylic acids on a preparative scale),[181] Falvey and Lee developed a covalently linked system (**Figure 14**).[182] They investigated two photosensitisers, anthracene and *N*,*N*-dimethylaniline, which were linked to the phenacyl uncaging group *via* ester bonds.

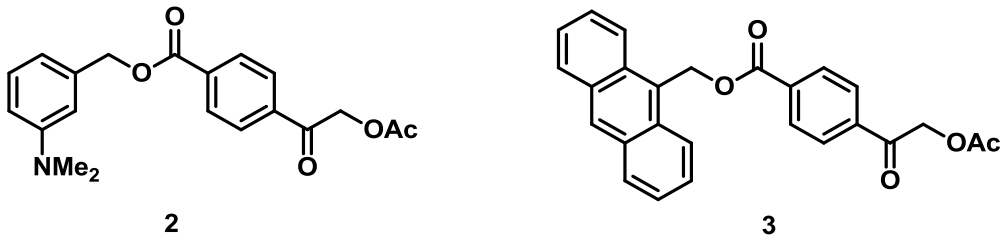

Figure 14: *Intramolecular PeT-based uncaging systems using* N,N-*dimethylaniline (left) and anthracene (right) as photosensitisers/electron donors bonded to a phenacyl acceptor/release group caging acetic acid.*[182]

Their photolysis studies (monitored by ^{1}H NMR) showed that the *N,N*-dimethylaniline system released acetic acid upon irradiation, while the anthracene-based system showed no uncaging. The failure of the anthracene system to uncage was attributed to the formation of an anthracene-based triplet state following its photoexcitation which did not lead to the formation of a charge-separated state. The overall quantum yield of uncaging for the aniline-based system was 0.02, with a free energy of electron transfer of −1.53 eV. Their kinetic analysis of the system established that back electron transfer (k_{-eT}) was dominating the reaction and limiting the quantum yield.

The mechanism proposed for uncaging *via* PeT is shown in **Figure 15**.

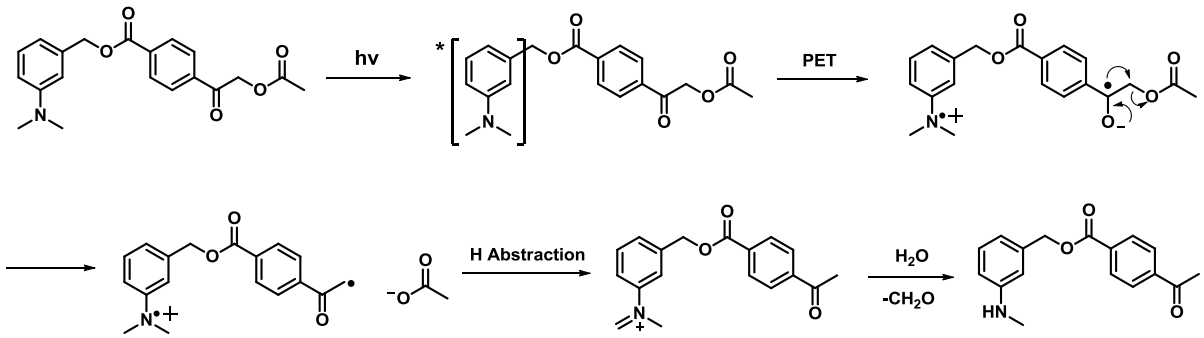

Figure 15: *The mechanism proposed by Falvey and Lee for intramolecular photo-induced electron transfer to a phenacyl derivative.*

Pulsed laser photolysis studies (308 nm, 500-80 mJ, 10 ns) showed the formation of peaks at 380, 480 and 580 nm immediately after the pulse. The peak at 480 nm corresponded to the dimethyl aniline radical while the other two were assigned to the ketyl radical. This assignment was confirmed by three experiments. Firstly, the introduction of oxygen (an anion radical quencher) eliminated the peaks at 380 and 580 nm while the peak at 480 nm remained. Secondly, independent laser photolysis studies of 4-carbomethoxyacetophenone and *N,N*-dimethylaniline showed similar transient absorption bands. Finally, to eliminate the

possibility of the formation of a phenacyl-localised triplet state, the triplet state of 4-carbomethoxyacetophenone was generated by laser flash photolysis of this compound alone. An absorption peak at 325 nm was observed, which was not present in the laser photolysis studies of the composite system.

Their investigations into the system established an important aspect of the molecular design which contributes to the mechanism. The yield of carboxylic acid was found to significantly reduce if the photosensitiser was unable to readily transfer a hydrogen atom, for example if aniline was used instead of *N*,*N*-dimethylaniline. This suggests that, in this case, the photosensitiser is responsible for quenching the radical produced by bond scission

After I had carried out approximately a year of research towards a two-photon uncaging system based on PeT, it became apparent that Jing Wang from Seth Marder's group (Georgia Institute of Technology, USA) had previously investigated the idea in unpublished work, to which I was granted access.[90]

The system initially investigated by Jing Wang consisted of a stilbene-based photosensitiser bound to phenacyl-protected acetic acid *via* an ester link (**Compound 4**, **Figure 16**).

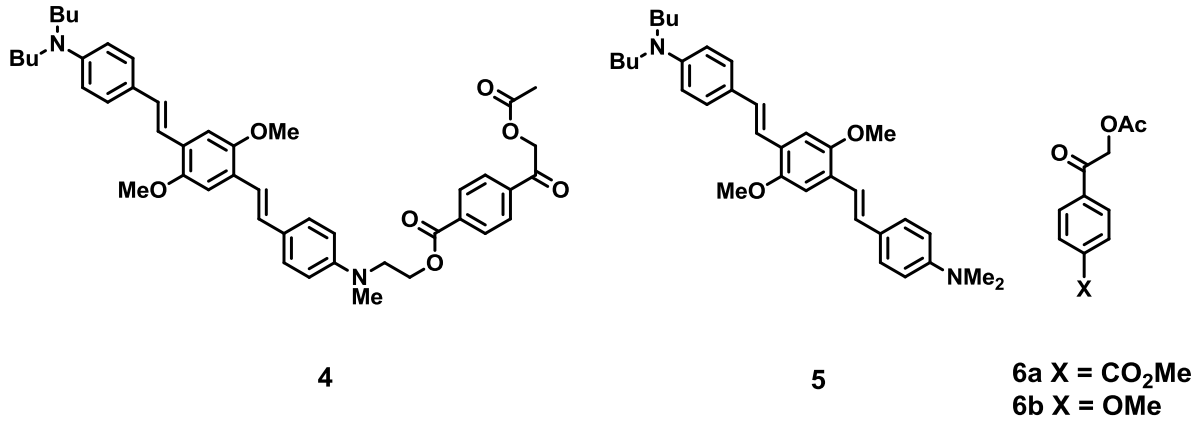

Figure 16: *The initial compound for intramolecular two-photon PeT uncaging (**4**) and the individual electron donor/photosensitiser (**5**) and electron acceptor/uncaging (**6**) components.*

Fluorescence measurements demonstrated a 98% reduction in the fluorescence quantum yield of **4** when compared to **5**. This quenching was attributed to PeT between the electron donor/sensitiser and electron acceptor/uncaging group, which was found to have a favourable free energy (−0.65 eV). However, **4** liberated no detectable amounts of acetic acid upon irradiation (419 nm) in benzene-d_6, suggesting that the charge-separated state decayed by back-electron transfer exclusively. Bimolecular uncaging experiments between **5** and **6a** in

benzene-d_6 corroborated this result. The reason for this failure appeared to be that the rate of the cleavage reaction (k_u in **Figure 13**) was too slow to compete with back-electron transfer (k_{-eT}). Marder and Wang hypothesised that this problem could be overcome by making the phenacyl group more electron-rich (as in **6b**) to accelerate cleavage.

The irradiation of **5** in the presence of **6b** did indeed result in the release of acetic acid, and these components were subsequently synthesised into an intramolecular PeT system. No measurement of the free energy of electron transfer was made for the ether-linked system, though electron transfer is likely to be less favourable as **6b** is more difficult to reduce than **6a** due to the electron-donating nature of the *para* oxygen. These investigations indicate that it is important to realise that favourable PeT is not a sufficient criterion to predict the operation of a PeT-based uncaging system.

In addition, their studies found that attachment of the phenacyl-protected species directly to the π-bridge led to far greater uncaging efficiency (**Figure 17**).

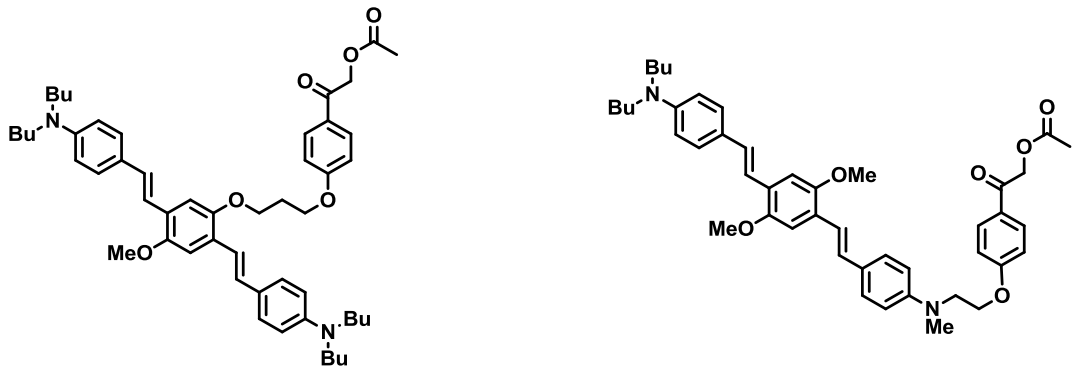

Figure 17: *Compounds for intramolecular two-photon PeT uncaging. In **7**, the uncaging group is attached at the π bridge, while in **8** it is attached to one of the aniline donors.*

Irradiation of **7** for 90 minutes in benzene-d_6 resulted in an NMR yield of acetic acid release of 92% while **8** yielded 47% in the same time. This could be related to closer proximity of the donor's excited state electron density to the acceptor in the case **7** compared to **8** (no possible explanation was given). No quantum yields of uncaging were discussed.

2.5 Photosensitisers for a Two-Photon PeT Uncaging System

There are no defined criteria for the suitability of a photosensitiser in a biologically compatible two-photon photoinduced electron transfer system, but some basic characteristics are suggested here:

1. A high two-photon cross-section (>100 GM).
2. A low oxidation potential (<0.5 eV).
3. A high excited state energy (>2.5 eV or <496 nm).
4. High water solubility at physiological pH (>1 mM).
5. A modular, high yielding synthesis.
6. A high fluorescence quantum yield (ϕ_f >0.75).

It is clear from these criteria that several compromises need to be made when considering the design of the photosensitiser. For example, in order to achieve a sufficiently high TPA cross-section, a molecule with a large, delocalised π-system is desired; however highly conjugated systems can exhibit reduced excited state energies. Similarly, molecules with large π-systems tend to be rigid and planar, two factors which lead to poor water solubility. A high fluorescence quantum yield is desired to indicate that no irreversible photochemical reactions occur upon photoexcitation.

From the literature survey in **Chapter 1** and the criteria stipulated above, I chose centrosymmetric quadrupolar fluorene systems as the basis for the photosensitisers in this research (**Figure 18**).

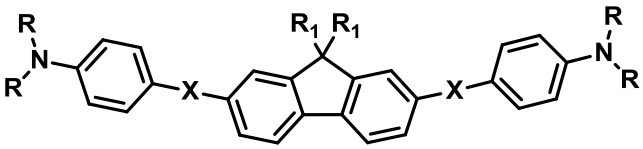

Figure 18: *The donor-acceptor-donor fluorene platform. Aniline-based donors are connected to the fluorene acceptor core* via *a conjugated link.*

In general, this platform combines a high two-photon cross-section (800-2000 GM) with high excited state energy (~3 eV).[33] Furthermore, fluorescence quantum yields of such derivatives are generally high (ϕ_f >0.70). The R_1 groups at the fluorene core provide an opportunity to attach the acceptor/uncaging group, while the additional R groups at the anilines' nitrogen atoms allow for the inclusion of solubilising groups.

2.6 Caging Groups for a PeT System

The following is a literature review of the mechanisms and photochemical parameters of caging groups which are suitable for PeT systems. For an examination of general caging groups, a very detailed review has recently been published.[91]

2.6.1 Phenacyl Esters

Although common conventional protecting groups for carboxylic acids (removable by reduction or hydrolysis)[92] phenacyl esters have more recently become the focus of PeT driven uncaging systems.

The photocleavage mechanism in a non-PeT system has been heavily discussed in the literature. In the first paper published on the photolysis of phenacyl groups, Sheehan *et al* studied the uncaging of *p*-methoxyphenacyl derivatives and made three observations. Firstly, decreased yields of the corresponding carboxylic acid were observed in the presence of water, no uncaging occurred in the presence of a triplet quencher, and in some cases, decarboxylation of the free carboxylic acid was noted.[93] In the presence of hydrogen donors and radical hydrogen donors, the yields of the carboxylic acid increased. This led them to propose a mechanism in which excitation of the phenacyl to a triplet state leads to homolytic bond scission. At this point, an unstable carboxylate radical will decompose or hydrogen donation will convert it to the free acid (**Figure 19**).

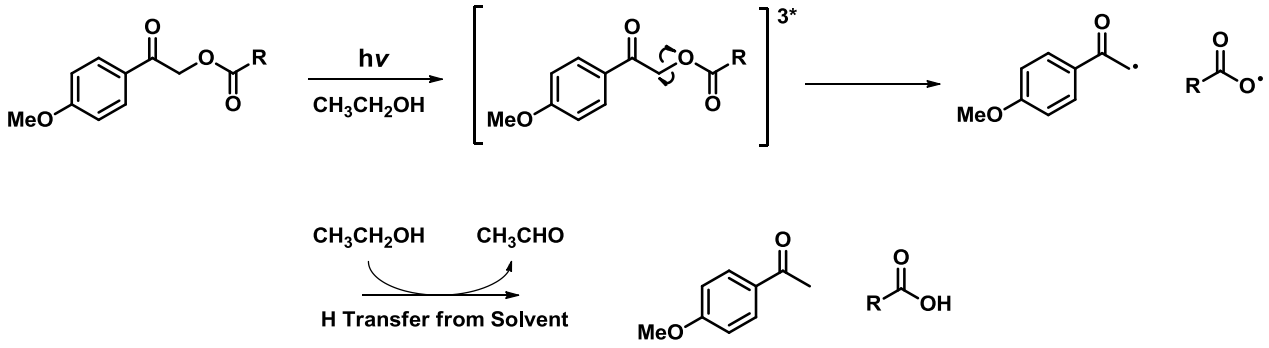

Figure 19: *The uncaging mechanism of phenacyl derivatives as proposed by Sheehan* et al.[201] *In the final step, ethanol is reduced to acetaldehyde to quench the products.*

Sheehan *et al* investigated the uncaging of many different carboxylic acids, including amino acids, and generally obtained very good isolated yields (up to 94%). No photochemical parameters, such as the quantum yield of uncaging, were reported.

In 1997, Givens and Park published a more extensive study of phenacyl derivatives, also varying the photolysis conditions.[94] Their study confirmed Sheehan's observation that in the presence of a hydrogen donor, such as methanol, uncaging occurs and results in an acetophenone-derived product. However, they reasoned that, because hydrogen donation from the solvent was required to initiate bond cleavage, reduction of the phenacyl ketone was the first step (**Figure 20**)

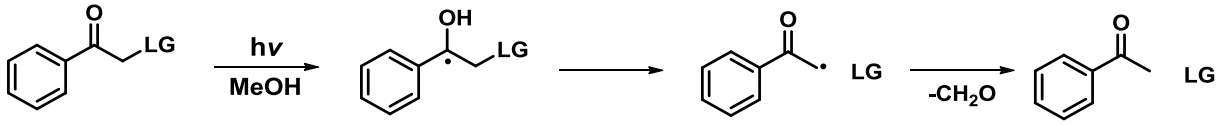

Figure 20: *Uncaging of the phenacyl group where photoreduction of the ketone is the first step.*

The Givens-Park mechanism, which is generally accepted, was extended by Falvey's group who proposed hydrogen donation from the solvent as the first photochemical step, and rejected the idea of homolytic bond scission (**Figure 21**).[95]

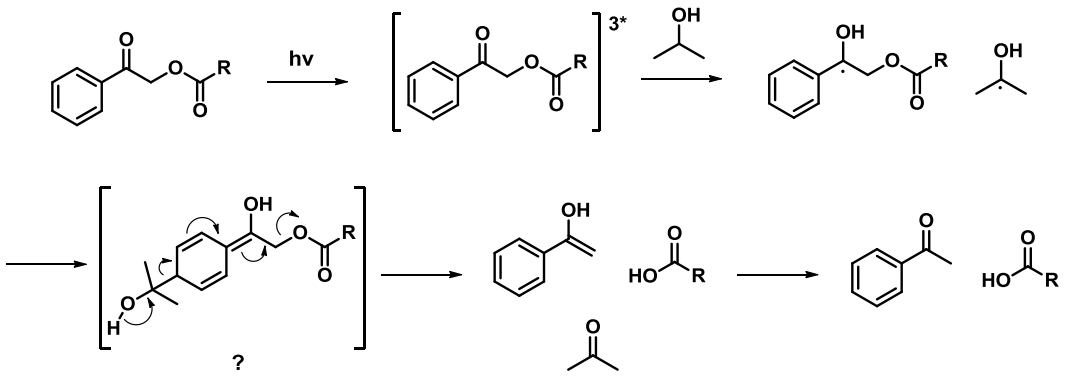

Figure 21: *The uncaging mechanism of phenacyl derivatives as proposed by Falvey* et al.[203]

This study was the first to provide experimental evidence for the intermediates of the reaction. Extensive laser flash photolysis studies detected a triplet excited state which rapidly decayed to form the phenacyl-based ketyl radical. Addition of a hydrogen donor increased the efficiency of uncaging, which would not be expected if homolytic bond cleavage were the means of photorelease. The intermediate (**?**) was not detected, but its presence was tentatively inferred from several observations. Laser flash photolysis studies indicated that the ketyl radical decays to a long-lived (>1 ms) species whose absorption does not correspond to acetophenone or its enol, and which subsequently decays in a second order fashion. Secondly, a metastable species has been reported in photochemical reactions between benzophenone

and 2-propanol, which has been assigned to the coupling of a 2-hydroxy-2-propyl radical to a benzophenone ketyl radical at the *ortho* or *para* position.[96]

Interestingly, photolysis of phenacyl groups which possess a hydroxyl or alkoxy group in the *para* position can result in profoundly different reactivity.[203] If hydrolytic conditions are used in the presence of derivatives with a *para*-oxygen, phenylacetic acid is formed. This requires a different mechanism to that proposed previously, in which electron transfer leads to the formation of a spirodienedione, which is hydrolysed to the phenylacetic acid (**Figure 22**).

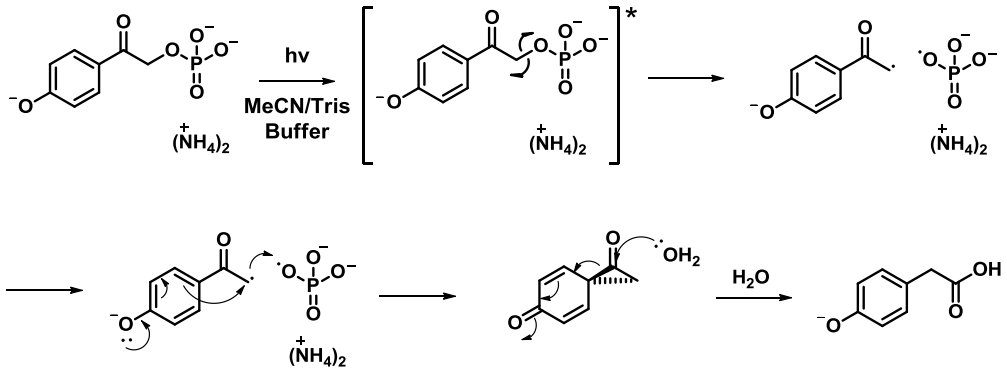

Figure 22: *The phenacyl uncaging mechanism as proposed by Givens and Parks*[95]

A simplified version of this mechanism, which eliminates the homolytic bond cleavage step, is now accepted (**Figure 23**).

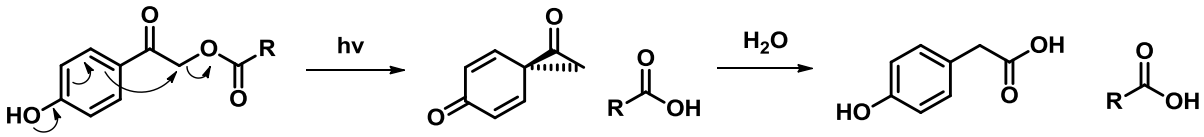

Figure 23: *Formation of phenacylacetic acid following photoexcitation without homolytic bond cleavage.*

The similarity of the spiroketone intermediate to the cyclopropanone intermediates proposed in Favorskii rearrangements has led to this reaction being referred to as the photo-Favorskii rearrangement.[97]

During this investigation into the mechanism, Falvey *et al* developed the first PeT uncaging system.[98] Their reasons for development of the PeT strategy were twofold; firstly, the proposed mechanism for phenacyl uncaging at the time involved releasing the protected species as free radicals. They noted that most applicable functional groups (for example, carboxylic acids) are highly unstable as free radicals and the H-abstraction was therefore in

competition with secondary fragmentation (**Figure 24**). The use of a photoinduced electron transfer to drive uncaging results in the formation of the corresponding radical anion, a much more stable species, and, as such, this problem is avoided.

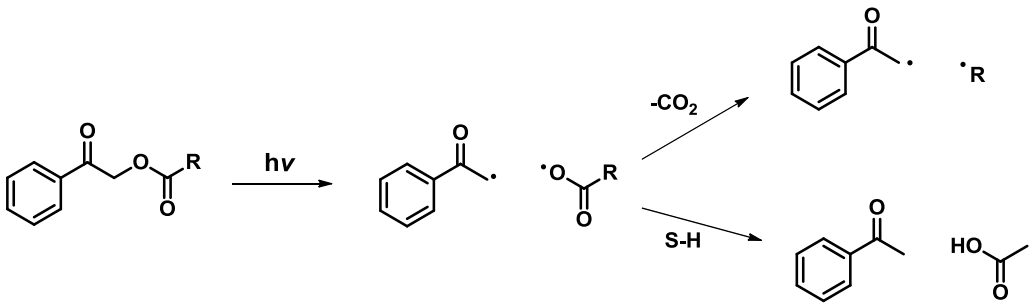

Figure 24: *The two possible outcomes of homolytic bond cleavage. Undesirable decarboxylation can be avoided by driving uncaging with a photoinduced electron transfer.*

Secondly, they identified that the use of a modular system, in which the absorption and release steps occur in independent parts of the system, allows for optimisation of each step independently.

Phenacyl groups are well-studied caging groups and generally exhibit very high chemical yields (>80%) and quantum yields of uncaging above 10%. Furthermore, as they have been demonstrated to uncage *via* two-photon PeT they were considered important compounds to investigate in this research.

2.6.2 Picolinium Esters

More recently, 4-picolyl esters have been investigated as photoremovable protecting groups for carboxylic acids (**Figure 25**).

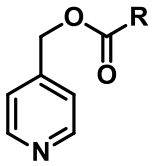

Figure 25: *The generic structure of 4-picolyl esters.*

They have previously shown to be versatile protecting groups for carboxylic acids in peptide synthesis,[99] released using electrolytic or chemical (e.g. Zn^0 or H_2, Pd/C) reduction.[100] When converted to their corresponding *N*-methyl-4-picolinium iodide, a charge transfer exists between the picolinium/iodide pair, resulting in an absorption band between 350 and 450 nm.

Direct irradiation of this transfer band results in C-O bond cleavage, producing the corresponding carboxylic acid in high yield (70-95%) (**Figure 26**).[101]

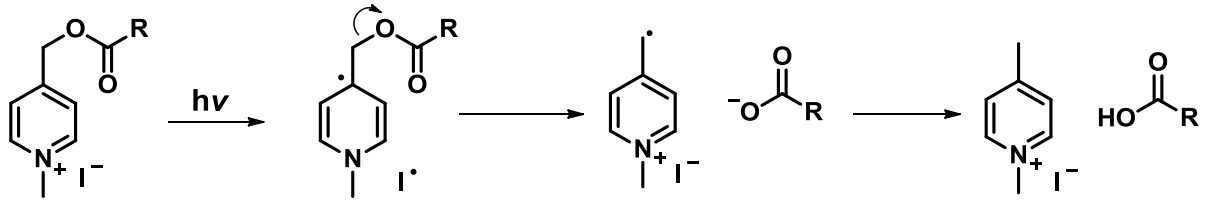

Figure 26: *Uncaging of picolinium derivatives by electron transfer from iodide.*

Absorption of light leads to a single electron transfer from iodide to the picolinium ester. The pyridyl radical subsequently releases the carboxylic acid, along with a pyridylmethyl fragment. The authors did not propose a mechanism for quenching the pyridylmethyl radical, though they report cleaner photolysis in methanol compared to acetonitrile, suggesting it occurs through reduction of the solvent.

By converting the iodide to another salt, perchlorate for example, charge transfer is eliminated, the absorption maximum falls below 300 nm, and a separate electron donor can be used to facilitate uncaging. That picolinium salts are capable of uncaging *via* PeT from a photoexcited donor was first established by Falvey *et al* in 2004. [102] The uncaging of acetic acid from *N*-methyl-4-picolinium acetate perchlorate *via* an intermolecular PeT from a variety of donors (including BODIPY, carbazole and coumarin derivatives) was demonstrated using ^{1}H NMR spectroscopy. The mechanism they proposed was analogous to that in **Figure 26**. Their evidence for this mechanism was based on laser flash photolysis, fluorescence quenching and radical trapping. Flash photolysis (355 nm, 50-80 mJ, 4-8 ns pulse) showed transient UV-Vis absorption at 410, 690 and 770 nm. The peak at 410 nm corresponds to the *N*-methyl-4-picolinium radical ion, confirmed by independent experiments on the picolinium. The other peaks are related to the donor radical cation.

An advantage of picolinium esters over many uncaging groups is their relatively high reduction potential (*ca* −1.5 eV). Falvey *et al* have demonstrated the versatility of such systems by uncaging a wide variety of carboxylic acids and phosphates in good yield with many different donors.[102] The caged compounds included biomolecules, such as glycine and serine, for which chemical yields ranged from 75 to 100%.

N-Methyl-4-picolinium esters represent an attractive prospect for an acceptor/release group because of their relative ease of reduction. In addition, the methylated picolinium salts are

water-soluble, so in a larger system, such as that proposed herein, they can act as solubilising groups.

2.6.3 *Ortho*-Nitrobenzyl Derivatives

Despite being the most common caging group, there are no examples of the uncaging of *ortho*-nitrobenzyl *via* photoinduced electron transfer. The group is very versatile, having been used to cage phosphates, carboxylic acids, alcohols and amines. In addition, there are several commercially available *o*-nitrobenzyl caging groups.[103]

The photochemical deprotection reaction has been shown to proceed *via* a Norrish Type II mechanism (**Figure 27**).[104]

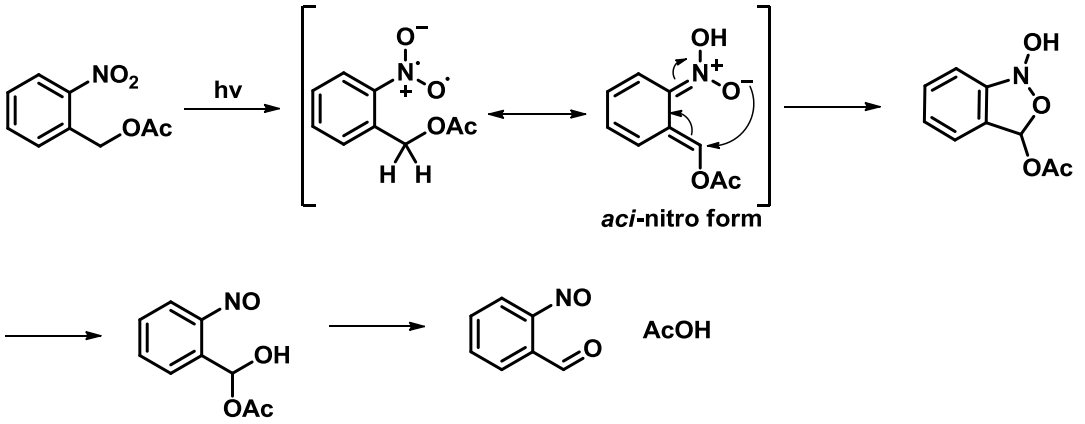

Figure 27: *General mechanism for the uncaging of* ortho-*nitrobenzyl derivatives.*

The excited nitro group abstracts a hydrogen atom intramolecularly, and subsequent electronic redistribution leads to the *aci*-nitro form. Intramolecular attack of the nitro-alcohol leads to a bicyclic system which rearranges, eliminating the carboxylic acid. The formation of the benzylic aldehyde is the driving force for the release.

In general, *o*-nitrobenzyl uncaging proceeds with high quantum yield (>0.1) however, the instability of the aldehyde photoproduct to biological conditions and relatively slow release rate make it less attractive as an uncaging group.

Attempts have been made to increase the sensitivity of the *o*-nitrobenzyl group to two-photon excitation by coupling with an efficient two-photon absorber. Rana *et al* developed a system using thioxanthone to induce uncaging *via* intermolecular triplet-triplet energy transfer.[105] Similarly, Steiner *et al* used the same photosensitiser in a covalently-linked system (**Figure**

28).[106] They investigated a number of different covalent links and used time-resolved laser spectroscopy to confirm the cleavage mechanism.[107]

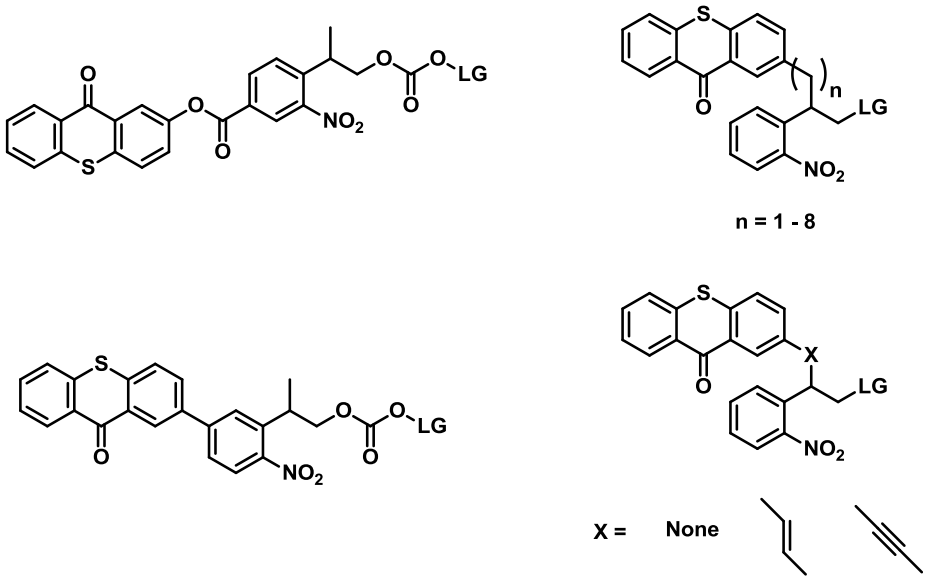

Figure 28: *The photoinduced triplet-triplet energy transfer systems employed by Steiner* et al.[107]

When compared to 2-(2-nitrophenyl)propoxycarbonyl groups alone, the sensitised systems demonstrated ε_u values between two and twenty times higher. Generally, these increases were the result of the improved absorption efficiency of the sensitised systems, as a decrease in quantum efficiency was observed in nearly all cases. Interestingly, the systems in which the sensitiser was not bonded to the benzene ring of the *o*-nitrobenzyl unit demonstrated the highest quantum yields (0.11-0.42), which approached or exceeded that of 2-(2-nitrophenyl)propoxycarbonyl itself (0.41).[108] Mechanistic investigations found that in those systems where the sensitiser was connected to the benzene ring of the *o*-nitrobenzyl group, the system acted as a single united chromophore, while the alkyl-linked systems demonstrated triplet-triplet energy transfer. In general, the yield of uncaging was found to decrease with increasing linker length in these systems.

2.7 Biologically-Active Molecules for Caging

As previously discussed, there are a huge variety of biologically-active molecules which have been caged. In general, the literature of uncaging research falls into one of two categories. There are those research groups who are primarily interested in the application of cages in biology, and so use simple, commercially-available photoremovable protecting groups to cage compounds for novel purposes. While in the other category, there are researchers mainly interested in developing new, synthetically-complex cages whose applications are demonstrated in well-established systems. My research mostly falls into the second category; it is concerned with developing novel, complex cages and demonstrating them in a biological environment. Initially, uncaging was investigated using simple carboxylic acids such as acetic or propanoic acid then, following the identification of a suitable system, a biologically-active compound was caged.

2.7.1 Caged Neurotransmitters

Arguably the most important application of caging groups is the photolabile protection of neurotransmitters.

Neurons transmit information through the brain *via* electrical impulses. At synapses, the junctions between neurons, the electrical impulse is converted to a biochemical signal and transferred across the synaptic cleft (**Figure 29**).

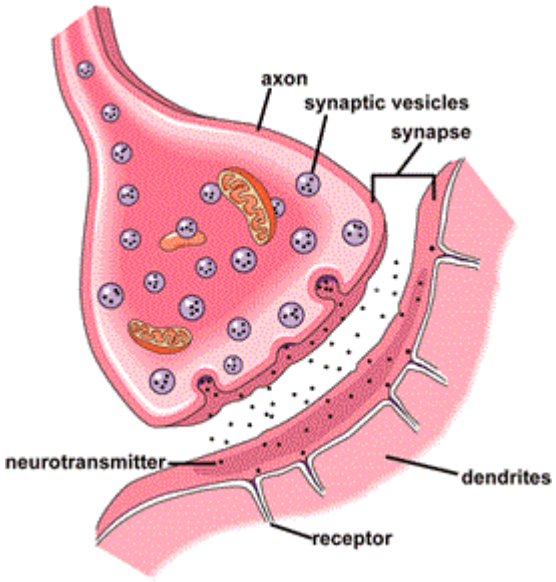

Figure 29: *A schematic representation of a synapse. Neurotransmitters are transmitted from the axon of the pre-synaptic cell to the dendrite of a post-synaptic cell across the synaptic cleft. Adapted from reference 109*

When a synapse fires, an impulse is transmitted from the axon of the pre-synaptic cell to the dendrite of the post-synaptic cell. This event is mediated by neurotransmitters which relay, amplify, or modulate the signal by controlling the activity of neuronal receptors.

Optical techniques have superceded electrode-based methods for the activation of individual neurons due to the difficulty in fabricating electrodes of the correct size and flexibility, as well as the practical considerations in the experimental set up. Two very simple neurotransmitters which are commonly caged are glutamic acid and γ-aminobutyric acid (GABA) (**Figure 30**).

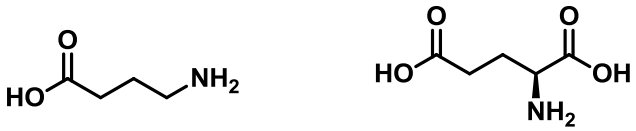

Figure 30: *Two commonly caged neurotransmitters.*

Glutamic acid (or glutamate) is one of the principal excitatory neurotransmitters in mammalian brains and is known to agonise three ion-channel receptors: the AMPA (amino-3-hydroxyl-5-methyl-4-isoxazole propionate), NMDA (*N*-methyl-D-aspartate) and kainate receptors. NMDA receptors are critical in the control of synaptic plasticity (the ability of a synapse signal to change in strength), an important process in memory formation. They operate by regulating the flow of calcium and sodium ions into and potassium ion flow out of the pre- and post-synaptic cells. Furthermore, it has been shown that a reduction in NMDA receptor activity can lead to behavioural changes characteristic of schizophrenia.[110]

There are a number of caged-glutamate compounds (including commercial products) which have been utilised for both one- and two-photon uncaging to great effect. Example studies using caged-glutamate include the analysis of channel-opening kinetics for several glutamate-sensitive ion channels,[111,112,113] and the increase in expression of postsynaptic AMPA receptors following the uncaging of glutamate in isolated dendritic spines.[114] Typically, the two-photon uncaging of neurotransmitters is performed *ex vivo* in brain slices or in cultured neurons, though recently, the first example of *in vivo* two-photon uncaging of glutamate was reported in live mice.[115] The transient currents observed in this study following two-photon uncaging were shown to be similar to normal excitatory post-synaptic currents (EPSCs). In

addition, a spatial resolution of glutamate uncaging of 0.6-0.8 μm to a depth of 200 μm was achieved meaning single spines could be stimulated.

Inhibition in the adult invertebrate central nervous systems is primarily controlled by GABA. Two types of GABA receptors are known: $GABA_A$ and $GABA_B$ receptors. $GABA_A$ receptors are ligand-gated chloride channels, while $GABA_B$ receptors are coupled to transmembrane potassium channels.

As a simple and readily-available carboxylic acid, it is an attractive candidate for caging. However, the research performed using caged-GABA compounds is not as advanced as caged-glutamate. In general, caged-GABA research focuses on the activation and mapping of individual GABA receptors in cultured neurons.[116] More advanced studies include the investigation of miniature pre-synaptic GABA signals and the excitatory properties of GABA.[117,118] In addition, two-photon uncaging of GABA has been demonstrated using a nitroindoline derivative in intact brain tissue.[119]

The reasons for the relative infancy of caged-GABA research are twofold: the low two-photon uncaging efficiency of current GABA cages (a problem for all commercial caged compounds) and that many caged-GABA compounds demonstrate antagonistic behaviour. Regarding two-photon uncaging efficiency, the two commercially available caged-GABA compounds most suitable for two-photon uncaging in biological systems, RuBi-GABA and DPNI-GABA, both have two-photon uncaging cross-sections of the order of 0.01 GM (**Figure 31**). [120,121] The only caged-GABA compound to demonstrate the *in vitro* release of GABA quantitatively with δ_u >1 GM is EANBP-GABA, the recent example from Specht *et al* [76,77]

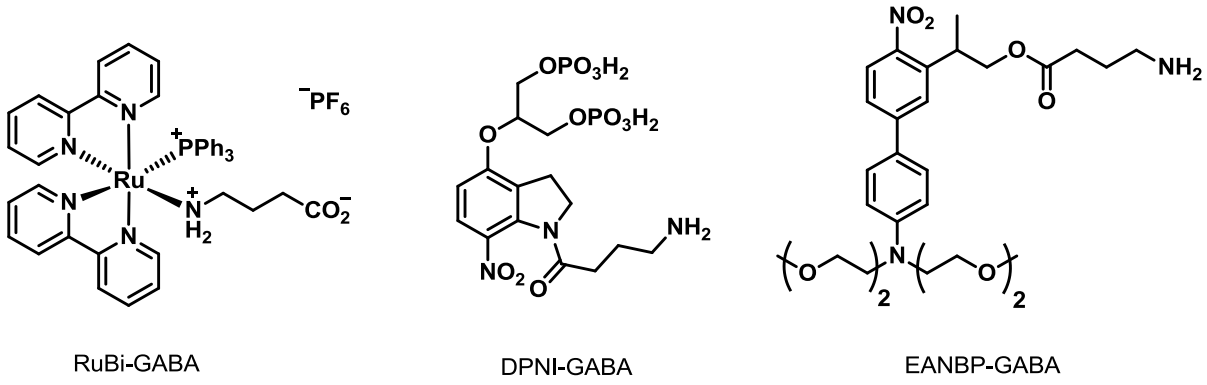

Figure 31: *Two commercially available caged-GABA compounds (RuBi- and DPNI-GABA) and EANBP-GABA, a promising cage from the recent literature.*[77]

Antagonistic behaviour indicates that in its caged form, some interaction between the cage and the target receptor is detected prior to the administration of the light dose. This generally means a significant amount of background activity is observed during experiments and a higher concentration of the cage is required to achieve an appreciable signal. Prediction and prevention of antagonist behaviour in caged-GABA compounds is a difficult problem to overcome. It has been proposed that charged cages show reduced interaction with GABA receptors, and DPNI-GABA certainly demonstrates weaker antagonisation than its non-charged predecessors.[122] However, EANBP-GABA is a neutral compound which exhibits no antagonisation, so the rule is obviously not absolute.

There is a clear need for the development of photoremovable protecting groups which exhibit fast, stoichiometric release of GABA with significant two-photon uncaging properties. For this reason, GABA will be the biologically active molecule used to demonstrate the photochemical properties of the caging groups developed in my research. A strategy employing charged compounds will be used where possible to attempt to minimise antagonisation.

Results and Discussion

2.8 Photosensitisers for Two-Photon Photoinduced Electron Transfer

For this section, photosensitisers for two-photon photoinduced electron transfer systems were synthesised and evaluated.

As an illustration of the overall strategy for designing a two-photon PeT uncaging system, the initial target is shown in **Figure 32**. This incorporated the photosensitiser platform chosen in **Section 2.5** and phenacyl-protected acetic acid. The solubilising groups are alkyl chains terminated by carboxylic acids.

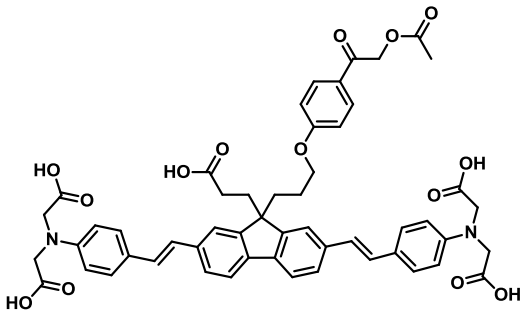

Figure 32: *An example structure for two-photon PeT uncaging*

Figure 33 illustrates how this structure could be constructed from simple building blocks.

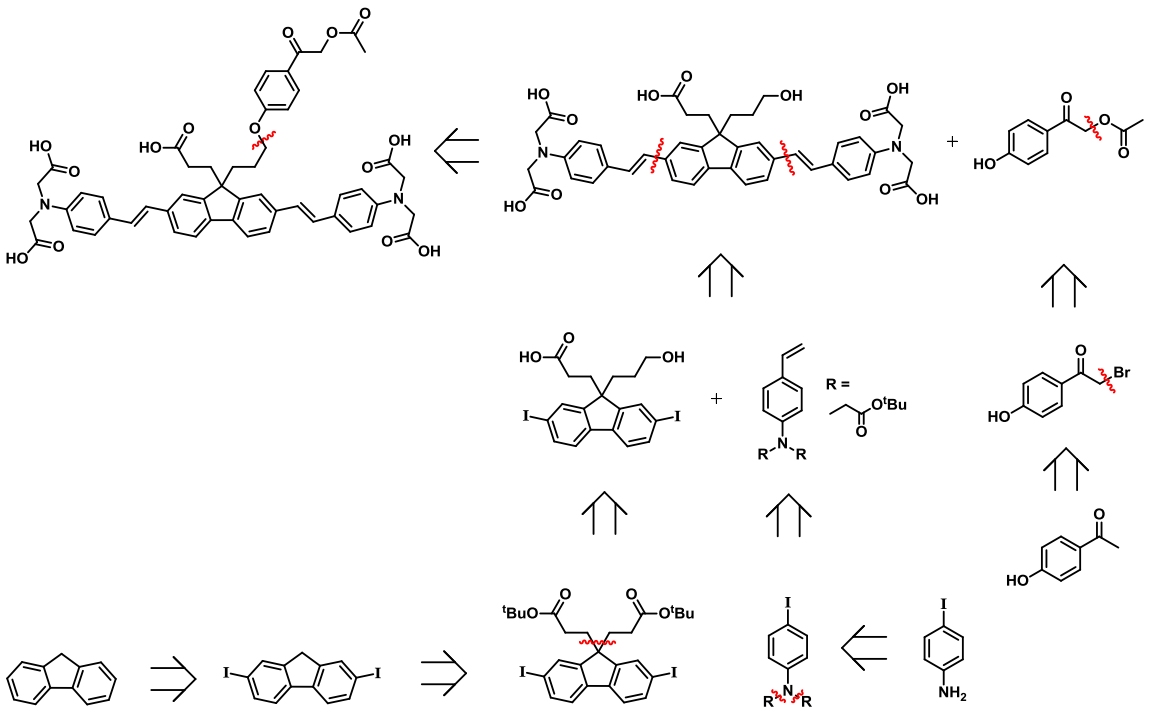

Figure 33: *A route towards the proposed donor-acceptor fluorene platform from simple building blocks. The starting compounds are commercially available at low cost.*

A modular approach to the synthesis allows for easy modification of the structure. The solubilising groups can be introduced by alkylating 4-iodoaniline, which is then modified with the alkene linker using palladium cross-coupling chemistry. A further cross-coupling reaction is used to form the full chromophore. To aid organic solubility during synthesis, the solubilising groups are protected as *tert*-butyl esters, which can be hydrolysed at a late stage in the synthesis. Reduction of one of the acid-terminated alkyl chains attached to the fluorene core allows for attachment of the acceptor/uncaging group.

2.8.1 Anionic Photosensitisers for PeT

The anionic photosensitiser platform is shown in **Figure 34**. Initially synthesising the photosensitiser without an uncaging group allowed for easy evaluation of its suitability as a donor.

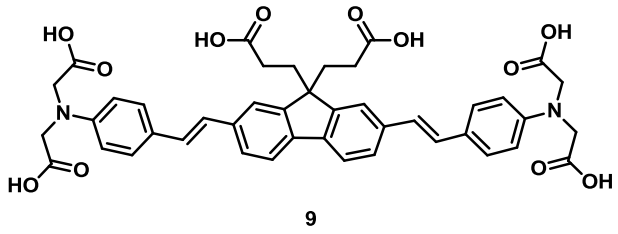

9

Figure 34: *The fluorene-based chromophore with carboxylic acid solubilising groups.*

The synthetic route towards the *tert*-butyl protected photosensitiser is shown in **Scheme 1**.

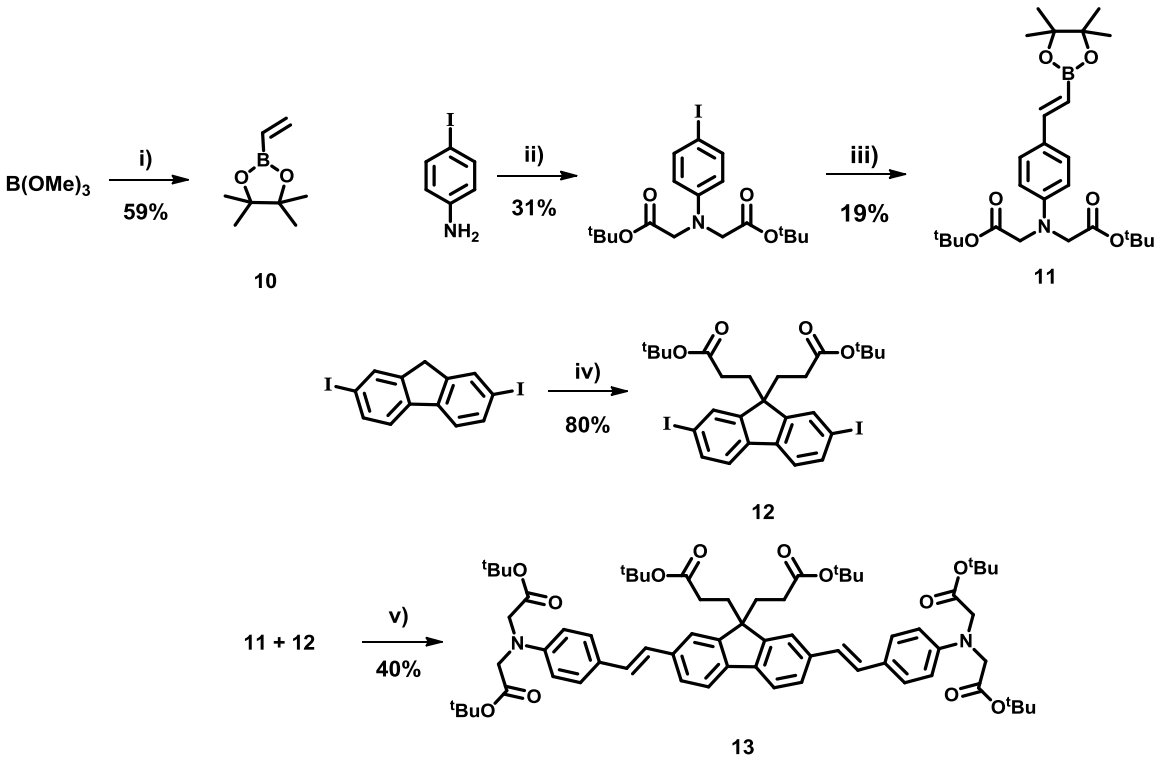

Scheme 1: *(i) CH_2=CHMgBr −78 °C, 30% HCl then pinacol (ii) tert-butyl bromoacetate, DMF, 90 °C, 3 days (iii) $Pd(OAc)_2$, $P(o\text{-}tol)_3$, AgOAc, Bu_3N, DMF, 90 °C, 24 h (iv) tert-butyl acrylate, TBAF, THF, rt, 2 h (v) $Pd_2(dba)_3$, $P(o\text{-}tol)_3$, KO^tBu, 66 °C, 4 h.*

Despite some low yielding steps, compound **13** was synthesised successfully. The main obstacle to this route was synthesising **10**, which resulted in highly variable yields. In addition, the Heck and Suzuki reactions were fairly low yielding despite attempts to optimise conditions. The photophysical and electrochemical properties of **13** were explored in order to investigate its suitability for a PeT system (**Figure 35**).

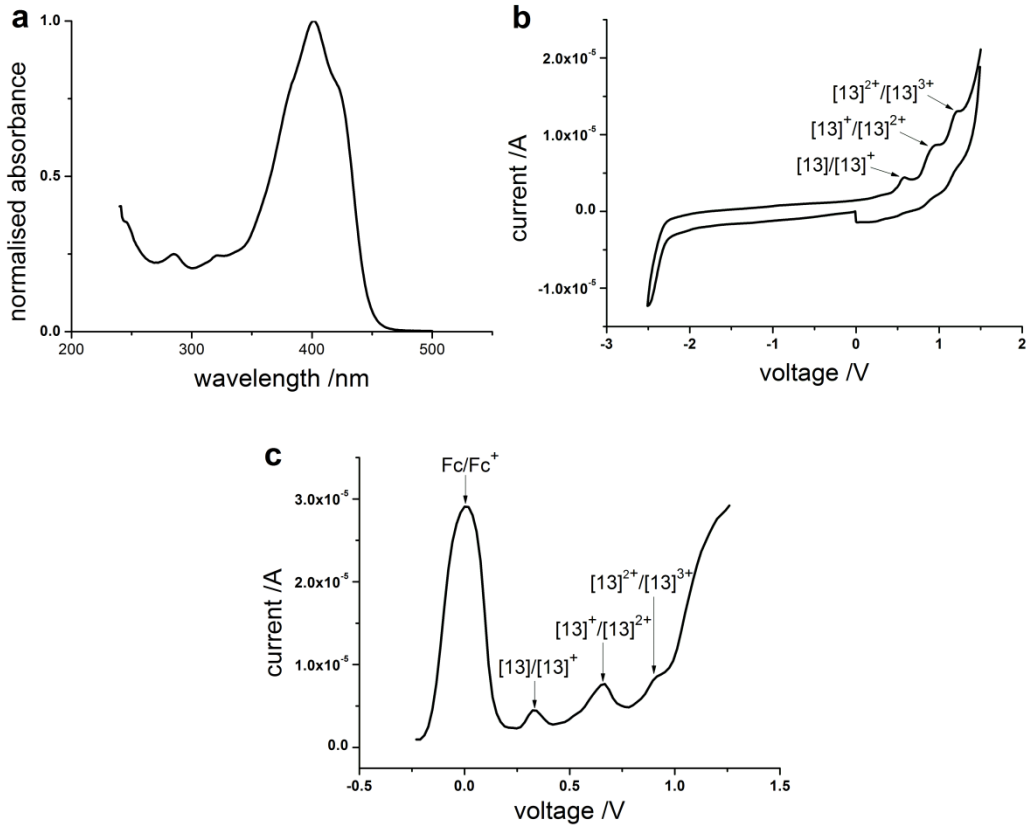

Figure 35: *(a) The absorption spectrum of **13** (b) the cyclic voltammogram of **13** in THF and (c) the square-wave oxidation of **13** in DCM. All electrochemistry was performed using Bu_4NPF_6 as an electrolyte (0.1 M) at 100 mV/s scan rate.*

The absorption of **13** (**Figure 35a**) extends to 470 nm with a peak at 397 nm. The fluorescence of this compound was not measured, but the excited state energy was estimated to be +2.75 eV (450 nm). Cyclic voltammetry showed three oxidation peaks and no visible reductions. The first oxidation appears at +0.31 eV relative to ferrocene (Fc/Fc^+). Interestingly, the oxidations are only partially reversible, suggesting that there are other pathways competing with electrochemical reduction.

For means of comparison and as a result of the difficulties in synthesising **13**, its acetylene analogue, **14** (**Figure 36**), was synthesised according to the synthetic route in **Scheme 2**.

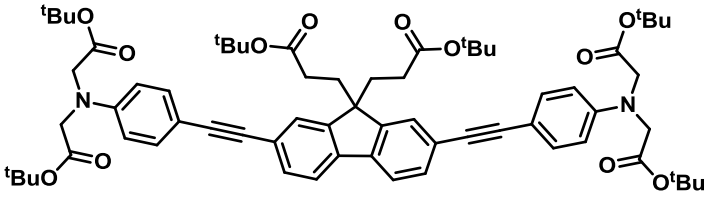

14

Figure 36: *The acetylene-bonded analogue of the photosensitiser,* ***14****.*

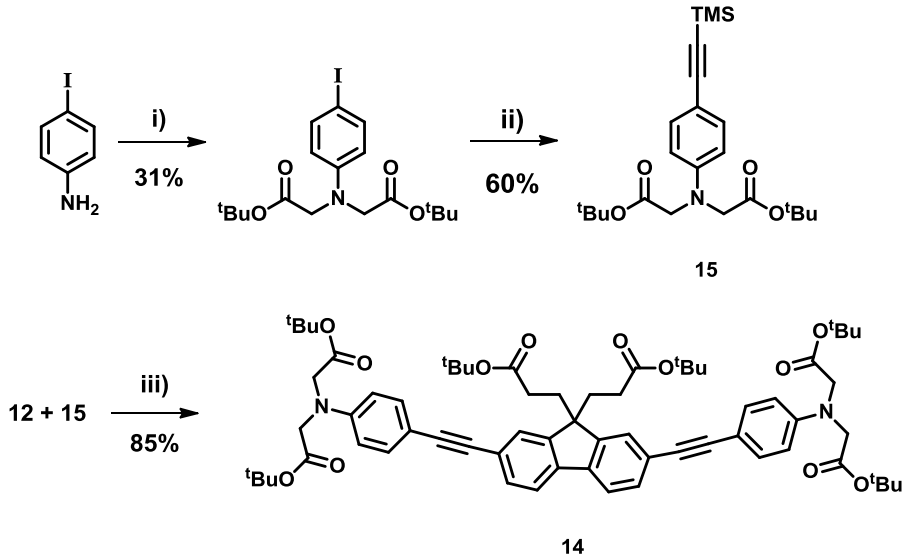

Scheme 2: *(i)* tert-*Butyl bromoacetate, DMF, 90 °C, 3 days (ii) TMS-acetylene, $Pd(OAc)_2$, PPh_3, DIPA, rt, 2 h (iii) $Pd(OAc)_2$, PPh_3, DIPA, TBAF, rt, 2 h.*

In general, this synthetic route proved far easier. The Sonogashira cross-coupling reactions were much higher yielding, and the *in situ* deprotection of the TMS-acetylene group with TBAF shortened the route.

Figure 37a shows the absorption and emission spectra of **14**. The absorption peaks at 377 nm ($\varepsilon \sim 90{,}000\ M^{-1}cm^{-1}$) with an emission maximum at 434 nm. The data in **Figure 37a**, was used to determine the excited state energy as 3.06 eV (405 nm). Cyclic voltammetry exhibited two close oxidations which again do not appear to be fully reversible. Square-wave voltammetry (**Figure 37c**) estimated the first oxidation potential at +0.55 eV relative to Fc/Fc^+ in DCM.

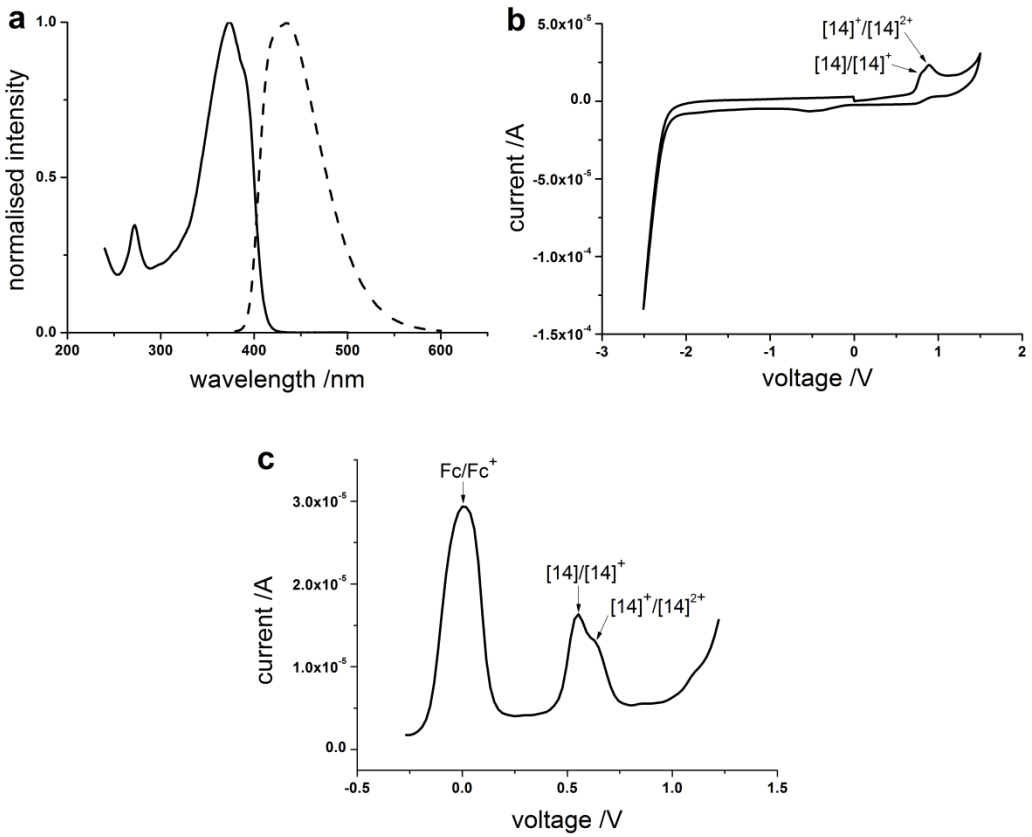

Figure 37: *(a) The absorption and emission spectra of **14** in THF (b) the cyclic voltammogram of **14** in THF and (c) the square-wave voltammogram of **14** in THF. All electrochemistry was performed using Bu_4NPF_6 as an electrolyte (0.1 M) at 100 mV/s scan rate.*

Figure 38 shows a comparison of the electrochemical and photophysical properties of **13** and **14**.

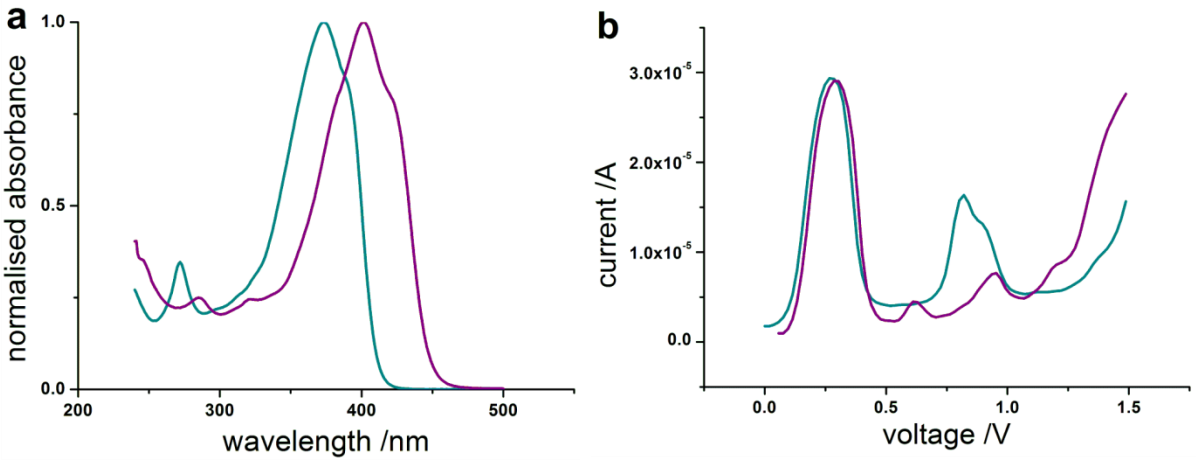

Figure 38: *(a) The absorption spectra of **13** (purple) and **14** (cyan) in THF (b) the square wave oxidation of **13** (purple) and **14** (cyan) in DCM relative to Fc/Fc^+. All electrochemistry was performed using Bu_4NPF_6 as an electrolyte (0.1 M) at 100 mV/s scan rate.*

As can be seen from **Figure 38b** the first oxidation potential of the **13** is lower in comparison to **14**. This is expected of a more electron rich system. A lower oxidation potential is advantageous in an electron transfer system as a lower excited state energy is then required to achieve PeT. However, as **Figure 38a** shows, the absorption of **13** is red-shifted by around 10 nm compared to the **14**, indicating a lower excited state energy and effectively cancelling out any advantage gained from the lower oxidation potential. Taking into account the similarity in the reported TPA cross-sections of chromophores similar to **13** and **14** (1130 GM and 1200 GM at 705 nm respectively),[32] the higher yielding and simpler synthesis of **14** made it the clear choice as a photosensitiser.

Hydrolysis of the *tert*-butyl ester groups to yield the free carboxylate photosensitiser was achieved using TFA (**Scheme 3**).

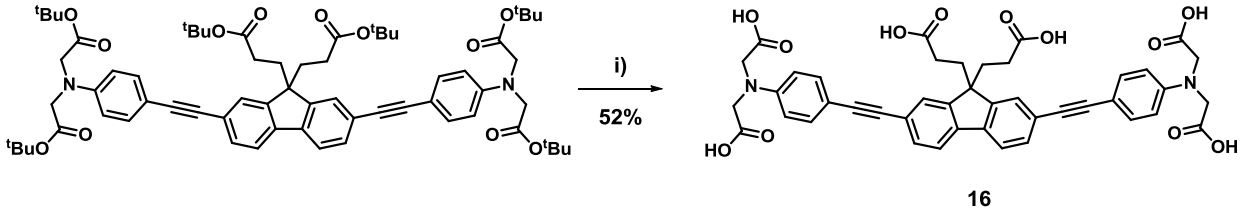

Scheme 3: *(i) TFA:$CHCl_3$ 1:1 (v:v), rt, 16 h.*

The free acid form of the carboxylate photosensitiser showed quite low solubility (<1 mM). A series of 1 mM solutions/suspensions were made up in deuterated solvents (**Table 2**).

Table 2: *The solubility of **16** in various deuterated solvents (1 mM).*

Solvent	***Water (pD 10)***	***Water (pD 12)***	***Methanol***	***DMSO***	***Tetrahydrofuran***
Appearance	Yellow suspension	Yellow solution	Yellow solution	Orange solution	Yellow suspension

^{1}H NMR experiments were performed at 1 mM in D_2O (pD 12) and DMSO-d_6 as they appeared to be the best solvents. The spectrum in DMSO-d_6 was significantly aggregated, showing broad lumps in the approximate regions where peaks would be expected. However, the spectrum in D_2O (pD 12) was sharper (**Figure 39**).

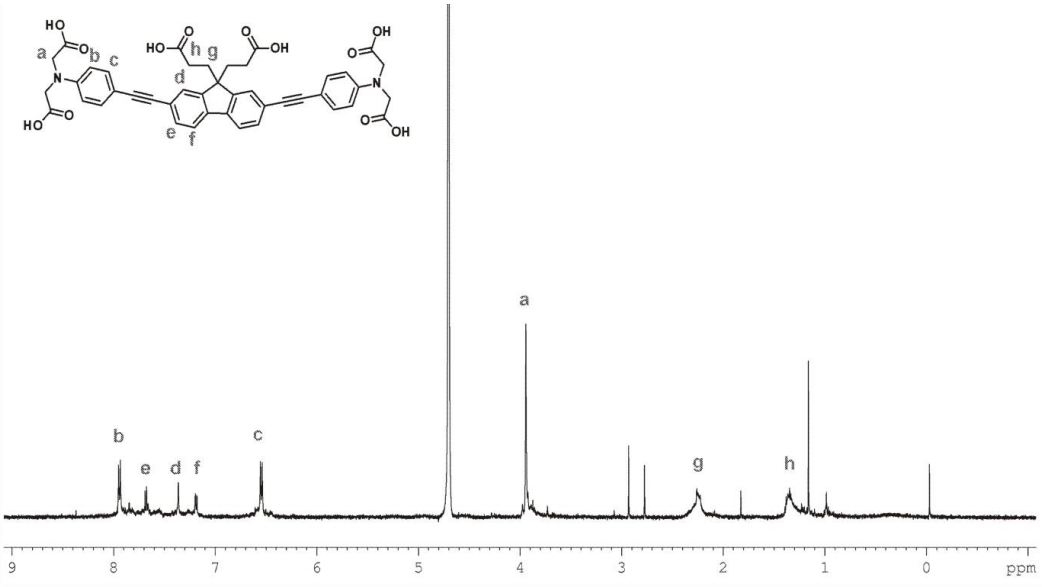

Figure 39: *The ^{1}H NMR spectrum (250 MHz) of **16** in NaOD (1 mM, pD = 12).The signal at 4.7 ppm is due to residual water.*

The absorption spectrum of **16** is shown in **Figure 40** (cyan). It was not expected that hydrolysis would have an effect on the absorption profile of the chromophore, so the broadened spectrum obtained is likely a result of aggregation in solution.

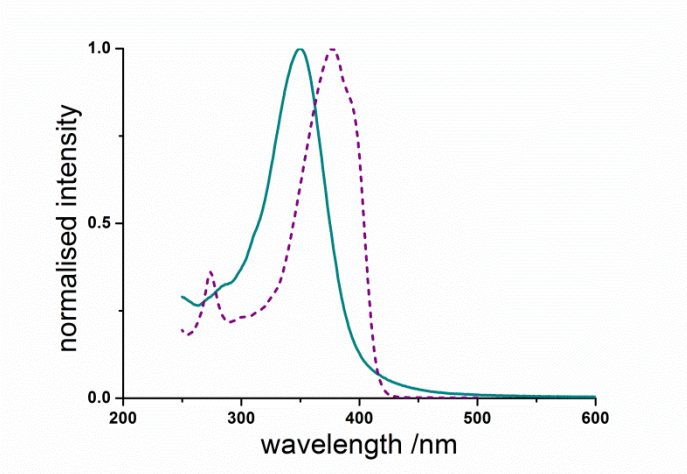

Figure 40: *The absorption spectrum of **16** (cyan) compared to **14** (purple).*

Aggregation due to the hydrophobic effect is common for large, planar π systems. It was hoped that electrostatic repulsion between the negatively charged carboxyl groups of adjacent molecules would be sufficient to disrupt such aggregation, but evidently this was not the case. In the final systems, the acceptor/uncaging groups at the fluorene core will sit out-of-plane with the rest of the molecule, which may prevent aggregation sufficiently to improve solubility.

2.8.2 A Neutral Photosensitiser for Intramolecular Uncaging

Due to the poor solubility of the anionic photosensitisers, an alternative, neutral photosensitiser was synthesised (**Figure 41**). There are two key differences in this evolution of the molecular design. Firstly, the solubilising groups attached to the aniline unit are hexaethylene glycol chains. Polyethylene glycols are neutral, bulky, polar groups with low associated toxicity, commonly used to improve the solubility of macromolecules both in the Anderson group and many others. In addition, both alkyl chains at the fluorene core have been reduced to primary alcohols and protected as *tert*-butyl-dimethylsilyl ethers. Both groups were reduced to simplify the synthesis towards the photosensitiser and the final PeT system.

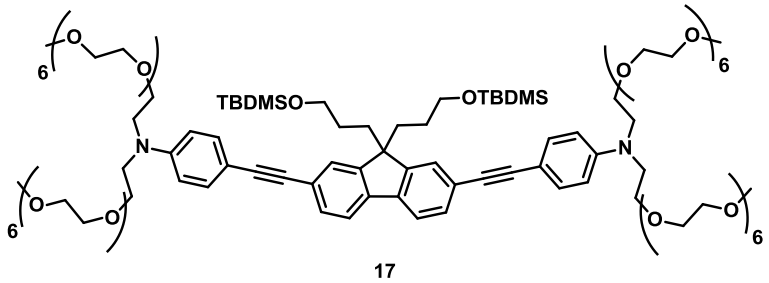

17

Figure 41: *The reference hexa-ethylenegycol photosensitiser.*

The synthetic route towards **17** is shown in **Scheme 4**.

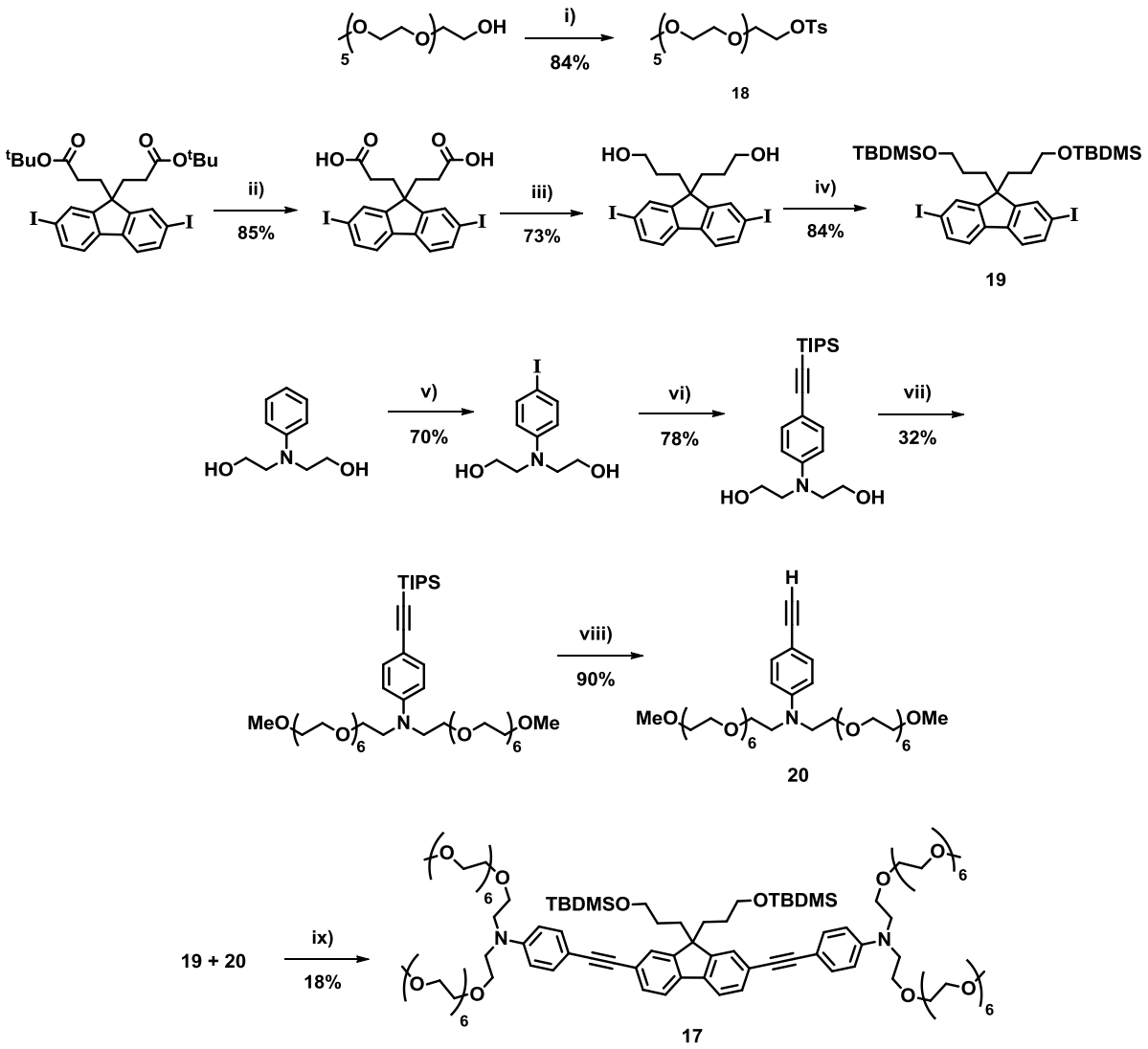

Scheme 4: *(i)* p-*Toluenesulfonyl chloride (ii) TFA, rt, 16 h (iii)* BH_3*.THF, 0 °C – rt (iv) TBDMS-Cl, DMF, rt (v)* I_2*, pyridine, rt (vi) TIPS-acetylene,* $Pd(OAc)_2$*,* PPh_3*, CuI, DIPA, rt, 2 h (vii)* ***18****, NaH, THF, reflux, 24 h (viii) TBAF, rt, 3 h (ix)* $Pd(OAc)_2$*,* PPh_3*, CuI, DIPA, rt 2 h.*

The components of this system are similar to those used in the synthesis of the **13** and **14**. Synthesis of the aniline derivatives proved more troublesome as the high polarity of the glycol chains complicated purification. This led to a route in which the chains were added at the last possible stage before Sonogashira cross-coupling of the aniline and fluorene components.

As expected, the photophysical properties of **17** are similar to that of **14**. Intense one-photon absorption in a variety of solvents, including water, was observed with peak absorption at 384

nm (ε ~100,000 $M^{-1}cm^{-1}$). In addition, the photosensitiser exhibits intense fluorescence at 462 nm (ϕ_f = 0.93 in ethanol) (**Figure 42**).

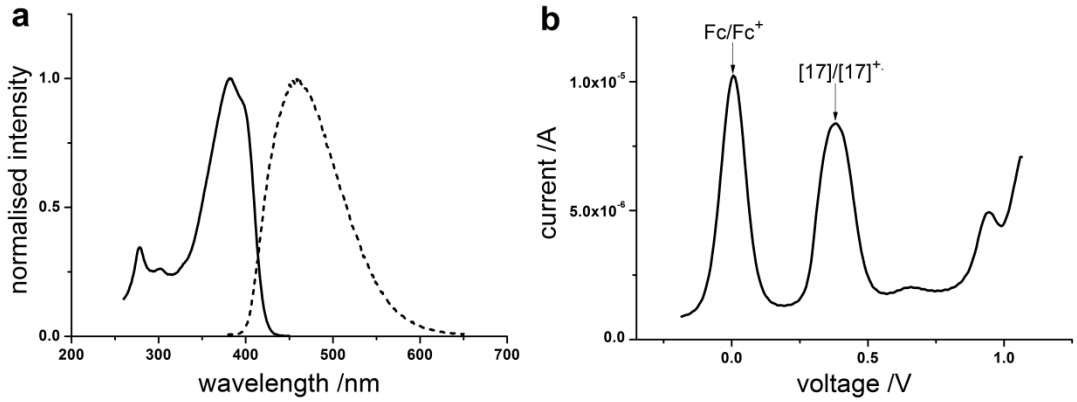

Figure 42: *(a) The normalised absorption and emission spectra of **17** in THF and ethanol respectively and (b) the square-wave oxidation of **17** in DCM relative to Fc/Fc^+ (0.1 M Bu_4NPF_6, 100 mV/s scan rate).*

From the data presented in **Figure 42**, the excited state energy was estimated at +2.99 eV (415 nm) and the first oxidation potential of the dye was determined to be +0.37 eV relative to Fc/Fc^+. In addition, the TPA cross-section (measured by Geoffrey Wicks of Prof. Aleks Rebane's group, Montana State University, USA) was determined to peak at 1200 GM at 700 nm, which corresponds well with previously reported data for this class of dye (**Figure 43**).[32]

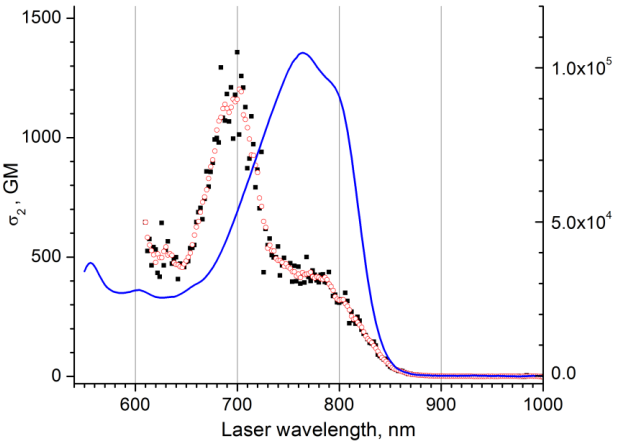

Figure 43: *The experimental two-photon absorption spectrum of **17** (black squares) with the wavelength-doubled absorption spectrum overlaid (blue). The red circles illustrate the fitted spectrum. Measured by Geoffrey Wicks.*

2.9 Caging Groups for Two-Photon Photoinduced Electron Transfer

Three photosensitisers which fulfil the criteria proposed in **Section 2.5** have been synthesised. In this section a number of caging/electron acceptor groups were synthesised and evaluated for a two-photon photoinduced electron transfer system.

2.9.1 The Phenacyl Group

As an extensively studied caging group with significant precedent as a photolabile protecting group for biologically active molecules, the phenacyl group was considered important to investigate in a two-photon PeT uncaging system. The position and nature of the covalent link between the photosensitiser/donor and the phenacyl group will have a significant impact on its properties. An electron withdrawing linker, such as an ester, will undoubtedly reduce the reduction potential of the phenacyl group, while an electron donating group will increase it. Based on literature precedent and commercially available starting materials, it was decided that both an ether and ester link in the *para* position would be investigated and as such, the ester and ether reference compounds in **Figure 44** were synthesised.

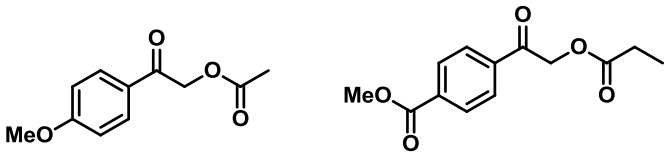

21 22

Figure 44: *The* para*-methoxy- and* para*-carboxymethyl-phenacyl reference compounds.*

The design of the reference compounds was chosen to mimic the final systems. As there is no electronic conjugation between the photosensitiser and uncaging group, it is sufficient to imitate the connection simply by methylating the ether and ester group. The model caged compound was chosen to be a carboxylic acid as many biologically active compounds (amino acids for example) contain carboxylate groups. NMR was chosen as the means of monitoring uncaging and so simple acids (acetic acid and propanoic acid) were investigated.

The synthesis of **21** and **22** is shown in **Scheme 5**.

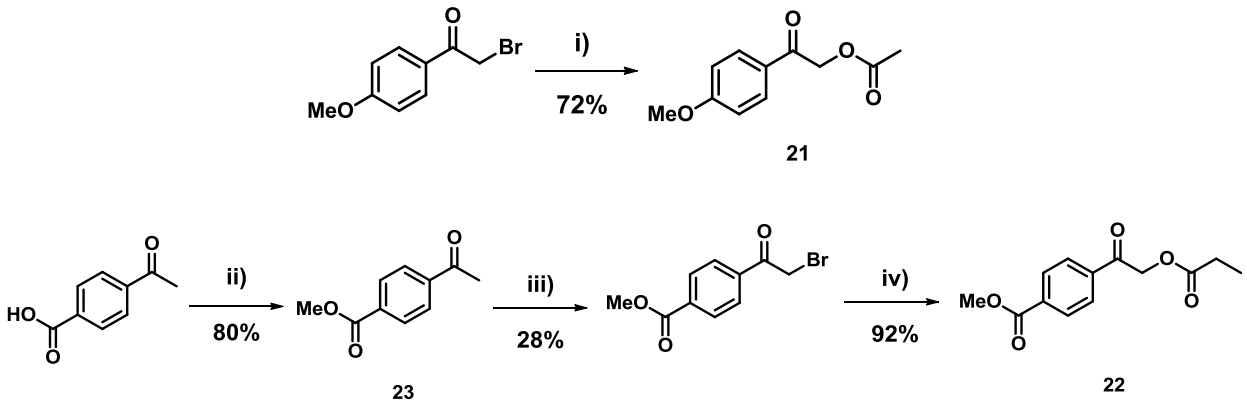

Scheme 5: *(i) Sodium acetate, EtOH, reflux, 3 h (ii) MeOH, conc. H_2SO_4, reflux, 8 h (iii) Br_2, AcOH, 0 °C, 30 mins (iv) propanoic acid, K_2CO_3, DMF, NaI, 90 °C, 2 h.*

Both reference compounds were synthesised in good yield. The bromination of **23** proved somewhat unreliable, though enough was isolated to complete the synthesis. Through investigation of the electrochemical and photophysical properties of these reference compounds, an insight was gained into their electron transfer characteristics and their suitability as acceptor/uncaging groups in conjunction with the photosensitisers identified in **Section 2.8**. In addition, the effect of the linker on these properties was investigated.

Figure 45 shows the photophysical and electrochemical properties of both **21** and **22**.

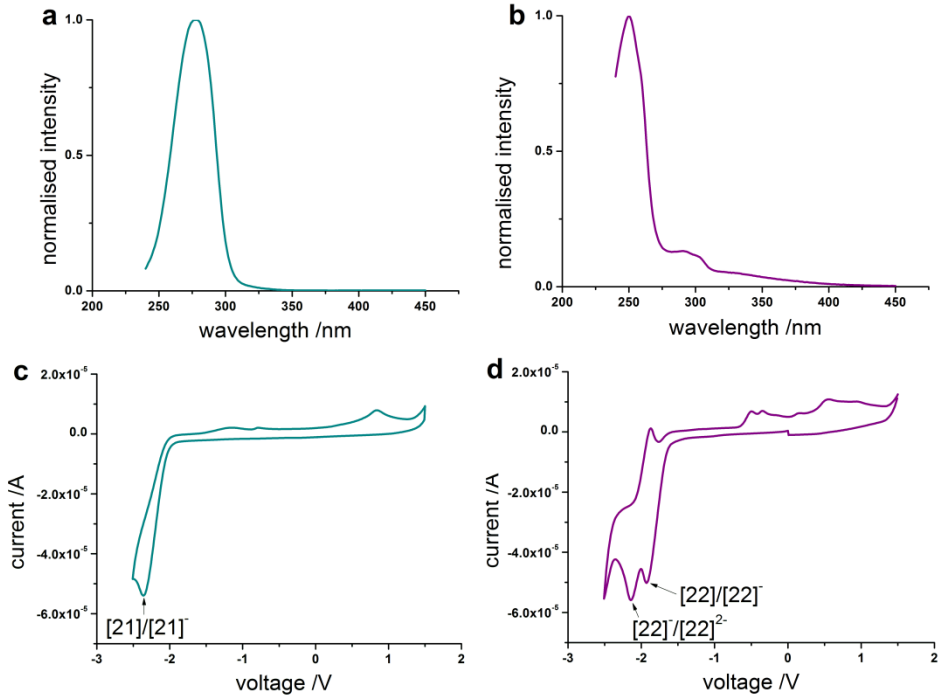

Figure 45: *The absorption spectra (THF) and cyclic voltammograms of **21** (a, c) and **22** (b, d) (THF, 0.1 M Bu_4NPF_6, 100 mV/s scan rate).*

There are some significant differences in the properties of these two compounds owing to their different linker groups. While the absorption spectrum of **21** has a red-shifted maximum when compared to **22**, its absorption extends to around 430 nm whereas the absorption of **21** does not extend beyond 350 nm (**Figure 46a**). This is the result of the increased conjugation of **22** caused by the carboxymethyl group.

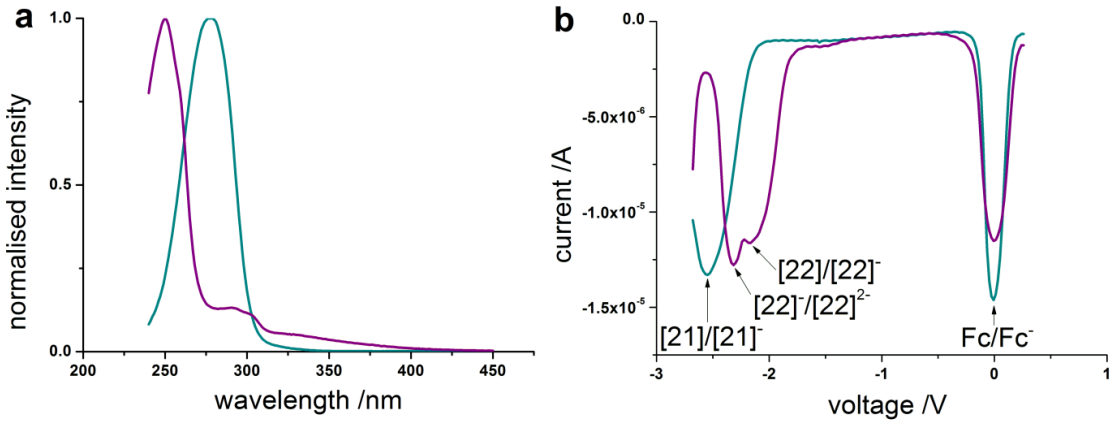

Figure 46: *(a) The absorption spectra of **21** (cyan) and **22** (purple) (b) the square-wave reduction of **21** (cyan) and **22** (purple) in THF relative to Fc/Fc^+ (0.1 M Bu_4NPF_6, 100 mV/s scan rate).*

Similarly, there are significant differences in the electrochemical properties (**Figure 46b**). While **21** has a single irreversible reduction at −2.74 eV, **22** exhibits two reductions, the first of which occurs at −2.24 eV and appears to be completely irreversible with the second at −2.39 eV, which is partially reversible. The carboxymethyl group has a clear effect here; the first reduction of **22** is easier than for **21** because of the relative electron-withdrawing nature of the carboxymethyl group compared to the methoxy group. The second reduction peak in the voltammogram of **22** is likely to be the reduction of the carboxymethyl linker group.

The irreversible nature of these reductions is not unexpected; it is the result of electrochemical uncaging during the experiment. At the point of reduction, an electron is transferred to the uncaging group, resulting in an uncaging event *via* the electron transfer mechanism. An irreversible process has occurred, so no peak is observed on the return to positive voltage. It should be possible to cycle the voltage rapidly enough that the reoxidation occurs before uncaging. This was attempted, however resolution was lost at high scan rates and so the results were inconclusive.

Both cyclic voltammograms in **Figure 45** were commenced at 0 V, cycled to −2.50 V then to +1.50 V and back to 0 V. The ill-defined peaks which occur in both voltammograms at more positive voltages than the reductions (on the return cycle) are the result of the products of uncaging. This was confirmed by commencing the cycle before those peaks, and sweeping to positive voltage first (**Figure 47**). The peaks did not appear in these experiments, so they must have been the result of the reduction.

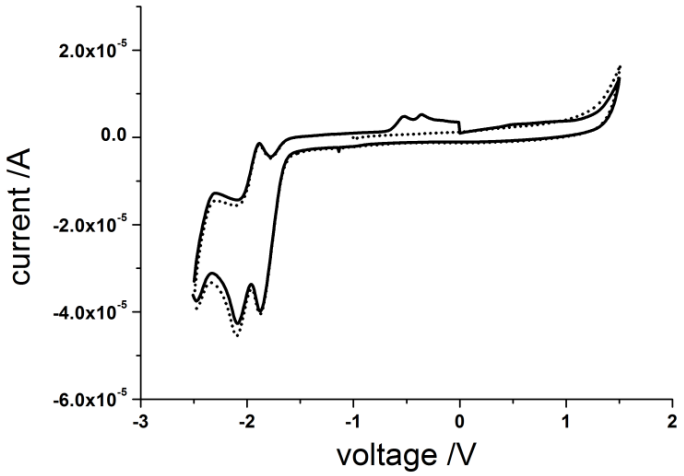

Figure 47: *Cyclic voltammograms of **22** commenced at 0 V (solid) and at −1 V (dotted).The ill-defined peaks between −0.8 and 0 V (solid) are not present in the voltammogram commenced at −1 V (dotted), demonstrating that they are the result of electrochemical reduction.*

An important consideration when evaluating caging groups for biological application is the physiological stability of the ester bond linking the caged compound to the caging group. It is likely that this bond will be hydrolysed under physiological conditions, so measuring the half-life of this hydrolysis is important. In order to evaluate the stability, a 1 mM solution of each reference caging group was made up in PBS at pD 7.4 in D_2O. Hydrolytic cleavage was monitored by ^1H NMR at 38 °C. **Figure 49** shows the change in integration of the signal indicated in **Figure 48** over time for compounds **21** and **22** relative to an internal standard (‘silicon grease’).

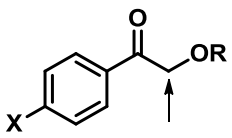

Figure 48: *An illustration of the NMR signal used to monitor hydrolysis. This signal was used as it appeared to mirror the increase in release of the corresponding carboxylic acid and was in a clear region of the spectrum.*

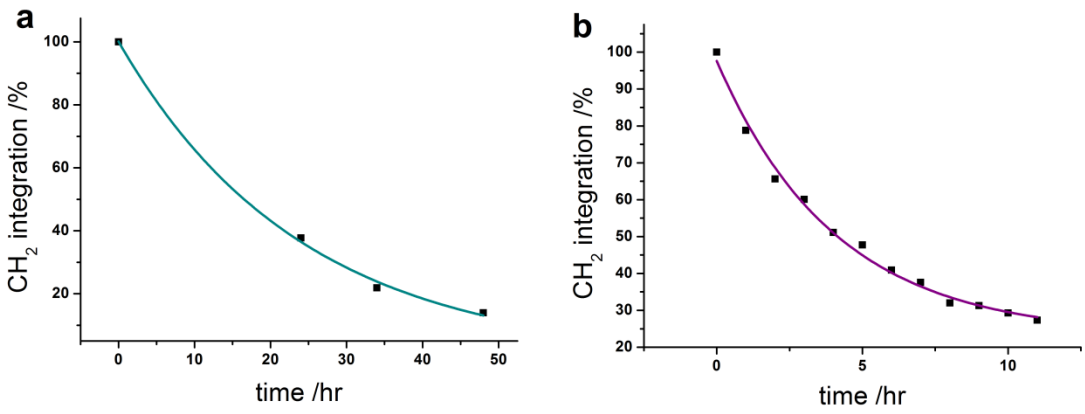

Figure 49: *(a) The ester hydrolysis of **21** and (b) the ester hydrolysis of **22** at pD 7.4 in PBS buffered D_2O at 38 °C.*

There is a large difference in the hydrolytic susceptibility of two compounds. Compound **21** has a hydrolytic half-life of 23 hours, while compound **22** has a half-life of just 4 hours. The electron-withdrawing nature of the carboxymethyl group must reduce the stability of the tetrahedral intermediate during hydrolysis compared to a methoxy group.

The Rehm-Weller equation (**Equation 5**) was used to assess the suitability of the phenacyl groups for a PeT system using **14** as a photosensitiser.

$$\Delta G_{eT} = (E_{OX} - E_{RED}) - E_{00} \qquad \textbf{Equation 5}$$

The data obtained from **Section 2.6.1** demonstrated that photosensitiser **14** has an oxidation potential (E_{OX}) of +0.55 eV and an excited state energy (E_{00}) of 2.99 eV. Thus, PeT between **14** and **22** (E_{RED} −2.24 eV) has a favourable free electron transfer (ΔG_{eT} −0.21 eV), while for **14** and **21** (E_{RED} −2.74 eV), PeT is not energetically favoured (ΔG_{eT} +0.29 eV). This suggests that an ester-linked phenacyl group is the most suitable candidate for an acceptor/uncaging group in a PeT system using **14**.

2.9.2 The *Ortho*-Nitrobenzyl Group

The following synthesis and photophysical evaluation was performed by Karolina Korzycka who was a first year DPhil student at the time of the research.

Two *ortho*-nitrobenzyl derivatives were investigated, mimicking an ester- and ether-linked system. As with the phenacyl group, the position of the linker groups will have an effect on the photophysics and electronics of the system. Based on commercially available starting materials, it was decided that the linker groups would be positioned *para* to the nitro group.

Scheme 6 shows the synthesis towards these two compounds.

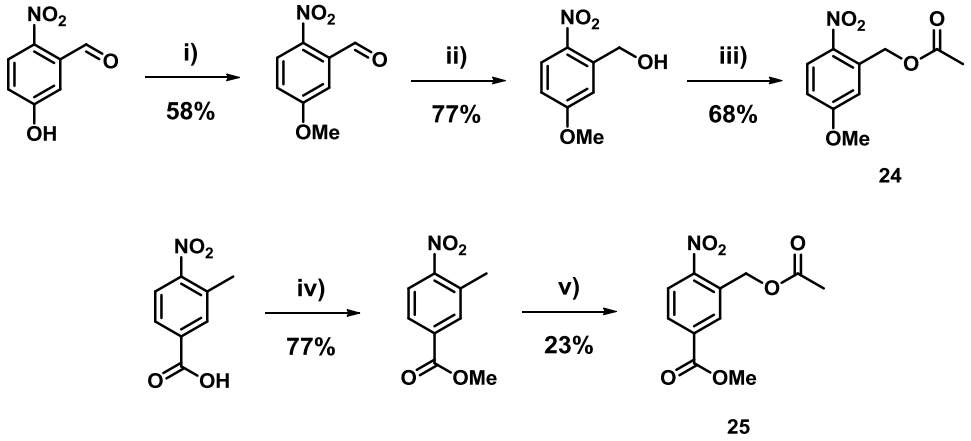

Scheme 6: *(i) Dimethylsulfate, NaOH, 50 °C, 48 h (ii) $NaBH_4$, 0 °C (iii) acetyl chloride, DMAP, 16 h (iv) conc. H_2SO_4, MeOH, reflux, 24 h (v)* N-*bromosuccinimide, benzoyl peroxide, CCl_4, 48 h, then sodium acetate, DMF, 70 °C, 24 h* .

The synthesis of compounds **24** and **25** was less straightforward than **21** and **22**, but reasonable yields were obtained. **Figure 50** shows the photophysical properties of **24** (cyan) and **25** (purple). The first reduction potentials of **24** and **25** are −1.80 V and −1.48 V respectively (in THF, relative to Fc/Fc^+), considerably less negative that the phenacyl groups.

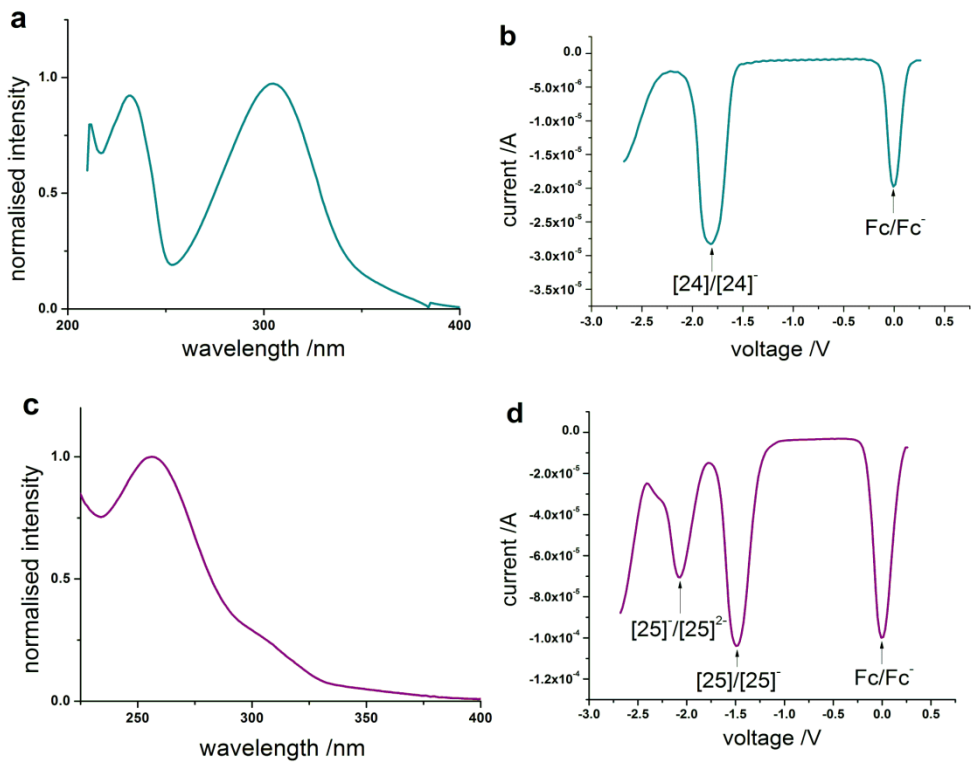

Figure 50: *(a) The absorption spectrum of **24** in THF and (b) its square-wave (c) the absorption spectrum of **25** and (d) its square-wave reduction. All electrochemistry was performed using Bu_4NPF_6 as an electrolyte (0.1 M) at 100 mV/s scan rate.*

Rehm-Weller analysis implied that PeT between **14** and both **24** and **25** is strongly favoured (ΔG_{eT} −0.71 eV and ΔG_{eT} −1.00 eV respectively) due to the relative ease with which both groups can be reduced. Both reductions were only partially reversible, suggesting that uncaging by electron transfer using these groups would be possible (**Figure 51**).

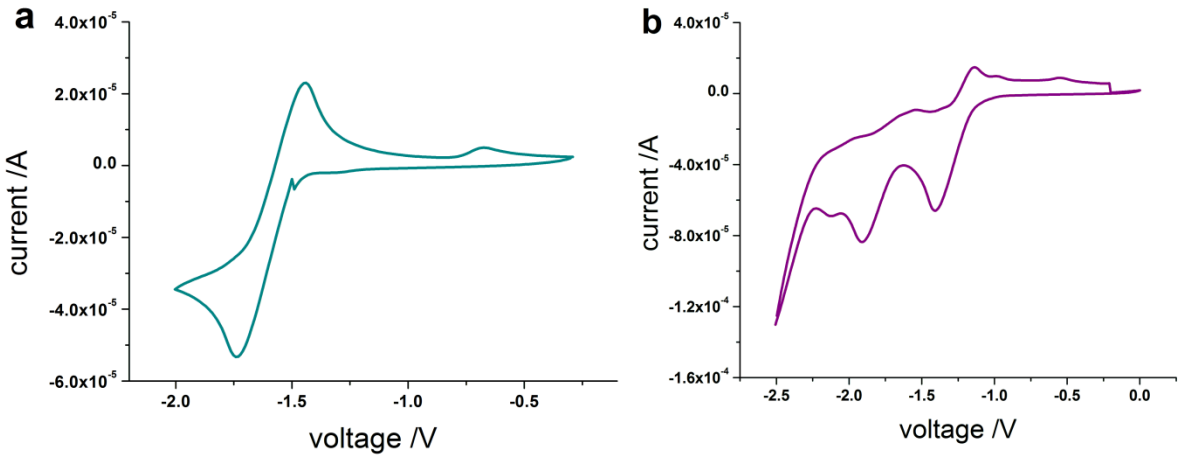

Figure 51: *Cyclic voltammograms showing the reductions of **24** (a) and **25** (b) in THF (0.1 M Bu_4NPF_6, 100 mV/s scan rate).*

Both compounds showed exceptional hydrolytic stability (>24 hours), though it should be noted that their poor water solubility meant that the final PBS (pD 7.4) solutions contained around 25% DMSO-d_6.

2.9.3 The Picolinium Group

The synthesis of the picolinium reference compound is shown in **Scheme 7**.

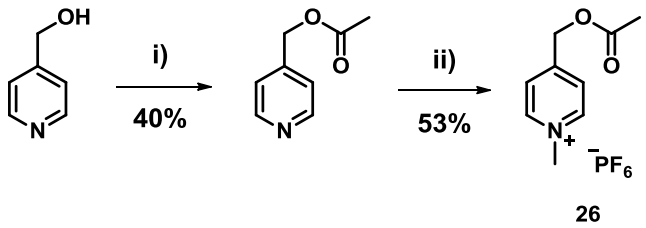

Scheme 7: *(i) Acyl chloride, Et_3N, 0 °C, 16 h (ii) MeI, rt, 16 h then precipitated using conc. ammonium hexafluorophosphate in methanol.*

Compound **26** was synthesised in moderate yield. The direct product of the methylation step is the iodide salt and the charge transfer between the iodide and the picolinium can be seen in the absorption spectrum (**Figure 52b**). The counter-ion was exchanged by precipitation with a concentrated solution of ammonium hexafluorophosphate, eliminating the charge transfer bands (**Figure 52a**).

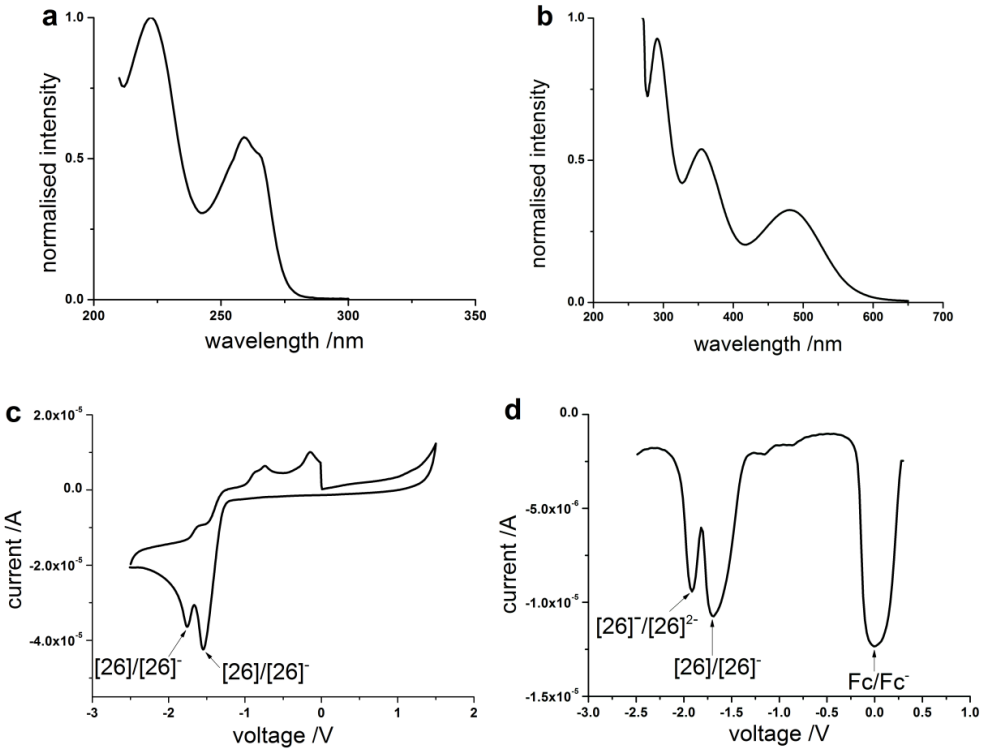

Figure 52: *(a) The absorption spectrum of **26** (cyan) in THF (b) the absorption spectrum* N*-methyl-4-picolinium acetate iodide (purple) in THF (c) the cyclic voltammogram of **26** in THF and (d) the square-wave reduction of **26** relative to* Fc/Fc^{+} *in THF. All electrochemistry was performed using* Bu_4NPF_6 *as an electrolyte (0.1 M) at 100 mV/s scan rate.*

Figures 55c & **d** show the cyclic and square wave voltammograms of **26** respectively. The familiar irreversible first reduction is present and occurs at −1.68 V, which is greater than 0.5 V more positive than the phenacyl groups under the same conditions. This results in a free energy of electron transfer for PeT between **14** and **26** of −0.83 eV, the second most favoured of the compounds measured here. **Figure 53** shows the hydrolytic stability of the picolinium salt. This caging group is the most stable to hydrolysis under the experimental conditions, with a half-life of approximately 40 hours.

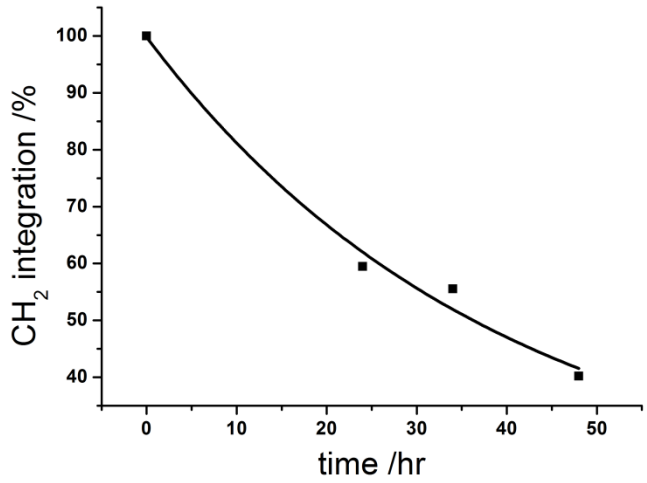

Figure 53: *Hydrolysis of **26** in PBS (D_2O, pD 7.4) at 38 °C.*

2.9.4 Summary of Donor and Acceptor Evaluation

Table 3 summarises the electrochemical and hydrolytic data gathered for the acceptor/uncaging groups. In addition, the free energies of electron transfer for PeT between each acceptor/uncaging group and **14** are presented.

Table 3: *Rehm-Weller analysis of the PeT donor-acceptor pairs and the corresponding hydrolytic half-life of the release group.*

	21	***22***	***24***	***25***	***26***
E_{RED}	−2.24 eV	−2.74 eV	−1.80 eV	−1.48 eV	−1.68 eV
Hyd. $t_{1/2}$	4 hr	23 hr	>24 hr	>24 hr	40 hr
ΔG_{eT}^{*}	−0.27 eV	+0.23 eV	−0.71 eV	−1.00 eV	−0.83 eV

The oxidation potential of donor/photosensitiser **14 used in these calculations was +0.55 eV and the excited state energy used was +3.06 eV.*

These data indicate that electron transfer between the acetylene-bonded anionic photosensitiser and all acceptor/uncaging groups except the ether-linked phenacyl group would be energetically favourable.

It is clear from these investigations that the most promising uncaging group is the picolinium acetate salt. Not only is the free energy of electron transfer predicted to be favoured, but the hydrolytic stability is also very high. Finally, the formal positive charge on the group should improve the water-solubility of the final system.

2.10 One-Photon Intermolecular PeT Uncaging

With a photosensitiser and several reference uncaging groups synthesised, it was possible to perform preliminary investigations into uncaging *via* PeT through intermolecular uncaging studies. In addition, these studies provided an opportunity to develop an experimental protocol.

It was proposed that the uncaging would be monitored by ^{1}H NMR. This provided a convenient technique to investigate, both qualitatively and quantitatively, the rate and products of irradiation.

The experimental procedure involved irradiating a 1 mM solution of the photosensitiser and uncaging group with a broad UV light source (300-400 nm)[123] in an NMR tube. A control sample, which contained the uncaging group at 1 mM concentration but no photosensitiser, was irradiated simultaneously. The uncaging experiments were performed in several solvents as the stability of the charge-separated state formed during electron transfer process is likely to be solvent dependent. An overview of these results is shown in **Table 4**.

Table 4: *An overview of the one-photon intermolecular PeT uncaging studies.*

Photosensitiser	***Uncaging group***	***Solvent***	***Evidence of uncaging?***	***Uncaging in control?***
14	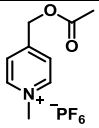 **26**	THF-d_8	Yes	No
		MeCN-d_3	-	-
		MeOH-d_4	-	-
14	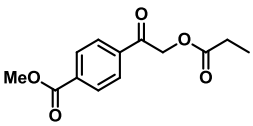 **21**	THF-d_8	Yes	Yes
		MeCN-d_3	Yes	Yes
		MeOH-d_4	No	Yes
14	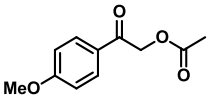 **22**	THF-d_8	No	Yes
		MeCN-d_3	No	No
		MeOH-d_4	No	No

Evidence of uncaging is defined as the presence of a signal relating to the corresponding free carboxylic acid whose integration increases over time.

For the phenacyl derivatives, it is difficult to draw solid conclusions. This is because the emission of the UV lamp overlaps with the absorption of the caging groups, so it is unclear whether uncaging was occurring by a direct irradiation mechanism or a PeT from the electron donor. However, these experiments still provided some useful information.

As Rehm-Weller analysis predicted PeT to be unfavourable, it was expected that no evidence of uncaging would be observed between **14** and **22**. That limited evidence of uncaging was observed even by irradiation of the phenacyl group alone is likely to be a result of poor overlap between the emission of the irradiation lamp and absorption of the uncaging group.

Irradiation of **21** in the presence of **14** exhibited uncaging in both THF and MeCN, while the control experiments also showed evidence of uncaging. Interestingly, in THF, uncaging in the control experiment progressed further in the same time compared to irradiation in the presence of the photosensitiser. A possible explanation for this is that most of (if not all) the uncaging is occurring by the direct irradiation mechanism rather than PeT. The superior absorption cross-section of the photosensitiser means it acts as a filter, preventing absorption by **21**. Unexpectedly, irradiation of **21** in the presence of **14** in methanol-d_4 resulted in little change in the NMR spectrum.

The clearest results were in the case of **26**. The absorption of this compound does not extend beyond 300 nm, which is outside the lamp emission range, ensuring that only the photosensitiser was absorbing during the irradiation. Therefore, any release of acetic acid observed must have occurred by means of a PeT from the **14** to **26**.

In THF-d_8, a decrease in the integration of the CH_2 signal alpha to the acetate ester ('b' in **Figure 54**) with a concurrent increase in integration at 1.9 ppm was observed. This peak was shown to be acetic acid by doping the final reaction mixture.

Figure 54 shows two spectra from a typical uncaging experiment between **14** and **26**. The upper spectrum is prior to irradiation and the lower is the final NMR from the uncaging, taken after 28 hours irradiation.

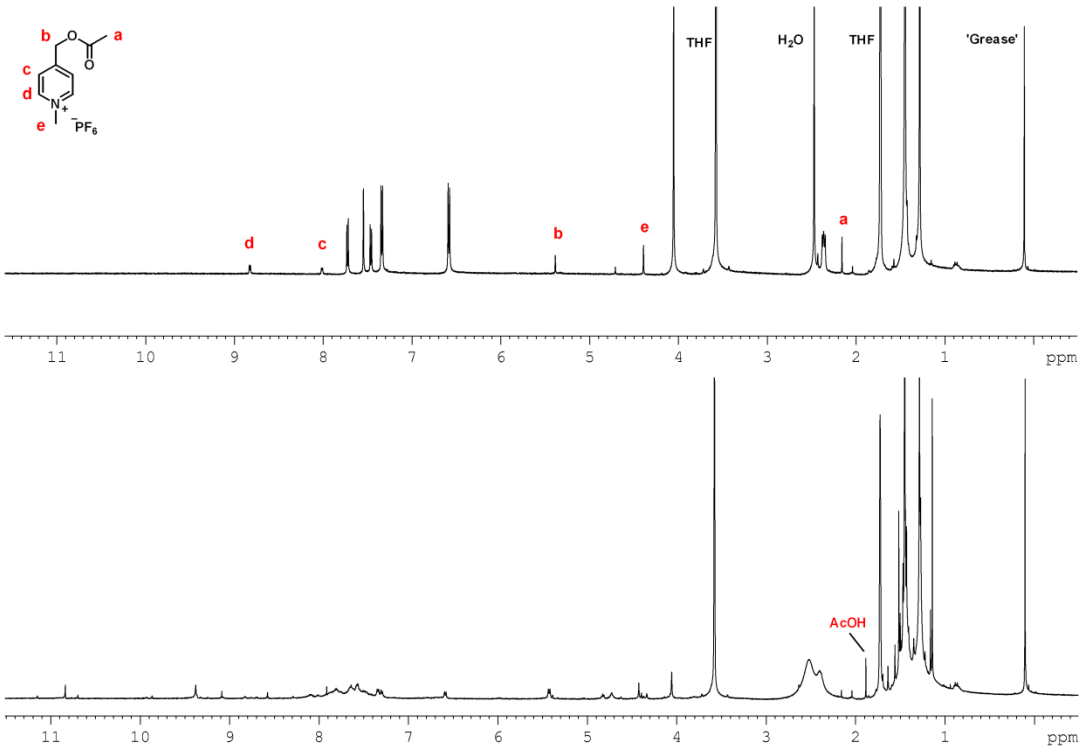

Figure 54: *^{1}H NMR spectra (500 MHz, THF-d_4) of an uncaging experiment between **14** and **26**, before irradiation (top) and after 28 hours irradiation (bottom) with a broad UV light source. The peaks not assigned are related to the photosensitiser.*

Here the disappearance of the singlet 'b' and the appearance of a singlet at 1.9 ppm (AcOH) are visible. Apart from these signals, it is difficult to determine the by-products of uncaging as the aromatic region is ill-defined.

The control experiment, in which no photosensitiser was present, showed no sign of a peak corresponding to acetic acid after the same irradiation time. **Figure 55** shows ^{1}H NMR spectra of the control experiment before irradiation and after 28 hours irradiation.

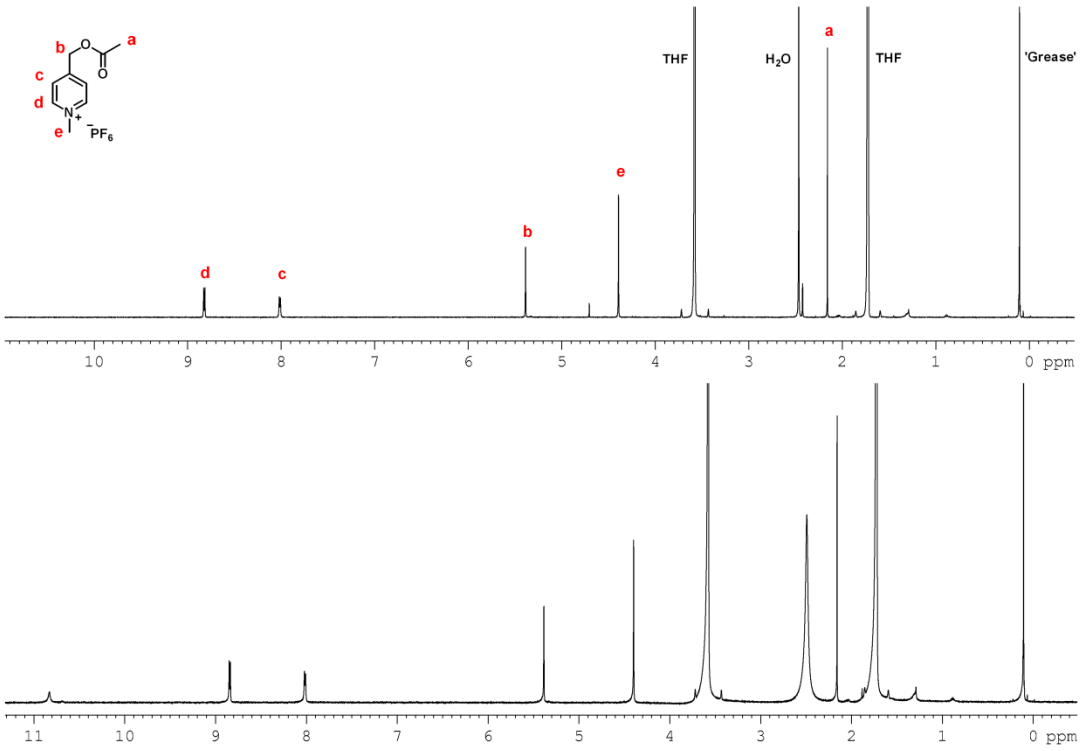

Figure 55: *^{1}H NMR spectra (500 MHz, THF-d_8) of a control experiment in which a 1 mM solution of **26** was irradiated simultaneously to the uncaging of **14** and **26**. The upper spectrum shows the experiment before irradiation, and the lower spectrum is after 28 hours irradiation.*

There are no significant new peaks in the spectrum and the change in integration of signal 'a' is only around 10%, which could be attributed to hydrolysis.

The peak at approximately 0.1 ppm corresponding to 'silicon grease' was used as an internal standard to investigate the rate and extent of uncaging. The relative integrations of the AcOH and 'b' to 'grease' over the period of irradiation were plotted against time in **Figure 56**.

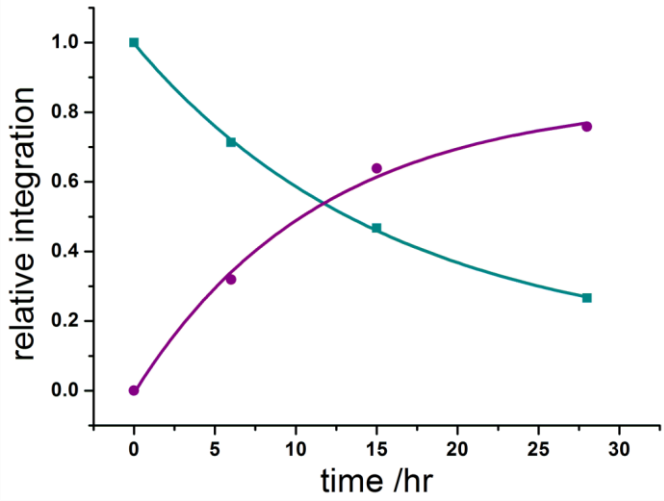

Figure 56: *Decay of 'b' (5.4 ppm) NMR signal (cyan) and concurrent release of acetic acid (1.9 ppm) (purple).*

Although the decay of the CH_2 signal is not necessarily direct evidence for uncaging, this signal was in a clear region of the spectrum and so was easier to analyse. In addition, it appeared to mirror the rising acetic acid signal.

The uncaging follows first order kinetics with a rate constant of 1.8×10^{-5} s^{-1}. After 28 hours of irradiation, the chemical yield of uncaging was around 70%. There is nothing to suggest that the uncaging would not have proceeded to completion, it was only time constraints that led to the termination of the experiment at this point. The uncaging took quite some time, but as the UV source was weak and the reaction was bimolecular this was not wholly unexpected.

This experiment served as a proof of principle, and demonstrated that the acetylene-bonded fluorene (**14**) and the *N*-methyl-4-picolinium acetate (**26**) uncaging group are a suitable donor-acceptor pair for uncaging *via* PeT. In addition, an experimental procedure was developed for uncaging which can identify whether uncaging has occurred, what products have resulted, and can quantify the rate and extent of that uncaging.

As a suitable system for uncaging had been identified, the photosensitiser/donor and uncaging/acceptor components could now be synthesised into a unimolecular system. In addition, the uncaging group was modified to cage a biologically active molecule.

2.11 Compounds for Intramolecular Uncaging

2.11.1 Anionic Compounds for Intramolecular Uncaging

This section documents the synthesis of a unimolecular system incorporating **14** and **26** (**Figure 57**). The system was designed to cage GABA.

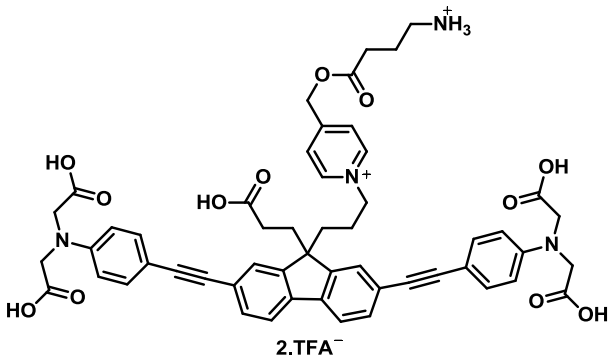

27

Figure 57: *An intramolecular two-photon PeT uncaging system incorporating **14** and **26**. The system is caging GABA.*

Compound **27** was synthesised according to the synthetic route in **Schemes 8** and **9**.

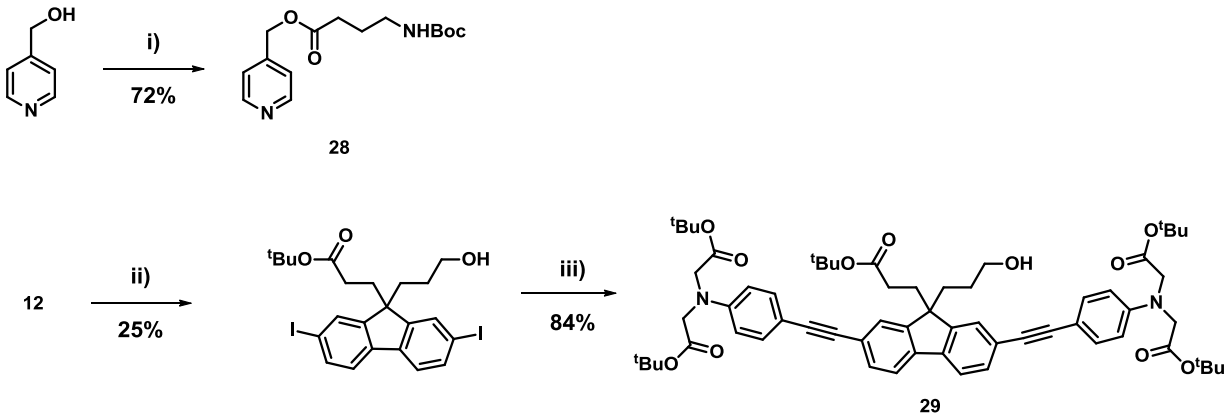

Scheme 8: *(i) Boc-GABA-OH, EDC, DMAP (ii) $LiAlH_4$, THF, 0 °C - rt (iii) $Pd(OAc)_2$, PPh_3, CuI, DIPA, rt, 2 h.*

The route towards the intramolecular uncaging system was initially analogous to the route towards **14**. When *in situ* deprotection of the acetylene was attempted, the Sonogashira reaction proceeded to completion, though the yield was poor. It was hypothesised that the TBAF deprotonates the alcohol group which can then react with the esters intramolecularly, reducing the product yield. To eliminate this possibility, the deprotection and Sonogashira cross-coupling were performed as separate steps.

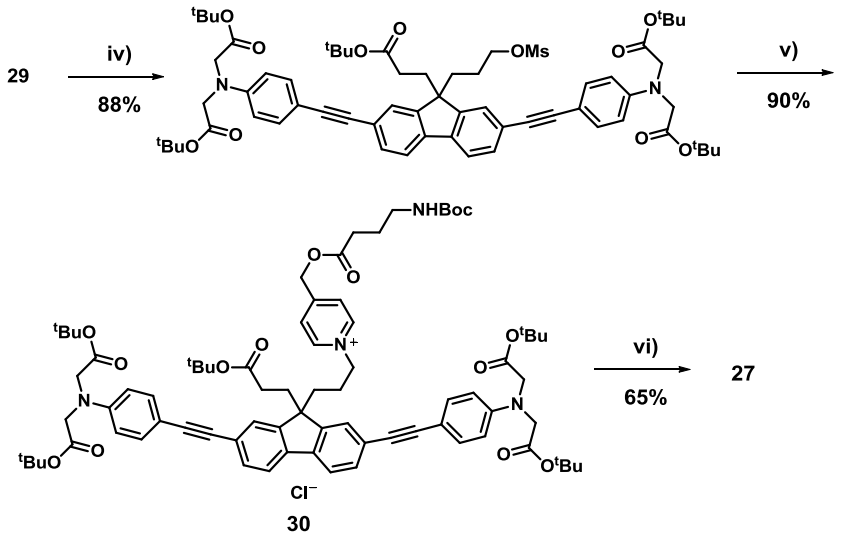

Scheme 9: *(iv) MsCl, Et_3N, 0 °C - rt (v)* ***28****, NaI (vi) $BF_3.Et_2O$, rt, 2 h.*

The synthesis towards compound **27** was generally high yielding and could be performed on scales above 100 mg. Purification of **30** by normal phase column chromatography proved difficult as the compound was sensitive to methanol. From purification by column chromatography using a mixture of chloroform and methanol, the presence of **30** could be confirmed by electrospray mass spectrometry of the column fractions. However, when these fractions were combined and the solvent evaporated, there was no sign of the product by mass spectrometry or any other analysis technique. Purification may have been possible by RP-HPLC or using an eluent mixture of chloroform and acetone, but instead the crude material was carried through to the next step.

The final deprotection step was initially attempted with trifluoroacetic acid in an analogous fashion to **14**. Unfortunately, this resulted in decomposition to many unidentifiable products. A fter attempting gentler acidic hydrolysis with formic acid and observing similar results, it became clear that the compound was highly sensitive to Brønsted acids. Previous research in the group had shown that Lewis acids such as boron trifluoride diethyl etherate ($BF_3.Et_2O$) could hydrolyse *tert*-butyl esters mildly and in the presence of pyridinium groups. This method proved successful and **27** was purified by semi-preparative reverse-phase HPLC in 65% yield.

Despite the increased steric bulk and polarity of the uncaging group, compound **27** displayed low solubility. Basic water (pH ~10) was the only solvent capable of dissolving the

compound, but the pyridinium group was sensitive to these conditions and decomposition occurred.

It was clear at this point that a biologically compatible uncaging system based on this photosensitiser would require different solubilising groups.

2.11.2 Neutral Compounds for Intramolecular Uncaging

Figure 58 shows the molecular design towards a two-photon PeT uncaging system for caging GABA, incorporating the neutral photosensitiser and uncaging group previously identified.

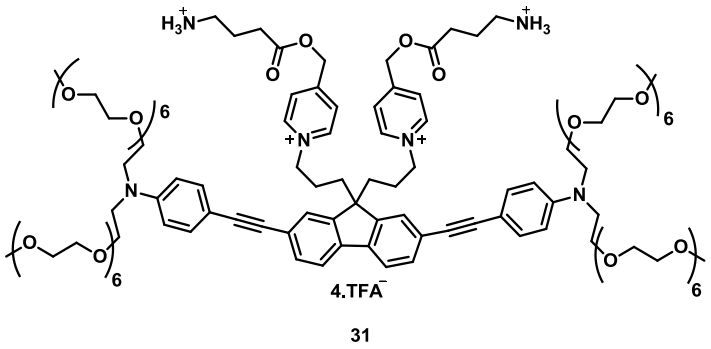

31

Figure 58: *The hexa-ethyleneglycol photosensitiser with two picolinium esters of GABA at the fluorene core.*

A convergent synthesis towards the product was designed in which the fluorene core was appended with the picolinium esters before conjugation with the substituted aniline units (**Scheme 10**).

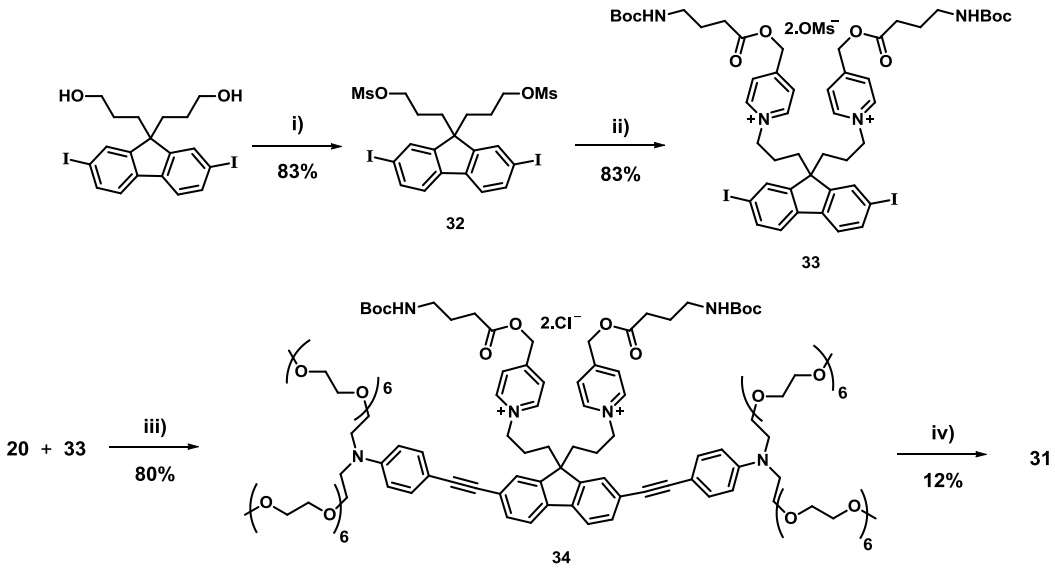

Scheme 10: *(i) MsCl, DCM, 0 °C - rt (ii)* ***28****, MeCN, reflux (iii) $Pd(OAc)_2$, PPh_3, CuI, DIPA, rt 2 h, (iv) BF_3. Et_2O, DCM, 0 °C - rt.*

Following alkylation of the fluorene core, the subsequent hydrolysis, reduction, mesylation, and attachment of the picolinium groups all proceeded in good yield with only recystallisation required for purification. Compounds **20** and **33** were coupled by means of Sonogashira cross-coupling cleanly and in high yield.

The final deprotection step required some modification from the synthesis of the anionic photosensitiser. Initially, a 10% solution of $BF_3.Et_2O$ in DCM was used as previously, and after around 15 minutes, reverse-phase HPLC showed that there was no starting material remaining and a more polar product had formed with the same absorption spectrum. Upon quenching with water and lyophilisation, the HPLC spectrum showed a single peak which had shifted to shorter retention time than before quenching and had an absorption spectrum blue-shifted by around 20 nm.

The reaction was repeated following a different procedure, which used twenty five equivalents of boron trifluoride per 'Boc' group. In addition, the reaction was quenched with saturated aqueous sodium bicarbonate to prevent the formation of a Brønsted acid. A product with the correct absorption spectrum was formed using this method, and **31** was isolated by reverse-phase HPLC in low yield. Compound **31** was characterised by ^1H NMR, HPLC, high-resolution ESI-MS+, electrochemistry, UV/visible spectroscopy and fluorescence spectroscopy.

It should be noted that if purification was performed without TFA as an additive, clean decomposition was observed by reverse-phase HPLC over around one hour. This is because, when the GABA amine is not protonated, it can cleave the ester bond which attaches GABA to the cage (**Figure 59**).

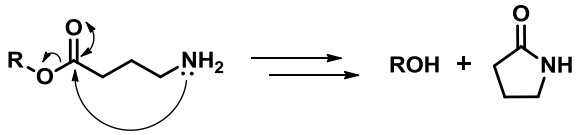

Figure 59: *The proposed intramolecular reaction of caged GABA when its amine group is not protonated.*

Compound **31** proved to be soluble in polar, non-polar and aqueous solvents, including water and PBS (pH 7.4) to 2-3 mM. Above this concentration, DMSO was the only suitable solvent.

In addition to synthesising **31**, attempts were made to synthesise a more general cage using a similar route (**Figure 60**).

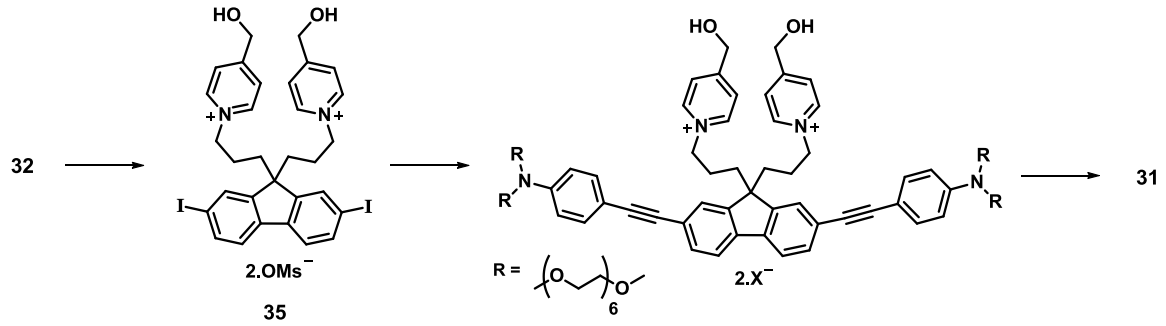

Figure 60: *The synthesis of a more general caging group based on the donor-acceptor pair.*

This route would be advantageous if the molecule being caged were precious, as the caged molecule is added at a later stage of the synthesis. However, the reaction to produce doubly-charged intermediate **35** proved to be highly unreliable and reproducible results could not be achieved.

Figure 61 shows the absorption, emission and electrochemical properties of compound **31**.

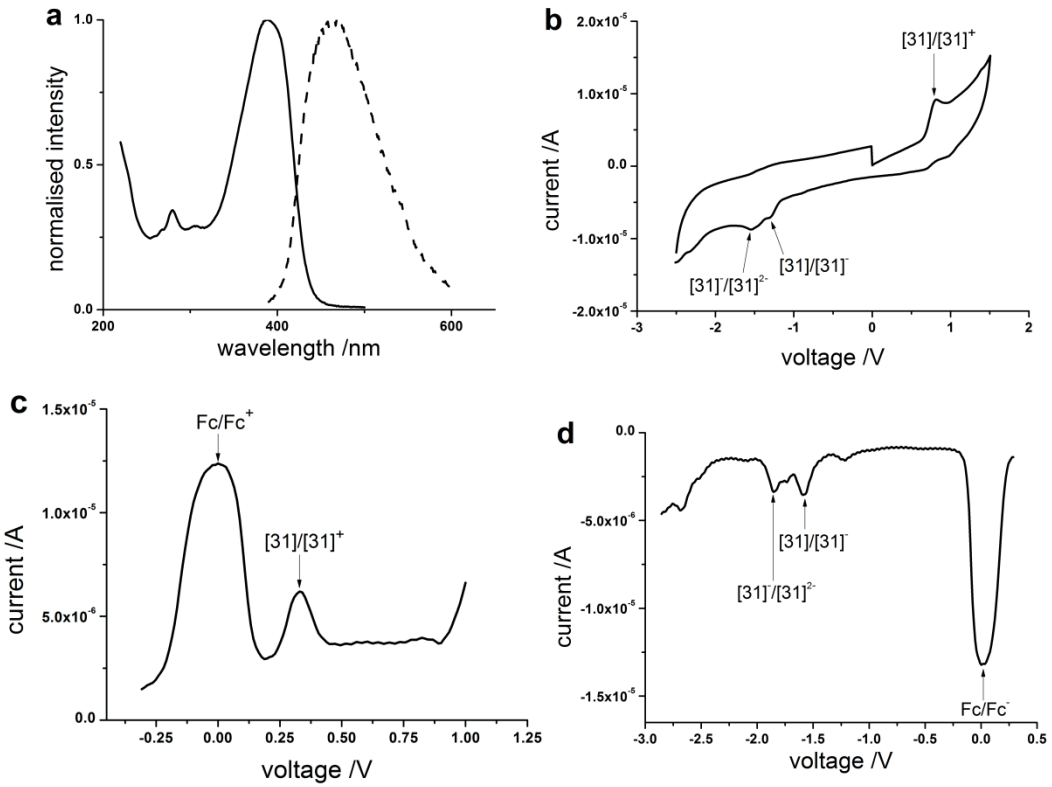

Figure 61: *(a) The absorption (solid) and emission (dashed) spectra in THF (b) the cyclic voltammogram (c) square-wave oxidation and (d) square-wave reduction of **31**. All electrochemistry was performed using Bu_4NPF_6 as an electrolyte (0.1 M) at 100 mV/s scan rate.*

The oxidation and reduction potentials of **31** (+0.33 eV and −1.59 eV respectively) correspond well with those of the individual components, **17** (+0.37 eV) and **26** (−1.68 eV). The absorption spectrum of **31** is essentially identical to that of the photosensitiser alone (**Figure 62**). When viewed on an extinction coefficient scale, it is easy to see how the absorption of **17** dwarfs that of **26**.

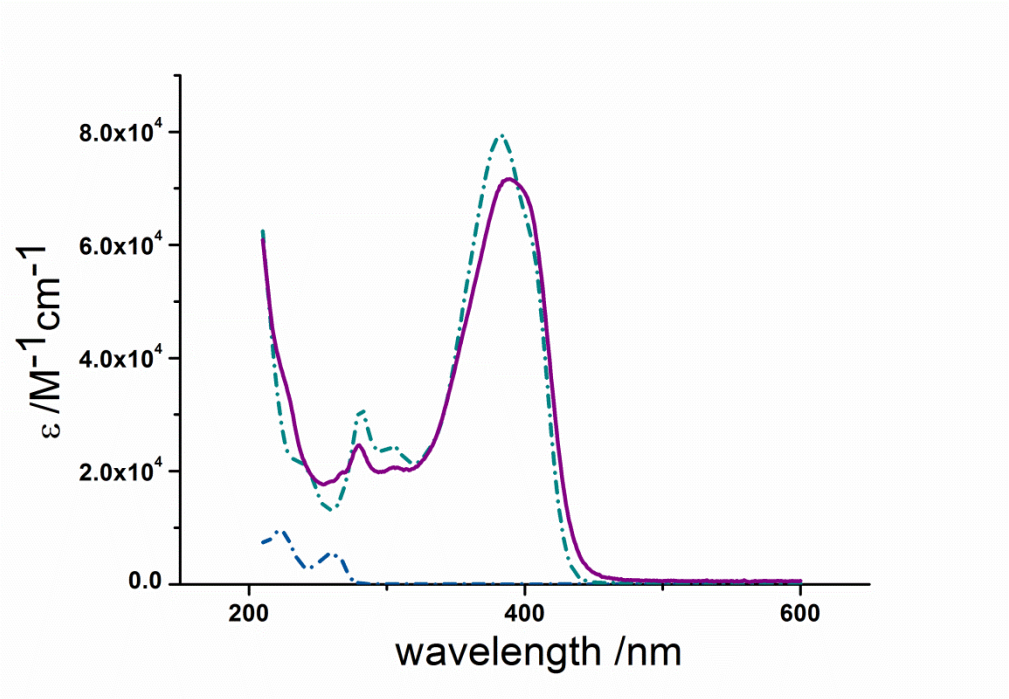

Figure 62: *The absorption spectra of **17** (cyan dashed), compound **30** (purple) **26** (blue dashed) on an extinction coefficient scale in water. The extinction coefficients of the compounds at λ_{max} are 79,000 (H_2O), 72,000 (H_2O), and 9,500 $M^{-1}cm^{-1}$(THF) respectively.*

The proximity of the two picolinium units to the photosensitiser almost completely quenches its fluorescence; compound **31** has a fluorescence quantum yield of 0.002 compared to 0.93 for **17**. This is to be expected if charge transfer between the donor and acceptor is occurring, and provides good evidence that PeT is taking place. Using this information and **Equation 6**, the quantum yield of charge transfer can be calculated.

$$\phi_{CT} = 1 - \frac{\phi_{f\ (linked\ system)}}{\phi_{f\ (parent\ dye)}} \qquad \textbf{Equation 6}$$

For **31**, the charge transfer quantum yield is 1, suggesting that essentially every excitation event leads to electron transfer to the picolinium group and thus the formation of the charge-separated state. The fate of this charge-separated state can be determined by investigation of the one-photon uncaging properties.

2.12 One-Photon Intramolecular Uncaging

The one-photon uncaging properties of **31** were investigated by NMR, building on the protocol developed in **Section 2.10**. Compound **31** was irradiated with a broad UV source (300-400 nm, peak 350 nm) in an NMR tube at 1 mM concentration. At this concentration, the transmittance of the solution is zero across the entire emission range of the light source.

One-photon uncaging using the conditions described demonstrated the release of GABA with a chemical yield of >95% (determined by NMR) (**Figure 63**).

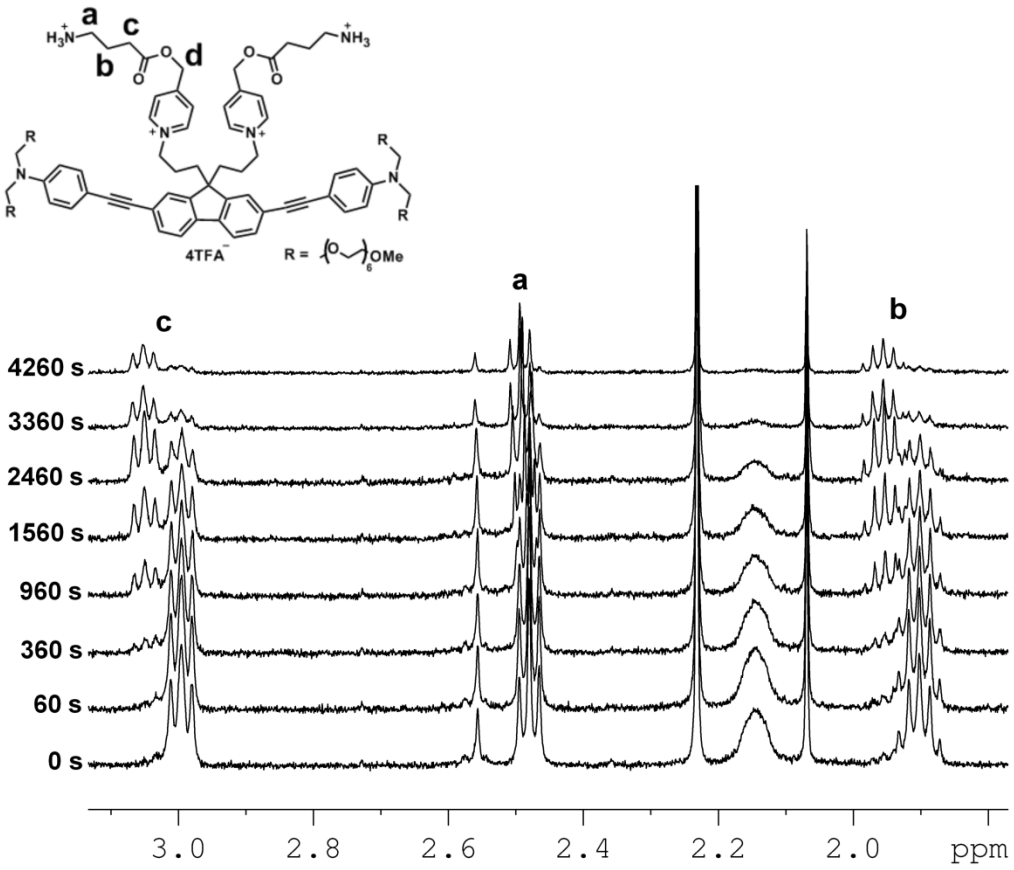

Figure 63: *^{1}H NMR spectra (500 MHz, D_2O) from a representative uncaging experiment which shows the disappearance of caged-GABA signals with a concurrent increase of a new set of multiplets later determined to be free GABA.*

The presence of uncaged GABA was confirmed by doping the irradiated solution with a genuine sample, which resulted in no new signals and an increase in the intensity of the suspected GABA signals (**Figure 64**).

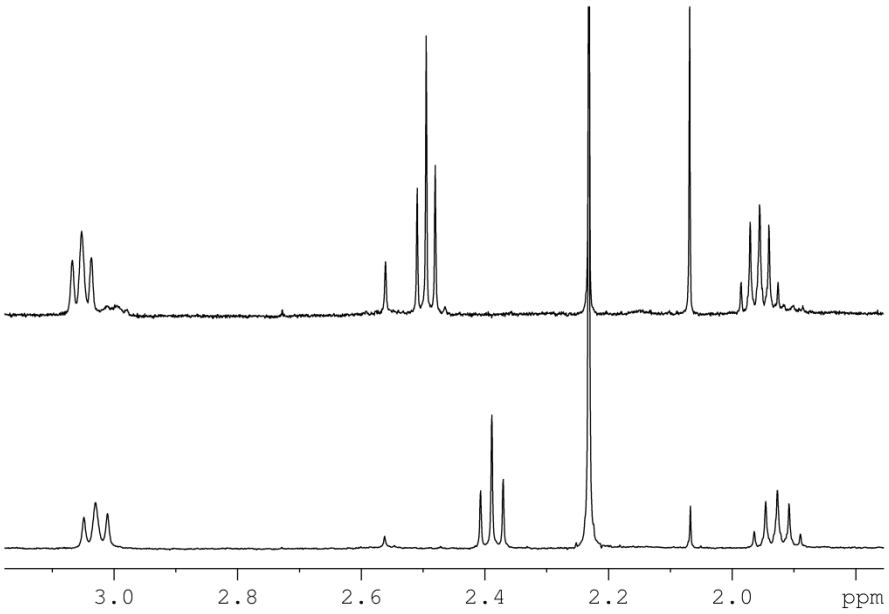

Figure 64: *A ^1H NMR spectrum (500 MHz, D_2O) of a completed uncaging experiment (top) and after the addition of one molar equivalent of GABA (400 MHz, D_2O) (bottom). The three multiplets of the suspected uncaged GABA approximately doubled in integration and no new peaks were observed in the region. The small shift in signal position is likely due to the differences in field strength and sample concentration between the two spectra.*

The GABA NMR signal at 'd' in **Figure 63** and uncaged GABA were integrated relative to an internal standard (*tert*-butanol) (**Figure 65**).

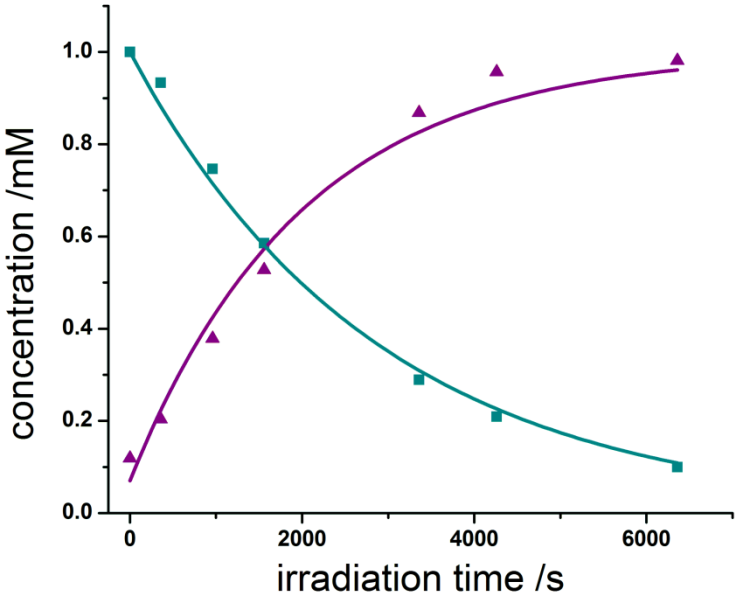

Figure 65: *Integration of CH_2 signal 'd' (cyan) and uncaged GABA (purple) relative to tert-butanol during irradiation.*

All uncaging experiments were fitted to an exponential curve of the general form y = A + Be^{Cx}, where 'C' is the rate of uncaging (k_u). Variable 'A' was fixed at 0 mM for decaying signals and 1 mM for rising signals. The gradients for the decay of signal 'd' and the rise of caged-GABA were 3.5×10^{-4} s^{-1} and 4.9×10^{-4} s^{-1} respectively. The close proximity of the caged- and uncaged-GABA signals at 'c' led to difficulty in obtaining a flat baseline for integration. The result of this was a translation of the decay of caged-GABA up the y-axis when integrating relative to *tert*-butanol (not shown) but a similar gradient (3.1×10^{-4} s^{-1}) was found. The signals in **Figure 65** mirrored each other well, and as no GABA intermediates were observed, subsequent analyses were performed using a constant total of GABA when integrating the caged and uncaged signals. An example of this analysis is shown in **Figure 66**.

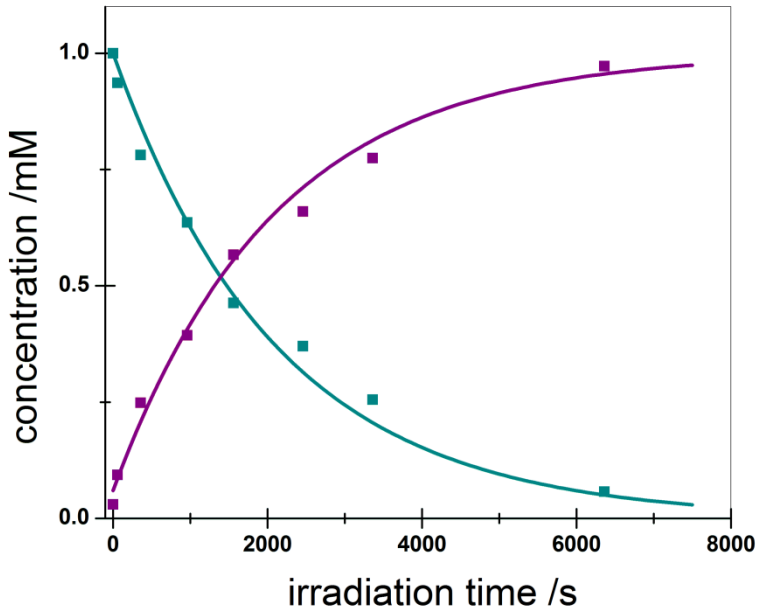

Figure 66: *The integration of signals 'c' (**Figure 63**) over time, using a constant total of GABA. The gradient of the exponential fit was 4.8×10^{-4} s^{-1}.*

Irradiation of **31** has been shown to result in the release of GABA, but the fate of photosensitiser is less clear as the aromatic region of the spectrum became weak and ill-defined (**Figure 67**).

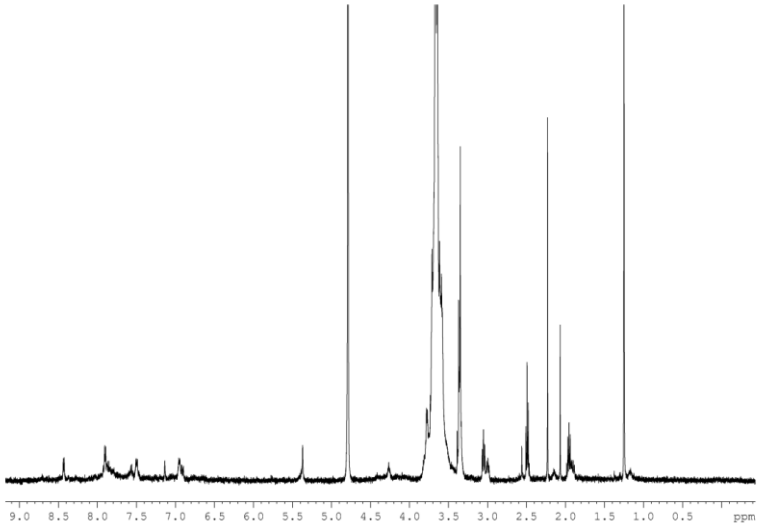

Figure 67: *A ^{1}H NMR spectrum (500 MHz, D_2O) of **31** during uncaging.*

No investigation into the mechanism of uncaging was performed. However, by combining the studies of Falvey *et al* into picolinium uncaging groups, and PeT uncaging using aniline-based donors, a mechanism similar to that in **Figure 68** might be expected.

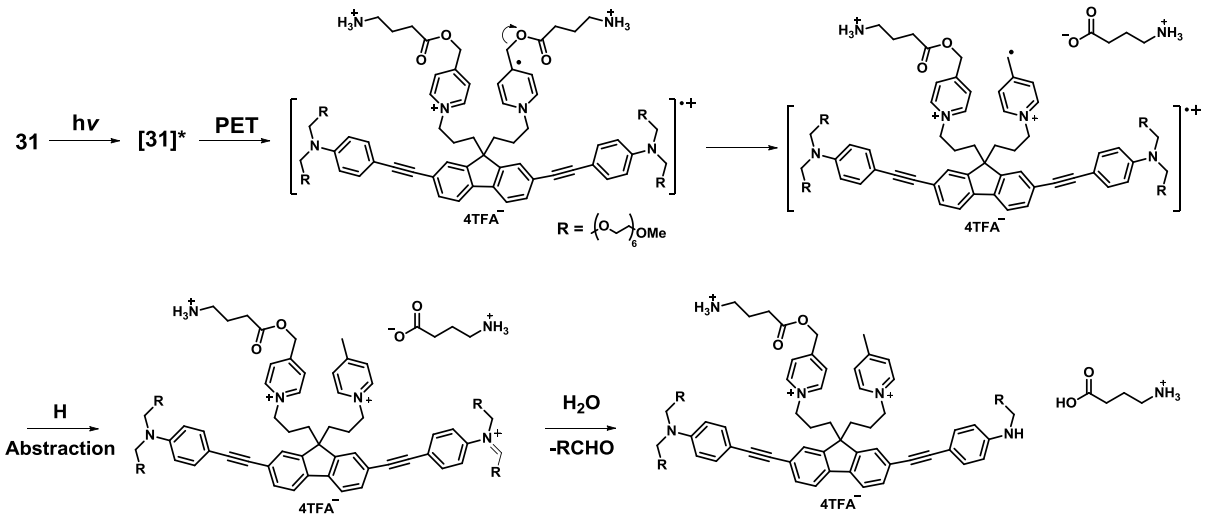

Figure 68: *The proposed uncaging mechanism of compound **31** in aqueous solution.*

Absorption of light leads to the formation of a photosensitiser-based singlet state, which is quenched by electron transfer to the picolinium uncaging group. The resulting pyridyl radical

releases GABA and the pyridinium ring re-aromatises. Radical quenching occurs by abstraction of a hydrogen atom from the position alpha to one of the aniline nitrogen atoms, and subsequent hydrolysis removes the solubilising group. The neutral photosensitiser is thus regenerated, and can undergo uncaging again to release the second GABA unit.

A product similar to that in **Figure 69** would be expected from the uncaging of both GABA compounds.

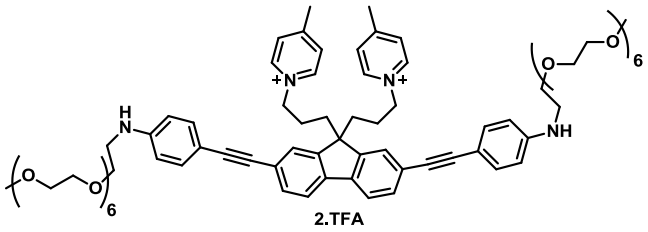

Figure 69: *The proposed product of uncaging based on observations by Falvey.*

Investigation into the fate of the photosensitiser yielded no definitive proof of a structure. As there is no obvious preference for which solubilising groups will be lost and rotation of the C-N bond is restricted by conjugation, there are several different products which can form, all with very similar NMR spectra.

The revere-phase HPLC trace from a typical uncaging reaction showed several products of similar polarity (**Figure 70**).

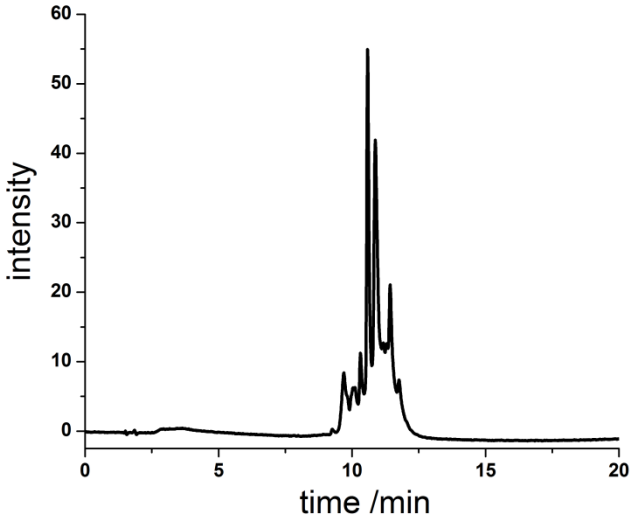

Figure 70: *A typical RP-HPLC trace (monitoring at 375 nm) of uncaged material. The two most intense peaks retain the absorption spectrum of the photosensitiser.*

The larger peaks all exhibited the same absorption profile as the photosensitiser, implying there is no loss of conjugation. In addition, solutions of the uncaged material showed no fluorescence, suggesting that the picolinium groups are still covalently linked. Mass spectrometry (MALDI-ToF) showed several signals within 100 m/z units of the mass of the compound in **Figure 69**, but isolation of the major products would be necessary to confirm a structure.

2.13 One-Photon Uncaging Quantum Yield

The quantum yield of uncaging of **31** was determined by comparison with the commercially-available compound, DPNI-GABA, which has a known uncaging quantum yield of 0.085 (**Figure 71**).[124]

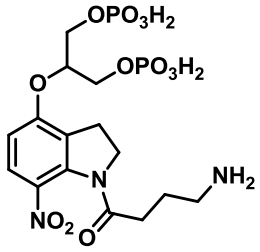

Figure 71: *The structure of DPNI-GABA.*

A solution of **31** and a solution of DPNI-GABA (1 mM, D_2O) were irradiated simultaneously using the same light source (300-400 nm, peak 350 nm). Despite the lower absorption coefficient of DPNI-GABA compared to **31** (4,000 $M^{-1}cm^{-1}$ and 35,000 $M^{-1}cm^{-1}$ at 350 nm respectively), at 1 mM concentration, there is zero transmittance through either solution. ^1H NMR analysis similar to that in **Figure 66** was used to determine their respective rates of uncaging (k_u) (**Figure 72**).

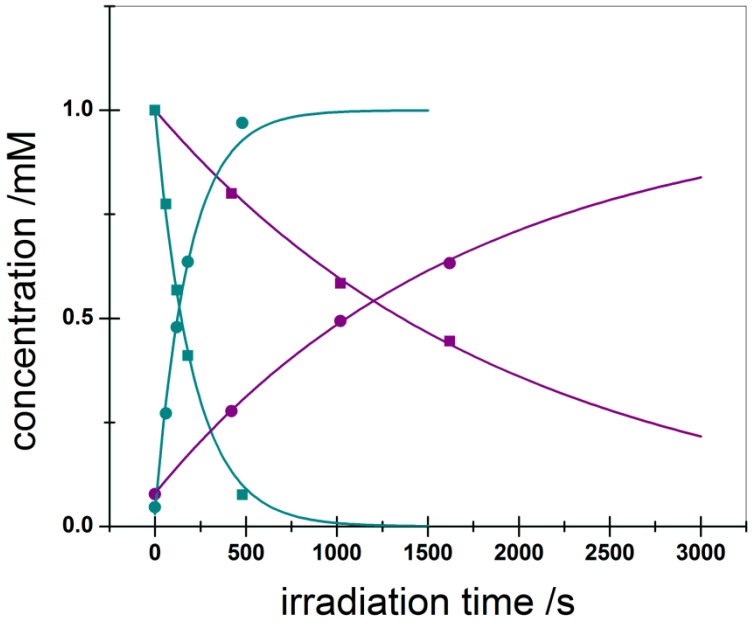

Figure 72: *The concentration of caged GABA over time during simultaneous irradiation of DPNI-GABA (cyan) and **31** (purple). Gradients of caged-GABA decay were 4.8×10^{-3} s^{-1} for DPNI-GABA (cyan, squares) and 5.1×10^{-4} s^{-1} for **31** (purple, squares), while gradients for GABA uncaging were 5.4×10^{-3} s^{-1} for DPNI-GABA (cyan, circles) and 5.4×10^{-4} s^{-1} for **31** (purple, circles).The rate of uncaging (k_u) was defined as the average of the two gradients.*

It is clear from the data in **Figure 72** that **31** uncages significantly more slowly than the commercial compound. The uncaging quantum yield of **31** was calculated relative to DPNI-GABA using the rates of uncaging of the two compounds (5.2×10^{-4} s^{-1} and 5.1×10^{-3} s^{-1} respectively) and **Equation 7**. When solved for compound **31**, it gives an uncaging quantum yield of 0.009 ± 0.003.

$$\phi_{u\,(\mathbf{31})} = 0.085\left(\frac{k_{u\,(\mathbf{31})}}{k_{u\,(DPNI-GABA)}}\right) \qquad \textbf{Equation 7}$$

The uncaging quantum yield was verified by ferrioxalate actinometry,[125] which determined the uncaging quantum yield for DPNI-GABA to be 0.088 ± 0.004 (in close accordance with the published value) and the quantum yield for **31** to be 0.009 ± 0.004.

With the data gathered it is possible to further understand the kinetics of the PeT system. It has been shown that the quantum yield of charge transfer is near unity, while the overall uncaging quantum yield is approximately 1%. This suggests that although formation of the charge-separated state is essentially certain, the rate of uncaging is much slower compared to the rate of back electron transfer.

Combining the quantum yield of uncaging with the measured two-photon absorption cross-section of the photosensitiser (1200 GM), results in a two-photon uncaging cross-section (δ_u) of 11 ± 3 GM at 700 nm. This is comparable to the highest reported value of δ_u by a conventional uncaging mechanism (11 GM)[20] and demonstrates a step forward in the design of two-photon caging groups.

Of the criteria proposed at the beginning of the chapter, several have already been fulfilled. It has been demonstrated that uncaging of a biologically active compound occurs and does so in aqueous media. The quantum yield is sub-optimal but the high two-photon absorption cross-section of the caging group overcomes this to give a two-photon uncaging cross-section comparable to the highest reported values.

2.14 Two-Photon Intramolecular Uncaging in a Biological System

At the time of submission, Dr Golnaz Borghei of the Paulsen group (Department of Physiology, University of Cambridge) was investigating the use of compound **31** as a tool for neurophysiology. Uncaging experiments under both a one- and two-photon regime were being investigated in cultured neurons, as well as a comparison of **31** with DPNI-GABA. The investigations up to the point of submission had not produced any conclusive results and so will not be discussed in this thesis.

2.15 Conclusions and Future Prospects

The research presented herein has resulted in the successful synthesis of a two-photon caging group with a two-photon uncaging cross-section which is comparable to the highest reported values. This was achieved by means of a two-photon photoinduced electron transfer between a photoexcited donor and an acceptor/release group; a mechanism not previously reported in the literature.

The advantages of this system are that the TPA cross-section of the photosensitiser and the uncaging quantum yield of the acceptor/release group can be optimised separately. A system was developed in which the TPA and formation of the charge-separated state are highly efficient. Subsequent decay of this state could be attributed to back electron transfer around 99% of the time. The system maintained a high two-photon uncaging cross-section due to its exceptional TPA properties.

An important aim of future research should be to investigate how changes in the free energy of electron transfer and the quantum yield of charge transfer affect the rate of uncaging. This

can most easily be achieved by changing the acceptor/uncaging group for those with higher/lower reduction potentials, or manipulating the electronics of the existing groups. Increasing the reduction potential of *N*-methyl-4-picolinium groups has been demonstrated by the inclusion of an electron withdrawing group (cyano) on the ring, which raises the reduction potential by approximately 0.5 eV.[126] This is a strategy which could be implemented for any of the acceptor/uncaging groups presented. An analogous approach could be used to reduce the favourability of the free energy of electron transfer, by including an electron donating groups (e.g. methoxy) to the acceptor/uncaging group. Alternatively, the position of the linker between the photosensitiser and the uncaging group could be changed. It is hard to predict whether increasing or decreasing the reduction potential will have the most beneficial effect. It could be argued that by reducing the energetic favourability of electron transfer, a more reactive radical is produced which will uncage faster. However, if electron transfer is poorly favoured energetically, it may not occur.

Another factor which would be interesting to investigate is the effect of rigidifying the link between the photosensitiser/donor and acceptor/release group on the rate of electron transfer. A rigid link should not only improve the efficiency of forward electron transfer but also prevent the possibility of the acceptor coming in close contact with the donor, eliminating back electron transfer by this mechanism. Spiro-cycloalkylfluorenes represent an interesting prospect for such a project,[127] and it may be possible to synthesise a compound such as the one shown in **Figure 73**.

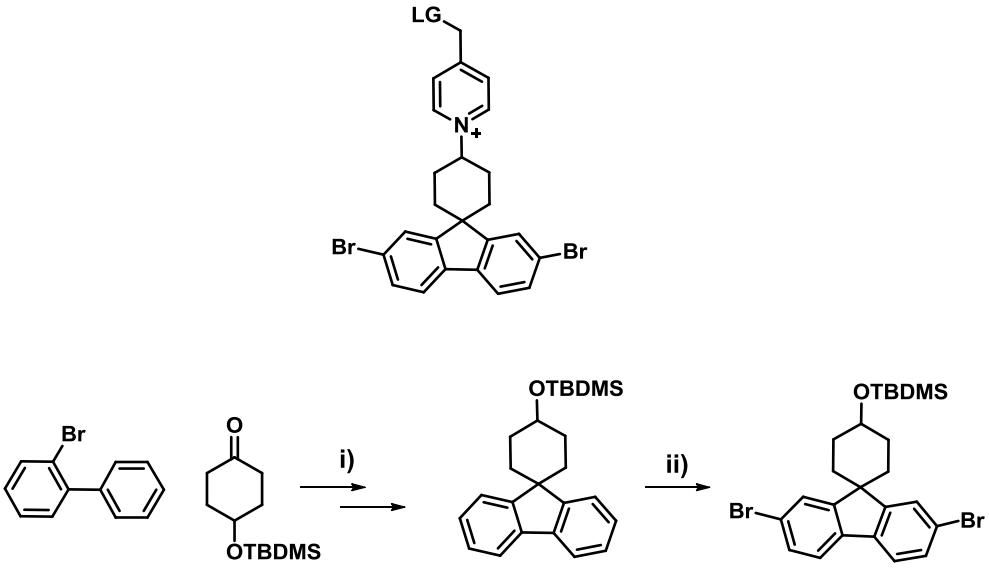

Figure 73: *Structure and proposed synthesis of the fluorene core for an* N*-methyl-4-picolinium ester caging group with a rigid linker; (i) n-BuLi, THF, then* p*-TsOH in benzene (ii)* Br_2, $FeCl_3$, $CHCl_3$.

Removal of the silyl protecting group and conversion of the subsequent alcohol to a good leaving group would produce a compound with which the *N*-methtyl-4-picolinium group could be reacted to produce an intermediate for Sonogashira cross-coupling with a substituted aniline.

The second aspect of this project that provides an opportunity for further development is the identity of the caged compound. Following discussion with neurophysiological collaborators, an obvious compound which would be synthetically easy to cage and would provide an interesting investigative tool is D-serine (**Figure 74**). There are some examples of caged D-serine in the literature,[128,129] and it is known to be a co-agonist of NMDA receptors with glutamate.[130] The significance of D-serine in the brain has only recently been realised,[131] and its role in neuron communication is far from fully explored. In particular, it is unknown whether D-serine can act as a neurotransmitter without the presence of a co-agonist. A caged form of the compound would be the perfect tool for such an investigation.

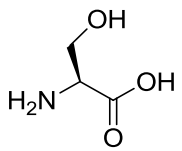

Figure 74: *D-serine.*

It is easy to see how this compound could be incorporated into a system such as the one described in this thesis. By protecting the alcohol side chain with an acid labile group, it could be deprotected in the final step of the synthesis.

For researchers interested in demonstrating synthetically complex cages in biological systems, receptors which respond to low agonist concentrations are an attractive prospect because synthesising large quantities of the cages can be problematic. However, in the brain, high affinity receptors often govern slow processes, so the advantages of releasing the agonist with high spatial and temporal control are less pronounced.

A recent study reported the caging and neurophysiological investigation of several less-commonly caged compounds (**Figure 75**).[132]

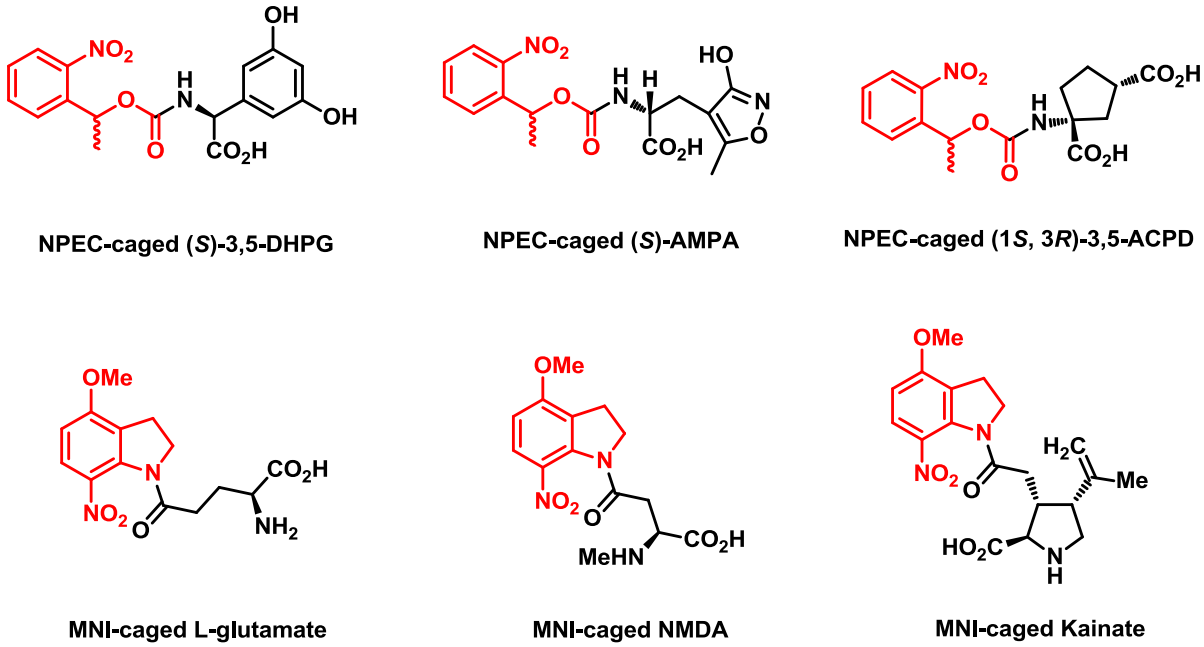

Figure 75: *A series of caged neuroactive compounds (caging groups are highlighted in red). Adapted from reference 132.*

From the perspective of developing the research discussed in this chapter, this study provides some useful information, as the optimum concentration required to give a physiological response was determined (**Table 5**)

Table 5: *The concentration of a selection of the caged compounds, as used during electrophysiological testing.*

Cage	MNI-kainate	MNI-NMDA	NPEC-AMPA	NPEC-DHPG	NPEC-ACPD
Conc.	100 µM	1 mM	200 µM	320 µM	1 mM

Kainate, AMPA and DHPG all produced a physiological response at sub-millimolar concentration, and would provide interesting means of demonstrating new cages. These compounds all contain carboxylic acids, which present an opportunity to cage them using the techniques described herein. The only complication is obtaining sufficient quantities of the compounds. Although all these compounds are available to purchase in their unprotected forms (excluding glutamate), they are very expensive (kainite, AMPA, DHPG and ACPD are £100-£300/10 mg). Alternatively, they could be synthesised as the synthetic procedures for most compounds are published.[133]

2.16 Experimental for Chapter 2

General Synthetic Procedures

All chemicals were purchased from Sigma-Aldrich or TCI Chemicals. DPNI-GABA was purchased from Tocris Biosciences. Dry acetonitrile (MeCN), tetrahydrofuran (THF) and dichloromethane (DCM) were obtained by passing the solvent through activated alumina. Diisopropylamine (DIPA) and triethylamine (TEA) were distilled from CaH_2 under nitrogen before use. All other reagents were used as supplied by commercial agents.

NMR spectra were recorded at ambient probe temperature using either a Bruker DPX400 (400 MHz), Bruker AVANCE AV400 (400 MHz) with a ^{13}C cryoprobe, Bruker DRX500 or a Bruker AVII 500. Chemical shift values are denoted in δ values (ppm) relative to residual solvent peaks ($CDCl_3$, δ_H = 7.26, δ_C = 77.16; DMSO-d_6, δ_H = 2.50, δ_C = 39.51 CD_3CN-d_3 δ_H = 1.94), coupling constants (J) are quoted in Hertz (Hz). Low resolution ESI-MS was carried out on a Micromass LCT platform. UV-Vis spectra were recorded on a Perkin Elmer Lambda 20 UV-Vis spectrometer. Fluorescence spectra were recorded on an ISA Spex FluoroMax-2 spectrometer. Electrochemical measurements (both cyclic and square wave) were performed on an Autolab PGSTAT12 potentiostat/galvanostat with a glassy carbon working electrode, Pt counter electrode and $Ag/AgNO_3$ reference electrode at a scan rate of 100 mV/s. Solutions of the compounds being measured were made up in THF or DCM containing 0.1 M tetrabutylammonium hexafluorophosphate at approximately 1 mg/mL concentration.

HPLC analysis and separation were carried out on an Agilent 1100 system equipped with a G1315B diode array detector, a G1311A quaternary pump and a G1316A fraction collector. Analytical HPLC were carried out using C8 5 μm, 3.9 × 150 mm Eclipse XDB-C8 column (Agilent) using 1 mL min^{-1} flow and linear gradients at 40 °C. Semi-preparative HPLC was carried out using C8 5 μm, 10 × 250 mm Eclipse XDB-C8 column (Agilent) using 3 mL min^{-1} flow and stepwise gradient at 40 °C. The chromatographic separations were monitored in the range 190 nm–900 nm.

Method A

Time /min	H_2O (0.1% TFA)	MeCN (0.1% TFA)
0	10	90
30	0	100

Method B

Time /min	H_2O (0.1% TFA)	MeCN (0.1% TFA)
0	100	0
20	0	100

General Procedure for One-Photon Uncaging Experiments

One-photon uncaging experiments were performed using a Rayonet RMR-600 or Philips CLEO 15 W lamps (300-400 nm) to irradiate vigorously stirred solutions in Wilmad 5 mm thin wall 7" 300 MHz NMR tubes. The rates of uncaging were measured by irradiating solutions (D_2O) of the respective compounds in NMR tubes (1 mM) with vigorous stirring (**Figure 76**).

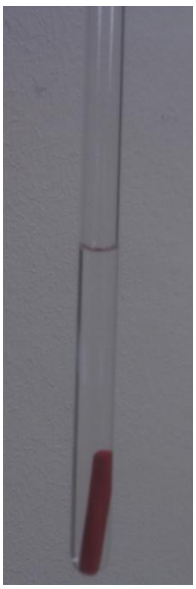

Figure 76: *A magnetic stirrer bar (red) in D_2O (0.5 mL) in an NMR tube. By placing the photolysis chamber on a magnetic stirrer, a satisfactory vortex could be created in the solution.*

At time intervals during the irradiation, the lamps were switched off and NMR spectra were measured on a Bruker AVII 500 MHz instrument. Following each measurement, irradiation and stirring were restarted. During transfer to and from the instrument, the samples were shielded from light.

General Procedure for Ferrioxalate Actinometry[125]

When exposed to light, potassium ferrioxalate ($K_3[Fe(C_2O_4)_3]$) decomposes as follows:

$$Fe(C_2O_4)_3^{3-} \xrightarrow{h\nu} Fe^{2+} + C_2O_4^{\bullet -} + 2C_2O_4^{2-}$$

$$Fe(C_2O_4)_3^{3-} + C_2O_4^{\bullet -} \xrightarrow{\Delta} Fe^{2+} + 2CO_2 + 3C_2O_4^{2-}$$

As the quantum yield of production of Fe^{2+} is well-known for a range of wavelengths (222 – 500 nm), it is possible to determine the photon flux irradiating a solution of ferrioxalate simply by measuring the amount of Fe^{2+} being produced. The quantity of Fe^{2+}formed during an irradiation period can be determined by complexing it with phenanthroline to form a coloured tris-phenanthroline complex (ε = 11,100 $M^{-1}cm^{-1}$ at λ_{MAX} = 510 nm), and measuring the absorption difference of two samples, with and without irradiation.

$$No.moles\ Fe(II) = \frac{V_1 V_3 \Delta A(510\ nm)}{10^3 V_2 l \varepsilon(510\ nm)}$$

where V_1(mL) is the irradiated volume, V_2 (mL) is the volume of the irradiated solution used for determining amount of Fe^{2+}, V_3 (mL) is the final volume after complexation with phenanthroline buffer, l (cm) is the optical pathlength of the quartz cuvette used for irradiation, ΔA (510 nm) is the difference in absorbance between the irradiated solution and that taken in the dark, and ε (510 nm) is the extinction coefficient of the complex ($Fe(phen)_3^{2+}$) at 510 nm.

The photon flux, *f*, irradiating the sample cell can then be determined:

$$f = \frac{moles\ Fe(II)}{(\Phi_\lambda t F)}$$

where Φ_λ is the quantum yield of Fe^{2+} production at the irradiation wavelength, *t* (s) is the irradiation time, and *F* is the fraction of light absorbed by the ferrioxalate solution. *F* was assumed to be 1, but can be calculated using the equation below:

$$F = (1 - 10^{-\varepsilon c l})$$

All procedures were carried out in the dark. A 0.006 M ferrioxalate solution was prepared by dissolving 600 mg of potassium ferrioxalate trihydrate ($K_3[Fe(C_2O_4)_3].3H_2O$) in 100 mL of 0.05 M H_2SO_4, while a 0.1% buffered phenanthroline solution was prepared by dissolving 22.5 g of $CH_3CO_2Na.3H_2O$ and 0.1 g of phenanthroline in 100 mL of 0.5 M H_2SO_4. 3 mL of this 0.006 M ferrioxalate solution was placed in a quartz cuvette and irradiated the Rayonet RMR-600 for 6 s, while an identical sample was kept in the dark. The irradiation time was chosen to ensure that no more than 10% of the ferrioxalate present in the solution was decomposed. 0.5 mL of the buffered phenanthroline solution was then added to each cuvette and their absorbance at 510 nm measured after 1 hour.

Synthesis of Charged Photosensitisers

4,4,5,5-tetramethyl-2-vinyl-1,3,2-dioxaboralane (10)

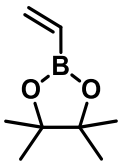

This compound was prepared according to a literature procedure.[134] To a stirred solution of trimethoxyborate (4.5 mL, 40 mmol) in dry ether (10 mL) cooled to −78 °C, was added vinylmagnesium bromide (50 mL of a 1.0 M solution, 50 mmol) dropwise over 1 h. The resulting suspension was stirred at room temperature for 1 h before the addition of hydrochloric acid (30% aqueous) and stirring for a further 30 mins. The reaction mixture was then extracted with ether, dried over sodium sulfate and concentrated to a small volume. This solution was added to a flask of dry ether (50 mL) with molecular sieves (5 g). Pinacol (7 g, 60 mmol) was added and the reaction stirred overnight under nitrogen at room temperature. The following day, the reaction mixture was filtered, concentrated and distilled under reduced pressure (45-48 °C, 6 mmHg) to afford a pungent, clear, colourless liquid (4.3 g, 70%); δ_H (400 MHz, $CDCl_3$) 1.26 (s, 8H), 6.62-5.80 (m, 2H); δ_C (125 MHz, $CDCl_3$) 24.7, 75.0, 83.3, 137.0; δ_B (160 MHz, $CDCl_3$) 29.7.

Di-tert-butyl 2,2'-((4-iodophenyl)azanediyl)diacetate

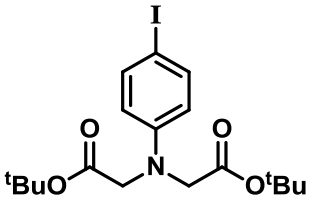

This novel compound was produced by adapting a reported procedure.[135] To a suspension of 4-iodoaniline (1.1 g, 4.6 mmol), sodium iodide (340 mg, 2.3 mmol) and sodium carbonate (2.4 g, 23 mmol) in anhydrous DMF (10 mL) was added *tert*-butylaminodiacetate (2.7 mL, 18 mmol). The reaction mixture was heated to 100 °C under nitrogen for 48 hours. The reaction mixture was poured into water (15 mL) and extracted with DCM (3 × 10 mL). The organic extractions were combined, washed with saturated sodium bicarbonate (3 × 10 mL) and brine (15 mL), dried over magnesium sulfate, filtered, and concentrated *in vacuo*. The product was purified by column chromatography (SiO_2 hexane:ethyl acetate 98:2) to yield the product as a white solid (640 mg, 31%); δ_H (400 MHz, $CDCl_3$) 1.46 (s, 18H), 3.97 (s, 4H), 6.36 (d, 2H), 7.45 (d, 2H); δ_C (125 MHz, $CDCl_3$) 28.0, 54.4, 79.2, 81.9, 114.5, 137.7, 147.7, 169.7.

(*E*)-di-*tert*-butyl 2,2'-((4-(2-(4,4,5,5-tetramethyl-1,3,2-dioxaborolan-2-yl)vinyl)phenyl)azanediyl)diacetate (11)

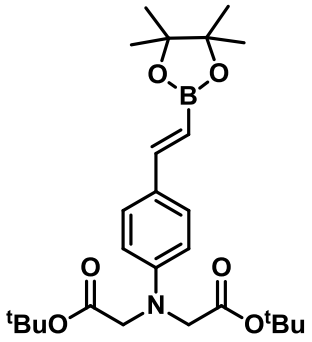

This novel compound was synthesised by adapting a reported procedure.[136] To an oven-dried Schlenk tube was added di-*tert*-butyl 2,2'-((4-iodophenyl)azanediyl)diacetate (1.0 g, 2.2 mmol), palladium(II) acetate (25 mg, 5.0 mol%), flame-dried silver(I) acetate (560 mg, 3.4 mmol), and tri-*ortho*-tolylphosphine (100 mg, 15 mol%). These solids were dried *in vacuo* for 15 mins before the addition of distilled tributylamine (0.5 mL), dry toluene (1 mL) and 4,4,5,5-tetramethyl-2-vinyl-1,3,2-dioxaboralane (520 mg, 3.4 mmol). The solution was

freeze-thaw degassed three times and then heated to 90 °C under nitrogen. After 2 h, the reaction mixture was cooled to room temperature, poured into brine and extracted with DCM (3 × 10 mL). The organic extractions were combined, dried over magnesium sulfate, filtered and the solvents removed *in vacuo*. Purification by column chromatography (SiO_2: DCM) afforded a brown oil (160 mg, 15%); δ_H (400 MHz, $CDCl_3$) 1.30 (s, 8H), 1.46 (s, 18H), 4.01, (s, 4H), 5.92 (d, 1H, *J* = 18.4 Hz, Olefin-*H*), 6.53 (d, 2H, *J* = 8.8 Hz, Ar-*H*), 7.29 (d, 1H, *J* = 18.4 Hz, Olefin-*H*), 7.36 (d, 2H, *J* = 8.8 Hz, Ar-*H*).

Di-*tert*-butyl 2,2'-((4-((trimethylsilyl)ethynyl)phenyl)azanediyl)diacetate (15)

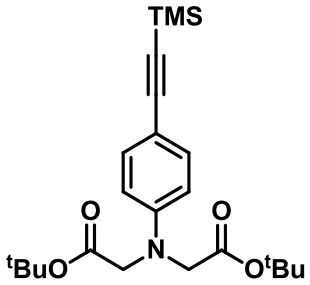

This novel compound was synthesised by adapting a reported procedure.[143] Di-*tert*-butyl 2,2'-((4-iodophenyl)azanediyl)diacetate (1.1 g, 2.2 mmol), palladium(II) diacetate (50 mg, 10 mol%), triphenylphosphine (120 mg, 0.45 mmol) and copper(I) iodide (30 mg, 0.20 mmol) were dried under vacuum in a pre-dried Schlenk tube. These reagents were dissolved in diisopropylamine (10 mL) and freeze-thaw degassed twice. Ethynyltrimethylsilane (950 µL, 6.7 mmol) was added *via* syringe and a final freeze-thaw degas cycle was performed. After stirring overnight at room temperature the reaction was poured into saturated aqueous ammonium chloride (15 mL) and extracted with DCM (3 × 10 mL). The combined organic extractions were washed with brine, dried over magnesium sulfate, filtered, and concentrated *in vacuo*. The product was purified by column chromatography (SiO_2: DCM) to afford a brown powder (550 mg, 59%); δ_H (400 MHz, $CDCl_3$) 0.23 (s, 9H), 1.45 (s, 18H), 4.00 (s, 4H), 6.46-6.51 (d, 2H), 7.30-7.35 (d, 2H); δ_C (125 MHz, $CDCl_3$) 0.0, 27.9, 54.3, 60.8, 81.8, 91.5, 105.8, 111.7, 133.0, 147.9, 169.6; *m/z* ESI-MS+ 418.22, $C_{23}H_{36}NO_4^+$ requires 418.24 (100%).

Di-*tert*-butyl 3,3'-(2,7-diiodo-9*H*-fluorene-9,9-diyl)dipropanoate (12)

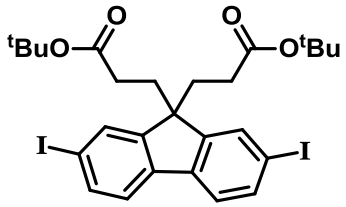

This compound was synthesised according to a literature procedure.[137] To a solution of 2,7-diiodofluorene (6.0 g, 14 mmol) in dry THF (300 mL) was added tetrabutylammonium fluoride (29 mL of a 1.0 M solution, 29 mmol) and the solution stirred for 5 minutes. The green solution became a deep red. Following this, *tert*-butylacrylate (8.3 mL, 57 mmol) was added and the reaction stirred at room temperature for 2 hr. Upon completion, the solvents were removed under reduced pressure and the product purified by column chromatography (SiO_2: 1:1 40-60 °C petrol ether:DCM) to give a white powder (7.3 g, 80%); δ_H (400 MHz, $CDCl_3$) 1.34 (s, 18H, ^{t}Bu), 1.44-1.49 (t, 4H), 2.27-2.31 (t, 4H), 7.40-7.43 (d, 2H), 7.68-7.70 (m, 3H); δ_C (125 MHz, $CDCl_3$) 28.0, 29.8, 34.3, 53.9, 80.4, 93.7, 121.7, 132.2, 136.9, 139.8, 149.9, 172.2; *m/z* ESI-MS- found 790.03, $C_{27}H_{32}I_2O_4$ requires 709.01 (100%).

***Tert*-butyl 3-(9-(3-hydroxypropyl)-2,7-diiodo-9*H*-fluoren-9-yl)propanoate**

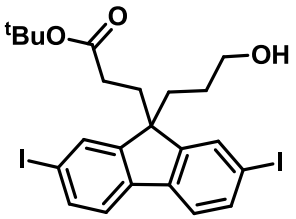

This novel compound was synthesised by adapting a literature procedure.[137] A pre-dried flask was charged with di-*tert*-butyl 3,3'-(2,7-diiodo-9*H*-fluorene-9,9-diyl)dipropanoate (1.0 g, 1.5 mmol) and dissolved in dry THF (100 mL). The solution was cooled to −78 °C in a dry ice/acetone bath after which, lithium aluminium hydride (590 µL of a 2.0 M solution in THF) was added dropwise *via* syringe. The reaction was stirred under nitrogen and allowed to warm to room temperature. TLC (98:2 DCM:MeOH) showed a mixture of starting material, mono-reduced and doubly-reduced material. The reaction was quenched with isopropanol, then methanol, then water and the aqueous layer extracted with DCM (3 × 10 mL). The organic extractions were combined, dried over magnesium sulfate, filtered and the solvents removed *in vacuo*. The crude material was purified by column chromatography (SiO_2: 99:1 DCM:methanol) to give a white crystalline solid (240 mg, 27%); δ_H (400 MHz, $CDCl_3$) 0.87 (m, 2H, C*H*$_2$), 1.06 (t, 1H, O*H*), 1.34 (s, 9H, O^t*Bu*), 1.48 (m, 2H, C*H*$_2$), 2.05 (m, 2H, C*H*$_2$), 2.28 (m, 2H, C*H*$_2$), 3.40 (m, 2H, C*H*$_2$), 7.42 (d, 2H, C*H*$_2$), 7.68-7.70 (m, 4H); δ_C (125 MHz,

$CDCl_3$) 27.0, 29.9, 34.3, 36.2, 54.3, 62.7, 62.8, 80.4, 93.6, 127.5, 132.1, 136.4, 136.7, 139.8, 150.7, 172.4; ESI-MS+ 627.03, $C_{23}H_{26}I_2O_3Na^+$ requires 626.99 (100%).

Tetra-*tert*-butyl 2,2',2'',2'''-((((1E,1'E)-(9-(3-(*tert*-butoxy)-3-oxopropyl)-9-(3-hydroxypropyl)-9*H*-fluorene-2,7-diyl)bis(ethene-2,1-diyl))bis(4,1-phenylene))bis(azanetriyl))tetraacetate (13)

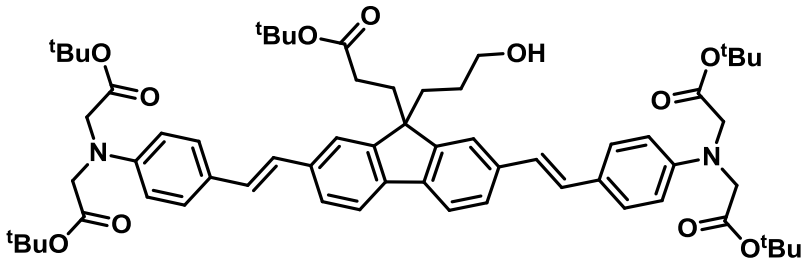

This novel compound was synthesised by adapting a reported procedure.[136] To an oven-dried Schlenk tube was added di-*tert*-butyl 3,3'-(2,7-diiodo-9*H*-fluorene-9,9-diyl)dipropanoate (116 mg, 192 µmol), tris(dibenzylidineacetone)dipalladium(0) (4.4 mg, 2.5 mol%), potassium *tert*-butoxide (32 mg, 290 µmol) and tri-*ortho*-tolylphosphine (6 mg, 10 mol%). These solids were dried *in vacuo* for 15 mins before the addition of dry THF (0.5 mL) and (*E*)-di-*tert*-butyl 2,2'-((4-(2-(4,4,5,5-tetramethyl-1,3,2-dioxaborolan-2-yl)vinyl)phenyl)azanediyl)diacetate (200 mg, 420 µmol) as a solution in dry THF (0.5 mL). The solution was freeze-thaw degassed three times and then heated to 67 °C under nitrogen. After 2 h, no starting material remained by TLC (98:2 DCM: ethyl acetate) and the mixture was poured into brine and extracted with DCM (3 × 10 mL). Following drying over magnesium sulfate, filtering and concentrating *in vacuo*, the final product was purified by column chromatography (SiO_2: 98:2 DCM:ethyl acetate) to give a tacky yellow solid (35 mg, 18%); δ_H (400 MHz, $CDCl_3$) 0.83-0.90 (m, CH_2), 1.30 (m, 12H, O^{t}Bu & CH_2), 1.48 (m, 39H, O^{t}Bu & CH_2), 2.15 (t, 2H, CH_2), 2.37 (t, 2H, CH_2), 3.38 (m, 2H, CH_2), 4.05 (s, 8H), 6.60 (d, 4H), 7.01 (d, 2H, J = 16.2 Hz, Olefin-CH_2), 7.08 (d, 2H, J = 16.2 Hz, Olefin-CH_2), 7.41-7.46 (m, 8H), 7.63 (d, 2H); δ_C (125 MHz, $CDCl_3$) 11.4, 14.0, 14.3, 18.7, 19.4, 20.4, 22.3, 22.6, 27.6, 27.7, 27.8, 27.9, 28.0, 28.1, 29.0, 29.7, 30.0, 31.2, 34.1, 36.0, 41.3, 54.5, 81.8, 112.4, 127.6, 170.0; *m/z* ESI-MS+ 1043.70, $C_{63}H_{82}N_2O_{11}$ requires 1042.59 (100%); λ_{max} ($CHCl_3$) 402 nm.

Tetra-*tert*-butyl 2,2',2'',2'''-((((9,9-bis(3-(*tert*-butoxy)-3-oxopropyl)-9*H*-fluorene-2,7-diyl)bis(ethyne-2,1-diyl))bis(4,1-phenylene))bis(azanetriyl))tetraacetate (14)

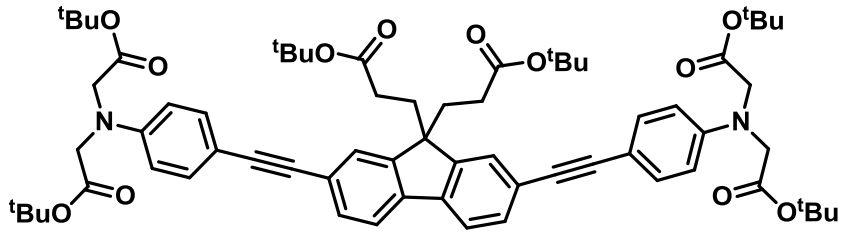

This novel compound was synthesised by adapting a reported procedure.[143] To an oven-dried Schlenk tube was added di-*tert*-butyl 3,3'-(2,7-diiodo-9*H*-fluorene-9,9-diyl)dipropanoate (100 mg, 290 µmol), palladium(II) diacetate (1.3 mg, 5.0 mol%), copper(I) iodide (1.1 mg, 5.0 mol%), triphenylphosphine (2.6 mg, 10 mol%) and di-*tert*-butyl 2,2'-((4-ethynylphenyl)azanediyl)diacetate (78 mg, 120 µmol). These solids were dried *in vacuo* for 15 mins before the addition of dry diisopropylamine (1.5 mL), freeze-thaw degassed three times and stirred at room temperature under nitrogen for 1 h. When no starting material remained by TLC (99:1 DCM:ethyl acetate) the mixture was poured into brine and extracted with DCM (3 × 10 mL). Following drying over magnesium sulfate, filtering and concentrating *in vacuo*, the crude product was purified by column chromatography (SiO_2 99:1 DCM:ethyl acetate) to give a yellow/orange solid (104 mg, 84%); δ_H (500 MHz, $CDCl_3$) 1.32 (s, 18H, O^{t}Bu), 1.47 (m, 41H, O^{t}Bu & CH_2), 2.35 (t, 4H, CH_2), 4.04 (s, 8H), 6.57 (d, 4H), 7.42 (d, 4H), 7.48-7.50 (m, 4H), 7.63 (d, 2H); δ_C (125 MHz, $CDCl_3$) 28.0, 28.0, 29.8, 34.5, 53.4, 54.4, 80.2, 82.0, 88.3, 91.1, 111.8, 172.5, 112.1, 120.0, 123.1, 125.8, 131.1, 132.8, 140.1, 148.0, 148.4, 169.7; λ_{max} (THF)/ nm (log ε) 274 (4.55), 377 (4.99); *m/z* 1131.61, $C_{67}H_{84}N_2O_{12}Na^+$ requires 1131.59 (100%).

2,2',2'',2'''-((((9,9-bis(2-carboxyethyl)-9*H*-fluorene-2,7-diyl)bis(ethyne-2,1-diyl))bis(4,1-phenylene))bis(azanetriyl))tetraacetic acid (9)

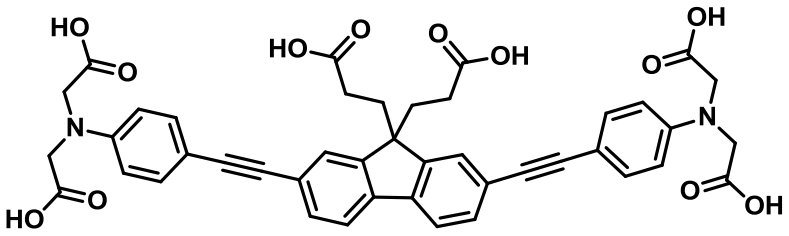

This novel compound was synthesised by adapting a reported procedure.[92] To a solution of tetra-*tert*-butyl 2,2',2",2"'-((((9,9-bis(3-(*tert*-butoxy)-3-oxopropyl)-9*H*-fluorene-2,7-diyl)bis(ethyne-2,1-diyl))bis(4,1-phenylene))bis(azanetriyl))tetraacetate (30 mg, 0.030 mmol) in chloroform (0.5 mL) was added dropwise trifluoroacetic acid (0.5 mL). The solution immediately became dark green. After stirring overnight, the solvents were removed *in vacuo* and traces of trifluoroacetic acid were removed by azeotroping with toluene (3 x 1 mL). A dark green powder resulted (20 mg, 86%); δ_H (500 MHz, $CDCl_3$) 1.38-1.33 (m, 4H), 2.26-2.23 (m, 4H), 3.94 (s, 8H), 6.55-6.54 (d, 4H), 7.20-7.28 (d, 2H), 7.36 (s, 2H), 7.68-7.69 (d, 2H), 7.93-7.95 (d, 4H); RP-HPLC (*Method B*) R_f 17.8 min.

Tetra-*tert*-butyl 2,2',2'',2'''-((((9-(3-(*tert*-butoxy)-3-oxopropyl)-9-(3-hydroxypropyl)-9*H*-fluorene-2,7-diyl)bis(ethyne-2,1-diyl))bis(4,1-phenylene))bis(azanetriyl))tetraacetate (29)

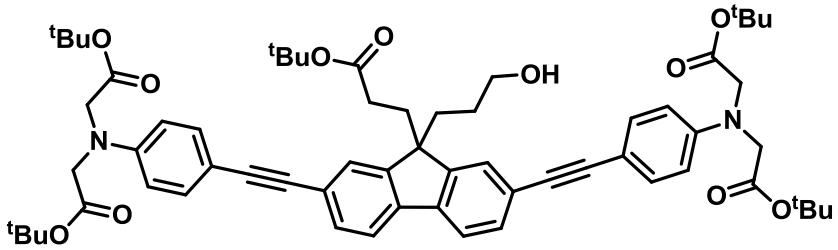

This novel compound was synthesised by adapting a reported procedure.[143] To an oven-dried Schlenk tube was added *tert*-butyl 3-(9-(3-hydroxypropyl)-2,7-diiodo-9*H*-fluoren-9-yl)propanoate (140 mg, 230 µmol), palladium(II) diacetate (2.6 mg, 5.0 mol%), copper(I) iodide (2.2 mg, 5.0 mol%), triphenylphosphine (6.0 mg, 10 mol%) and di-*tert*-butyl 2,2'-((4-((trimethylsilyl)ethynyl)phenyl)azanediyl)diacetate (240 mg, 570 µmol). These solids were dried *in vacuo* for 15 mins before the addition of dry diisopropylamine (2 mL), freeze-thaw degassing three times and stirring at room temperature under nitrogen for 1 h. When no starting material remained by TLC (99:1 DCM:ethyl acetate) the mixture was poured into

brine and extracted with DCM (3 × 10 mL). Following drying over magnesium sulfate, filtering, and concentrating *in vacuo*, the crude product was purified by column chromatography (SiO_2 99:1 DCM:ethyl acetate) to give a yellow/orange solid (74 mg, 84%); δ_H (400 MHz, $CDCl_3$) 1.32 (s, 18H, O^{t}Bu), 1.47 (m, 41H, O^{t}Bu & CH_2), 7.63 (d, 2H), 2.09-2.13 (t, 2H, CH_2), 2.31-2.36 (t, 4H, CH_2), 3.36-3.40 (q, 2H, CH_2), 4.04 (s, 8H), 6.57 (d, 4H), 7.42 (d, 4H), 7.48-7.50 (m, 4H); δ_C (125 MHz, $CDCl_3$) 27.2, 28.0, 28.0, 29.9, 34.5, 36.4, 53.9, 54.4, 60.8, 62.9, 80.1, 88.4, 91.0, 111.9, 112.0, 120.0, 123.0, 125.7, 130.9, 132.8, 140.7, 148.0, 149.2, 169.7, 172.7; λ_{max} (THF)/ nm (log ε) 274 (4.55), 377 (4.99); *m/z* ESI-MS+ 1039.62, $C_{63}H_{78}N_2O_{11}$ requires 1039.56 (100%).

Tetra-*tert*-butyl 2,2',2'',2'''-((((9-(3-(*tert*-butoxy)-3-oxopropyl)-9-(3-iodopropyl)-9*H*-fluorene-2,7-diyl)bis(ethyne-2,1-diyl))bis(4,1-phenylene))bis(azanetriyl))tetraacetate

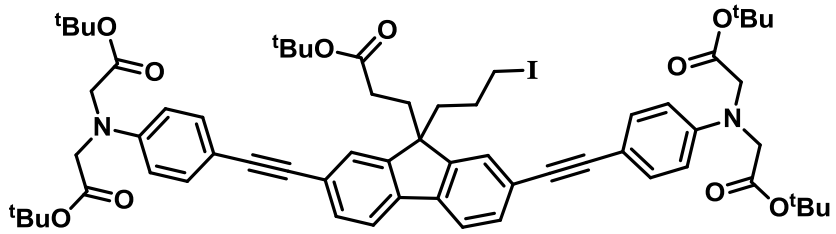

This novel compound was synthesised by adapting a reported procedure.[138] Tetra-*tert*-butyl 2,2',2",2'"-((((9-(3-(*tert*-butoxy)-3-oxopropyl)-9-(3-hydroxypropyl)-9*H*-fluorene-2,7-diyl)bis(ethyne-2,1-diyl))bis(4,1-phenylene))bis(azanetriyl))tetraacetate (60 mg, 0.060 mmol) was dissolved in dry DCM (2 mL) with triethylamine (25 µL, 0.20 mmol). The mixture was cooled in an ice/water bath and methanesulfonyl chloride (10 µL, 0.10 mmol) was added *via* syringe. After warming to room temperature, the reaction was stirred for 30 mins before quenching with saturated aqueous sodium bicarbonate and extracted with DCM (3 × 10 mL). The combined organic extractions were washed with brine, dried over magnesium sulfate, filtered and the solvent removed *in vacuo* to give a yellow solid (50 mg, 80%)

The crude residue was dried, dissolved in dry acetone (2 mL) with NaI (17 mg, 0.12 mmol) and heated at reflux for 2 h. When no starting material remained by TLC (99:1 DCM:methanol), the reaction mixture was poured into brine, washed with DCM (2 × 10 mL), dried over magnesium sulfate, filtered and dried *in vacuo* to give a yellow solid (36 mg, 55%); δ_H (400 MHz, $CDCl_3$) 1.11-1.14 (m, 2H), 1.25 (s, 9H), 1.47 (m, 38H), 2.30-2.34 (t, 2H), 2.80-2.92 (t, 2H), 4.03 (s, 8H), 4.13-4.14 (m, 2H), 6.55-6.57 (d, 4H), 7.41-7.50 (m, 8H), 7.64 (d, 2H).

1-(3-(2,7-bis((4-(bis(2-(*tert*-butoxy)-2-oxoethyl)amino)phenyl)ethynyl)-9-(3-(*tert*-butoxy)-3-oxopropyl)-9*H*-fluoren-9-yl)propyl)-4-(((4-((*tert*-butoxycarbonyl)amino)butanoyl)oxy)methyl)pyridin-1-ium (30)

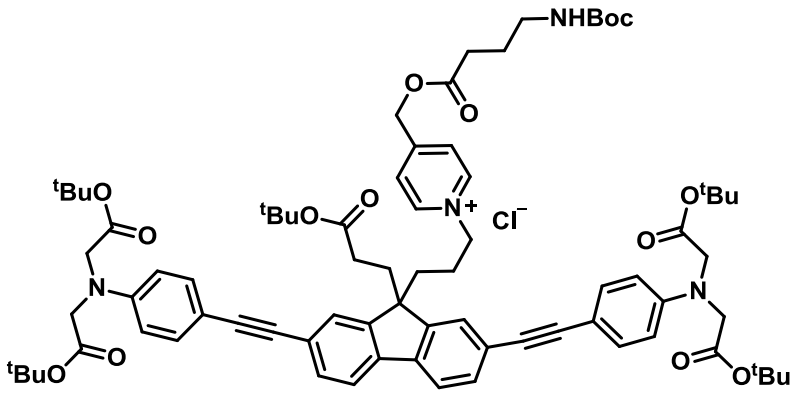

This novel compound was synthesised by adapting a reported procedure.[143] Tetra-*tert*-butyl 2,2',2",2"'-((((9-(3-(*tert*-butoxy)-3-oxopropyl)-9-(3-iodopropyl)-9*H*-fluorene-2,7-diyl)bis(ethyne-2,1-diyl))bis(4,1-phenylene))bis(azanetriyl))tetraacetate (100 mg, 0.10 mmol) and pyridin-4-ylmethyl 4-((*tert*-butoxycarbonyl)amino)butanoate (128 mg, 0.440 mmol) were dissolved in dry acetonitrile (2 mL) and heated to reflux. When no more starting material remained by HPLC (*Method A*) the reaction was cooled to room temperature and the solvents removed under reduced pressure. The crude material was dissolved in chloroform and washed with a semi-saturated aqueous ammonium chloride until a constant and reproducible absorption spectrum was observed. The organic layer was dried over magnesium sulfate, filtered and dried *in vacuo* to afford an orange/red solid (5 mg, 4%); δ_H (500 MHz, CD_3CN) 1.29 (s, 9H), 1.42 (s, 9H), 1.48, (s, 38H), 1.82-1.84 (m, 2H, GABA-CH_2), 2.43-2.46 (m, 2H, GABA-CH_2) 3.06-3.10 (m, 2H, GABA-CH_2), 4.07 (s, 8H), 5.15 (s, 2H), 6.62-6.64 (d, 4H, *J* = 8.6 Hz), 7.33-7.34 (d, 2H, *J* = 6.7 Hz), 7.41-7.43 (d, 2H, *J* = 8.6 Hz), 7.51-7.55 (m, 5H), 7.99-7.80 (d, 2H, *J* = 8.3 Hz), 7.87-7.88 (d, 2H, *J* = 6.7 Hz, Py-C*H*), 8.40-8.41 (d, 2H, *J* = 6.7 Hz, Py-C*H*), 8.54-8.56 (d, 2H, *J* = 8.6 Hz); δ_C (125 MHz, CD_3CN) 27.1, 27.3, 27.6, 27.7, 29.4, 29.8, 30.5, 30.8, 30.9, 79.7, 81.4, 88.1, 90.9, 110.9, 112.1, 112.6, 112.9, 120.4, 123.1, 125.4, 125.8, 131.1, 132.6, 140.2, 143.9, 148.5, 148.7, 169.5, 171.9, 172.7; λ_{max} (MeCN /nm) 272 (4.19), 374 (4.61); *m/z* ESI-MS+ 1315.72, $C_{78}H_{99}ClN_4O_{14}$ requires 1315.72 (100%).

Synthesis of Neutral Photosensitisers

2,5,8,11,14,17-hexaoxanonadecan-19-yl 4-methylbenzenesulfonate (18)

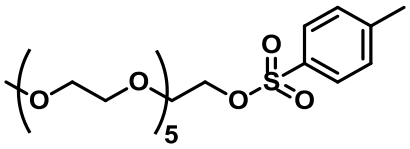

This compound was synthesised by adapting a literature procedure.[141] To a suspension of -*para*-toluenesulfonyl chloride (2.92 g, 15.0 mmol) in dry DCM (5 mL) at 0 °C was added a solution of hexa-ethyleneglycol monomethylether (3.5 g, 12 mmol) and distilled triethylamine (3.3 mL) in dry DCM (5 mL). The reaction was stirred at room temperature overnight. The reaction was quenched with cold water, extracted with DCM (2 × 10 mL) and ether (3 × 10 mL). The organic extractions were combined, dried over magnesium sulfate, filtered and concentrated *in vacuo* to yield a pale yellow oil (4.5 g, 84%); δ_H (400 MHz, $CDCl_3$) 2.20 (s, 3H), 3.11 (s, 3H), 3.27-3.44 (m, 22H), 3.90 (m, 2H), 7.12 (d, 2H), 7.53 (d, 2H); δ_C (125 MHz, $CDCl_3$) 21.7, 59.0, 68.7, 69.7, 70.6-70.7, 72.0, 128.1, 130.2, 133.3, 145.0; *m/z* ESI-MS+ 473.2, requires 473.2 (100%).

2,2'-(4-iodophenylazanediyl)diethanol

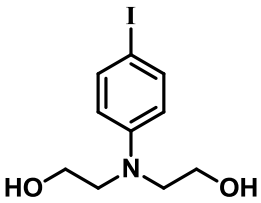

This compound was prepared according to the literature procedure.[207] *N,N'*-phenyldiethanoloamine (1.0 g, 5.5 mmol) was dissolved in dioxane and pyridine (1:1, 30 mL) and cooled to 0 °C in the ice bath. Iodine (4.20 g, 16.5 mmol) was added and the reaction was stirred for 1 h. After this time an additional portion of iodine was added (1.4 g, 5.5 mmol) and the ice bath was removed. The solution was left stirring for 3 h at room temperature. After this time a saturated aqueous solution of sodium thiosulfate (15 mL) was added and reaction mixture was extracted with ethyl acetate (20 mL). The organic phase was dried over magnesium sulfate and evaporated. The crude product was recrystallised from DCM/hexane to give the desired product as a white powder; (1.2 g, 70% yield); δ_H (400 MHz, $CDCl_3$) 3.41 (m, 4H), 3.53 (m, 4H), 6.55 (d, J = 9.1 Hz, 2H), 7.39 (d, J = 9.1 Hz, 2H); δ_C (125 MHz,

$CDCl_3$) 53.7, 58.5, 75.8, 114.3, 137.6, 148.0; *m/z* ESI-MS+ 330.0, $C_8H_{10}INO_2Na$ requires 330.0 (100%).

2,2'-((4-((triisopropylsilyl)ethynyl)phenyl)azanediyl)diethanol

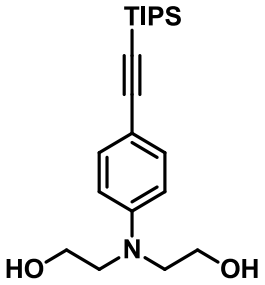

This compound was synthesised according to a literature procedure.[139] 2,2'-(4-iodophenylazanediyl)diethanol (800 mg, 2.6 mmol), palladium(II) diacetate (120 mg, 0.50 mmol), triphenylphosphine (270 mg, 1.0 mmol) and copper(I) iodide (65 mg, 0.30 mmol) were dried in an oven-dried Schlenk tube and the system was flushed with nitrogen. Distilled DIPA (12 mL) was added and reaction mixture was freeze-thaw degassed twice. Ethynyltriisopropylsilane (1.6 mL, 7.0 mmol) was added and additional freeze-thaw cycle was run. The reaction was left stirring at 50 ºC for 12 h. After this time reaction mixture was allowed to cool to room temperature and ethyl acetate (20 mL) was added. The organic phase was washed with water (20 mL) and a saturated solution of ammonium chloride (20 mL). The organic layer was dried over magnesium sulfate and the solvents removed by evaporation. The product was purified by column chromatography to yield a brown oil (SiO_2 96:4 chloroform:methanol). (740 mg, 78%); δ_H (400 MHz, $CDCl_3$) 1.21 (m, 21H), 3.55 (m, 4H), 3.79 (m, 4H), 3.99 (bs, 2H), 6.56 (d, J = 8.5 Hz, 2H), 7.34 (d, J = 8.5 Hz, 2H); δ_C (125 MHz, $CDCl_3$) 11.4, 18.7, 55.2, 60.6, 87.8, 107.9, 111.1, 111.9, 133.3, 147.5.

***N*,*N*-di-(2,5,8,11,14,17,20-heptaoxadocosan-22-yl)-N-(4-((trimethylsilyl)ethynyl)phenyl) amine**

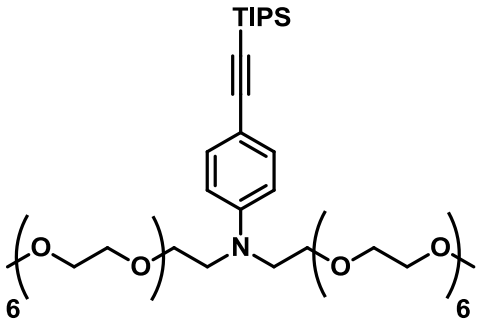

This novel compound was synthesised by adapting a literature procedure.[214] 2,2'-((4-((triisopropylsilyl)ethynyl)phenyl)azanediyl)diethanol (90 mg, 0.25 mmol) and sodium hydride (50 mg, 2 mmol) were heated to reflux in dry THF (2 mL) under nitrogen for 1 h. The mixture was then cooled to room temperature, and 2,5,8,11,14,17-hexaoxanonadecan-19-yl 4-methylbenzenesulfonate (260 mg, 0.60 mmol) was added as a solution in dry THF (3 mL) *via* syringe. The resultant mixture was heated at reflux under nitrogen for 2 days. Following this, the reaction was quenched with brine and extracted with chloroform (3 × 10 mL). The organic extractions were combined, dried over magnesium sulfate, filtered, and concentrated *in vacuo*. The crude product was purified by column chromatography (SiO_2: 98:2 $CHCl_3$:methanol) to yield the final product as a brown oil (90 mg, 39%); δ_H (400 MHz, $CDCl_3$) 1.11 (s, 21H), 3.38 (s, 6H), 3.54-3.67 (m, 64H), 6.61-6.63 (d, 2H), 7.30-7.32 (d, 2H); δ_C (125 MHz, $CDCl_3$) 1.7, 11.3, 19.0, 50.8, 59.0, 68.2, 70.6, 71.9, 87.5, 108.2, 111.4, 116.6, 133.4, 147.4; *m/z* ESI-MS+ 940.5, $C_{41}H_{75}NO_{14}SiNa^+$ requires 940.6 (100%).

***N*-(2,5,8,11,14,17,20-heptaoxadocosan-22-yl)-*N*-(4-ethynylphenyl)-amine (20)**

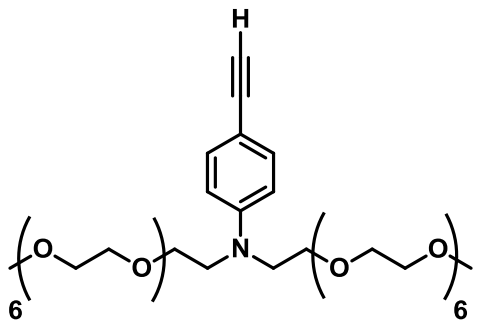

This novel compound was synthesised by adapting a reported procedure.[140] To a solution of *N*,*N*-di-(2,5,8,11,14,17,20-heptaoxadocosan-22-yl)-*N*-(4-((trimethylsilyl)ethynyl)phenyl) amine (172 mg, 0.190 mmol) in dry THF (5 mL) cooled to 0 °C was added

tetrabutylammonium fluoride (1.9 mL of a 1.0 M solution in THF, 1.9 mmol) dropwise *via* syringe. After overnight stirring at room temperature, the reaction mixture was poured onto a short silica plug and eluted with 98:2 DCM:methanol to yield the product as a yellow oil (100 mg, 70%); δ_H (400 MHz, $CDCl_3$) 3.43 (s, 6H), 3.58-3.71 (m, 64H), 6.66-6.69 (d, 2H), 7.35-7.39 (d, 2H); δ_C (125 MHz, $CDCl_3$) 50.8, 58.8, 68.2, 70.5, 71.9, 75.2, 84.5, 108.4, 111.2, 133.2, 147.9; *m/z* ESI-MS+ 784.3, $C_{32}H_{58}NO_{14}Na^+$ requires 784.4 (100%).

3,3'-(2,7-diiodo-9*H*-fluorene-9,9-diyl)dipropanoic acid

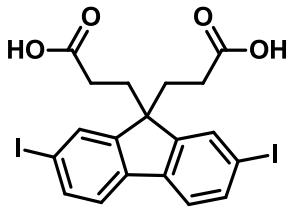

This compound was prepared according to a literature procedure.[137] To a solution of di-*tert*-butyl 3,3'-(2,7-diiodo-9*H*-fluorene-9,9-diyl)dipropanoate (2.50 g, 3.70 mmol) in DCM (6 mL) was added trifluoroacetic acid (5.6 mL, 600 mmol) dropwise. After stirring overnight at room temperature, the solvents were removed by evaporation. Traces of trifluoroacetic acid were removed by azeotroping with toluene. The solid was filtered, washing with cold toluene and dried *in vacuo* yielding a white solid (1.8 g, 85%); δ_H (400 MHz, $CDCl_3$) 1.28-1.33 (m, 4H), 2.30-2.34 (m, 4H), 3.45 (br, 2H), 7.68-7.70 (d, 2H), 7.74-7.76 (d, 2H), 7.95 (s, 2H).

3,3'-(2,7-diiodo-9H-fluorene-9,9-diyl)bis(propan-1-ol)

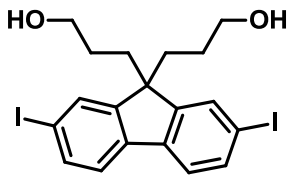

This novel compound was synthesised by adapting a reported procedure.[137] To a suspension of 3,3'-(2,7-diiodo-9*H*-fluorene-9,9-diyl)dipropanoic acid (1.80 g, 3.20 mmol) in dry THF (10 mL) cooled to 0 °C was added borane tetrahydrofuran complex (13 mL of a 1.0 M solution in THF, 13 mmol) dropwise *via* syringe. The solution was allowed to warm to room temperature. When TLC showed completion (99:1 chloroform:methanol), the reaction was quenched with isopropanol, then methanol and finally water. The solution was acidified with 1 M hydrochloric acid (10 mL) and extracted with ethyl acetate (3 × 10 mL). The organic extractions were combined, washed with brine (1 × 15 mL), dried over magnesium sulfate,

filtered and solvents evaporated. The product was purified by recrystallisation (THF/hexane) to yield a white solid (1.25 g, 73%); δ_H (400 MHz, $CDCl_3$/10% MeOH-d_4) 0.79-0.86 (m, 4H), 1.98-2.02 (m, 4H), 3.30-3.33 (m, 4H), 7.39-7.42 (d, 2H), 7.62-7.67 (d, 2H), 7.67 (s, 2H); δ_C (125 MHz, DMSO-d_6) 27.7, 35.7, 55.2, 61.2, 94.4, 122.6, 132.2, 136.3, 139.7, 152.4; *m/z* ESI-MS+ 557.0, $C_{19}H_{20}I_2O_2Na^+$ requires 556.9 (100%).

(((2,7-diiodo-9H-fluorene-9,9-diyl)bis(propane-3,1-diyl))bis(oxy))bis(trimethylsilane) (19)

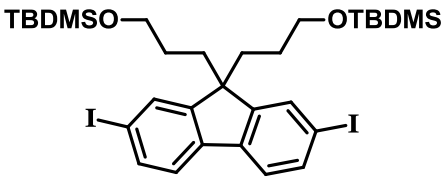

This compound was synthesised by adapting a literature procedure.[141] 3,3'-(2,7-diiodo-9H-fluorene-9,9-diyl)bis(propan-1-ol) (100 mg, 0.20 mmol), *tert*-butyl-di-methyl-silylchloride (210 mg, 1.4 mmol) and imidazole (90 mg, 1.3 mmol) were dissolved in THF (4 mL). After 1 h, TLC showed ($CHCl_3$) completion and the reaction was quenched with brine (15 mL) and extracted with chloroform (3 × 10 mL), dried over magnesium sulfate, filtered, and concentrated *in vacuo*. The crude mixture was passed over a plug of silica (chloroform) to yield the pure product as a white powder (120 mg, 84%); δ_H (400 MHz, $CDCl_3$) −0.06 (s, 12H), 0.76-0.80 (m, 4H), 0.85 (s, 18H), 1.99-2.03 (m, 4H), 3.32-3.36 (t, 4H), 7.39-7.41 (m, 2H), 7.64-7.66 (m, 4H); δ_C (125 MHz, $CDCl_3$) −5.3, 18.3, 26.0, 27.2, 36.3, 55.0, 62.9, 93.3, 121.6, 132.1, 136.3, 139.8. 151.9; *m/z* ESI-MS+ 762.5, $C_{25}H_{36}I_2O_2Si_2$ requires 762.1 (100%).

(2,7-diiodo-9*H*-fluorene-9,9-diyl)bis(propane-3,1-diyl) dimethanesulfonate (32)

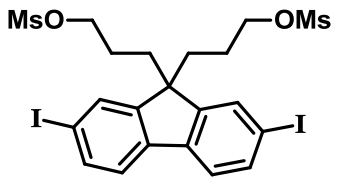

This novel compound was synthesised by adapting a reported procedure.[142] A solution of 3,3'-(2,7-diiodo-9H-fluorene-9,9-diyl)bis(propan-1-ol) (950 mg, 1.90 mmol) and triethylamine (1.60 mL, 11.2 mmol) in dry THF (10 mL) was cooled to 0 °C and methanesulfonyl chloride (560 µL, 7.50 mmol) added dropwise *via* syringe. After around 10 min, precipitation was observed. When the reaction was shown to be complete by TLC (98:2

$CHCl_3$:methanol), the reaction mixture was poured into brine and extracted with DCM (3 × 10 mL). The organic extractions were combined, dried over magnesium sulfate, filtered and concentrated *in vacuo*. The compound was purified by column chromatography (SiO_2: $CHCl_3$) to give an off-white powder (1.0 g, 83%); δ_H (400 MHz, $CDCl_3$) 0.98-1.05 (m, 4H), 2.09-2.13 (t, 4H), 2.94 (s, 6H), 3.95-3.98 (t, 4H), 7.43-7.45 (d, 2H), 7.68-7.73 (m, 4H); δ_C (125 MHz, $CDCl_3$) 23.6, 35.7, 37.4, 54.3, 69.5, 93.7, 121.9, 131.9, 137.0, 139.8, 150.1; *m/z* ESI-MS+ 712.9, $C_{21}H_{24}N_2O_6S_2Na^+$ requires 712.9 (100%).

1,1'-((2,7-diiodo-9H-fluorene-9,9-diyl)bis(propane-3,1-diyl))bis(4-(hydroxymethyl)pyridin-1-ium) (35)

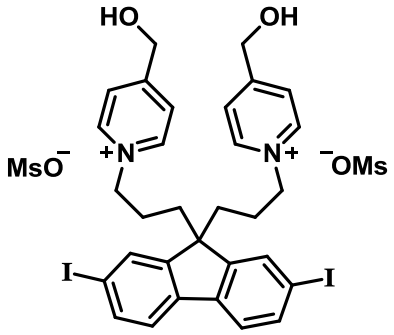

This novel compound was synthesised by adapting a reported procedure.[143] (2,7-diiodo-9H-fluorene-9,9-diyl)bis(propane-3,1-diyl) dimethanesulfonate (250 mg, 0.36 mmol) and 4-pyridinemethanol (210 mg, 0.90 mmol) were dissolved in dry acetonitrile (5 ml) and heated to reflux overnight. The product precipitated out as a red solid. The solvent was decanted and the red solid triturated with acetonitrile (3 × 5 mL). The product was dried under vacuum and used without further purification (CARE: very hygroscopic) (190 mg, 58%); δ_H (400 MHz, D_2O) 1.00-1.06 (m, 4H), 1.91-1.95 (m, 4H), 4.11-4.14 (m, 4H), 4.85 (s, 4H), 7.41-7.43 (d, 2H), 7.47 (s, 2H), 7.78-7.80 (d, 4H), 8.28-8.30 (d, 4H); δ_C (125 MHz, D_2O) 25.5, 34.5, 38.9, 54.3, 60.8, 62.0, 93.9, 124.0, 125.0, 132.2, 137.4, 140.2, 143.7, 150.1, 162.3.

1,1'-((2,7-diiodo-9H-fluorene-9,9-diyl)bis(propane-3,1-diyl))bis(4-(((4-((*tert*-butoxycarbonyl)amino)butanoyl)oxy)methyl)pyridin-1-ium) methanesulfonate (33)

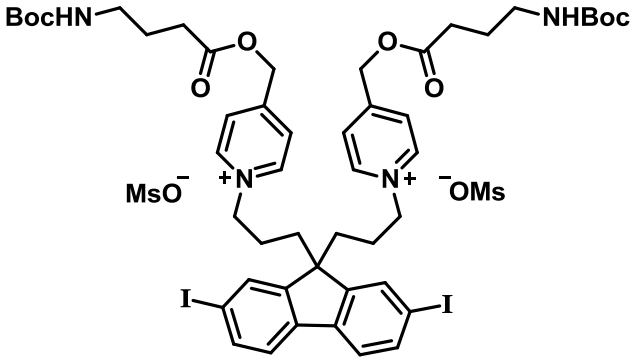

This novel compound was synthesised by adapting a reported procedure.[143] A solution of (2,7-diiodo-9*H*-fluorene-9,9-diyl)bis(propane-3,1-diyl) dimethanesulfonate (300 mg, 0.43 mmol) and pyridin-4-ylmethyl 4-((tert-butoxycarbonyl)amino)butanoate (320 mg, 1.30 mmol) was refluxed in dry MeCN (5 mL) for 36 h. The solution became a deep red colour and NMR spectroscopy showed the reaction was complete. The solvent was concentrated and the residue taken up in water. The aqueous solution was washed with toluene (3 × 5 mL) and chloroform (3 × 5 mL) to remove the excess starting reagent, then concentrated *in vacuo* to give a red solid (CARE: Very hygroscopic) (460 mg, 83%); δ_H (400 MHz, $CDCl_3$) 1.33-1.39 (m, 22H, ^{t}Bu and CH_2), 1.77-1.84 (s+m, 4H, GABA-CH_2), 2.07 (br, 4H, CH_2), 2.47-2.51 (t, 4H, GABA-CH_2), 2.69 (s, 6H, OMs-CH_3) 3.11-3.13 (m, GABA-CH_2) 4.55 (br, 4H, CH_2), 5.25 (br, 2H, NHBoc), 5.36 (s, 4H), 7.36-7.38 (d, 2H), 7.61-7.63 (s+d, 4H), 7.97-7.98 (d, 4H, Py-H), 8.94-8.96 (d, 4H, Py-H); δ_C (125 MHz, CD_3CN) 25.0, 26.1, 28.2, 30.8, 34.4, 39.4, 39.5, 53.9, 60.9, 63.0, 93.6, 116.7, 121.9, 125.5, 132.1, 136.9, 139.3, 144.6, 150.1, 156.1, 156.3, 172.3.

4,4'-((9,9-bis(3-((trimethylsilyl)oxy)propyl)-9H-fluorene-2,7-diyl)bis(ethyne-2,1-diyl))bis(*N*,*N*-bis(2-(2-methoxyethoxy)ethyl)aniline) (17)

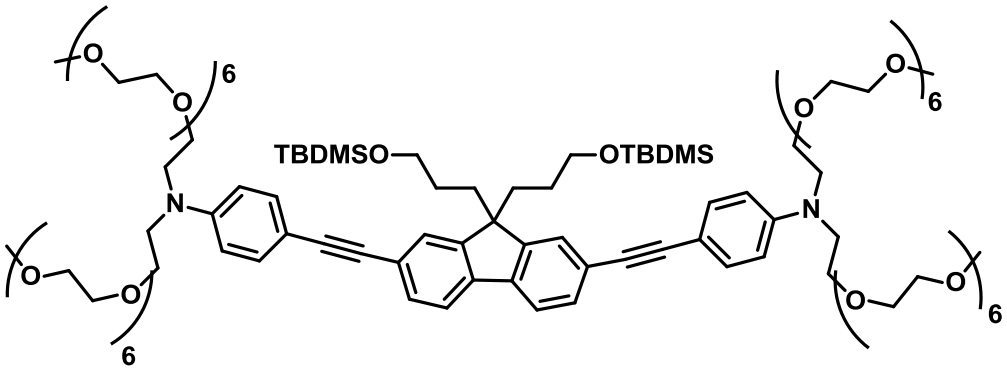

This novel compound was synthesised by adapting a reported procedure.[144] (((2,7-diiodo-9H-fluorene-9,9-diyl)bis(propane-3,1-diyl))bis(oxy))bis(trimethylsilane) (50 mg, 0.10 mmol), palladium(II) diacetate (1 mg, 5 mol%), copper iodide (1 mg, 5 mol%) and triphenylphosphine (2 mg, 10 mol%) were dried under vacuum in a pre-dried Schlenk tube. The reagents were suspended in diisopropylamine (1 mL) and freeze-thaw degassed once. *N*-(2,5,8,11,14,17,20-heptaoxadocosan-22-yl)-*N*-(4-ethynylphenyl)-2,5,8,11,14,17,20-heptaoxadocosan-22-amine (110 mg, 0.14 mmol) was added as a solution in DIPA (1.0 mL) and the mixture was freeze-thaw degassed twice more. The reaction was stirred at 40 °C under nitrogen. After 2 hours TLC (1:1 DCM: petrol ether) showed completion, and the reaction was quenched with saturated aqueous ammonium sulfate (10 mL) and extracted with chloroform (3 × 10 mL). The organic extractions were combined, washed with brine (1 × 15 mL), dried over magnesium sulfate, filtered, and concentrated *in vacuo*. The crude mixture was purified by semi-preparative RP-HPLC to yield the product as a yellow oil (25 mg, 18%); δ_H (400 MHz, $CDCl_3$) −0.02 (s, 12H), 0.89 (s, 18H), 2.10-2.13 (m, 4H), 3.37-3.40 (t, 4H), 3.42 (s, 6H), 3.58-3.60 (m, 8H), 6.71-6.73 (d, 4H), 7.42-7.44 (d, 4H), 7.50-7.52 (m, 4H), 7.65-7.66 (d, 2H); δ_C (125 MHz, $CDCl_3$) −4.90, 18.7, 26.4, 27.6, 36.9, 51.3, 54.9, 59.5, 63.6, 68.8, 71.0, 71.0, 71.1, 71.2, 72.4, 88.8, 91.2, 110.5, 111.8, 120.2, 123.3, 126.2, 130.9, 133.3, 140.5, 148.1, 150.7; *m/z* ESI-MS+ 2029.91, $C_{107}H_{180}N_2O_{30}Si_2$ requires 2030.22 (100%); λ_{max} (ethanol)/ nm (log ε) 384 (5.01), 273 (4.62); Φ_{max} (ethanol)/ nm (ϕ_f) 468 (0.93).

1,1'-((2,7-bis((4-(bis(2-(2-methoxyethoxy)ethyl)amino)phenyl)ethynyl)-9*H*-fluorene-9,9-diyl)bis(propane-3,1-diyl))bis(4-(hydroxymethyl)pyridin-1-ium)

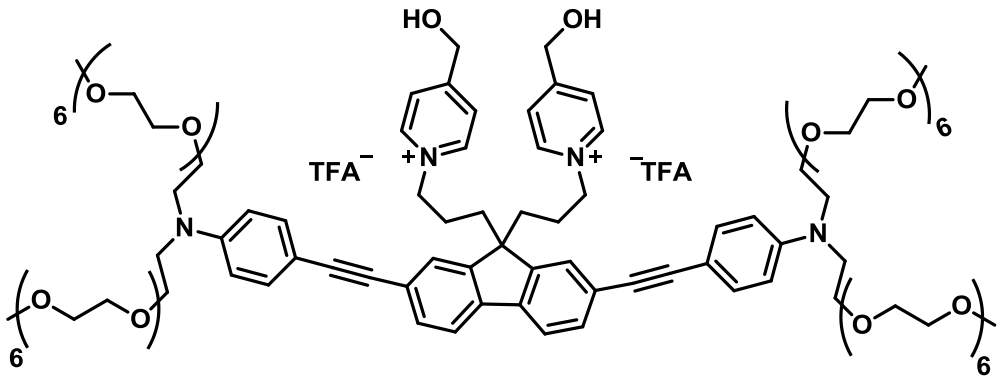

This compound was synthesised by adapting a reported procedure.[142] 1,1'-((2,7-diiodo-9H-fluorene-9,9-diyl)bis(propane-3,1-diyl))bis(4-(hydroxymethyl)pyridin-1-ium) (90 mg, 0.10 mmol), tris(dibenzylidinediacetone)dipalladium(0) (2.3 mg, 2.5 mol%), copper(I) iodide (0.5 mg, 2.5 mol%) and triphenylphosphine (1.3 mg, 5.0 mol%) were dried under vacuum in a pre-dried Schlenk tube. The reagents were suspended in diisopropylamine (1 mL) and freeze-thaw degassed once. *N*-(2,5,8,11,14,17,20-heptaoxadocosan-22-yl)-N-(4-ethynylphenyl)-2,5,8,11,14,17,20-heptaoxadocosan-22-amine (160 mg, 0.20 mmol) was added as a solution in dry acetonitrile (1 mL) and the mixture was freeze-thaw degassed twice more. The reaction was stirred at room temperature under nitrogen for two hours. After this time, RP-HPLC showed consumption of the fluorene starting material and the reaction was quenched with saturated aqueous ammonium chloride (10 mL). The aqueous layer was extracted with chloroform (3 × 10 mL). These extractions were combined, washed with brine, dried over magnesium sulfate, filtered and concentrated. The compound, an orange/brown oil, was used without further purification (24 mg, 12%); δ_H (500 MHz, $CDCl_3$) 1.18-1.22 (m, 4H), 2.16 (m, 4H), 3.26 (s, 12H), 3.48-3.63 (m, 140H), 4.28-4.30 (t, 4H), 6.97-6.99 (d, 4H), 7.40 (m, 8H), 7.66-7.68 (d, 2H), 8.12-8.14 (d, 4H), 8.49-8.50 (d, 4H).

TBFHEG-Py-BocGABA (34)

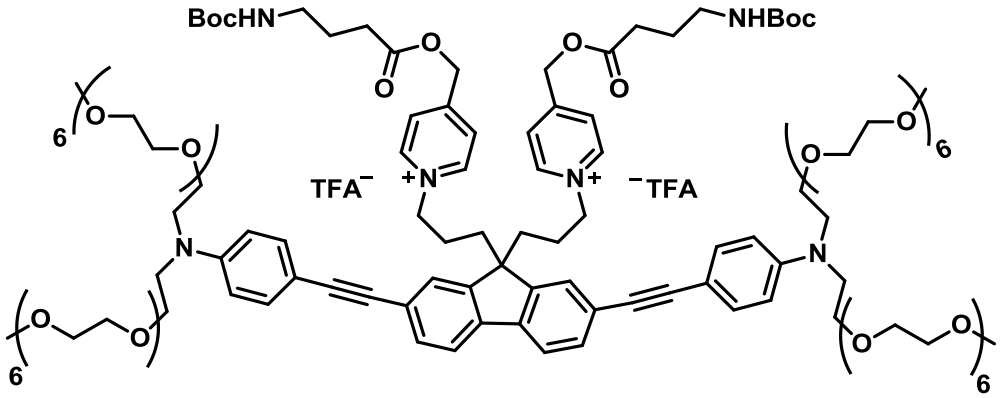

This compound was synthesised by adapting a reported procedure.[142] To a suspension of 1,1'-((2,7-diiodo-9H-fluorene-9,9-diyl)bis(propane-3,1-diyl))bis(4-(((4-((*tert*-butoxycarbonyl)amino)butanoyl)oxy)methyl)pyridin-1-ium) methanesulfonate (110 mg, 0.090 mmol), palladium(II) diacetate (1 mg, 5 mol%), triphenylphosphine (2 mg, 10 mol%) and copper iodide (0.8 mg, 5 mol%) in diisopropylamine (2 mL) in a pre-dried Schlenk tube, was added *N*-(2,5,8,11,14,17,20-heptaoxadocosan-22-yl)-N-(4-ethynylphenyl)-2,5,8,11,14,17,20-heptaoxadocosan-22-amine (150 mg, 0.20 mmol) as a solution in dry MeCN (2 mL). The resulting solution was freeze-thaw degassed three times and allowed to warm to room temperature. After 1 hr, HPLC showed a single peak at 15 mins (*Method B*) with the desired absorption spectrum. The reaction mixture was concentrated *in vacuo* and the residue taken up in water. The aqueous suspension was washed with toluene (3 × 10 mL) to remove triphenylphosphine, then a small volume of brine was added and the solution extracted with chloroform until the aqueous phase became colourless. The organic extractions were combined, dried over magnesium sulfate, filtered, and the solvents removed *in vacuo* to afford a dark red oil (150 mg, 76%); δ_H (400 MHz, CD_3CN) 1.19 (br, 4H), 1.39 (s, 18H), 1.72-1.75 (m, 4H, GABA-CH_2), 2.12-2.16 (br, 4H), 2.41-2.45 (t, 4H, GABA-CH_2), 3.06 (br, 4H, GABA-CH_2), 3.29 (s, 12H, HEG-CH_3), 3.46-3.65 (m, 112H, HEG), 4.24-4.26 (t, 4H), 5.30 (s, 4H), 5.42 (br, 2H, NHBoc), 6.78-6.80 (d, J = 8.9 Hz, 4H), 7.35-7.37 (d, J = 8.9 Hz, 4H), 7.42 (s, 2H), 7.49-7.50 (d, J = 7.9 Hz, 2H), 7.74-7.76 (d, J = 7.9 Hz, 2H), 7.85-7.87 (d, J = 6.4 Hz, 4H, Py-H), 8.40-8.41 (d, J = 6.4 Hz, 4H, Py-H); δ_C (125 MHz, CD_3CN) 18.1, 25.0, 25.7, 27.7, 30.5, 35.1, 39.2, 50.5, 53.9, 57.9, 60.8, 62.9, 68.0, 68.1, 69.9, 70.1, 70.2, 70.2, 70.4, 71.6, 78.2, 71.6, 78.2, 88.0, 88.1, 91.6, 91.6, 108.7, 111.9, 120.4, 123.3, 125.3, 125.5, 131.0, 132.6, 140.0, 144.1, 148.4, 148.5, 156.1, 157.0, 172.4; λ_{max} (H_2O) /nm (log ε) 280

(4.59), 389 (5.07); λ_{max} (EtOH)/ nm (log ε) 281 (4.68), 383 (5.07); Φ_{max} (CH_3CN)/ nm (ϕ_f) 468 (0.002).

TBFHEG-Py-GABA (31)

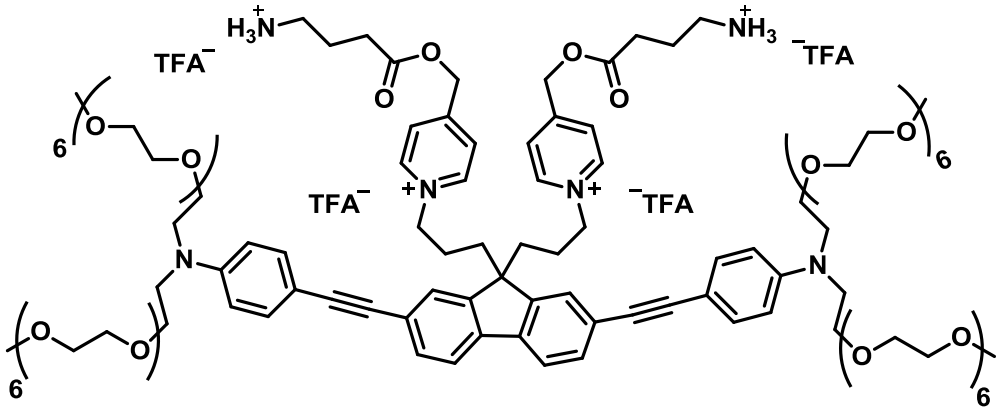

This compound was synthesised by adapting a literature procedure.[145] TPBG (30 mg, 0.010 mmol) was dissolved in dry DCM (2 mL) in a flame-dried round-bottomed flask with approximately eight 4 Å molecular sieves. The reaction mixture was cooled to 0 °C and BF_3. Et_2O (160 µL, 0.60 mmol) added slowly *via* syringe. The reaction was stirred vigorously for 5 hours, after which time, HPLC showed no starting material at 14 mins and a new peak at 10.5 minutes (*Method B*). The reaction was quenched with saturated aqueous sodium acetate and extracted with DCM (3 × 5 mL). The organic extractions were combined, dried over magnesium sulfate, filtered, and concentrated *in vacuo*. The residue was taken up in the minimum amount of water and purified by semi-preparative HPLC to afford a yellow oil (3 mg, 12%); δ_H (500 MHz, D_2O) 1.08 (br, 4H), 1.80-1.83 (dt, 4H, GABA-CH_2), 2.06 (br, 4H), 2.37-2.40 (t, 4H, GABA-CH_2), 2.89-2.92 (m, 4H, GABA-CH_2), 3.26 (s, 12H, HEG-CH_3), 3.56-3.71 (m, 112H, HEG), 4.18 (t, 4H), 5.29 (s, 4H), 6.82-6.84 (d, 4H, J = 8.9 Hz), 7.03 (s, 2H), 7.39-7.40 (d, 4H, J = 8.9 Hz), 7.47-7.48 (d, 2H, J = 8.0 Hz), 7.77-7.78 (d, 2H, J = 8.0 Hz), 7.81-7.82 (d, 4H, J = 6.3 Hz, Py-H), 8.34-8.35 (d, 4H, J = 6.3 Hz, Py-H); δ_F (470 MHz, D_2O) −75.7; λ_{max} (H_2O) /nm (log ε) 279 (4.36), 389 (4.82); *m/z* ESI-MS+ 1078.1286, $[C_{115}H_{178}N_6O_{32}]^{2+}$ requires 1078.1254 (100%); λ_{max} (H_2O)/nm (log ε) 279 (4.36), 389 (4.82); λ_{max} (MeCN)/nm (log ε) 280 (4.43), 389 (4.86); Φ_{max} (H_2O)/ nm (ϕ_f) 468 (0.002).

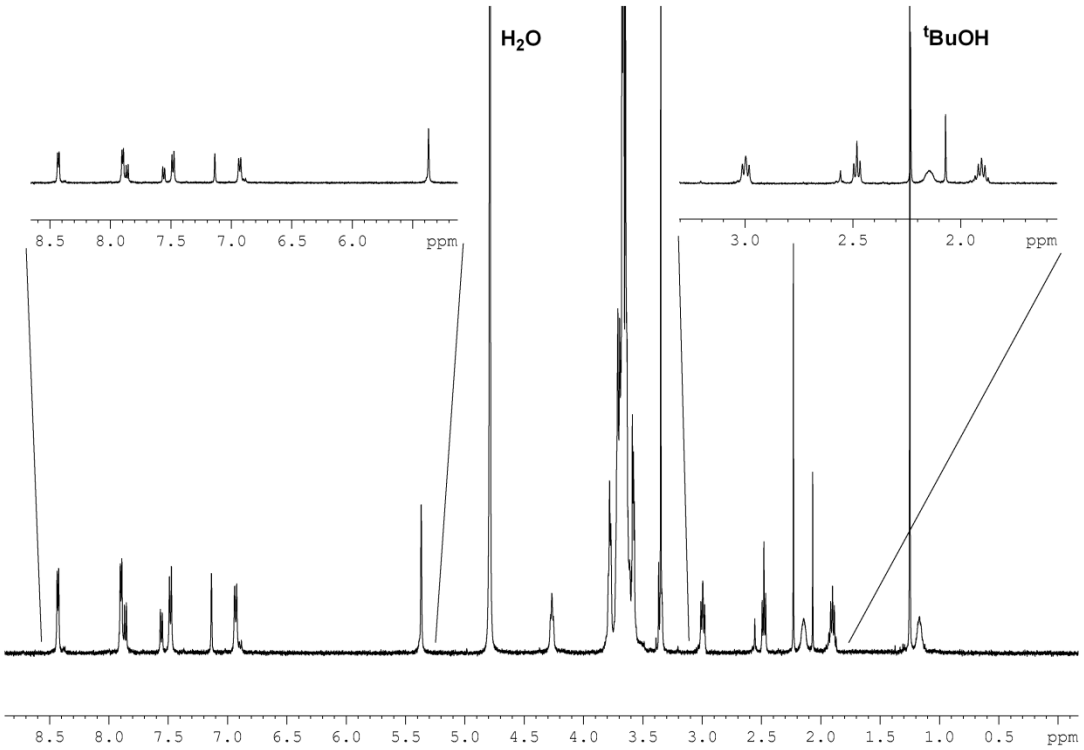

Figure 77: *A representative ^{1}H NMR spectrum (500 MHz, D_2O) of compound **31**.*

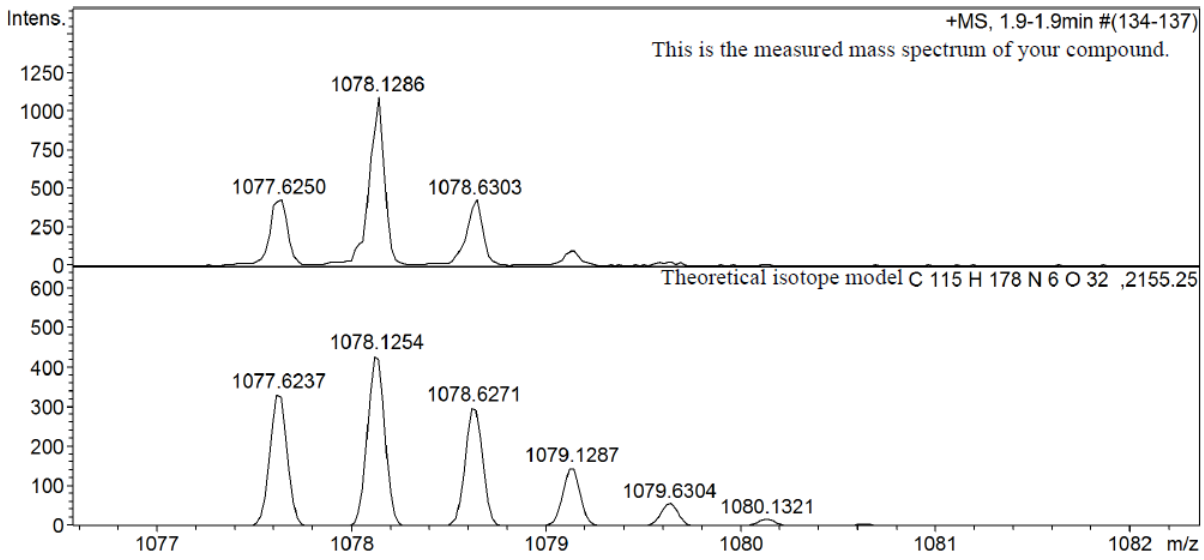

Figure 78: *The positive ion electrospray mass spectrum of **31**.*

Synthesis of Uncaging Groups

2-(4-methoxyphenyl)-2-oxoethyl acetate (21)

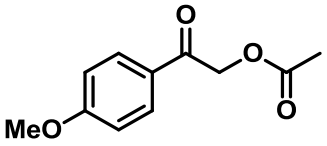

This compound was prepared according to a reported procedure.[146] To a suspension of 4-methoxyphenacyl bromide (1.0 g, 4.4 mmol) in ethanol (4.5 mL) was added a solution of sodium acetate trihydrate (713 mg, 5.24 mmol) in 10% aqueous acetic acid. The reaction mixture was heated to reflux until no more starting material remained by TLC (hexane:ethyl acetate 1:1). The reaction was quenched with semi-saturated sodium bicarbonate and extracted with ethyl acetate (3 × 10 mL). The organic extractions were combined and washed with brine (15 mL), dried over sodium sulfate, filtered, and concentrated *in vacuo* to yield the product as a white solid (815 mg, 95%); δ_H (400 MHz, $CDCl_3$) 2.23 (s, 3H), 3.88 (s, 3H), 5.30 (s, 2H), 6.95 (d, 2H), 7.90 (d, 2H); δ_C (125 MHz, $CDCl_3$) 20.6, 55.5, 65.7, 114.0, 127.2, 130.0, 164.0, 170.5, 190.6; *m/z* ESI-MS+ 231.04, $C_{11}H_{12}NaO_4^+$ requires 231.06 (100%).

2-(4-methoxyphenyl)-2-oxoethyl acetate (*See Appendix 1*)

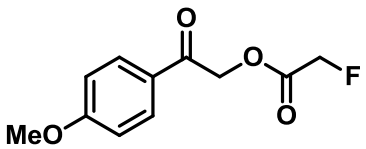

This compound was prepared according to a reported procedure.[147] To a solution of 4-methoxyphenacyl bromide (760 mg, 3.3 mmol) in DMF (10 mL) was added sodium fluoroacetate (1 g, 10 mmol). The reaction mixture was heated to 90 °C until no more starting material remained by TLC (hexane:ethyl acetate 1:1). The reaction was quenched with semi-saturated sodium bicarbonate and extracted with ethyl acetate (3 × 10 mL). The organic extractions were combined and washed with brine (15 mL), dried over sodium sulfate, filtered, and concentrated *in vacuo* to yield the product as a white solid (500 mg, 67%); δ_H (400 MHz, $CDCl_3$) 1.58 (d, 3H), 3.88 (3H), 4.91-5.03 (d, 2H), 6.08 (q, 1H), 6.96 (d, 2H), 7.92 (d, 2H); δ_C (125 MHz, $CDCl_3$) 17.4, 55.5, 72.0, 78.1, 114.1, 126.7, 130.8, 164.1, 167.2, 194.0; δ_F (370 MHz, $CDCl_3$) −230.5; *m/z* ESI-MS+ 263.05, $C_{11}H_{12}KO_4^+$ requires 265.03 (100%).

Methyl 4-acetylbenzoic acid (23)

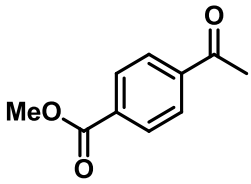

This compound was synthesised according to a reported procedure.[92] To a suspension of 4-acetyl benzoic acid (750 mg, 3.1 mmol) in methanol (10 mL) was added conc. sulfuric acid (60 µL). The suspension was heated to reflux, upon which a solution formed. After 6 hours, no starting material remained by TLC (1:1 hexane:ethyl acetate) and the solvents were removed *in vacuo*. The residue was taken up in diethyl ether (20 mL) and washed with saturated aqueous sodium bicarbonate (3 × 10 mL) and brine (10 mL). The organic layer was dried over magnesium sulfate, filtered, and the solvent removed *in vacuo*. The product was precipitated from DCM/petroleum ether to give a fine cream powder (650 mg, 80%); δ_H (400 MHz, $CDCl_3$) 2.63 (s, 3H), 3.94 (s, 3H), 7.98-8.00 (d, 2H), 8.10-8.12 (d, 2H); δ_C (125 MHz, $CDCl_3$) 26.9, 52.4, 128.2, 129.8, 133.8, 140.2, 166.2, 197.5.

Methyl 4-(2-bromoacetyl)benzoate

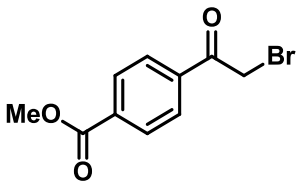

This compound was synthesised according to a reported procedure.[89] Methyl 4-acetylbenzoic acid (300 mg, 2.3 mmol) was suspended in acetic acid (15 mL) and heated to 70 °C until a solution was formed. Bromine (120 µL, 2.3 mmol) was added dropwise *via* syringe and the solution was allowed to cool to room temperature until the strong orange colour disappeared, at which time the solution was cooled in an ice/water bath. The precipitate formed was filtered, washing with ice cold 1:1 water:methanol to give a cream powder (120 mg, 28%); δ_H (400 MHz, $CDCl_3$) 3.96 (s, 3H), 4.47 (s, 2H), 8.03-8.05 (d, 2H), 8.14-8.16 (d, 2H); δ_C (125 MHz, $CDCl_3$) 30.7, 52.6, 128.9, 130.0, 134.6, 137.1, 165.9, 190.8.

Methyl 4-(2-(propionyloxy)acetyl)benzoate (22)

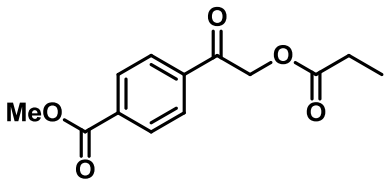

This compound was synthesised by adapting a reported procedure.[89] Methyl 4-(2-bromoacetyl)benzoate (100 mg, 0.40 mmol), potassium carbonate (270 mg, 1.9 mmol) and sodium iodide (12 mg, 0.10 mmol) were suspended in dry DMF (2 mL). Propionic acid (150 µL, 1.9 mmol) was added and the reaction mixture stirred at 90 °C under nitrogen. After 3 hours no starting material remained by TLC (98:2 DCM:methanol) so the reaction was cooled to room temperature and poured into brine. This was extracted with DCM (3 × 10 mL) and the combined organic extractions were dried over magnesium sulfate, filtered and evaporated to dryness. A tacky yellow solid resulted (90 mg, 92%); δ_H (400 MHz, $CDCl_3$) 1.23-1.20 (t, 3H), 2.55-2.49 (q, 2H), 3.95 (s, 3H), 5.34 (s, 2H), 7.95-7.97 (d, 2H), 8.13-8.15 (d, 2H); δ_C (125 MHz, $CDCl_3$) 9.0, 27.2, 52.5, 66.0, 127.7, 130.0, 134.5, 137.4, 166.0, 173.8, 192.0.

5-Methoxy-2-nitrobenzaldehyde

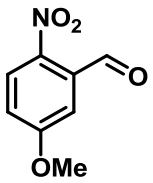

To a solution of 5-hydroxy-2-nitrobenzaldehyde (1.0 g, 6.0 mmol) in absolute ethanol (5 mL), dimethylsulfate (2.0 mL, 21 mmol) was added. The mixture was cooled to 0 °C and sodium hydroxide (1.2 g, 30 mmol) in water (3 mL) was added dropwise. The reaction mixture was stirred at 50 °C for 2 days. After cooling to room temperature, water (10 mL) was added and reaction mixture was extracted with DCM (3 × 10 mL). The organic extractions were combined, dried over magnesium sulfate and concentrated *in vacuo*. The compound was purified by column chromatography (SiO_2 hexane:ethyl acetate 95:5) to yield the product as yellow solid (640 mg, 58%); δ_H (400 MHz, $CDCl_3$) 3.72 (s, 3H), 7.15 (dd, J = 2.8 Hz, J = 9.0 Hz, 1H), 7.3 (d, J = 2.8 Hz, 1H), 8.15 (d, J = 9.0 Hz, 1H); δ_C (125 MHz, $CDCl_3$) 56.3, 113.3, 118.6, 127.3, 134.3, 142.3, 164.1, 188.5.

(5-methoxy-2-nitrophenyl)methanol

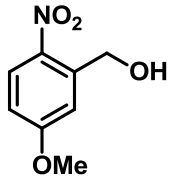

4-Methoxy-2-nitrobenzaldehyde (600 mg, 3.3 mmol) was dissolved in methanol (10 mL) and cooled to 0 °C. Sodium borohydride (63 mg, 1.7 mmol) was added dropwise and reaction mixture was stirred at room temperature for 1 h. After this time reaction was acidified to pH 7 with 2 M hydrochloric acid. Water (20 mL) was added and the reaction mixture was extracted with DCM (3 × 10ml). The organic extractions were combined, dried over magnesium sulfate and evaporated to dryness. The product, a yellow solid, was used without further purification (470 mg, 77%); δ_H (400 MHz, $CDCl_3$) 3.92 (s, 3H), 5.01 (s, 2H), 6.89 (dd, J = 2.5 Hz, J = 8.6 Hz, 1H), 7.22 (d, J = 2.5 Hz, 1H), 8.18 (d, J = 8.6 Hz, 1H).

5-Methoxy-2-nitrobenzyl acetate (24)

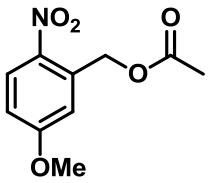

(4-Methoxy-2-nitrophenyl)methanol (60 mg, 0.32 mmol), acetyl chloride (0.030 mL, 0.34 mmol) , DMAP (5 mg, 0.04 mmol) and triethylamine (0.1 mL, 0.7 mmol) were dissolved in THF (2 mL). The reaction mixture was stirred at room temperature overnight, following which, the solvent was evaporated to dryness the product isolated by column chromatography (SiO_2: hexane:ethyl acetate 90:10) to yield a white solid (50 mg, 68%); δ_H (400 MHz, $CDCl_3$) 2.19 (s, 3H), 3.91 (s, 3H), 5.53 (s, 2H), 6.90 (dd, J = 2.6 Hz, J = 9.3 Hz, 1H), 7.04 (d, J = 2.6 Hz, 1H), 8.20 (d, J = 9.3 Hz, 1H); δ_C (125 MHz, $CDCl_3$) 20.7, 55.9, 63.2, 112.4, 114.0, 128.07, 135.5, 140.2, 163.8, 170.4.

Methyl-3-methyl-4-nitrobenzoate

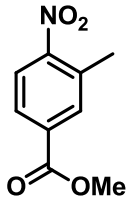

3-Methyl-4-nitrobenzoic acid (5.0 g, 28 mmol) was suspended in methanol (50 mL) and concentrated sulphuric acid (0.5 mL) was added. The reaction mixture was heated at reflux for 24 hr, cooled to room temperature and the methanol was evaporated. The solid obtained was dissolved in ethyl acetate (50 mL), washed with saturated sodium bicarbonate (50 mL), water (50 mL), dried over magnesium sulfate and concentrated *in vacuo* to give the product as a white solid (4.2 g, 77%); δ_H (400 MHz, $CDCl_3$) 2.61 (s, 3H), 3.96 (s, 3H), 7.96 (m, 2H); δ_C (125 MHz, $CDCl_3$) 8.02, 20.1, 52.7, 124.5, 128.0, 133.7, 134.0, 151.8, 165.3.

Methyl 3-(acetoxymethyl)-4-nitrobenzoate (25)

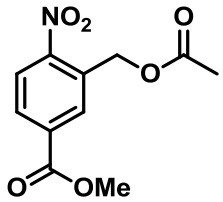

3-Methyl-2-nitrobenzoic acid methyl ester (2.0 g, 10 mmol) and *N*-bromosuccinimide (2.0 g, 11 mmol) were suspended in tetrachloromethane (50 mL) and heated to reflux. Benzoyl peroxide (500 mg, 2.0 mmol) was added and reaction was stirred for 48 h. Following cooling to room temperature, the solvents were removed *in vacuo* and the residue was dissolved in ethyl acetate (30 mL). The organic phase was washed with 1:1 mixture of sodium bicarbonate and sodium thiosulfate (50 mL), water (50 mL), dried over magnesium, filtered, and concentrated *in vacuo*. The crude benzyl bromide was dissolved in DMF (5 mL) and sodium acetate (1.7 g, 21 mmol) was added. The reaction mixture was heated at 70 ºC for 24 h. After cooling to room temperature the solvent was evaporated to give orange solid which was dissolved in ethyl acetate (30 mL) and washed with brine (30 mL). The organic phase was dried over magnesium sulfate, filtered and evaporated to dryness. The product was purified by column chromatography (SiO_2: DCM) to yield the product as a yellow solid (600 mg, 23%); δ_H (400 MHz, $CDCl_3$) 2.20 (s, 3H), 4.01 (s, 3H), 5.51 (s, 2H), 8.14 (m, 2H), 8.26 (s,

1H); δ_C (125 MHz, $CDCl_3$) 20.7, 52.9, 62.5, 125.1, 129.9, 130.4, 132.3, 134.5, 150.0, 165.0, 170.3.

4,5-dimethoxy-2-nitrobenzyl 2-fluoroacetate (*See Appendix 1*)

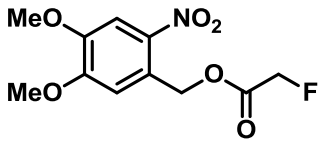

This novel compound was synthesised by adapting a reported procedure.[143] A solution of 2-nitro-4,5-dimethoxy-6-nitrobenzylbromide (460 mg, 3.30 mmol), sodium monofluoroacetate (500 mg, 10 mmol) and sodium iodide (50 mg, 0.7 mmol) suspended in dry DMF (5 mL) was heated to 100 °C under nitrogen. After 3 hours, TLC showed completion (DCM) and the reaction was quenched with brine (15 mL). The aqueous suspension was extracted with DCM (3 × 10 mL) and the organic extractions were combined and dried over magnesium sulfate, filtered and concentrated. The product was purified by column chromatography (SiO_2: DCM) to yield the product as a white powder (650 mg, 71%); δ_H (400 MHz, $CDCl_3$) 3.96 (s, 3H), 3.99 (s, 3H), 4.89-5.01 (d, 2H, CH_2F), 5.63 (s, 2H), 7.04 (s, 1H), 7.73 (s, 1H); δ_C (125 MHz, $CDCl_3$) 56.4, 64.0, 76.7, 78.5, 108.3, 110.9, 125.6, 140.1, 148.6, 153.5, 167.2, 167.4; δ_F (470 MHz, $CDCl_3$) −230.05-−229.80 (t); *m/z* ESI-MS+ 296.05, $C_{11}H_8O_6NFNa^+$ requires 296.05 (100%); λ_{max} ($CHCl_3$) /nm 303, 343.

Pyridin-4-ylmethyl acetate

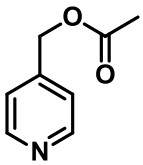

This compound was synthesised according to a reported procedure.[148] To an ice-cold solution of pyridine-4-ylmethanol (5.0 g, 46 mmol) and triethylamine (13 mL, 92 mmol) in toluene (25 mL) was added acyl chloride (6.0 mL 80 mmol) as a solution in toluene (15 mL), dropwise. The reaction was stirred overnight at room temperature before being poured into water, extracted with DCM (3 × 20 mL), dried over magnesium sulfate, filtered, and concentrated *in vacuo*. The residue was purified by column chromatography (SiO_2: 99:1 DCM:methanol) to give a yellow powder (553 mg, 40%); δ_H (400 MHz, $CDCl_3$) 2.14 (s, 3H),

5.10 (s, 2H), 7.23 (d, 2H), 8.58 (d, 2H); δ_C (125 MHz, $CDCl_3$) 20.8, 64.2, 121.9, 144.8, 150.0 170.5.

4-(Acetoxymethyl)-1-methylpyridin-1-ium iodide

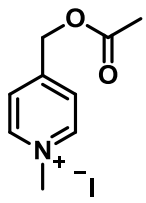

This compound was synthesised by adapting a reported procedure.[147] To a solution of pyridin-4-ylmethyl acetate (200 mg, 1.3 mmol) in methanol (2 mL) was added methyl iodide (120 µL, 2.0 mmol) and the resulting mixture stirred overnight at 50 °C. The following day, the solvents were removed *in vacuo* and the desired product was recrystallised from methanol to yield bright orange/yellow crystals (290 mg, 75%); δ_H (400 MHz, CD_3CN) 2.19 (s, 3H), 4.36 (s, 3H), 5.38 (s, 2H), 8.00 (d, 2H), 8.77 (d, 2H); δ_C (125 MHz, CD_3CN) 20.4, 48.5, 63.5, 117.8, 125.4, 157.0, 170.6; *m/z* ESI-MS+ 167.08, $C_9H_{13}NO_2H^+$ requires 167.09 (100%); λ_{max} (CD_3CN)/ nm 271, 294, 357, 482.

4-(Acetoxymethyl)-1-methylpyridin-1-ium hexafluorophosphate(V) (26)

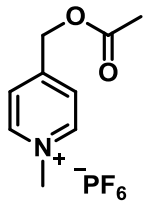

Ammonium hexafluorophosphate (10 mg) was added to a portion of the solid (35 mg) dissolved in the minimum amount of methanol. The resulting precipitate was washed with DCM and recrystallised from methanol to give the product as a white powder (28 mg, 80%); ESI-MS+ 166.08, $C_9H_{13}NO_2$ requires 167.09 (100%), λ_{max} (CD_3CN)/ nm (log ε) 273 (3.98).

Pyridin-4-ylmethyl 4-((*tert*-butoxycarbonyl)amino)butanoate (28)

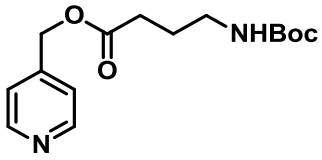

This novel compound was synthesised by adapting a reported procedure.[147] To a suspension of boc-γ-aminobutyric acid (920 mg, 4.1 mmol), 1-ethyl-3-(3-dimethylaminopropyl)carbodiimide (640 mg, 4.1 mmol) and dimethylamino pyridine (50 mg, 10 mol%) in dry THF (5 mL) was added 4-pyridylmethanol (500 mg, 4.6 mmol) in dry THF (5 mL). The reaction was stirred overnight at room temperature after which, the reaction was quenched with brine, extracted with chloroform (3 × 10 mL), dried over magnesium sulfate, filtered, and reduced to a small volume *in vacuo*. The residue was purified by column chromatography (SiO_2: $CHCl_3$ to 99:1 $CHCl_3$:methanol) to afford a white powder (960 mg, 72%); δ_H (400 MHz, $CDCl_3$) 1.41 (s, 9H), 1.81-1.85 (m, 2H), 2.42-2.46 (t, 2H), 3.15-3.17 (m, 2H), 4.77 (br, 1H), 5.11 (s, 2H), 7.21-7.23 (d, 2H), 8.57-8.58 (d, 2H); *m/z* ESI-MS+ 295.2, $C_{15}H_{23}N_2O_4^+$ requires 295.2.

Pyridin-4-ylmethyl propionate

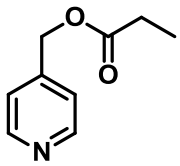

Propionic acid (620 µL, 8.3 mmol) dimethylaminopyridine (100 mg, 0.83 mmol) and dicyclohexylcarbodiimide (1.72 g, 8.34 mmol) were dissolved in dry THF (10 mL) and stirred for 15 mins. To this solution was added 4-pyridyl methanol (1.0 g, 9.2 mmol) and the reaction left to stir overnight under nitrogen at room temperature. The following day, the reaction mixture was filtered and extracted with DCM. The organic extractions were combined and washed with saturated aqueous ammonium chloride (10 mL) and water (10 mL). The crude product was purified by column chromatography (SiO_2: 99:1 DCM:methanol) to afford an orange oil (950 mg, 69%); δ_H (400 MHz, $CDCl_3$) 1.13-1.19 (t, 3H), 2.40-2.45 (q, 2H), 5.28 (s, 2H), 7.22-7.24 (d, 2H), 8.57-8.59 (d, 2H); δ_C (125 MHz. $CDCl_3$) 9.0, 27.4, 64.1, 121.8, 145.0, 150.0, 173.9.

Chapter 3: Peptide-conjugated porphyrin dimers for photodynamic therapy

This chapter discusses the use of porphyrin dimers as photosensitisers for two-photon photodynamic therapy (TP-PDT) as well as methods of improving their biocompatibility. The synthesis of three peptide-appended dimers is described, formed by the reaction of short hydroxylamine-appended peptides with a bis-aldehyde porphyrin dimer to form an oxime-linked system. This reaction is investigated before the photophysical properties, in vitro *cytotoxicity, pharmacokinetic, and one-photon PDT efficacy of the dimers is explored.*

3.1 Introduction to PDT and Historical Overview

Modern photodynamic therapy combines two individually non-toxic components (laser light and a photosensitiser) to produce a cytotoxic effect *via* the excitation of cellular oxygen. It is used to treat any condition characterised by an abnormal and unwanted growth of cells,[149,150] with its two main applications being the treatment of cancer and age-related macular degeneration (AMD).[151,152] Despite its relative infancy, as a clinical technique it is sufficiently developed that it is considered the fourth strategy in the treatment of cancer, behind surgery, chemo- and radio-therapy.

Light has been used as a therapy for various diseases (including psoriasis, vitiligo and skin cancer) for thousands of years.[153] The earliest report of the use of light in combination with a chemical to induce cell death was by Oscar Raab in 1900, who observed that certain wavelengths of light were lethal to infusoria (*paramecium caudatum*) in the presence of acridine.[154] Tetrapyrroles, the basis of most modern PDT drugs, were identified as valuable photosensitisers by Friedrich Meyer-Betz in what was the first example of photodynamic therapy on a human subject in 1913. After injecting 200 mg of hematoporphyrin (Hp) into his own hands, Friedrich observed their reddening and swelling upon exposure to light. [155]

The modern era of PDT began in the 1960s with the further investigation of hematoporphyrin. Following observations by fluorescence spectroscopy, Lipson and Baldes noted the accumulation of Hp in neoplastic tissue after administration to a live patient.[156,157] They noted that the impurities in Hp were a more effective tumour marker than Hp itself, which led to the development of an optimised preparation of the active components known as Hematoporphyrin derivatives (HpD).[158,159] This consists of a mixture of hematoporphyrin oligomers formed as by-products in the synthesis. In 1972, Diamond postulated that the combination of phototoxicity and tumour-localisation observed in many porphyrin derivatives could be exploited in the treatment of cancer.[160] The first significant breakthrough to this end was achieved by Dougherty, who reported that a combination of HpD and red light resulted in the eradication of mammary tumour growth in mice.[161,162] Similar results were reported by Kelly and co-workers for the treatment of bladder carcinoma in mice.[163] This flurry of promising results quickly led to clinical trials of HpD in humans. In 1976, Kelly initiated a study on bladder cancer in which five patients were diagnosed using HpD. Another patient with recurrent bladder cancer, who had not responded to traditional treatment, exhibited slowing of tumour growth and tumour necrosis in areas treated with

PDT.[164] A further trial by Dougherty used HpD to treat 25 patients with a total of 113 primary or secondary skin tumours. A complete response was observed in 98 tumours; while 13 showed a partial response and 2 were treatment resistant.[165] The results of these trials led to the clinical approval of a partially purified HpD preparation in 1995, which became the first PDT drug, marketed under the name Photofrin.

3.1.1 Mechanism and Clinical Procedure

PDT drugs are administered to the patient either by injection or, in the case of skin conditions, topical application. The protocol is generally simple, with superficial lesions often only requiring local anaesthetic. Due to the limits of light penetration through skin, the administration of a light dose to internal organs requires more complex procedures. Hollow organs such as the oesophagus and lungs can be irradiated endoscopically, while less accessible tumours can be reached by interstitial probes.[166,167]

The light dose is administered after a prescribed period of time to allow the photosensitiser to accumulate in the diseased cells. Following the absorption of light, the photosensitiser enters a long-lived triplet excited state *via* a short-lived singlet state. The photosensitiser can return to the ground state by one of two mechanisms: Type I or Type II.[168] Type I reactions involve the formation of radical species in the cellular environment which react with oxygen to produce cytotoxic reactive oxygen species whereas type II reactions result in the formation of singlet oxygen ($^1O_2$) directly *via* a spin-allowed triplet-triplet interaction between the photosensitiser and cellular oxygen.[169] In practice, both of these mechanisms operate simultaneously, but Type II is thought to dominate.[170] Because PDT is an oxygen-dependent treatment, anoxic regions of tissue are not affected, and it has been shown that induction of hypoxia *in vivo* eliminates the PDT effect.[171]

The primary cytotoxic species produced by PDT is singlet oxygen. Due to its highly reactive nature, this species has a typical lifetime of 3 μs in biological systems and an action radius on the sub-cellular scale (0.02 - 2 μm).[172,173] Therefore, in order to achieve a PDT effect, a significant amount of the photosensitiser must accumulate in the diseased tissue and, if possible, a tumour-targeting approach is favoured. The formation of singlet oxygen can kill cells directly by inducing non-specific necrosis, or by initiating apoptosis, autophagy or both. Apoptosis and autophagy commonly occur after damage to the mitochondria or endoplasmic reticulum.[174] The supply of nutrients and oxygen to tissue through blood vessels is important to cell viability, so targeting the tumour vasculature can induce cell death indirectly through

effects such as hypoxia and anoxia.[175] It is thought that PDT can result in cell death by eliciting an immune response. In the 1980s and 1990s, it was reported that tissue treated with PDT was infiltrated with leukocytes, lymphocytes and macrophages, suggesting an immune response had been triggered.[176,177]

Following the PDT procedure, dead cells are removed or reabsorbed by the organism, and re-epithelialisation results in little or no scarring. These excellent cosmetic results make PDT an invaluable technique for lesions on exposed areas of skin. In contrast to chemo- and radio-therapies, there is no dose limit associated with PDT, so it can be used repeatedly or in conjunction with other treatment.[178]

3.1.2 Commercial and Clinical Photosensitisers

There are several commercial photosensitisers which are licensed for clinical use. **Figure 79** shows those most commonly used.

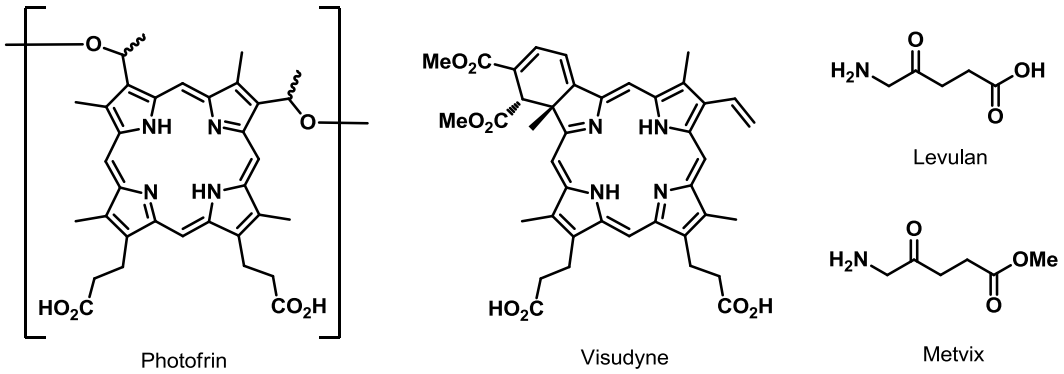

Figure 79: *Four photosensitisers for one-photon PDT which are approved for clinical use in the USA and/or Europe.*

The majority of photosensitisers available today and those currently in clinical trials are based on a tetrapyrrolic structure. There are several reasons why derivatives of this structure (which includes porphyrins and chlorins) are popular.[179] In general, they exhibit absorption at long wavelengths which minimise cell photodamage and maximise tissue penetration, they are known to form triplet excited states which can lead to efficient singlet oxygen formation and they are often highly fluorescent, so biodistribution can be monitored orthogonally. Furthermore, their synthesis is well-developed and, as previously mentioned, they show tendency to accumulate in malignant tissue.

Photofrin, the most common non-dermatological photosensitiser, is used for the treatment of oesophageal cancer, non-small cell lung cancer and Barrett's oesophagus. In addition, it is

prescribed to treat bladder, cervical, and stomach cancer. Excitation of the photosensitiser occurs at 630 nm, a wavelength at which Photofrin's absorption is relatively weak, allowing for tissue penetration of 4-6 mm.[66] The light dose is administered between 48 and 72 hours after drug administration, which indicates relatively slow accumulation in diseased tissue. Skin photosensitivity can persist for 4-6 weeks after application, which causes considerable inconvenience to the patient.[180] Despite this, and perhaps owing to the lengthy clinical trials required to develop a replacement, Photofrin is still the most popular photosensitiser for this application.

For dermatological applications, the haem precursor 5-aminolevulinic acid (5-ALA, Levulan) is the most common photosensitiser.[181] It is approved for the treatment of the non-malignant skin disorder actinic keratosis in the USA,[182] while its methyl ester is licensed for the same purpose in Europe.[183] 5-ALA is a pro-drug which is enzymatically converted to the endogenous chromophore protoporphyrin IX (PpIX) in nucleated cells.[184] It tends to accumulate in malignant tissue due to its deficiency in the enzyme ferrochelatase, which converts PpIX into the non-photoactive compound, haem. Due to its application to superficial lesions, it is most often applied topically, 3-6 hours before the light dose (which can use red, green or blue light). The maximum penetration into tissue which can be achieved is 2 mm.[180]

A second generation of photosensitisers resulted in the development of verteporfin, and its commercial formulation, Visudyne.[185] A highly successful treatment for the wet form of AMD, this photosensitiser represents a significant improvement in clinical applicability.[186] Following intravenous infusion, only a 15 minute wait is required before the light dose (690 nm, 600 mW cm^{-2}) is applied for approximately 1.5 minutes through the front of the eye.[187] As well as its rapid clinical procedure, the photosensitiser is excreted quickly and no photosensitisation is seen after 24 hours.

The major disadvantage of the current clinical photosensitisers is that light penetration into tissue is low due to absorption by endogenous chromophores and scattering. The region of the spectrum where light transmittance through tissue is highest does not correlate with the absorption maxima of the clinical photosensitisers described so far. In addition, a rational approach to photosensitiser design would aim to improve biodistribution, water-solubility and pharmacokinetic properties.

3.1.3 Two-Photon PDT

The use of two-photon absorption to excite PDT photosensitisers offers an opportunity to reduce the difficulties caused by the absorption of endogenous chromophores and scattering. Two-photon absorbing chromophores typically exhibit peak TPA in the near-IR region, which coincides with the region at which the transmittance of animal tissue is highest (**Figure 80**). Furthermore, excitation by TPA is effectively limited to the focal volume of the laser; hence highly targeted PDT could be envisaged.

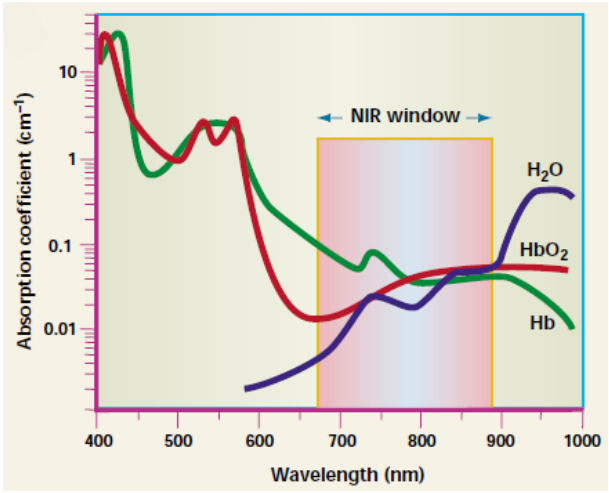

Figure 80: *The relative absorption coefficients of water (blue) oxygenated haemoglobin (red) and deoxygenated haemoglobin (green). There exists a window between approximately 700 and 900 nm in which the relative absorption of these species is at its lowest. Adapted, with permission, from reference 188.*

If two-photon absorption itself could not be realised until the invention of the laser, it took until the invention of the femtosecond-pulse laser before TP-PDT could be properly investigated. Earlier experiments using nanosecond-pulse lasers were limited by the high irradiation powers required to achieve TP-PDT, which led to hyperthermia and non-specific tissue damage. In these experiments, it was unclear whether the dominant mode of cell death was by means of a PDT mechanism or the result of photothermal effects.[189,190] Following the introduction of the femtosecond pulse laser, TP-PDT experiments could be performed at powers low enough to minimise photothermal damage. The first report of two-photon PDT used a Ti:Sapphire laser to excite a psoralen derivative, and demonstrated PDT by killing *Salmonella typhimurium* cells.[191] The first extensive and quantitative proof of a photodynamic effect by two-photon absorption was performed by the groups of Prof. Brian C. Wilson and Prof. Harry Anderson.[192] Using the commercially available photosensitisers Photofrin and Visudyne, a quadratic dependence of TP-PDT on light intensity was

demonstrated for the first time. Despite the availability of suitable light sources for TP-PDT, the clinical photosensitisers accessible at this point were not efficient two-photon absorbers (Photofrin δ_a = 10 GM and Visudyne δ_a = 50 GM).

Significant research towards a rationally designed TP-PDT photosensitiser performed has also been reported by the Anderson group. In 2004, the photophysical evaluation of a series of π-conjugated porphyrin dimers with exceptionally high TPA cross-sections was reported (**Figure 81**).[13]

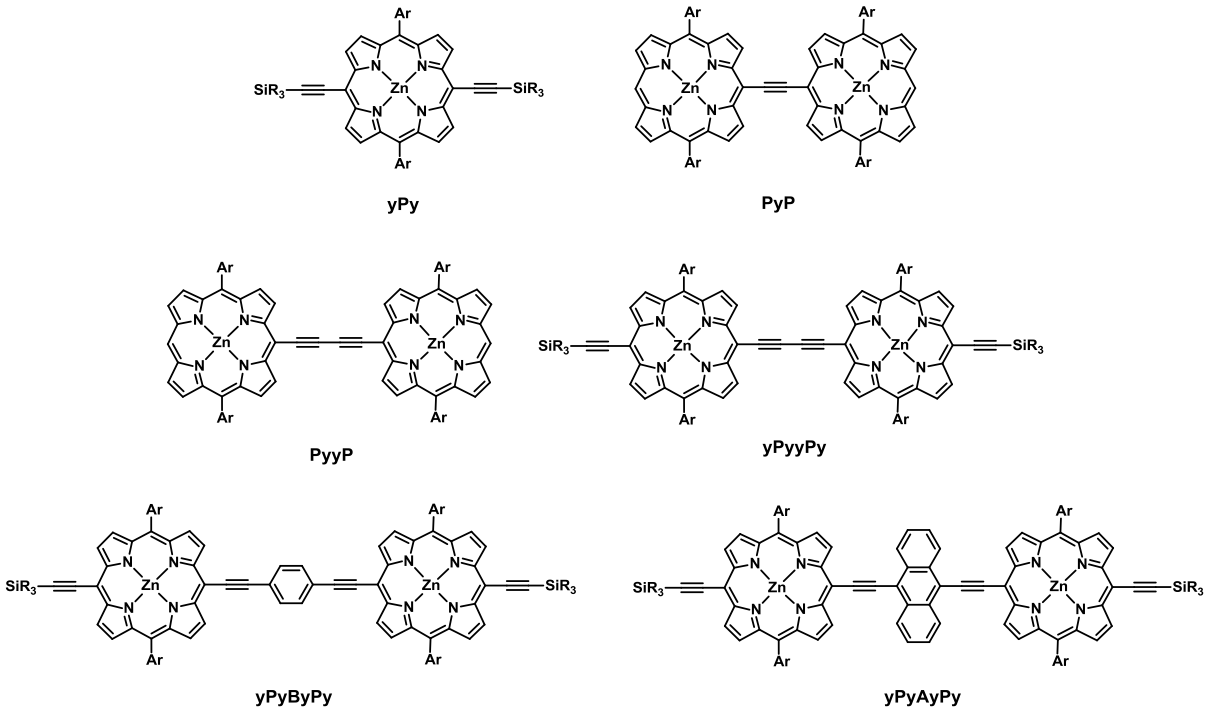

Figure 81: *A series of conjugated porphyrins with high TPA cross-sections. All the dimers exhibited a pronounced TPA peak at 820-890 nm, with TPA cross-sections ranging from 3-10 × 10^3 to 10^4GM. The highest cross-sections were observed for* ***yPyyPy*** *(9.1×10^3 GM) and* ***yPyAyPy*** *(1×10^4 GM). These were some of the highest TPA cross-sections reported at the time.*

Taking the butadiyne-linked structure (**yPyyPy**) as a basis, a series of A-π-D-π-A dimers were synthesised in an attempt to maximise the suitability for clinical TP-PDT.[36]

A major challenge for the design of TP-PDT photosensitisers is overcoming the poor solubility of two-photon chromophores. As discussed, compounds which exhibit intense TPA contain a large, planar π-conjugated chromophore, characteristics which lead to poor solubility, particularly in water. To improve the water-solubility of the porphyrin dimers, tri-ethyleneglycol substituted aryl groups were added at the 5 and 15 positions of each porphyrin

core. In addition, a variety of solubilising groups attached at the remaining meso positions were investigated (**Figure 82**).

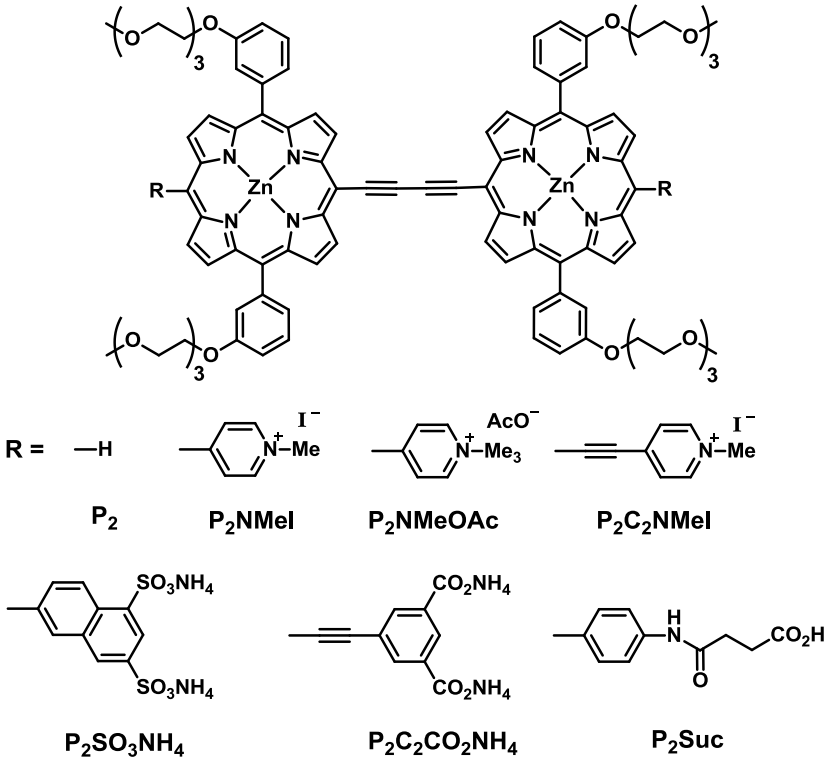

Figure 82: *The series of conjugated porphyrin dimers developed by the Anderson group as candidates for two-photon PDT photosensitisers.*

All the dimers exhibited strong one-photon absorption in the 650-800 nm range and fluorescence at 700-800 nm, with singlet oxygen quantum yields ranging from 0.5-0.9 in methanol. Their two-photon absorption properties were exceptional, with cross-sections ranging from 8,000-17,000 GM between 830 and 916 nm. Some aggregation was observed in aqueous solution, which led to a reduction in fluorescence and singlet oxygen quantum yields (ϕ_Δ). However, aggregation was demonstrated to be less of a problem under physiological conditions. Fluorescence measurements in aqueous bovine serum albumen (BSA) solution showed that protein binding disrupted aggregation, resulting in a quantum efficiency of singlet oxygen production closer to that observed in methanol. These data are summarised in **Table 6**.

Table 6: *A summary of the photophysical properties of the porphyrin dimer series.*

	OPA λ_{max} /nm	log ε_{max}	TPA λ_{max} [b] /nm	$\delta_{a\ max}$ /GM	Em λ_{max} /nm	ϕ_Δ [a] (D_2O)
P_2	482	5.62	830	5,500	712	0.14
P_2NMeI	458	5.31	838	8,700	760	0.50
P_2C_2NMeI	471	5.45	916	17,000	800	0.25
P_2NMe_3OAc	455	5.36	830	8,300	733	0.36
$P_2C_2CO_2NH_4$	463	5.57	878	14,000	725	0.59
$P_2SO_3NH_4$	458	-	725	-	780	0.24
P_2Suc	460	5.40	838	10,000	729	0.43

[a] *versus Chla in ether,* [b] *TPA λ_{max} is the wavelength at which the highest two-photon absorption cross-section was measured.*

One-photon phototoxicity studies *in vitro* showed that none of the dimers were significantly toxic to SK-OV-3 cells in the absence of light at concentrations up to 20 μM, and only exhibited mild dark toxicity up to 40 μM. All dimers, except **$P_2C_2CO_2NH_4$**, exhibited some cytotoxicity following irradiation with red light (657 nm). **P_2NMe_3OAc** (LD_{50}(light) 2.5 ± 0.3 min), **P_2C_2NMeI** (LD_{50}(light) 3.1 ± 0.8 min) and **P_2NMeI** (LD_{50}(light) 4.7 ± 0.2 min) showed the most pronounced PDT effect (**Figure 83**).[193]

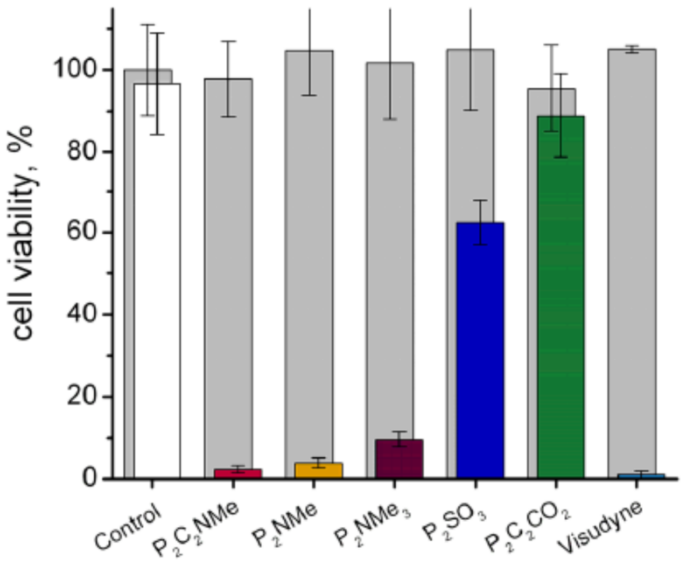

Figure 83: *The effect of incubation of the porphyrin dimers on the viability of SK-OV-3 cells with (black) and without (grey) a one-photon light dose (657 nm). Reproduced, with permission, from reference 192.*

Despite having more intense absorption at the irradiation wavelength, the dimers' one-photon PDT efficacy was found to be lower than that of the commercial photosensitiser Visudyne (LD_{50}(light) 0.5 ± 0.1 min).

Optimisation of photosensitiser concentration, incubation time and irradiation length resulted in the selection of **P_2C_2NMeI** as the most effective all round photosensitiser, and this compound was tested under two-photon conditions. Discrete areas (230 μm x 230 μm) of a monolayer of SK-OV-3 cells incubated with **P_2C_2NMeI** were irradiated (920 nm, 300 fs, 6.8 mW) for increasing periods of time (**Figure 84**).

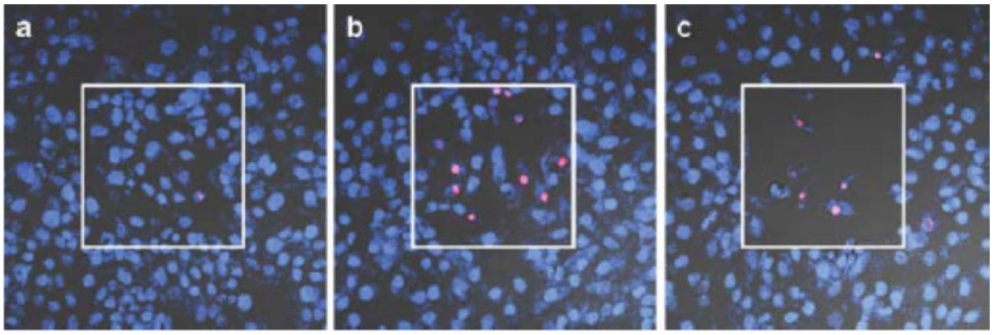

Figure 84: *Confocal fluorescence images from two-photon PDT experiments on SK-OV-3 cells with **P_2C_2NMeI**. Only the region enclosed in the white box (230 μm x 230 μm) was irradiated. The combined transmission and fluorescence images are shown. Cells were stained with Hoescht 33258 (blue) and cells with compromised plasma membranes are co-stained with Sytox orange (magenta). The central region was irradiated at 920 nm for (a) 60 scans (b) 100 scans and (c) 320 scans. Reproduced, with permission, from reference 192.*

Subsequent cell viability staining demonstrated an increase in the levels of cell death with increasing irradiation time. A plot of log[LD_{50}(light)] against log[(laser power)$^{-1}$] exhibited a linear dependence, proving that the cytotoxicity was the result of two-photon absorption at 920 nm. Comparison of **P_2C_2NMeI** with Visudyne under identical two-photon excitation conditions demonstrated the porphyrin dimer's greater cytotoxic efficiency (LD_{50}(light) 110 ± 30 s) over Visudyne (LD_{50}(light) 180 ± 30 s). This is in contrast to the one-photon PDT efficacy; the dimer's vastly superior two-photon absorption cross-section compensates for its lower PDT efficacy.

Studies on the dimer's biodistribution *in vitro* suggested that **P_2C_2NMeI** localised mostly in lysosomes. Investigations were recently made into the *in vivo* biodistribution and pharmacokinetics of **P_2C_2NMeI**.[194] Fluorescence spectroscopy performed on organ samples analysed *ex vivo* showed localisation of the photosensitiser in the liver, kidneys and heart as well tumours, but the concentration in plasma was 5-10 times higher than in other tissues. In

most tissues, the fluorescence signal peaked at 3-12 hours after injection and, over the 24 hour analysis period, a shift in the fluorescence maximum was observed, suggesting metabolism of the photosensitiser was occurring.

3.1.4 Project Aim

In summary, the previous research of the Anderson group represents a significant step forward in the development of photosensitisers for the photodynamic treatment of cancer and other neoplastic disorders. The porphyrin dimer has been extensively evaluated as a potential TP-PDT photosensitiser and has demonstrated excellent absorption, singlet oxygen production and TP-PDT characteristics. Investigations into biological compatibility have shown significant aggregation of the dimer under aqueous conditions, while pharmacokinetic and biodistribution studies have shown some propensity for tumour localisation and moderate tissue accumulation times. Now that a photosensitiser with optimised two-photon photophysical characteristics has been established, the next generation of two-photon PDT photosensitisers can be designed, focussing on the optimisation of the biological compatibility, pharmacokinetics, and biodistribution.

The aim of this project is to investigate how conjugating the porphyrin dimer with biomolecules known to facilitate cell uptake and/or target specific organelles or cellular processes affect its photophysical, biological and pharmacokinetic properties.

3.2 Targeted Two-Photon Photodynamic Therapy

3.2.1 Peptide-Conjugation for Improved Drug Delivery

Biological membranes are natural barriers through which only compounds within a narrow range of molecular size, net charge, and polarity are able to diffuse effectively.[195] As such, one of the main constraints on the design of drugs whose targets of interest are located within cells is membrane permeability.[196] The use of cell-penetrating and cell-targeting peptides to facilitate the uptake and localisation of foreign molecules is well established, and there are numerous examples of the uptake of oligonucleotides,[197,198] nanoparticles,[199,200] and organic macromolecules[201,202] using this strategy.

Peptides offer an attractive prospect because of their low toxicity and because several sequence-specific interactions with membrane receptors are known. For PDT, they are of particular interest because of their general resistance to radical oxidation.[203] The downside of

using peptides is that they are easily digested by enzymes *in vivo*. Despite this, the use of peptide conjugation for targeted or improved cellular drug delivery is a large and growing field.[204] There are a number of peptides which have been shown to improve the uptake of organic compounds, including the HIV-1-derived Tat protein and Antennapedia (marketed commercially as Penetratin).[205] Studies of these sequences led to the discovery that, in general, peptide sequences with a high proportion of cationic residues (arginine (R) or lysine (K)) gave improved cell penetration.[206] Interestingly, L-arginine has been shown to be more effective than D-arginine, presumably because many digestive enzymes cannot act upon it.[207] The proposed mechanism of cell uptake begins with the interaction of the peptide with the numerous anionic residues at the cell surface, facilitating its subsequent translocation by endocytosis.[208] Cell-targeting peptide research has generally focused on the RGD sequence (the first identified tumour-targeting peptide), which is known to interact strongly with integrin receptors (see **Section 3.3.2**). Cell-targeting peptides can be identified by structural elucidation of the binding sequence (e.g. X-ray crystallography), phage display, or using combinatorial peptide libraries.[226]

In PDT research, many peptide-conjugated porphyrin photosensitisers have been reported which show enhanced properties.[209] Pertinent examples include tetraphenylporphyrin (TPP) derivatised with the peptide sequence Asp-Tyr-Trp-Lys-Pro-Pro-Arg which demonstrated a twenty-five fold increase in uptake rate compared to TPP alone, as well as a tenfold increase in phototoxicity.[210] The peptide sequence is known to bind neuropilin-1, a cell membrane surface receptor commonly over-expressed in cancer cells, and was coupled to TPP *via* aminohexanoic acid using solid-phase synthesis. However, the hydrophilicity of the photosensitiser and peptide limited its use in a clinical setting.

A derivative of chlorin (a porphyrin derivative in which one pyrrole alkene is reduced) appended with the nucleus-targeting peptide sequence Asp-Pro-Pro-Lys-Lys-Lys-Arg-Lys-Val-Gly-Asp-Pro from the simian virus T antigen. The peptide was coupled by activation of the native carboxylic acid on the chlorin and reaction with the *N*-terminus of the peptide during solid-phase peptide synthesis. This peptide conjugate showed improved cellular uptake compared to the non-conjugated photosensitisers, and an enhanced cytotoxic effect was observed as a result of oxidative damage to DNA.[211] Extension of this research by another group led to the development of bifunctional peptide-conjugated porphyrins which contained a single linear sequence consisting of both a nucleus-localising sequence and a

cell-penetrating peptide.[212] Again, conjugation was achieved by amide formation between the peptide and a functionalised porphyrin during solid-phase peptide synthesis. The peptide conjugates demonstrated significantly increased accumulation in HEp2 cells compared to the non-conjugated dimer and showed enhanced cytotoxicity.

3.3 Peptide Selection

3.3.1 Targeting Cancer

The term cancer covers a broad range of over one hundred diseases, all characterised by the deregulation of various cellular processes resulting in uncontrolled cell proliferation.[213] This behaviour occurs following the accumulation of discrete genetic abnormalities, resulting in deviation from the homeostatic mechanisms that control normal cell growth.[214] More recently, focus has been laid on the importance of reprogrammed metabolic pathways in tumour formation and development.[215,216]

That cancerous cells exhibit deregulated processes and genetic abnormalities allows the designers of targeted cancer treatments to gain some selectivity for cells which, in many respects, are indistinguishable from non-cancerous cells. There are thought to be six acquired capabilities which cancerous cells develop during their progress from normality to neoplasticity: self-sufficiency in growth signals, insensitivity to anti-growth signals, tissue invasion and metastasis, limitless replicative potential, sustained angiogenesis and evasion of apoptosis.[48] A selection of these capabilities will be discussed in the context of targeted photodynamic therapy.

3.3.2 Angiogenesis

Angiogenesis is the process of new blood vessel development, and is essential for cell growth and repair, particularly during embryogenesis.[217] During rapid cell proliferation, avascular diffusion cannot provide sufficient oxygen and nutrients to support the cell multiplication occurring, so the growth of new blood vessels becomes essential. Tumour growth is characterised by rapid cell proliferation and thus the occurrence of angiogenesis. Whereas angiogenesis related to wound healing is tightly regulated, in association with cancer it is persistent and abnormal.[52] Angiogenesis can also induce metastasis by providing conduits for the transport of tumour cells to new sites.[218]

PDT is already known to prevent angiogenesis and cause tumour regression by the induction of hypoxia either through the direct destruction of the tumour vasculature,[219] or through vasoconstriction.[220] The various receptors associated with angiogenesis, and their ligands, provide interesting targets for PDT. **Figure 85** describes the mechanism of angiogenesis and how it can result in tumour metastasis.

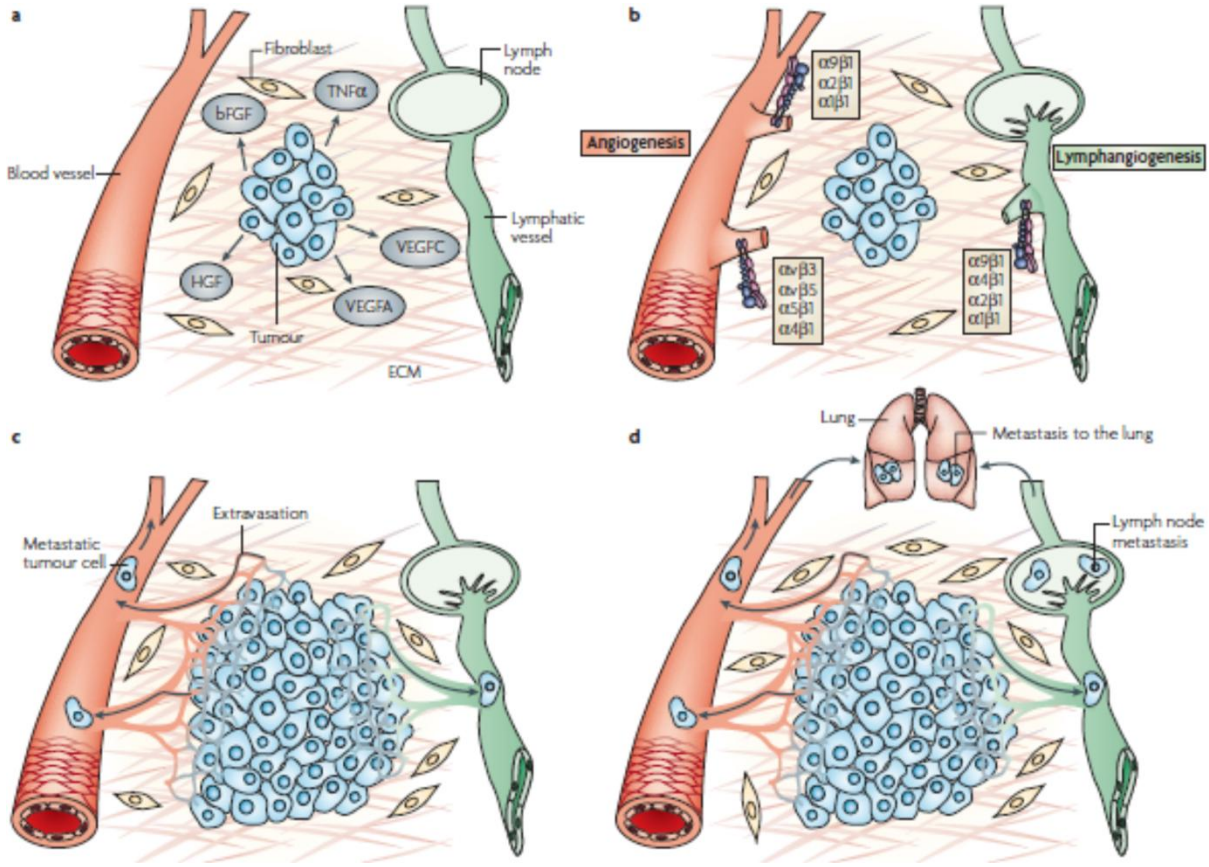

Figure 85: ***Mechanisms regulating angiogenesis and lymphangiogenesis, the formation of new lymph vessels (adapted with permission from reference 217):*** *(a) Tumour cells near pre-existing blood vessels secrete growth factors, including vascular endothelial growth factor A (VEGFA), basic fibroblast growth factor (bFGF) and tumour necrosis factor α (TNFα), that stimulate quiescent vascular endothelium to enter the cell cycle, (b) These growth factors upregulate the expression of integrins including $\alpha_1\beta_1$, $\alpha_2\beta_1$, $\alpha_4\beta_1$, $\alpha_5\beta_1$ and $\alpha_v\beta_3$ in blood vessels, while tumour-derived VEGFC promotes new lymph vessel growth in draining lymph nodes, (c) These integrins promote endothelial cell migration and survival during the invasion of tumour tissue, resulting in the formation of new vessels, which promote tumour growth by removing waste and providing nutrients to the growing tissue. The new blood and lymph vessels also provide a pathway for metastasis to occur, (d) Lymphangiogenesis promotes metastasis to the lymph nodes and sometimes more distant tissue, while angiogenesis promotes metastasis to local and distant sites such as the lungs and ECM.*

A key aspect to the process of angiogenesis is the role that integrins play. Integrins are a family of heterodimeric, non-covalently bound transmembrane receptors for (among others) extracellular matrix proteins.[217] Ligation of integrins promotes a variety of effects including intracellular signal transduction as well as cell survival and migration during angiogenesis

and lymphangiogenesis. Their dimeric structure consists of an α and β sub-unit of which eighteen α and eight β units exist, combining to form 24 different integrin receptors. A number of endothelial cell integrins have been implicated in the regulation of angiogenesis in a variety of ways, and their upregulation in tumour tissue is well known. Of particular interest to targeted cancer therapy is the $\alpha_v\beta_3$ receptor, which is widely expressed on blood vessels in human tumour biopsy samples, but not on vessels in normal human tissue.[217]

Many integrin receptors (including $\alpha_v\beta_3$) recognise the tripeptide Arg-Gly-Asp (RGD) in their ligands, a motif first identified from the interaction of the ECM protein fibronectin with the extra cellular receptors.[221,222] The crystal structure shows that the arginine residue binds the α sub-unit while the metal ion of the β sub-unit coordinates the aspartate residue.[223] Derivatives of this structure have been investigated for their binding capabilities, as the sequences flanking the RGD motif can have a significant effect on integrin selectivity.[224,225,226] This short peptide chain represents an interesting candidate peptide for conjugation to the porphyrin dimer core for promoting the localisation of the sensitiser in tumour cells.

There exists a large number of RGD-based strategies for contemporary cancer therapy, drug delivery and cancer diagnosis.[227,228] In addition to the selectivity for cancer cells they provide, antagonisation of the $\alpha_v\beta_3$ integrin receptor has been shown to induce endothelial cell apoptosis, increase the activity of tumour suppressor p53, increase levels of the cell cycle inhibitor $p21^{WAF1/CIP1}$, and decrease levels of the anti-apopototic protein BAX.[229] Furthermore, studies have shown that $\alpha_v\beta_3$ antagonisation initiates the caspase 8-dependent cell death pathway.[230] Of the potential targets, the simple RGD sequence and c(RGDfK) appear the most promising (**Figure 86**).

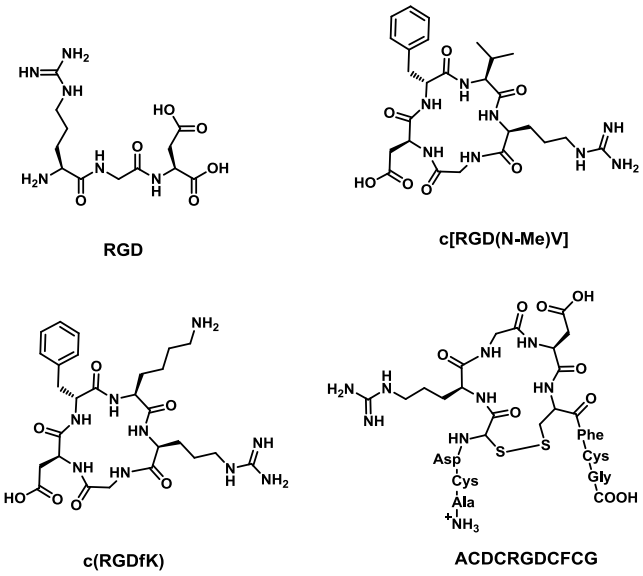

Figure 86: *Peptides containing the RGD motif which are known to ligate the $\alpha_v\beta_3$ integrin receptor.*

Cyclic RGD peptides have been shown to be more effective ligands than linear sequences, owing to their more rigid structure and enhanced stability to physiological conditions.[231] Furthermore, the presence of the lysine residue on the c(RGDfK) sequence provides a free amine which is not directly involved in integrin binding, for conjugation. Protoporphyrin IX conjugated to c(RGDfK) *via* the free lysine has been shown to demonstrate enhanced tumour localisation compared to PpIX, while maintaining the porphyrin's PDT efficacy.[232]

For my research, the simple linear RGD and c(RGDfK) were chosen as peptides for conjugation with the porphyrin dimer.

3.3.3 Mitochondria

Mitochondria are membrane-enclosed organelles found in the majority of eukaryotic cells and are their primary source of adenosine triphosphate (ATP).[233] Furthermore, they are the site from which apoptosis is activated. It is well known that cancerous cells produce most of their ATP through glycolosis, and it has been postulated that a primary factor in cell immortality and carcinogenesis is the impairment of mitochondria followed by the activation of glycolosis pathways.[234]

Oxidative stress of the mitochondria has been shown to activate apopototic pathways in cells and so they represent an important sub-cellular target for PDT.[235,236] Furthermore, it has already been established that the mode of action of the photosensitiser 5-ALA involves destruction of the mitochondria.[237] *In vitro* localisation studies of the charged porphyrin

dimers of **Section 3.1.3** have not suggested that there is significant localisation in the mitochondria, so targeting this organelle represents an opportunity to improve PDT efficacy.

As a result of their microbial origins, mitochondrial membranes share structural similarities with their bacterial ancestors; namely a large proportion of anionic lipids in their membranes. Therefore, they are susceptible to cationic peptides, as well as those with an α-helical structure. Electrostatic interactions between such peptides and the mitochondrial membrane lead to selective localisation in this membrane, while the zwitterionic phospholipids of the plasma membrane remain unperturbed. A common feature of mitochondria-targeting peptides is the presence of several arginine residues. The guanidinium moieties found on the side chain of arginine infer on the peptide the cationic properties known to allow for selective mitochondrial localisation.

There are several molecules known to preferentially localise in the mitochondria, some of which are shown in **Figure 87**.[235]

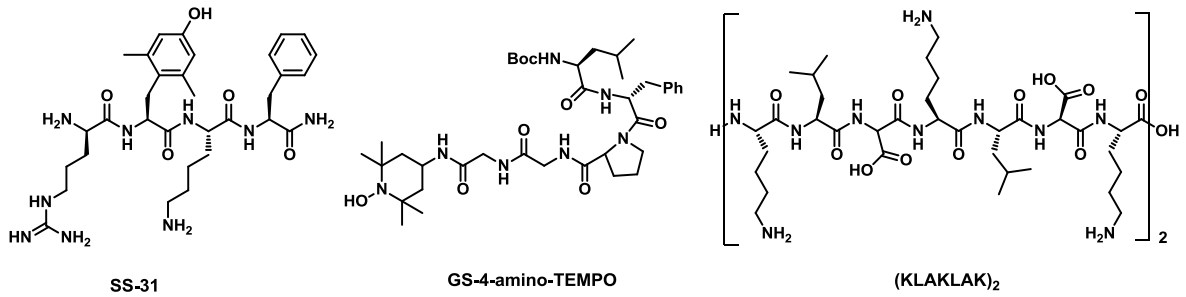

Figure 87: *Three examples of peptides and peptide derivatives which have been shown to localise in the mitochondrial membrane.*[235]

The peptide sequence **(KLAKLAK)$_2$** is a cationic, alpha-helical peptide known to localise in the mitochondrial membrane and is a realistic target for peptide conjugation with the dimer.

3.4 Peptide Conjugation Strategies

The simplest way to conjugate the porphyrin dimer with the peptides would be to couple the *N*-terminus of the peptide with a carboxylic acid-appended dimer during solid-phase synthesis. However, previous research in the group established that it is difficult to conjugate porphyrin dimers with peptides during solid-phase synthesis as poor conversion and mixtures of products are observed. In addition, the final peptide deprotection reaction with trifluoroacetic acid results in demetallation of the porphyrin. Another issue here is that direct coupling of the two components *via* an amide bond can result in poor selectivity over amino

acid side chain functional groups. The bioconjugation of macromolecules to peptides commonly includes a small linker group into the synthesis of either the macromolecule or the peptide, which is then coupled with the other component in a selective manner to produce a bond which is stable to physiological conditions.[238,239]

Selective ligation of unprotected peptides using a linker group has been examined by Tam *et al*, who investigated ligation through condensation of a hydroxylamine, cysteine or hydrazide derivative with an aldehyde (forming an oxime, thiazolidine or hydrazone bond respectively).[240] A particular attraction of these ligation techniques is that water is the only by-product from the reaction.

Thiazolidine formation offers an attractive prospect as cysteine residues can be introduced into solid-phase synthesis, good selectivity is observed, and thiazolidine formation occurs under mild conditions (37 °C, pH 4.0-5.0). Similarly, hydrazone formation occurs under mild conditions over wide pH range (pH 4.0-8.0). The disadvantage of this reaction compared to thiazolidine and oxime formation is that the resulting bond is more susceptible to hydrolysis.

For my research, an aldehyde-appended dimer was coupled to hydroxylamine-appended peptides to form an oxime link. This bond is the most hydrolytically stable of the three and has recently been used to efficiently form a variety of bioconjugates.[241,242]

So that the linker could be incorporated into the solid-phase synthesis of the peptide, it was designed to mimic an amino acid (**Figure 88**).

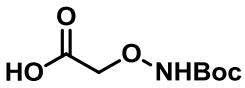

Figure 88: *The hydroxylamine or amino-oxy (AO) group which was attached to each peptide to allow for selective ligation to an aldehyde-appended porphyrin dimer.*

The carboxylic acid was coupled with the *N*-terminus of an amino acid during solid-phase synthesis. By protecting the hydroxylamine with a *tert*-butoxycarbonyl (Boc) group, it could be deprotected along with the amino acid side-chains in the final stage of peptide synthesis.

Results and Discussion

3.5 Synthesis of Peptide-Conjugated Porphyrin Dimers

The following sections report the synthesis of an aldehyde-appended porphyrin dimer and amino-oxy-appended peptides in preparation for the synthesis of peptide-conjugated porphyrin dimers.

3.5.1 Porphyrin Synthesis

An aldehyde-appended porphyrin dimer was synthesised according to **Scheme 11** by simple modification of the published procedure towards the charged dimers of **Section 3.1.3**.

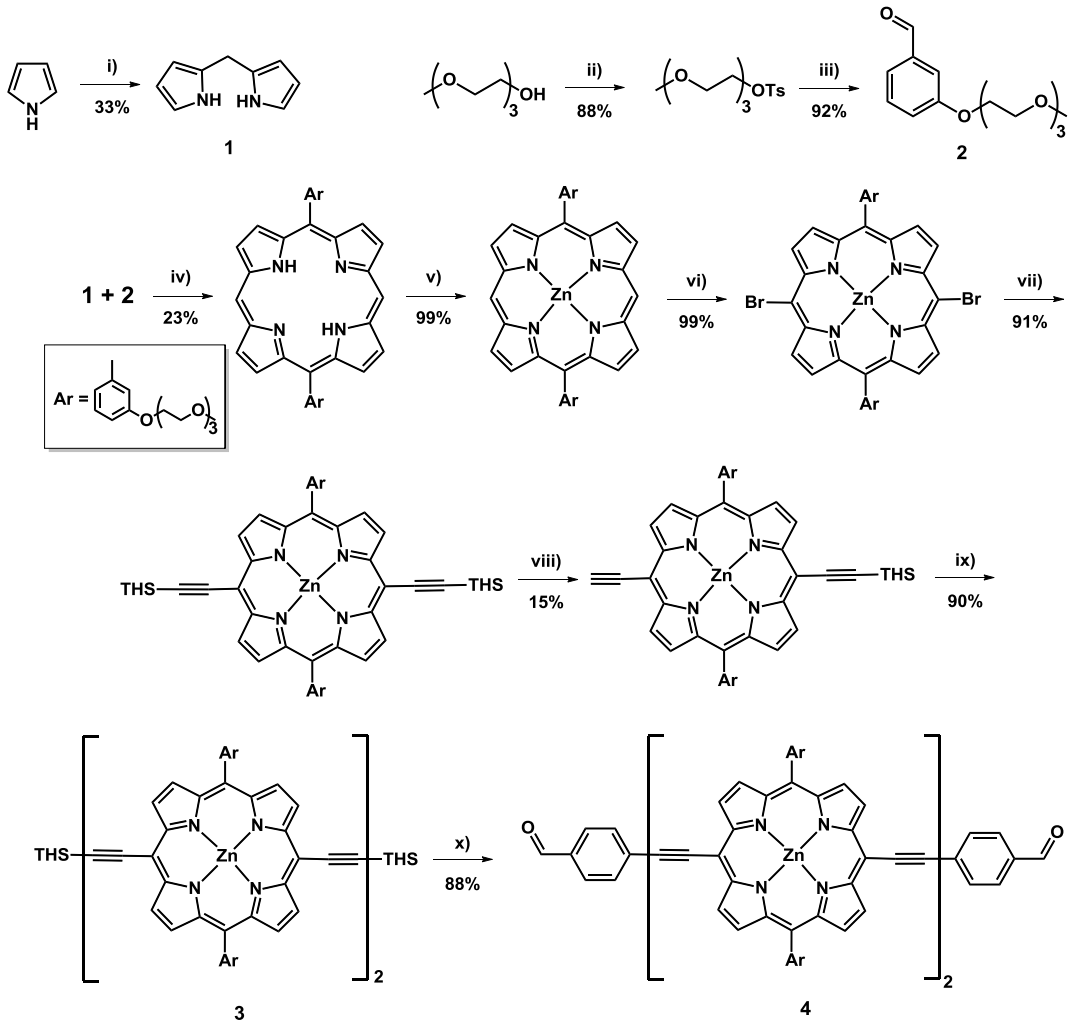

Scheme 11: *(i) Formaldehyde, TFA then DDQ (ii)* para-*toluenesulfonyl chloride, Et_3N, 0 °C – rt (iii) 3-hydroxybenzaldehyde, K_2CO_3, MeCN, reflux (iv) TFA, rt (v) $Zn(OAc)_2$, rt (vi) NBS, pyridine, rt (vii) THS-acetylene, $Pd(PPh_3)_2Cl$, CuI, PPh_3, DIPA, rt (viii) TBAF, rt (ix) Cu(I)Cl, O_2, rt, 1h (x) 4-iodobenzaldehyde, $Pd_2(dba)_3$, PPh_3, DIPA, rt (xi)* N-*hydroxysuccinimide, DCC, rt (xii) PEPTIDE, DIPA, rt, then TFA (xiii) AcOH, aniline, DMSO, 40 °C.*

As a well established synthetic route within the group, the steps to the key intermediate **3** proceeded smoothly. The final silylether deprotection and Sonogashira cross-coupling reaction could be combined in one step through *in situ* tetrabutylammonium fluoride deprotection, to give the bis-benzaldehyde porphyrin dimer in excellent yield. Compound **4** was characterised by ^{1}H NMR, ^{13}C NMR, RP-HPLC, UV-visible spectrometry and MALDI-ToF mass spectrometry.

3.5.2 Peptide Synthesis

Peptide synthesis can be most easily achieved using solid-phase synthetic techniques.[243,244] Sequential coupling and deprotection of Fmoc-protected amino acids on resin allows for easy separation of by-products and unreacted reagents from the desired products (**Scheme 12**).[245]

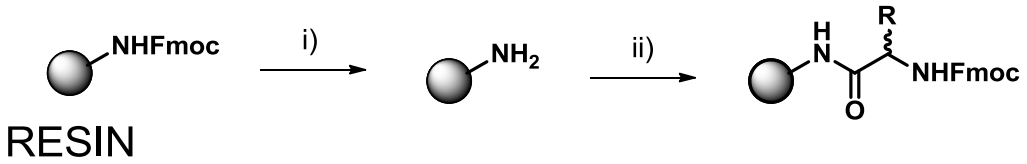

Scheme 12: *(i) 20% piperidine in DMF (ii) amino acid, coupling agent, DIPEA.*

Resins were chosen to have high acid sensitivity, so that peptides could be cleaved without deprotecting their side-chain functional groups. A variety of peptide coupling reagents are available, all of which activate the carboxylic acid group of the amino acid. For my research, coupling was achieved using either PyBOP or HBTU (**Figure 89**).

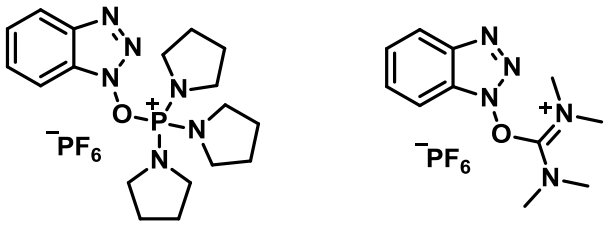

Figure 89: *Benzotriazole-1-yloxytripyrrolidinophosphonium hexafluorophosphate (HBTU) and O-benzotriazole-N, N, N', N'-tetramethyluronium hexafluorophosphate (PyBOP), the peptide coupling agents used in solid-phase peptide synthesis.*

The synthesis of the linker group and its subsequent attachment to the peptide is shown in **Scheme 13**. The linker was synthesised as an *N*-hydroxysuccinimide-activated ester and could be coupled to the peptide on- or off-resin.

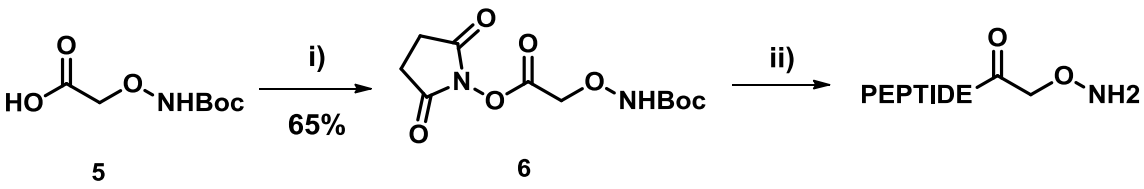

5 6

Scheme 13: *(i)* N-*hydroxysuccinimide, DCC, rt (ii) PEPTIDE, DIPA, rt, then TFA.*

3.5.3 Oxime Chemistry and Peptide Conjugaton

In order to investigate the oxime formation reaction without using precious peptide material, a simple test molecule consisting of glycine bonded to the hydroxylamine linker group was synthesised (**Scheme 14**). This compound was subsequently used to optimise peptide conjugation with **4**.

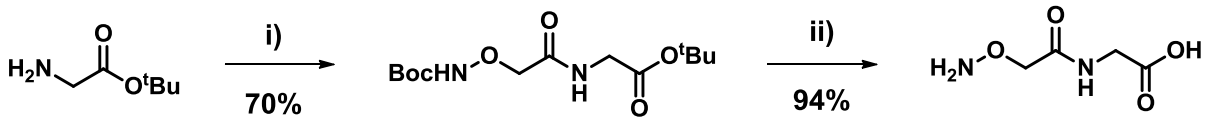

7 8

Scheme 14: *(i)* ***6****, DIPEA, DMF, rt (ii) TFA, rt.*

A literature survey suggested two possible options for optimisation of oxime formation. Firstly, oxime condensation can be catalysed by the addition of aniline.[246,247] Initial imine formation creates a more reactive intermediate which then facilitates oxime formation. Secondly, the optimum pH for oxime condensation is pH 4-5,[144] so the addition of acetic acid to reduce the reaction pH was investigated. Finally, as a bimolecular reaction, the concentration will clearly have an effect on the reaction rate.

Initially, the concentration at which all reactions would be performed was determined. Aggregation of porphyrin dimers in solution is a common problem, so it was proposed that all conjugation reactions should be performed at concentrations where no aggregation occurred. The presence of aggregation was determined by ^{1}H NMR; aggregated samples are easily identified by the broadened signals they produce. Dimethylsulfoxide-d_6 was the chosen solvent as most of the peptides were soluble only in DMSO or water, and the dimer's solubility in water was found to be very low. Initially, a concentration of 25 mM was used and this gave a very broad NMR spectrum. Reduction to 12.5 mM gave a much sharper spectrum, and so this concentration was chosen for the reaction.

The reaction between **4** and **8** (**Scheme 15**) was performed by mixing the two components in a 1:2.2 molar ratio of **4** to **8** in DMSO to give a final concentration of **4** of 12.5 mM.

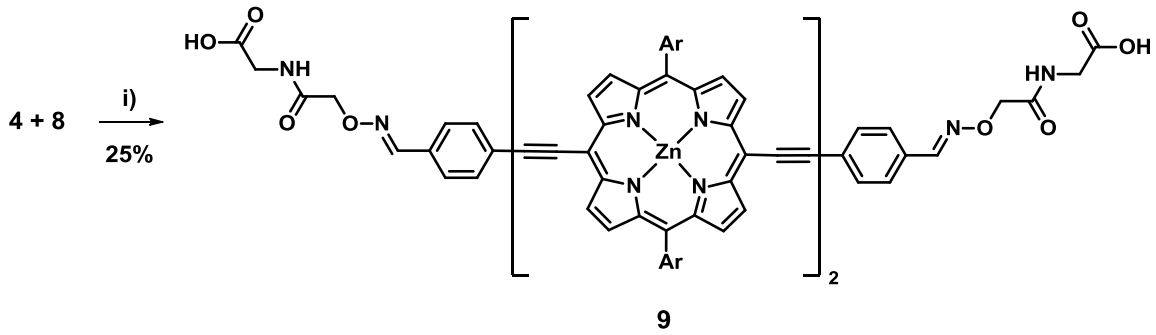

9

Scheme 15: *(i) Acetic acid:aniline 1:10 (v:v), DMSO.*

Progress was monitored by HPLC, with excellent resolution between the starting dimer, mono-substituted, and bis-substituted dimer observed. The initial reaction conditions resulted in a small amount of product formation after 2 hours. Aniline and acetic acid (1% and 10% by volume respectively) were subsequently added to catalyse the reaction, which led to an approximately equal mixture of the three components (**Figure 90a**) after further reaction for two hours.

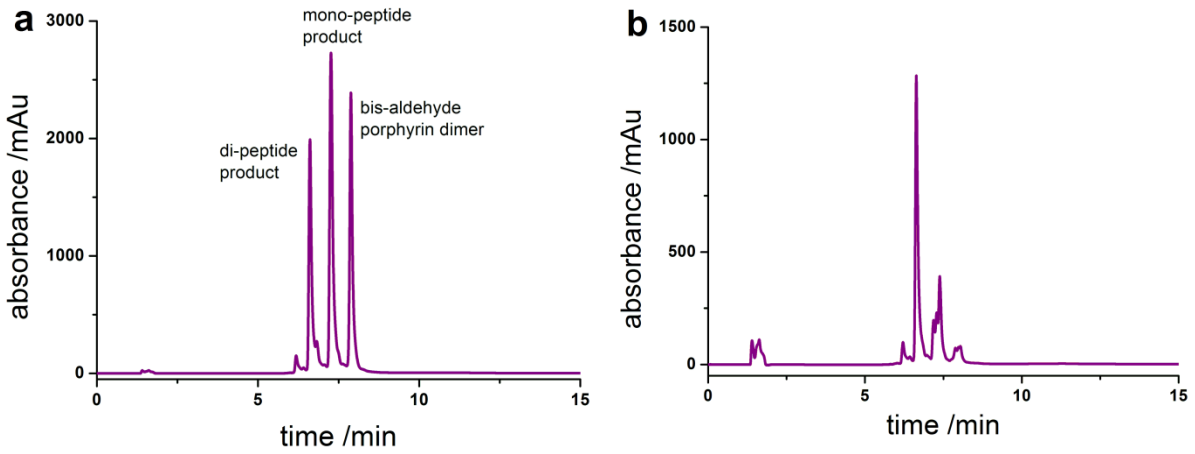

Figure 90: *Reverse-phase HPLC traces (740 nm) showing the progress of the reaction between **4** and **8**. (a) shows the excellent resolution observed between the three components, while (b) shows the reaction at completion.*

Little progress was observed from this point, so an additional 2.2 equivalents of **8** as a solution in DMSO (100 mM) was added, which led to almost complete conversion of the starting material and a high proportion of product formation (**Figure 90b**). The reaction was terminated at this point and the bis-substituted product was isolated using semi-preparative reverse-phase HPLC to give 6 mg (53%) of the desired product. Novel compound **9** was characterised by RP-HPLC, ^{1}H NMR, and MALDI-ToF mass spectrometry.

In conclusion, the reaction optimisation studies indicated that catalysis of oxime formation may be possible using a combination of acidic conditions and aniline. An amino acid conjugated porphyrin dimer was synthesised using the conditions investigated, but an excess (4.4 equivalents) of the amino acid component was still required.

3.5.4 Linear RGD

The synthesis of this compound was performed by Dr Sébastian Ulrich and *in vitro* evaluation performed with his collaboration.

The structure of linear RGD appended with the amino-oxy linker is shown in **Figure 91**.

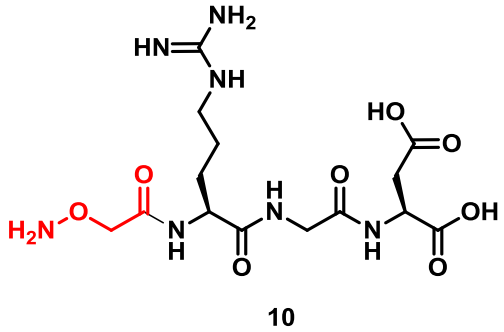

Figure 91: *The linear RGD peptide, appended with the amino-oxy linker group (red).*

The synthesis of this compound and its corresponding conjugated dimer are shown in **Scheme 16**.

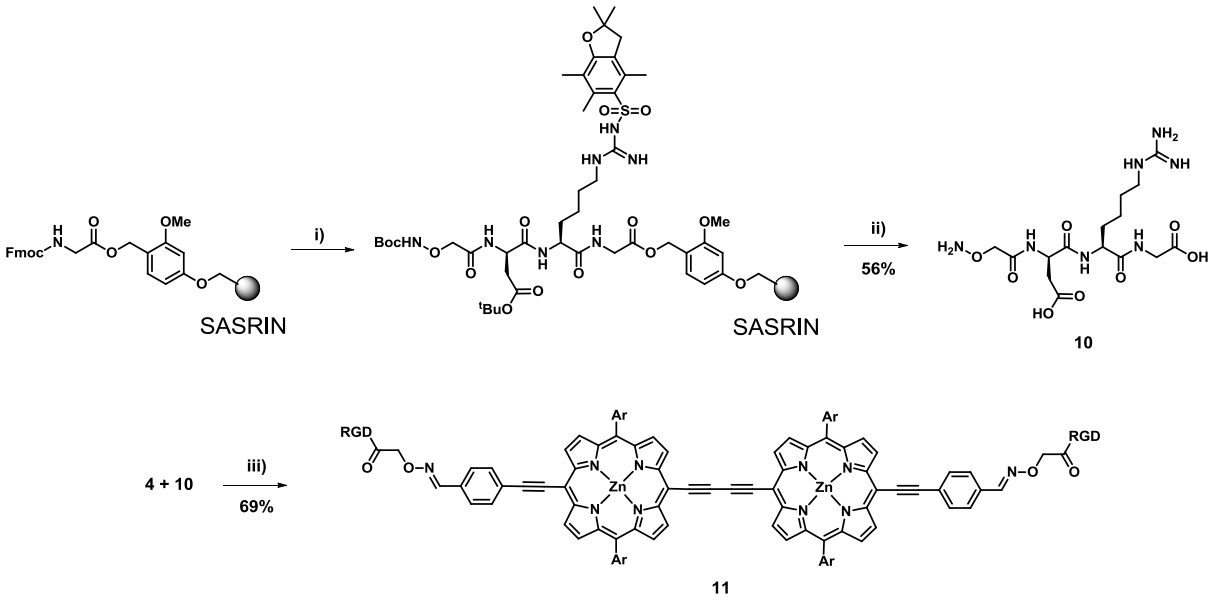

Scheme 16: *(i) 20% piperidine DMF, then amino acid, DIPEA, DMF (ii) HFIP:DCM 1:1, then TFA:DCM 1:1 (iii) DMSO, rt, 4 h.*

This peptide was synthesised using standard Fmoc solid-phase techniques on super acid-sensitive resin (SASRIN) appended with Fmoc-protected glycine. Cleavage from the resin was achieved using hexafluoroisopropanol, and deprotection of the peptide side chains was achieved using trifluoroacetic acid to yield the amino-oxy appended peptide in moderate yield. This was reacted with the porphyrin dimer (**4**) in DMSO directly to give the peptide-conjugated dimer in good yield (69%). Compound **11** was characterised by RP-HPLC and MALDI-ToF mass spectrometry.

3.5.5 Cyclic RGDfK

The structure of cyclic RGDfK, including the amino-oxy linker is shown in **Figure 92**.

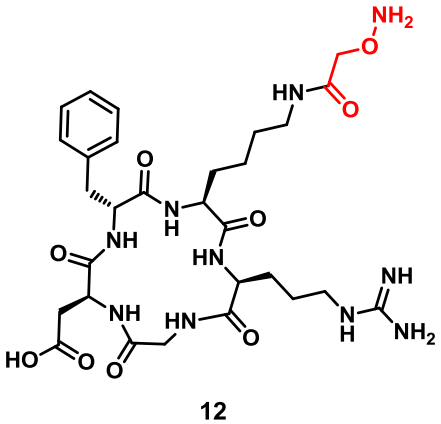

12

Figure 92: *The structure of cyclic RGDfK appended with the amino-oxy linker (red).*

The synthetic route towards this compound is shown in **Scheme 17**.

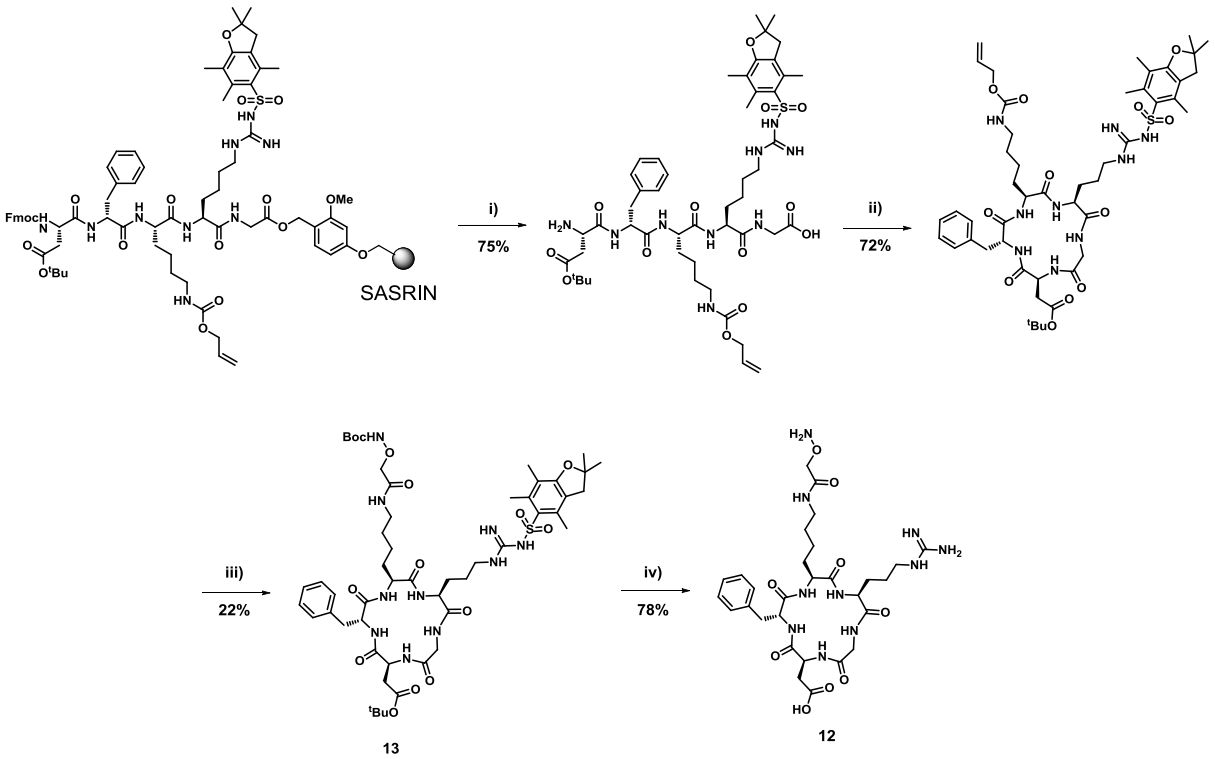

Scheme 17: *(i) Hexafluoroisopropanol, DCM, 3 × 2 min (ii) HBTU, DIPEA, 0.5 mM, rt, 16 h (iii) Pd(0)(PPh_3)$_4$, TIPS, DMF then* ***6*** *and DIPEA (iv) TFA:TIPS:H_2O 95:2.5:2.5 (v:v:v) then precipitation from ice cold diethyl ether.*

Initial solid-phase synthesis of the linear RGDfK unit was performed using the same Fmoc-Gly-SASRIN resin used to synthesise linear RGD. In addition, the same coupling and deprotection conditions were employed. Cleavage of the linear sequence was performed using hexafluoroisopropanol, yielding a compound with a single peak in the RP-HPLC trace and a mass spectrum corresponding to the desired product. This indicated that all coupling reactions had been successful and that the side-chain protecting groups remained intact.

Following cyclisation, selective deprotection of the allyoxycarbonyl (alloc) protecting group was achieved using tetrakistriphenylphosphine palladium(0) in the presence of the hydride donor phenylsilane.[248] It was found that this reaction gave best results when good quality (i.e. bright yellow) tetrakistriphenylphosphine palladium(0) was used. The free amine was then reacted with the amino-oxy activated ester compound to give compound **13**. The amino acid protecting groups were subsequently removed by acid hydrolysis to yield compound **12**, which was purified by RP-HPLC. Analysis of **12** and the intermediates isolated after initial

on-resin synthesis was performed by ^{1}H NMR because published data relied only on mass spectrometry for characterisation and to confirm purity.[249]

A modified route towards the product was investigated in which deprotection of the alloc group and coupling of the amino-oxy linker was performed on resin (**Scheme 18**). This is likely not part of the published procedure for two reasons: firstly the palladium catalysed deprotection is oxygen sensitive (freeze-thaw degas cycles are used in the published procedure) and secondly, diisopropylethylamine is used in the amino-oxy coupling, to which the Fmoc group may be sensitive. On-resin attachment was attempted because the solid-phase synthetic procedure already requires vigorous nitrogen bubbling in order to mix the resin and solution-phase reactants, and there is also precedent for the activated ester reaction occurring without a base present.[250,251] This strategy proved successful, and furnished compound **9** in a similar yield to the published procedure using a route which is far more convenient.

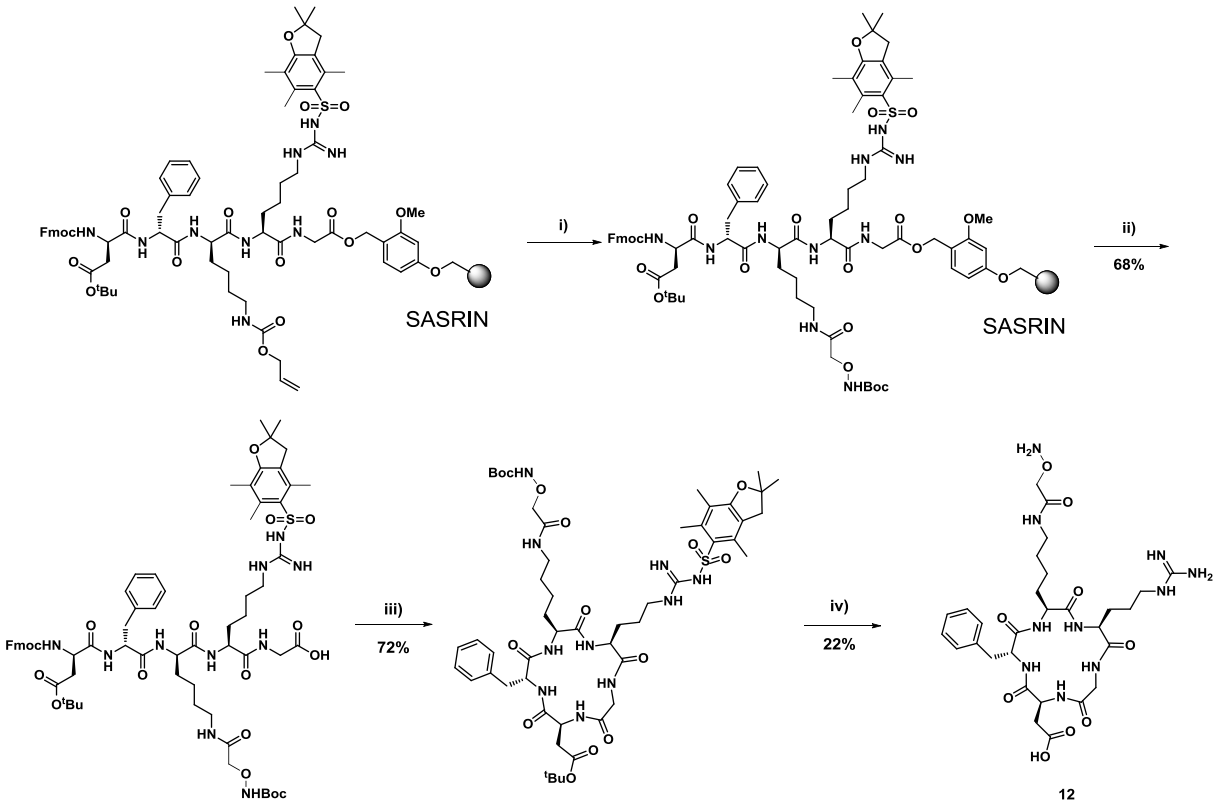

Scheme 18: *(i) $Pd(PPh_3)_4$, $PhSiH_3$ then **6**, DMF (ii) hexafluorisopropanol, DCM, 4 × 2 min (iii) HBTU, DIPEA, 0.5 mM, rt, 16 h (iv) TFA:TIPS:H_2O 95:2.5:2.5 (v/v/v) then precipitation from ice cold diethyl ether.*

The reaction between **12** and **4** was performed using the optimised conditions developed for compound **9**. The reaction proceeded similarly, with high conversion observed by RP-HPLC (**Figure 93**).

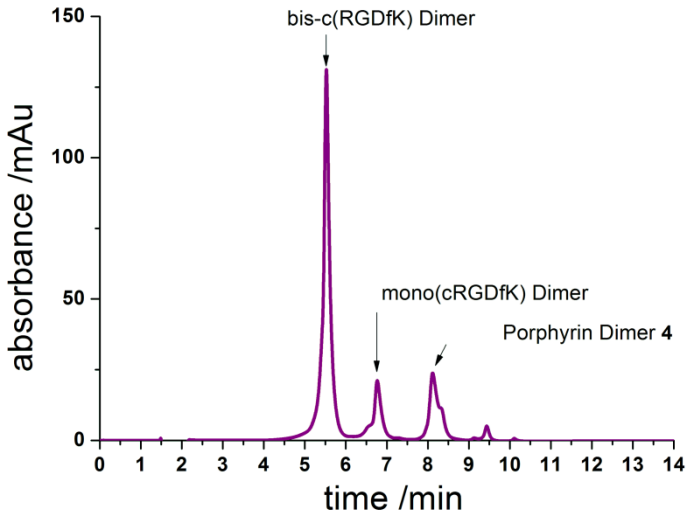

Figure 93: *An RP-HPLC trace (740 nm) showing the bis-peptide conjugated dimer, the mono-conjugate and the unsubstituted dimer (**4**).*

Subsequent purification using semi-preparative RP-HPLC appeared to result in decomposition of the product at 5.6 mins. As with previous peptide conjugates, the fractions were combined, the organic solvents were removed by rotary evaporation and then water was removed by lyophilisation. This resulted in profound changes in the HPLC trace and absorption spectrum (**Figure 94**).

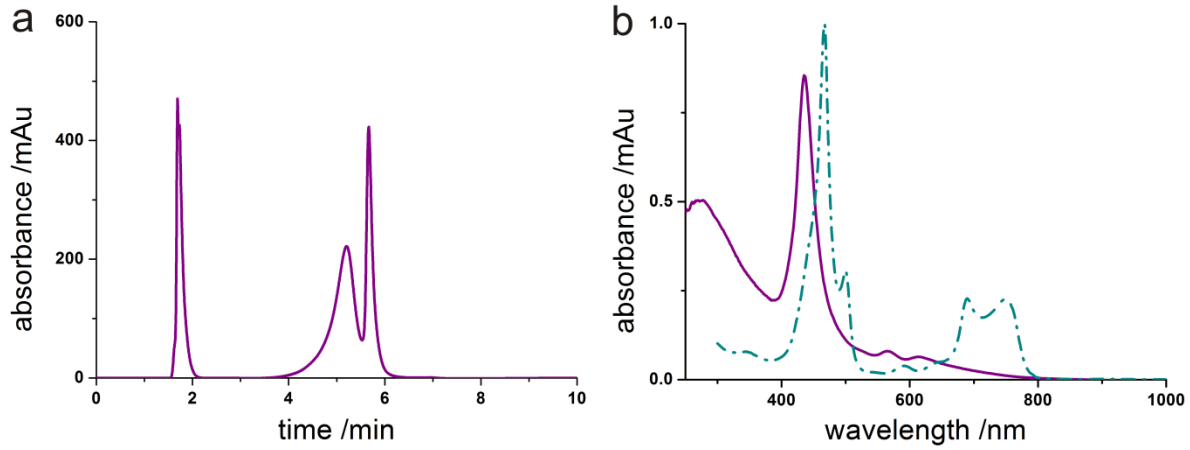

Figure 94: *(a) RP-HPLC trace (740 nm) of the bis-c(RGDfK) dimer following lyophilisation of the fractions collected by semi-preparative RP-HPLC (b) the absorption spectrum of the peak in (a) at 5.9 min material (purple) with the absorption spectrum of **4** (cyan dashed) overlaid.*

In addition, the NMR spectrum showed was not clean (**Figure 95**). The presence of a singlet peak at 10.4 ppm suggests that an aldehyde was present in the isolated material.

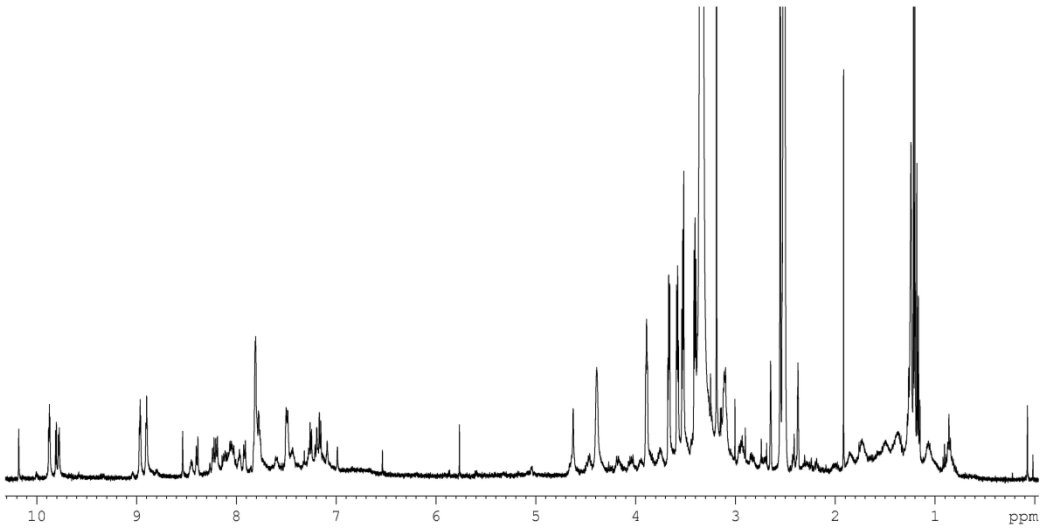

Figure 95: *A ^{1}H NMR spectrum (500 MHz, DMSO-d_6) of the product isolated by semi-preparative RP-HPLC.*

Repetition of the synthesis gave similar results. Size-exclusion chromatography was attempted as an alternative purification technique but the product could not be isolated using this method.

The manual solid-phase peptide synthesis apparatus available limited the scale on which **12** could be synthesised to 0.5 mmol and normally 5-10 mg was isolated. The lengthy and low yielding synthesis as well as the tendency of the porphyrin conjugate to decompose meant no further investigation of this compound was made.

3.5.6 $(KLAKLAK)_2$ Synthesis

The synthesis of this compound was performed by Dr Sébastian Ulrich and *in vitro* evaluation performed with his collaboration.

The structure of **AO-$(KLAKLAK)_2$** appended with the amino-oxy linker is shown in **Figure 96**.

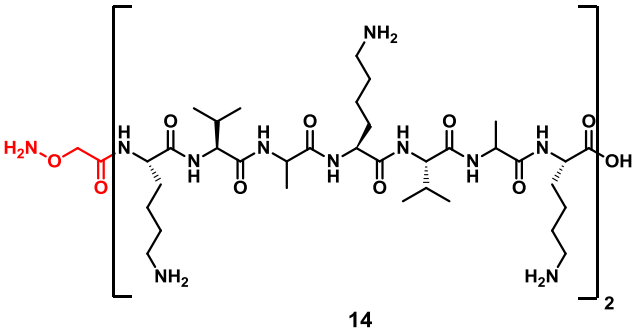

14

Figure 96: *The structure of **AO-$(KLAKLAK)_2$**. The amino-oxy linker is highlighted in red.*

This peptide was prepared using an automated solid-phase synthesiser with the highly acid-sensitive RINK resin and DCC and as a coupling reagent. The linker group was attached on-resin by mixing **6** with the peptide-appended resin in DMF. Subsequent cleavage using HFIP yielded the protected amino-oxy-appended peptide, deprotection of which was performed using a cocktail of TFA, TIPS and H_2O. Coupling of the **14** and **4** was performed in DMSO at 15 mM concentration (**Scheme 19**).

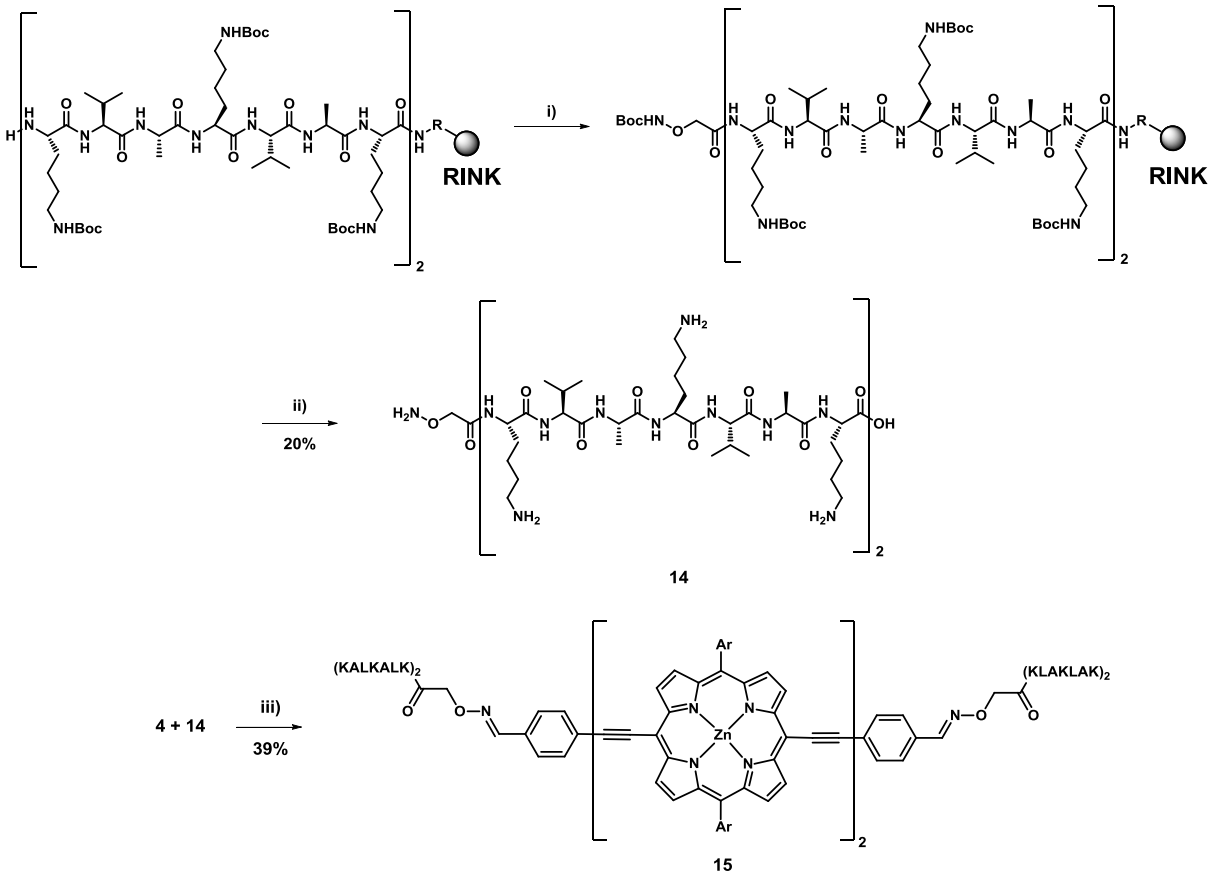

Scheme 19: *(i)* ***8****, DMF (ii) TFA:TIPS:H_2O 95:2.5:2.5 (v:v:v) then precipitation from ice cold diethyl ether (iii) DMSO.*

Compound **15** was isolated in 52% yield by RP-HPLC and characterised using this technique and UV/visible spectroscopy.

3.6 One-photon *In Vitro* Testing

The following sections document the *in vitro* one-photon PDT, fluorescence imaging and uptake studies performed on the dimers synthesised in the previous sections.

One-photon *in vitro* experiments were performed on HeLa cells seeded in 96-well plates. Irradiation was performed using the light box developed by the Anderson group (**Figure 97**). The LED arrangement allows for the irradiation of six out of eight wells in up to ten out of the twelve columns. The outer wells are left unused to eliminate the possibility of ambient light affecting the experiments. Each column of LEDs can be controlled individually, so the effect of the length of the light dose on cell viability can be evaluated. The experiments were designed so that for every column of wells irradiated there is an adjacent column which does not receive a light dose, thus the PDT efficacy after each time period can be examined. As the wells in each column are under identical conditions, each column represents six replicates of the same experiment.

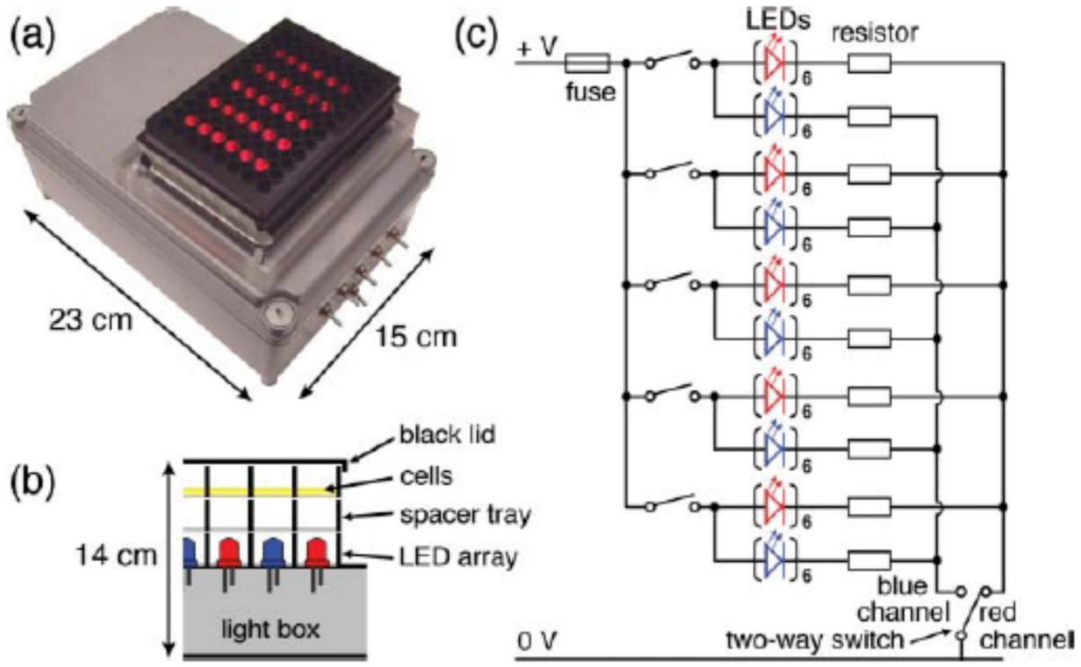

Figure 97: *The experimental set-up for one-photon PDT experiments: (a) the LED arrangement for the irradiation of cells in a 96-well plate, (b) a cross-section of the light box and (c) its circuit diagram. The LED array is powered by a 24 V rechargeable battery which, with 680 Ω resistors, results in 9.4 mW cm^{-2} light intensity for the red (657 nm) LEDs. This data was reproduced, with permission, from reference 192.*

There are three variables in a typical PDT experiment: the incubation time, the irradiation time, and the photosensitiser concentration. The optimised conditions from Anderson group

research used a photosensitiser concentration of 10 μM, an incubation time of 18 hours and irradiation times of 10, 20, 30 and 40 minutes.[192] As control experiments, two columns of wells (one irradiated and one not irradiated) were seeded with cells but no photosensitiser.

Following incubation, a viability assay based on 3-(4,5-dimethylthiazol-2-yl)-5-(3-carbocymethoxyphenyl)-2-(4-sulfophenyl)-2H-tetrazolium (MTS) reduction was used to determine the percentage of viable cells (Promega CellTiter96). This is a colourimetric assay consisting of a novel tetrazolium compound which is bio-reduced by viable cells to a formazan product (**Figure 98**).[252]

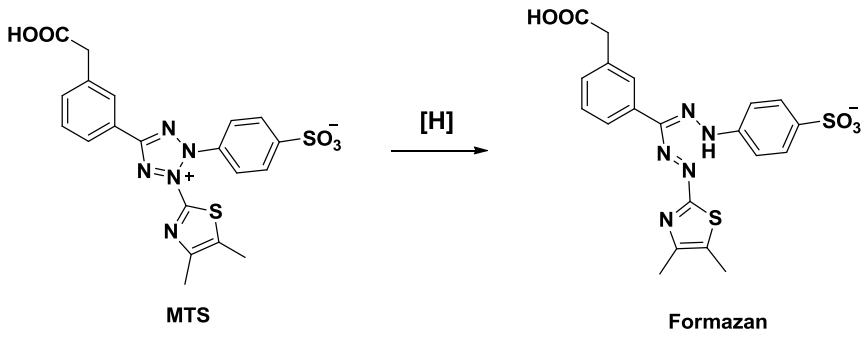

Figure 98: *The reduction of MTS to formazan, which forms the basis of the cell viability assay used to determine the percentage of viable cells in PDT experiments. The reduction only occurs in viable cells and produces a fluorescent compound from a non-fluorescent one, thus cell survival can be determined by a fluorescence assay. In cells, the reaction is thought to be performed by NADH.*

The quantity of the formazan product (which is determined by absorbance measurement at 490 nm), is directly proportional to the number of viable cells. As a control, the absorption intensity of the cell culture medium itself was measured and subtracted from all results.

Before investigating any peptide-conjugated dimers, PDT experiments were repeated in collaboration with Dr Sébastian Ulrich on **P_2C_2NMeI** to ensure that the procedures were being followed correctly (**Figure 99**). The studies in this research were all performed using HeLa cells rather than SK-OV-3 cells, due to their lower tendency to aggregate and simpler culturing protocols.

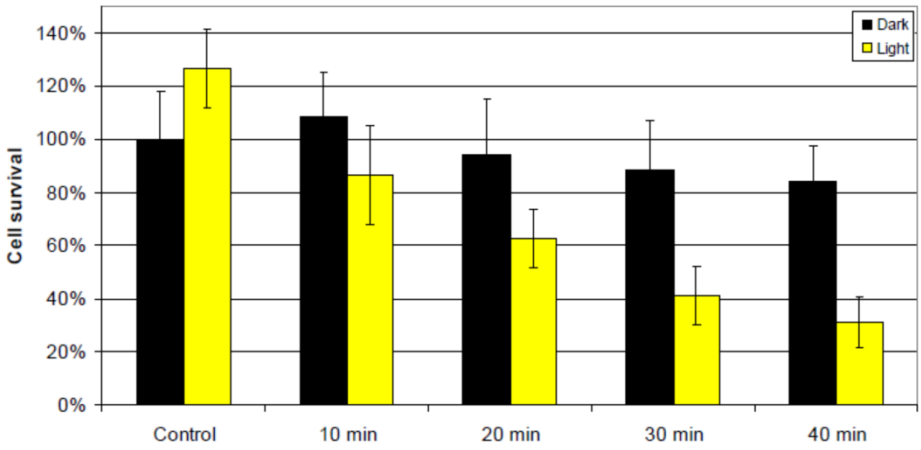

Figure 99: In vitro *PDT experiment on* ***P_2C_2NMeI*** *(10 µM) in HeLa cells. The cells were incubated with the photosensitiser for 18 hours prior to irradiation at 657 nm for 10 to 40 mins. Yellow bars represent irradiated cells, black bars represent non-irradiated cells. The error bars represent one standard deviation from six replicates.*

The studies indicated no significant dark toxicity and a clear contrast in cell viability between the irradiated and non-irradiated columns. The apparent increase in toxicity over time in the non-irradiated columns with increasing length of light dose was attributed to a photothermal effect arising from the irradiation of adjacent wells. No toxicity was observed in the control experiments.

3.6.1 Integrin-Targeting Dimer

Figure 103 shows the results from the PDT experiments on compound **11**. It is clear that, at this concentration, the RGD-appended dimer is highly toxic as both the irradiated and non-irradiated cells showed similar, very high levels of toxicity.

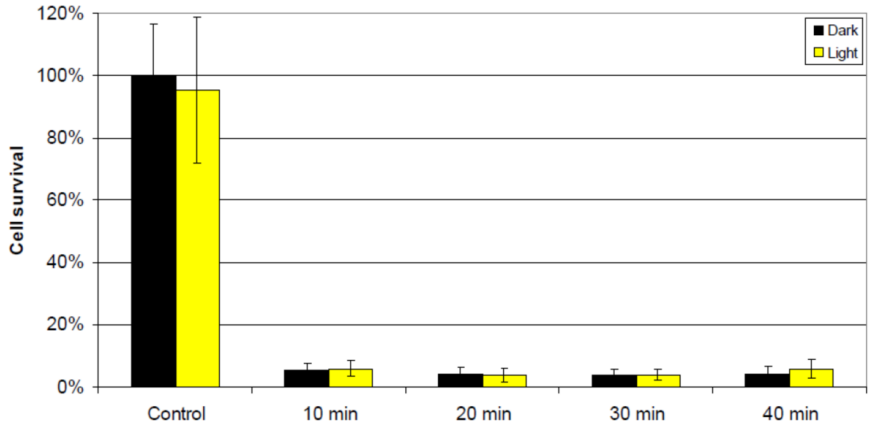

Figure 100: *The results of* in vitro *PDT experiments on* ***11*** *(10 µM) in HeLa cells. The cells were incubated with the photosensitiser for 18 hours prior to irradiation at 657 nm for 10 to 40 mins. Yellow bars represent irradiated cells, black bars represent non-irradiated cells. The error bars represent one standard deviation from six replicates*

Following this, investigations into the lethal concentration (LD_{50}) were made. For such experiments, the only variable was the photosensitiser concentration; no irradiation was performed and the incubation time was maintained at 18 hours. The six columns of the 96-well plate were used to test the dark toxicity at six different concentrations, ranging from 100 nM to 40 µM.

Investigation into the lethal concentration confirmed the high toxicity at 10 µM and above (**Figure 101**). There was a marked increase in cell survival below 1 µM and the LD_{50} for this compound was estimated at 2 µM. Even at very low concentration, it appeared that the mean cell survival is lower than that of **P_2C_2NMeI**.

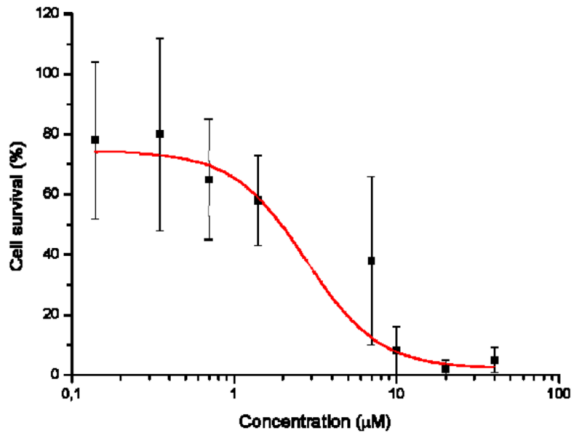

Figure 101: *Dark toxicity studies on **11** (10 µM) after 18 hours incubation with HeLa cells. The error bars represent one standard deviation from six replicates. The correlation coefficient of the sigmoidal fit is 0.96.*

Another concentration-dependent experiment, which included 40 minutes of irradiation after 18 hours incubation, yielded a similar LD_{50} value (3 µM) (**Figure 102**). This implied that there would be no PDT effect even at a low enough concentration that dark toxicity was negligible.

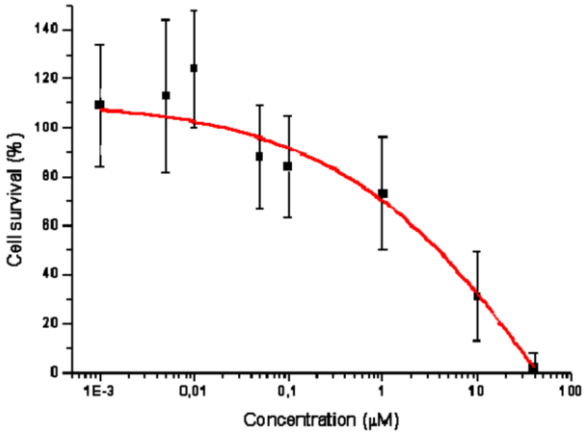

Figure 102: *Concentration-dependent toxicity studies after 18 hours incubation and irradiation for 40 mins. The error bars represent one standard deviation from six replicates. The sigmoidal fit coefficient is 0.98.*

Co-staining of **11** with Lysotracker (a dye known to localise in lysosomes, organelles found throughout the intracellular fluid) in SK-OV-3 cells demonstrated that rather than localising in the cells, it forms small aggregates in the extracellular matrix (**Figure 103**). There are three possible explanations for this: either the compound interacts with integrins at the membrane's surface and does not cross the membrane, after 18 hours incubation **11** has been excreted, or inside the cells the photosensitiser fluorescence is quenched. The incubation period is sufficient to expect excretion could have occurred, though, if metabolism had taken place, it might be expected that the porphyrin's emission characteristics would be different, which was not observed.

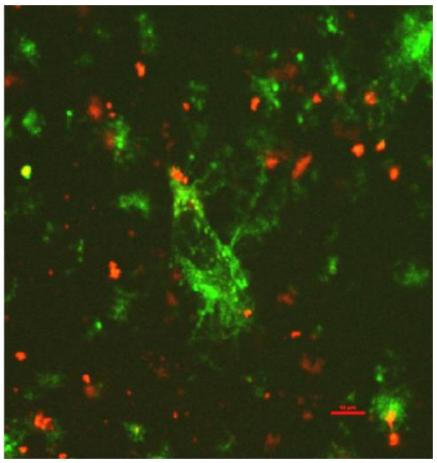

Figure 103: *Fluorescence imaging (λ_{ex} 488 nm) of SK-OV-3 cells with **11** (10 µM) (red) co-stained with Lysotracker Yellow (green) after 18 hours incubation. Experiment performed by Dr Marina Kuimova, Imperial College London (ICL).The scale bar reads 10 µm.*

The increase in dark toxicity and the lack of evidence for a PDT effect, even at lower concentrations, was unexpected and is not easily explained. There is no evidence relating to the mechanism of cell death, so it is difficult to speculate on the cause of the increased toxicity over the non peptide-conjugated dimer.

3.6.2 Mitochondria-Targeting Dimer

The initial *in vitro* PDT studies, again using the optimised conditions developed for **P_2C_2NMeI**, are shown in **Figure 104**. The peptide conjugate showed little evidence of a PDT effect, there was significant dark toxicity and little difference in cell survival with or without a light dose. There was also an increase in dark toxicity over time of around 20%, which could be caused by the photothermal effect of irradiating the adjacent cells for prolonged periods.

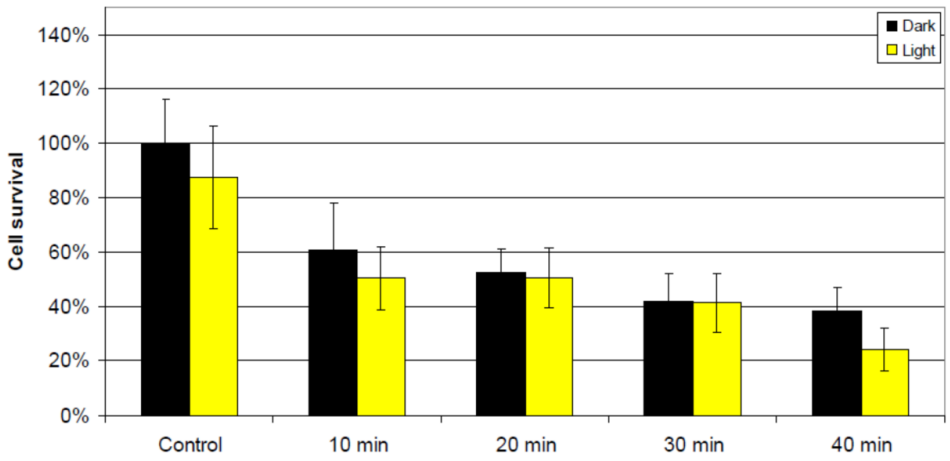

Figure 104: In vitro *PDT experiment on **15** (10 µM) in HeLa cells. The cells were incubated with the photosensitiser for 18 hours prior to irradiation at 657 nm for 10 to 40 mins. Yellow bars represent irradiated cells, black bars represent non-irradiated cells. The error bars represent one standard deviation from six replicates*

Concentration dependent dark toxicity studies confirmed the high toxicity at 10 µM and indicated an LD_{50} of 0.05 µM (**Figure 105**).

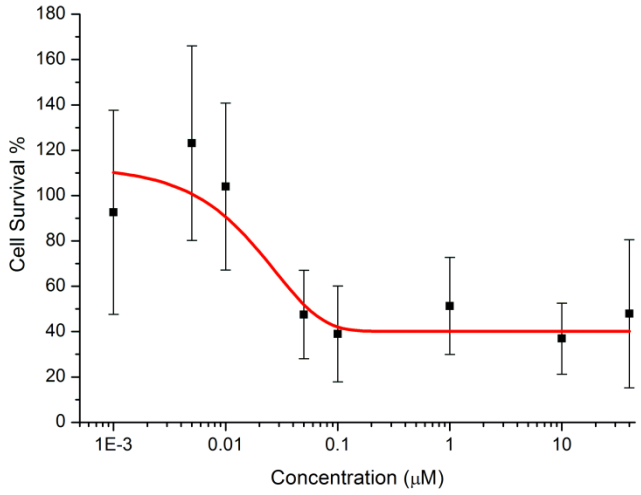

Figure 105: *Dark toxicity studies on **15** (10 μM) after 18 hours incubation with HeLa cells. The error bars represents one standard deviation from six replicates. The correlation coefficient of the sigmoidal fit is 0.79.*

Encouragingly, fluorescence microscopy studies suggested that **15** partially localised in the mitochondria. **Figure 106** shows confocal fluorescence images in which **P_2C_2NMeI** and **15** were co-localised with Rhodamine-123 (a mitochondrial stain),[253] demonstrated some overlap after 18 hours incubation.

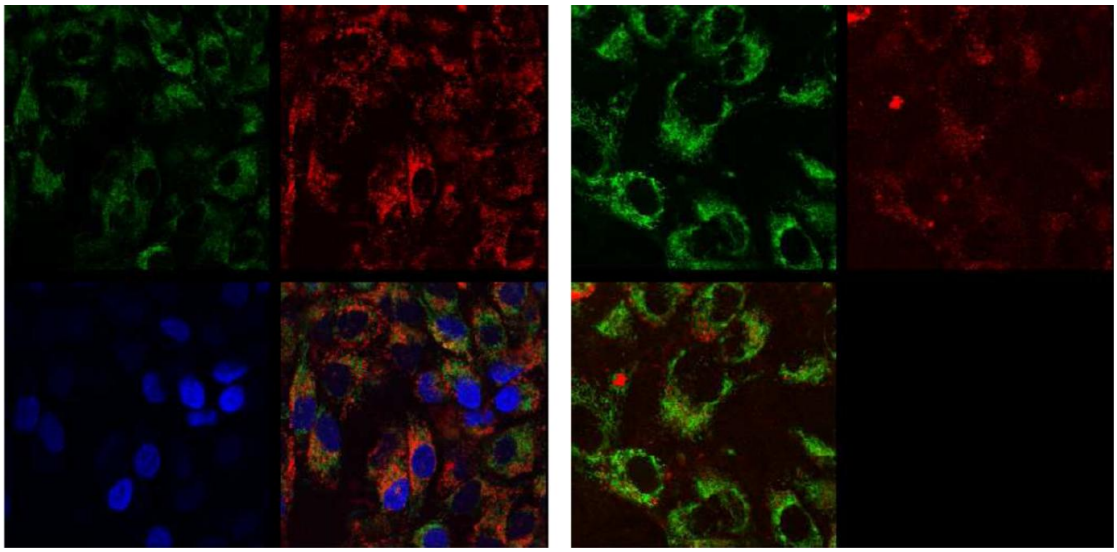

Figure 106: *Fluorescence imaging experiments on **P_2C_2NMeI** (left) and **15** (right) (10 μM) in SK-OV-3 cells after 18 hours incubation. The compounds (λ_{ex} = 633 nm, λ_{em} = 700-800 nm) were co-stained with Rhodamine-123 (λ_{ex} = 488 nm, λ_{em} = 550 nm), DAPI-blue (λ_{ex} = 405 nm, λ_{em} = 480 nm). Experiments performed by Dr Kuimova, ICL.*

Subsequent fluorescence-based uptake studies found that the distribution of **15** after the original 18 hour incubation time was punctated, while soon after incubation was started, a more even distribution was observed (**Figure 107**).

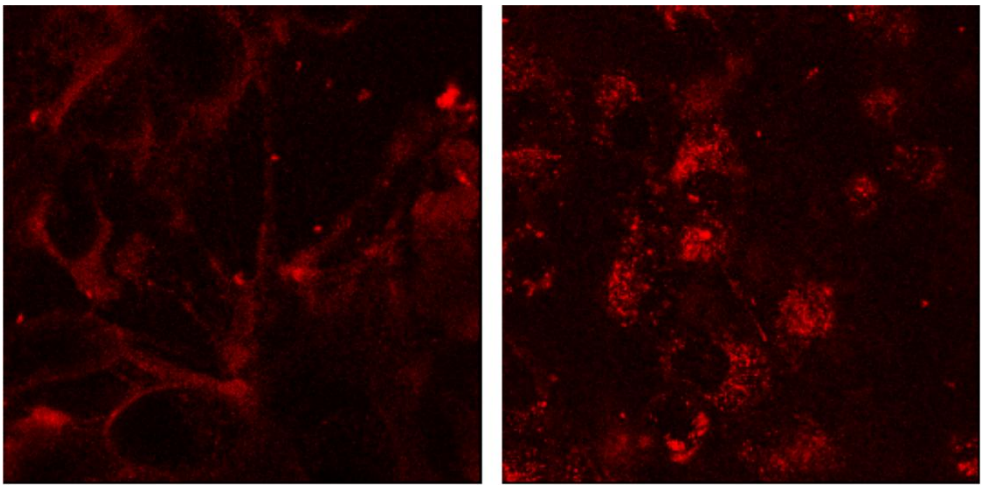

Figure 107: *Confocal fluorescence imaging study of **15** (10 μM) in SK-OV-3 cells after 12 minutes (left) and 18 hours incubation (right). Experiments performed by Dr Kuimova, ICL.*

This gave cause to investigate whether the uptake rate of **15** was faster, as the data suggested that after 18 hours, the cell had begun to metabolise or otherwise excrete the foreign species.

Indeed, further uptake studies showed that **15** was taken up by the cells more rapidly than **P_2C_2NMeI** (**Figure 108**).

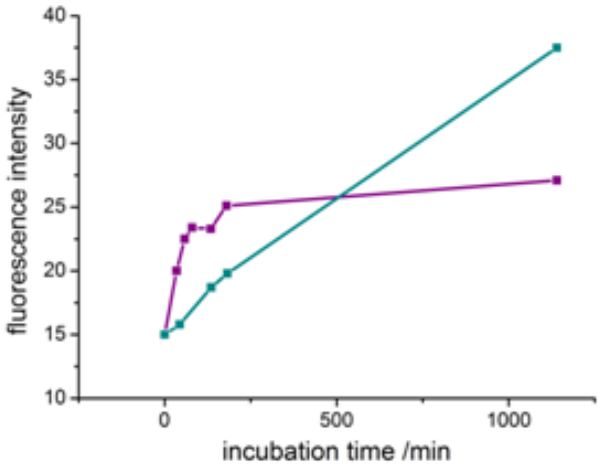

Figure 108: *Uptake studies in which the subcellular fluorescence intensity of **15** (purple) and **P_2C_2NMeI** (cyan) was measured over-time during incubation with SK-OV-3. Experiments performed by Dr Kuimova, ICL.*

While **P_2C_2NMeI** demonstrated a steady rate of uptake over the 18 hour period, **15** was taken up much more rapidly over the first 3 hours than **P_2C_2NMeI**, after which it reached its maximum concentration, around 60% of the maximum observed for **P_2C_2NMeI** (assuming the two compounds have similar fluorescence characteristics).

This result was encouraging and suggested that if a PDT effect was observed below the LD_{50} a photosensitiser with significantly improved pharmacokinetics could be developed. Unfortunately, a concentration study with the application of a light dose gave a very similar profile to the dark toxicity study (**Figure 109**).

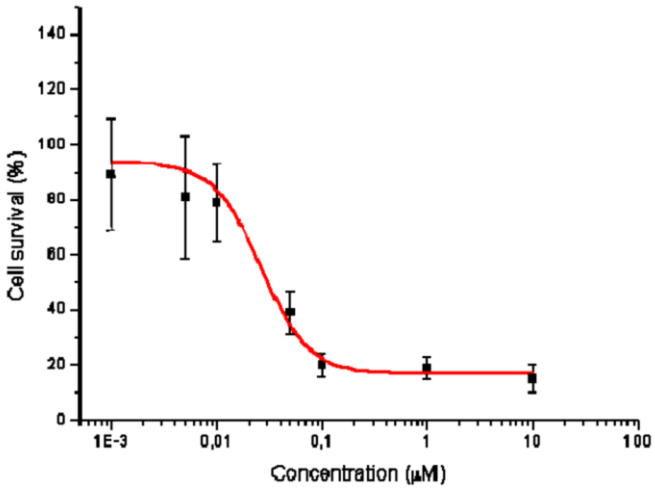

Figure 109: *Concentration-dependent studies on **15** after 18 hours incubation with HeLA cells. The error bars represent one standard deviation from six replicates. The cells at each concentration were irradiated for 40 mins (657 nm) following incubation. The correlation coefficient of the sigmoidal fit is 0.98. The estimated LD_{50} value is 0.03 µM, essentially the same as the LD_{50} without a light dose (0.05 µM).*

This suggested that at a concentration sufficiently low to negate the effect of dark toxicity, the quantity of photosensitiser would not be sufficient to result in significant cytotoxicity. Although it appears to be a common factor among the peptide-conjugated dimers that their toxicity is greater than that of **P_2C_2NMeI**, in the case of **15**, this may be explained by its antimicrobial origins. The **$(KLAKLAK)_2$** peptide has been recently shown to have antibiotic properties based on its localisation in the mitochondria, which results in permeablisation of the membrane.[254] Generally, permeablisation of the mitochondrial membrane releases factors which initiate apoptosis, which could explain the high levels of dark toxicity observed.

3.7 Conclusions and Future Prospects

In conclusion, two peptide-conjugated porphyrin dimers have been synthesised and evaluated for their pharmacokinetic properties. Co-staining experiments demonstrated partial localisation of **15** in the target organelle, as well as an increase in rate of uptake over the first three hours of incubation when compared to **P_2C_2NMeI**. However, in common with **11**, peptide conjugation led to a significant increase in dark toxicity of the porphyrin dimers. Both **15** and **11** were found to be highly toxic at 10 μM, with LD_{50} values of 0.08 and 2.0 μM respectively. This was unexpected, as the conjugation of macromolecules with peptides is a well-known strategy for the modification of their pharmacokinetic properties. It is possible that the antibacterial properties of **$(KLAKLAK)_2$** contributed to this, but the increase in toxicity was found to be a general trend both in the peptides presented here and from other research in the group. Interestingly, a recent publication in which the same porphyrin dimer was appended with carbohydrates observed similar results.[255] In this case, the carbohydrates glucose, mannose, or lactose was appended to the meso positions of the porphyrins. Toxicity studies on each carbohydrate-conjugated dimer demonstrated nearly identical LD_{50} values both with and without a light dose. It is interesting that two different but related strategies demonstrated comparable results, and it suggests there may be a more fundamental problem with increasing the size and polarity of the dimers.

Regarding a c(RGDfK)-conjugated dimer, the problems with obtaining a useful quantity of the product prevented any photobiological evaluation and in general, the oxime formation reaction proved less simple and reliable than anticipated. There are many other techniques used to couple peptides to macromolecules[256] and, in the last 5-10 years, copper-catalysed '*N*-click' chemistry has emerged as a popular technique for conjugating peptides to organic/inorganic molecules,[257,258] including porphyrins.[259] Copper-catalysed click chemistry between an azide-appended peptide and an acetylene-appended macromolecule is generally easy, quick and efficient and known to be highly stable to hydrolysis. The application of click chemistry to the porphyrin dimers could be realistically envisaged as an intermediate in the dimer synthesis contains two acetylene bonds to which an azide-appended peptide could be attached (**Figure 110**).

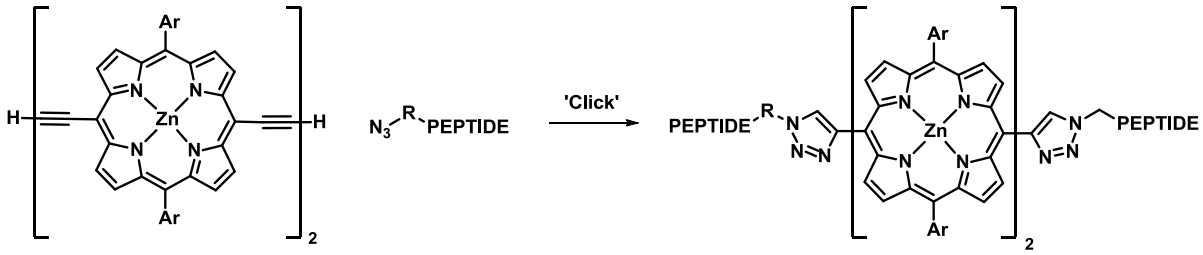

Figure 110: *An example of how the porphyrin synthesis could be simply modified to investigate peptide conjugation using click chemistry.*

This would of course have a detrimental impact on the TPA cross-section, but would provide an insight into the viability of the technique and more information on the toxicity of such compounds.

3.8 Experimental for Chapter 3

General Methods

Manipulation of all air- and water-sensitive compounds was carried out using standard high vacuum techniques. Dry toluene, tetrahydrofuran (THF) and dichloromethane (DCM) were obtained by passing the solvent through activated alumina. Dimethylformamide (DMF), diisopropylamine (DIPA) and triethylamine (Et_3N) were distilled from CaH_2 under nitrogen before use. All other reagents were used as supplied by commercial agents. All other reagents were used as supplied by commercial agents. Analytical thin layer chromatography (TLC) was carried out on Merck aluminium backed silica gel 60 GF254 plates and visualisation, when required, was achieved using UV light (254 nm). Where mixtures of solvents were used, ratios reported are by volume.

NMR spectra were recorded at ambient probe temperature using either a Brucker DPX400 (400 MHz), Brucker AVANCE AV400 (400 MHz), Brucker DPX250 (250 MHz) or a Brucker DRX500 with a ^{13}C cryoprobe. Chemical shift values are denoted in δ values (ppm) relative to residual solvent peaks ($CDCl_3$, δ_H = 7.26, δ_C = 77.16; DMSO-d_6, δ_H = 2.50, δ_C = 39.51; CD_3CN-d_3 δ_H = 1.94), coupling constants (J) are quoted in Hertz (Hz). Low resolution ESI-MS was carried out on a Micromass LCT platform. UV-Vis spectra were recorded on a Perkin Elmer Lambda 20 UV-Vis spectrometer.

HPLC analysis and separation were carried out on either a Hitachi/VWR LaChrom ELITE HPLC system equipped with L-2130 quaternary pump, L-2455 diode array detector, L-2200 autosampler, L-2350 column oven and Foxy Jr. fraction collector or an Agilent 1100 system equipped with a G1315B diode array detector, a G1311A quaternary pump and a G1316A fraction collector. Analytical HPLC were carried out using C8 5 μm, 3.9 × 150 mm Eclipse XDB-C8 column (Agilent) using 1 mL min^{-1} flow and linear gradients at 40 °C. Semi-preparative HPLC was carried out using C8 5 μm, 10 × 250 mm Eclipse XDB-C8 column (Agilent) using 3 mL min^{-1} flow and stepwise gradient at 40 °C. The chromatographic separations were monitored in the range 190-900 nm.

Reverse-Phase HPLC Methods

The tables below show the solvent gradients used to achieve resolution of the components. Following the stated gradient, the column was washed with the least polar solvent for 3-5 mins before a 5 minute gradient returning to starting conditions was performed.

HPLC Method A

Time /min	H_2O (0.1% TFA)	MeCN (0.1% TFA)
0.00	90	10
30.00	0	100

HPLC Method B

Time /min	H_2O (0.1% TFA) /%	MeOH /%	THF /%
0.00	68	2.0	30
9.00	8.0	2.0	90

HPLC Method C

Time /min	H_2O (DiCHAP*)	MeOH	DMSO
0.00	24	48	28
3.00	0	0	100
15.00	0	0	100

* DiCHAP = Dicyclohexyl Ammonium Phosphate buffer (2.5 g/L)

HPLC Method D

Time /min	H_2O (0.1% TFA) + 30% THF /%	MeOH /%	THF /%
0.00	98	2.0	0
12.90	12	2.0	86

Manual Solid-Phase Peptide Synthesis

Method I: SASRIN resin was swelled in DCM then DMF by bubbling nitrogen through a suspension of the resin for 30 mins each. After washing with DMF 2-3 times, the Fmoc group was deprotected with a solution of 20% piperidine in DMF for 30 mins. Each subsequent amino acid attachment was performed as follows: a solution of the amino acid (3 eq), PyBOP (3 eq) and DIPEA (7.5 eq) in DMF ([amino acid] = 0.1 M) was stirred for 3-5 mins before being added to the deprotected resin. After 30 mins, the resin was washed with DMF and the TNBS test was used to check that all amines had reacted.[260] Deprotection of the Fmoc group was again performed by treatment of the resin with a solution of 20% piperidine in DMF for 30 mins. The TNBS test was then used to detect free amines on the resin.[160] After the final coupling, the resin was thoroughly washed with DMF, then DCM. It was dried overnight under vacuum and the product was cleaved from the solid support by treatment with TFA/TIPS/H_2O 95:2.5:2.5 for 3-4 hours. Most of the solution was then evaporated by N_2 bubbling. Precipitation with cold ether and centrifugation for 5-10 mins at 4 °C afforded a solid material which was dissolved in aqueous solvent and lyophilized.

Method II: Wang resin (200-400 mesh) was swelled with DCM and DMF by bubbling nitrogen through a suspension of resin for 30 mins each. After washing with DMF 2-3 times, the Fmoc group was deprotected with a solution of 20% piperidine in DMF for 30 mins. Each amino acid attachment was then performed as follows: a solution of the amino acid (2.5 eq), HBTU (2.5 eq) and *N*-methyl morpholine (NMM) (10 eq) in DMF ([amino acid] = 0.1 M) was stirred for 3-5 mins before adding to the deprotected resin. After 30 mins the resin was washed with DMF. The TNBS test was used to check that no free amine groups remained.[1] After the first amino acid coupling, any free hydroxyl sites on the resin were capped with acetic anhydride (2 eq) and NMM (2 eq). Following this the resin was washed with DMF (3 x 5 mL) and amino acid coupling was continued as before. After the final coupling, the resin was deprotected with 20% piperidine in DMF and *N*-tert-butoxy-carbonyl-amino-oxy-acetic acid-2,5-dioxypyrrolidin-1-yl ester (0.1 M) in DMF was coupled to the peptide. After overnight reaction, the resin was washed with DMF followed by DCM. The product was cleaved from the solid support by treatment with TFA/TIPS/H_2O 95:2.5:2.5 for 3 hours. The product was precipitated from the solution with cold ether and collected by centrifugation before overnight lyophilisation.

Cell Manipulation Methods

Cell culture: Human epithelial cervical cancer cells (HeLa) were grown in phenol red-free Dulbecco's modified Eagle's medium (DMEM, Gibco) supplemented with 2 mM L-glutamine, 100 U mL^{-1} penicillin (Sigma), 100 μg mL^{-1} streptomycin (Sigma) and 10% foetal bovine serum (Sigma). The cells were maintained at 37 °C in a humidified, 5% CO_2 atmosphere.

In vitro *one-photon photodynamic therapy:* The cells were seeded in flat 96-well plates (Corning) in the tissue culture medium (100 μL). The cells were irradiated 18 h after seeding and at the required time before the light dose, the media was replaced with a solution of the photosensitiser. The plates were shielded from light during and after incubation. Following incubation the wells requiring light exposure were irradiated and then the cells were washed (3 × 100 μL medium) and incubated in new media (100 μL) for 48 h. After this time the cell viability was determined using CellTiter 96 Aqueous Proliferation Assay (MTS) according to the manufacturer's instructions. An average background absorbance reading of the medium was recorded and subtracted from the average absorbance of each replicate group before data manipulation.

LD_{50} studies: The cells were seeded in flat 96-well plates in the tissue culture medium (100 μL). After 2 h incubation, the medium was replaced with the photosensitiser solution at concentrations between 1 nM and 40 μM and incubated for a further 18 h. Following this, all wells were irradiated, the cells were washed (3 × 100 μL medium) and then incubated for a further 48 h. After this time the cell viability was determined using CellTiter 96 Aqueous Proliferation Assay (MTS) according to the manufacturer's instructions. An average background absorbance reading of the media was recorded and subtracted from the average absorbance of each replicate group before data manipulation. To determine dark toxicity, the irradiation step was left out.

Fluorescence Imaging Techniques

Imaging was performed using a confocal laser scanning microscope (Leica TCS SP2), coupled to a CW argon-ion laser (488 nm) by Dr Marina Kuimova at ICL. The fluorescence emission of the photosensitisers in the cells was spectrally dispersed using a prism and detected using a photomultiplier tube. Either dry 40× (NA = 0.75) or water immersion 63× objectives (NA = 1.2) were used to image. For the imaging experiments, the cells were

seeded at 104 cells per well in 0.2 mL of culture medium in untreated 8-well coverglass chambers (Lab-TekTM, Nunc) and allowed to grow to confluence for 24 h. The culture media was replaced with the medium containing the porphyrin dimers and incubated for 1–24 h. Following incubation, the chambers were washed twice with PBS and images were collected at 25 °C. The mean fluorescence intensities from the images were obtained at different incubation times and plotted to determine the rate of uptake into cells.

Synthesised Compounds

Porphyrin Derivatives

Dipyrromethane (1)

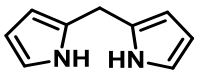

This compound was synthesised according to a literature procedure.[36] Formaldehyde (37-40 % w/v in water, 4.9 mL, 0.060 mol) was added to pyrrole (100 mL) and the solution was freeze-thaw degassed three times. Trifluoroacetic acid (0.50 mL, 3.1 mol) was added with vigorous stirring and the reaction was allowed to proceed for 5 minutes before DCM (100 mL) was added, followed by saturated aqueous sodium carbonate (100 mL). The organic layer was washed with saturated aqueous sodium carbonate (2 × 100 mL) and water (100 mL). The organic layer was concentrated giving a brown oil, which was distilled under reduced pressure (200 °C, 0.12 mmHg) to give the product as a white crystalline solid (2.90 g, 33%); δ_H (250 MHz, $CDCl_3$) 3.99 (s, 2H), 6.02-6.09 (m, 2H), 6.11-6.22 (m, 2H), 6.59-6.72 (m, 2H), 7.80 (br, 2H); δ_C (125 MHz, $CDCl_3$) 26.34, 106.51, 108.31, 117.41, 129.14.

2-(2-(2-(methoxyethoxy)ethoxy)ethyl 4-methylbenzenesulfonate

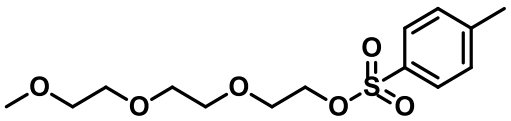

This compound was prepared according to a reported procedure.[261] To a solution of *para*-toluene sulfonyl chloride (18 g, 0.090 mol) in dry DCM (40 mL) was added a solution of triethylene glycol monomethyl ether (10.0 mL, 0.06 mol) and dry triethylamine (17 mL, 0.12 mol) in dry DCM (7 mL), dropwise at 0º C under argon. The reaction mixture was stirred at room temperature overnight and monitored by TLC (10:1 DCM:MeOH). When no tri-

ethyleneglycol monomethyl ether remained, the reaction mixture was poured into water (50 mL) and extracted with DCM (4 × 15 mL). The extractions were combined, washed with 2 M hydrochloric acid (1 × 15 mL), half saturated aqueous sodium bicarbonate (4 × 15 mL) and brine (1 × 20 mL). The solvents were removed by evaporation and the resulting pale yellow oil was dried *in vacuo* (17 g, 88%); δ_H (400 MHz, $CDCl_3$) 2.42 (s, 3H) 3.36 (s, 3H) 3.52 (m, 2H) 3.55-3.60 (m, 7H) 3.68 (t, 2H) 4.16 (t, 2H) 7.28 (d, 2H) 7.78 (d, 2H).

3-(2-(2-(2-methoxy-ethoxy)ethoxy)ethoxy)benzaldehyde (2)

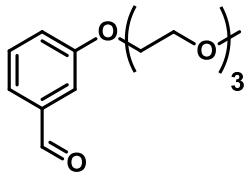

This compound was synthesised according to a literature procedure.[36] 3-Hydroxybenzaldehyde (3.1 g, 26 mmol), tri-ethyleneglycol monomethyl ether tosylate (6.8 g, 20 mmol) and potassium carbonate (5.9 g, 41 mmol) were dissolved in dry acetonitrile (15 mL). The reaction mixture was stirred at reflux for 16 h under nitrogen. When no tri-ethyleneglycol monomethyl ether tosylate remained by TLC (1:1 Petrol Ether:EtOAc), the reaction was cooled, diluted with diethyl ether (100 mL), filtered, and dried *in vacuo*. The resulting oil was distilled under reduced pressure (160 °C, 0.11 mmHg) to yield a colourless oil. This was washed with 1 M sodium hydroxide (2 × 10 mL) to remove the excess 3-hydroxybenzaldehyde, and brine (1 × 20 mL) then dried *in vacuo* to give a colourless oil (4.9 g, 92%); δ_H (400 MHz, $CDCl_3$) 3.25 (s, 3H), 3.42-3.44 (m, 2H), 3.52-3.55 (m, 6H), 3.55-3.58 (m, 2H), 3.61-3.63 (m, 2H), 3.76-3.79 (m, 2H), 7.08 (s, 1H), 7.27-7.33 (m, 3H), 9.83 (s, 1H); δ_C (125 MHz, $CDCl_3$) 58.9, 67.6, 69.5, 70.5, 70.6, 70.7, 71.8, 113.0, 121.9, 123.4, 130.0, 137.6, 159.3, 192.1.

5,15-bis-3-(2-(2-(2-methoxy-ethoxy)ethoxy)ethoxy)phenyl porphyrin

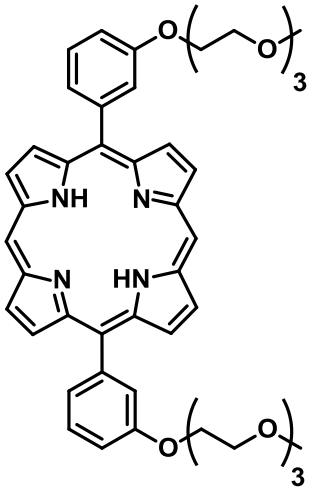

This compound was synthesised according to a literature procedure.[36] A fresh Winchester of DCM (2.5 L) was degassed by purging with nitrogen for 1 h. To this, dipyrromethane (1.8 g, 12 mmol) was added, followed by 3-(2-(2-(2-methoxy-ethoxy)ethoxy) ethoxy)benzaldehyde (3.2 g, 12 mmol) and trifluoroacetic acid (600 µL). The reaction was shielded from light with aluminium foil and stirred at room temperature for 3 h. When no dipyrromethane remained by TLC (99:1 DCM:methanol), 2,3-dichloro-5,6-dicyano-1,4-benzoquinone (DDQ) (3.6 g, 16 mmol) was added and the reaction mixture stirred for a further 30 mins. The reaction mixture was neutralised with triethylamine (10 mL) and passed through a silica plug. Initially DCM removed the DDQ residues then the product was isolated by eluting with 99:1 DCM:methanol. Further purification by column chromatography (SiO_2, 99:1 DCM:methanol) and precipitation from hexane gave the product as a fine purple powder (2.1 g, 23%); δ_H (400 MHz, $CDCl_3$/1% pyridine-d_5) -3.10 (s, 2H) 3.32 (s, 6H), 3.47-3.49 (m, 4H), 3.62-3.63 (m, 4H), 3.67-3.70 (m, 4H), 3.92-3.94 (m, 4H), 4.32-4.34 (m, 4H); δ_C (125 MHz, $CDCl_3$/1% pyridine-d_5) 59.0, 67.7, 69.9, 70.5, 70.7, 70.9, 71.9, 105.3, 114.2, 118.8, 121.5, 127.8, 128.0, 131.1, 131.6, 142.7, 147.1, 147.3, 157.49; *m/z* MALDI-ToF+ 786.84, $C_{46}H_{50}N_4O_8$ requires 786.36 (100%).

5,15-bis-3-(2-(2-(2-methoxy-ethoxy)ethoxy)ethoxy)phenyl zinc porphyrin (Zinc porphyrin)

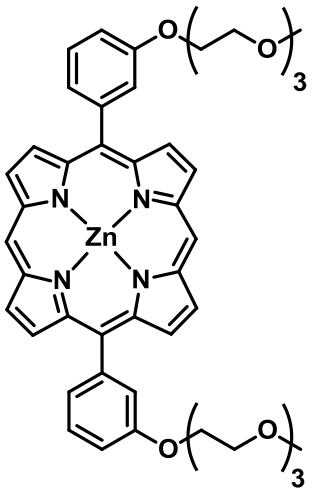

This compound was synthesised according to a literature procedure.[36] To a stirred solution of 5,15-bis-3-(2-(2-(2-methoxy-ethoxy)ethoxy)ethoxy)phenyl porphyrin (1.5 g, 1.9 mmol) in chloroform (210 mL), was added a solution of zinc acetate (2.1 g, 9.5 mmol) in methanol (20 mL). The mixture was stirred at room temperature until none of the starting material remained by TLC (95:5 DCM:methanol). The solvent was removed by evaporation and the product isolated by flash chromatography followed by column chromatography (SiO_2, 99:1 DCM:methanol) to yield a dark red glass (1.6 g, 99%); δ_H (400 MHz, $CDCl_3$/1% pyridine-d_5) 3.32 (s, 6H), 3.47-3.49 (m, 4H), 3.60-3.62 (m, 4H), 3.66-3.68 (m, 4H), 3.74-3.76 (m, 4H), 3.90-3.93 (t, 4H), 4.31-4.34 (t, 4H), 7.33-7.36 (m, 2H), 7.63-7.67 (t, 2H), 7.86-7.88 (m, 4H), 9.12 (d, J = 4.4 Hz, 2H, *β-H*), 9.36 (d, J = 4.4 Hz, 2H, *β-H*), 10.20 (s, 2H, *meso-H*); %); δ_C (125 MHz, $CDCl_3$/1% pyridine-d_5) 59.0, 67.6, 69.8, 70.5, 70.7, 71.8, 72.3, 105.9, 113.6, 119.2, 121.7, 127.3, 128.2, 131.6, 132.3, 144.7, 149.5, 149.9, 157.1; *m/z* MALDI-ToF+ 848.75, $C_{46}H_{48}N_4O_8Zn$ requires 848.28 (100%).

1,10-bromo-5,15-bis-3-(2-(2-(2-methoxy-ethoxy)ethoxy)ethoxy)phenyl zinc porphyrin

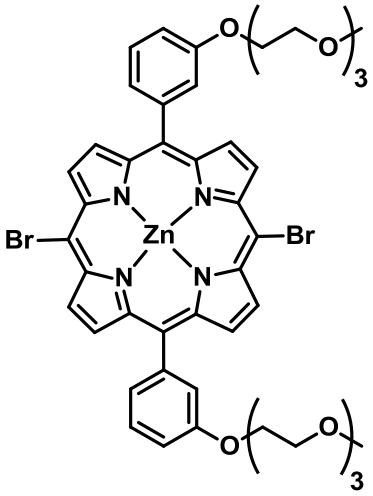

This compound was synthesised according to a literature procedure.[36] Zinc porphyrin (1.43 g, 1.68 mmol) was dissolved in chloroform (130 mL) with pyridine (1 mL). To this solution was added *N*-bromosuccinimide (299 mg, 1.68 mmol) in chloroform (40 mL) and pyridine (240 µL) dropwise over 30 mins. After 15 mins, an aliquot was removed and analysed by NMR. Integration showed 50% of the material had reacted, so a further solution of *N*-bromosuccinimide (299 mg, 1.68 mmol) in chloroform (40 mL) and pyridine (240 µL) was added dropwise over 30 mins. After 15 mins, the reaction was quenched with acetone (5 mL). The solvents were removed under reduced pressure and the product was eluted from a silica plug with 99:1 DCM:methanol. Evaporation of the solvent gave the product as a purple glass (1.68 g, 99%); δ_H (400 MHz, $CDCl_3$/1% pyridine-d_5) 3.37 (s, 6H), 3.67-3.69 (m, 4H), 3.74-3.75 (m, 4H), 3.83-3.84 (m, 4H), 4.00-4.02 (m, 4H), 4.38-4.40 (m, 4H), 7.32-7.33 (m, 2H), 7.64-7.66 (m, 2H), 7.78-7.79 (m, 4H), 8.94 (d, J = 4.6 Hz, 4H), 9.68-9.69 (d, J = 4.6 Hz, 4H); *m/z* MALDI-ToF+ 1007.05, $C_{46}H_{50}Br_2N_4O_8Zn$ requires 1006.10 (100%).

1,10-bis(trihexylsilylacetylene)-5,15-bis-3-(2-(2-(2-methoxy-ethoxy)ethoxy)ethoxy)phenyl zinc porphyrin

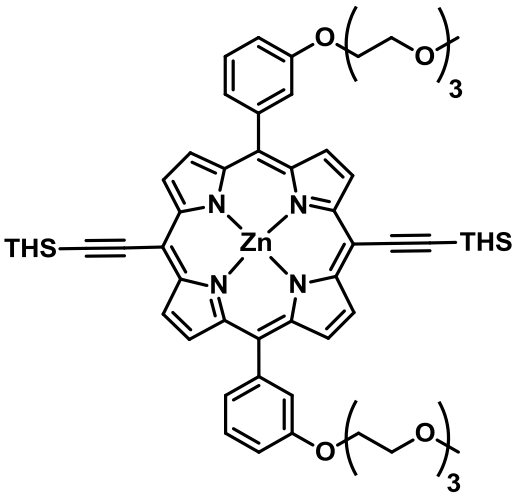

This compound was synthesised according to a literature procedure.[36] To a pre-dried Schlenk was added 1,10-bromo-5,15-bis-3-(2-(2-(2-methoxy-ethoxy)ethoxy)ethoxy)phenyl zinc porphyrin (670 mg, 0.66 mmol), bis(triphenylphosphine)palladium(II) chloride (23 mg, 5.0 mol%) and copper(I) iodide (13 mg, 10 mol%). After drying under vacuum, the solids were dissolved in dry toluene (15 mL) and freshly distilled diisopropylamine (7.5 mL) and the suspension was freeze-thaw degassed once. Trihexylsilylacetylene (620 mg, 2.0 mmol) was added by syringe and the resulting mixture was freeze-thaw degassed twice more and stirred at 40 °C under nitrogen. After 3 hr, no more starting material remained by TLC (199:1 DCM:MeOH) and the reaction was diluted with toluene (50 mL), washed with saturated aqueous ammonium chloride (1 × 100 mL) and brine (1 × 100 mL). The organic layer was dried over magnesium sulfate, filtered and the solvent evaporated. The crude mixture was purified by column chromatography (SiO_2: 99:1 DCM:methanol) to afford a green glass (1.7 g, 85%); δ_H (400 MHz, $CDCl_3$/1% pyridine-d_5) 0.86-0.90 (m, 18H), 0.97-1.02 (m, 12H), 1.32-1.43 (m, 24H), 1.49-1.56 (m, 12H), 1.71-1.79 (m, 12H), 2.24 (s, 3H), 3.31 (s, 6H), 3.48-3.50 (m, 4H), 3.61-3.66 (m, 8H), 3.68-3.70 (m, 4H), 3.77-3.80 (m, 4H), 3.94-3.97 (m, 4H), 4.33-4.35 (m, 4H), 7.31-7.34 (m, 2H), 7.59-7.63 (m, 2H), 7.74-7.75 (m, 4H), 8.85 (d, J = 4.6 Hz, 2H), 9.61-9.62 (d, J = 4.6 Hz, 2H), *m/z* MALDI-ToF+ 1462.76 $C_{86}H_{124}N_4O_8Si_2Zn$ requires 1460.82 (100%).

1-trihexylsilylacetylene-5,15-bis-3-(2-(2-(2-methoxy-ethoxy)ethoxy)ethoxy)phenyl zinc porphyrin

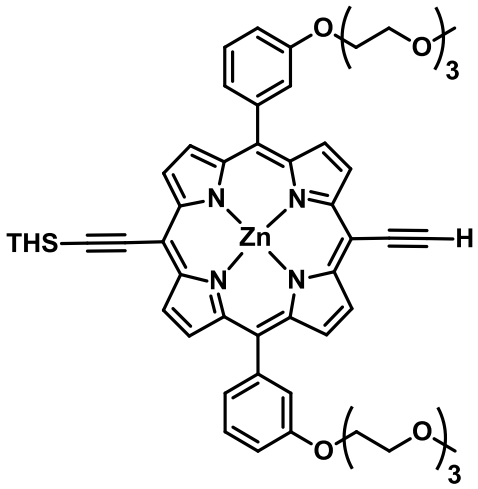

This compound was synthesised according to a literature procedure.[36] To a solution of 1,10-bis(trihexylsilylacetylene)-5,15-bis-3-(2-(2-(2-methoxy-ethoxy)ethoxy)ethoxy)phenyl zinc porphyrin (800 mg, 0.55 mmol) in chloroform (200 mL) was added tetrabutylammonium fluoride (320 µL of a 1.0 M solution in THF, 0.36 mmol). The reaction was monitored by TLC (10:1 DCM:ethyl acetate) and additional tetrabutylammonium fluoride solution (up to 1 equivalent) was added until bis-deprotected product was visible, at which point the reaction was quenched with calcium chloride. The product was purified by column chromatography (SiO_2: 10:1 DCM:ethyl acetate) to afford the product as a green glass (100 mg, 10%); δ_H (400 MHz, $CDCl_3$/1% pyridine-d_5) 0.92-0.95 (m, 12H), 1.04-1.07 (m, 6H), 1.29-1.32 (m, 6H), 1.37-1.47 (m, 12H), 1.55-1.61 (m, 8H), 1.78-1.84 (m, 6H), 2.09 (s, 1H), 3.36 (s, 6H), 3.53-3.55 (m, 4H), 3.67-3.68 (m, 4H), 3.73-3.75 (m, 4H), 3.82-3.84 (m, 4H), 4.00-4.02 (m, 4H), 4.14-4.19 (m, 4H), 4.38-4.40 (m, 4H), 7.37-7.39 (m, 2H), 7.64-68 (m, 2H), 7.79-7.80 (m, 4H), 8.90-8.93 (dd, J = 4.6 Hz, 4H), 9.67-9.69 (t, 4H).

Copper(I) chloride

This compound was prepared by a reported procedure.[25] Copper(II) chloride (16.0 g, 103 mmol) in water (100 mL) was added to a solution of sodium sulfite (15 g, 120 mmol) in water (100 mL). The suspension was immediately poured into concentrated hydrochloric acid (3 mL) and sodium sulfite (1.5 g, 12 mmol) in water (1 L). The solid was collected by filtration, washing with acetic acid (125 mL), ethanol (125 mL) and ether (125 mL) to yield a greenish white solid (3 g), which was dried *in vacuo*.

Bis-trihexylsilylacetylene porphyrin dimer (3)

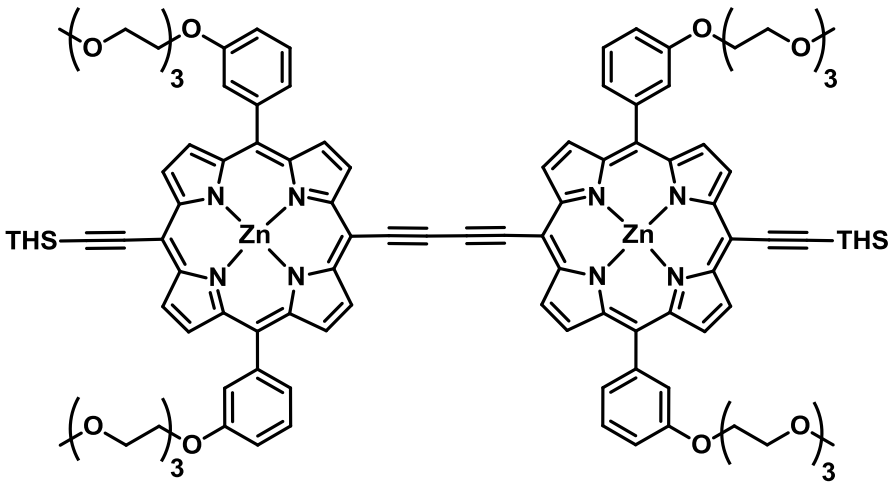

This compound was synthesised according to a literature procedure.[36] To a vigorously stirred solution of 1-trihexylsilylacetylene-5,15-bis-3-(2-(2-(2-methoxy-ethoxy)ethoxy)ethoxy)phenyl zinc porphyrin (180 mg, 0.15 mmol) in DCM (70 mL) was added freshly prepared copper(I) chloride (450 mg, 4.6 mmol), followed by tetramethylehtylenediamine (690 µL, 4.6 mmol). The reaction mixture was stirred vigorously for 1 hr, after which it was quenched with water (150 mL). The organic solution was washed with water until no blue colour persisted, then it was dried over magnesium sulfate, filtered, and concentrated to a small volume. The product was purified by column chromatography (SiO_2: 199:1 DCM:MeOH) to afford the product as a green glass (200 mg, 72%); δ_H (400 MHz, $CDCl_3$/1% pyridine-d_5) 0.89-0.93 (m, 18H), 1.00-1.05 (m, 12H), 1.35-1.45 (m, 28H), 1.52-1.59 (m, 12H), 1.74-1.82 (m, 12H), 3.31 (s, 12H), 3.49-3.51 (m, 8H), 3.64-3.65 (m, 8H), 3.69-3.72 (m, 8H), 3.78-3.81 (m, 8H), 3.96-3.99 (m, 8H), 4.36-4.38 (m, 8H); *m/z* MALDI-ToF+ 2358.92, $C_{136}H_{170}N_8O_{16}Si_2Zn_2$ requires 2358.08 (100%).

Bis-benzaldehyde porphyrin dimer (4)

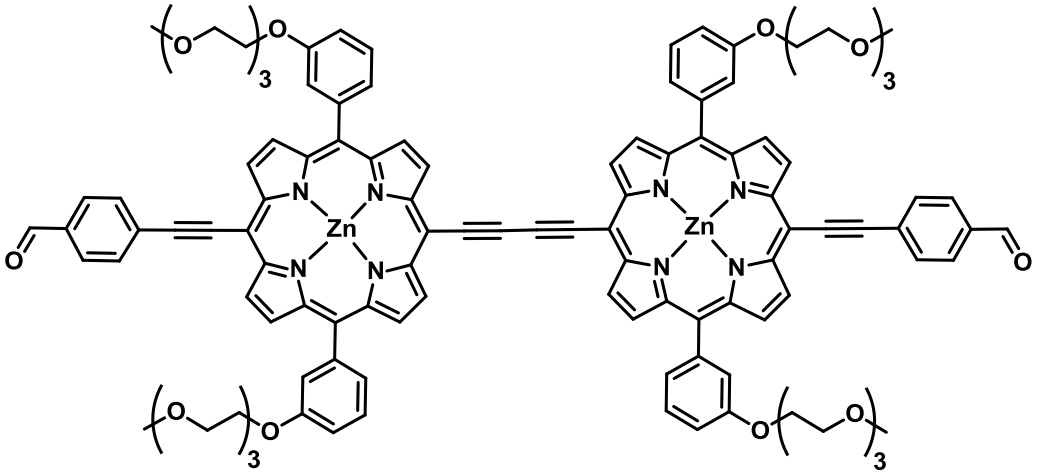

This novel compound was synthesised by adapting a literature procedure.[36] Bis-THS-protected porphyrin dimer (50 mg, 0.02 mmol), 4-iodobenzaldehyde (98 mg, 0.40 mmol), tris(dibenzylidineacetone)palladium(0) (5.0 mg, 25 mol%), copper(I) iodide (1.0 mg, 4.0 μmol), triphenylphosphine (6.0 mg, 0.020 mmol) were dried under vacuum in a pre-dried Schlenk tube. Dry diisopropylamine (1.5 mL) and dry toluene (2 mL) were added and the solution freeze-thaw degassed three times. The reaction mixture was allowed to warm to room temperature upon which, tetrabutylammoniumfluoride (170 μL of a 1.0 M solution in THF, 0.17 mmol) was added and the reaction stirred overnight at room temperature. When the reaction was complete by TLC (DCM:methanol 99:1), the reaction was diluted with toluene (70 mL), washed with saturated aqueous ammonium chloride (100 mL) and water (2 × 100 mL). The organic layer was concentrated *in vacuo* and the crude product was purified by column chromatography (SiO_2: DCM:methanol 99:1) followed by size-exclusion chromatography (THF) then recrystallision ($CHCl_3$/MeOH) to give the pure product as a green powder (42 mg, 100%); δ_H (400 MHz, $CDCl_3$:pyridine-d_5 1:1) 8.67 (d, 4H, J = 8.6 Hz, β-*H*) 8.65 (s, 2H, CO*H*) 8.51 (d, 4H, J = 8.6 Hz, β-*H*), 9.21 (d, 4H, J = 4.6 Hz, β-*H*), 9.17 (d, 4H, J = 4.6 Hz, β-*H*), 8.14 (d, 4H, J = 8.2 Hz), 8.02 (d, 4H, J = 8.2 Hz), 8.01 (s, 4H, Ar-H), 7.96 (d, 4H), 7.77 (t, 4H, Ar-*H*), 7.51 (d, 4H), 4.72 (br, 6H, TEG-O-CH_2), 4.44 (t, 8H, TEG-CH_2), 4.04 (t, 8H, TEG-CH_2), 3.86 (t, 8H, TEG-CH_2), 3.77 (t, 8H, TEG-CH_2), 3.70 (t, 8H, TEG-CH_2), 3.55 (t, 8H, TEG-CH_2) 3.34 (s, 12H, TEG-O-CH_3); δ_C ($CDCl_3$:Pyridine-d_5, 125 MHz) 57.2, 66.3, 68.4, 69.1, 69.2, 69.4, 70.5, 81.4, 87.4, 94.7, 96.3, 98.5, 99.3, 112.7, 120.0, 121.3, 126.1, 126.4, 128.4, 128.7, 129.5, 129.6, 130.0, 130.4, 131.6, 131.9, 142.3, 148.8, 149.0, 150.7, 151.8, 155.9, 189.6; *m/z* MALDI-ToF+ 2002.25, $C_{114}H_{102}N_8O_{18}Zn_2$ requires

2002.59 (100%); λ_{max} ($CHCl_3$) /nm (log ε) 467 (5.08), 500 (4.57), 591 (3.67), 690 (4.44), 748 (4.44); RP-HPLC (*Method D*) R_f: 9 min.

_N_-methyl-pyridyl Porphyrin Dimer (P_2C_2NMeI)

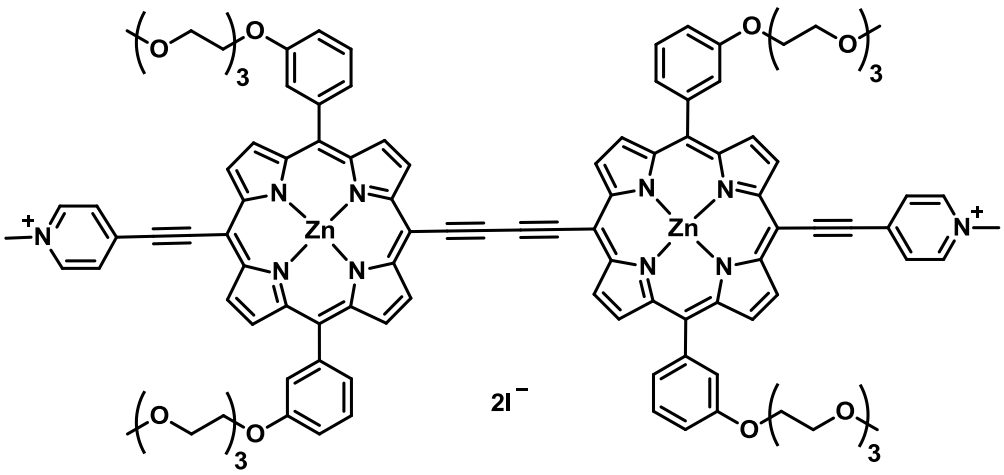

This compound was synthesised by following a reported procedure.[36] Methyl iodide (2.6 mL, 0.040 mol) was added to a solution of di-pyridyl porphyrin dimer (100 mg, 5.1 μmol) in anhydrous DMF (10 mL) and the mixture stirred at 40º C for 1 h. The reaction was monitored by RP-HPLC (*Method C*). The product was precipitated from the solution with ether (15 mL) then redissolved in DMF and crystallised from toluene. Microfiltration yielded a dark green powder (72 mg, 63%); δ_H (400 MHz, DMSO-d_6/5% d_5-pyridine) 3.14 (s, 12H, O-CH_3) 3.87-3.89 (m, 8H, CH_2) 4.42 (s, 6H, N-CH_3) 7.49-7.51 (m, 4H, Ar-H) 7.75-7.86 (m, 16H, β-H) 8.77 (d, J = 5.9 Hz, 4H, Pyr-CH_2) 9.15 (d, J = 5.9 Hz, 4H, py-CH); *m/z* MALDI-ToF+ 1978.4, $C_{112}H_{106}N_{10}O_{16}Zn_2I_2^-$ requires 1978.6 (100 %); λ_{max} (DMF/1% pyridine)/ nm (log ε) 471 (5.36) 594 (4.04) 710 (4.81) 770 (4.99).

Peptide Synthesis

_N_-tert-butoxy-carbonyl-amino-oxy-acetic acid-2,5-dioxypyrrolidin-1-yl ester (6)

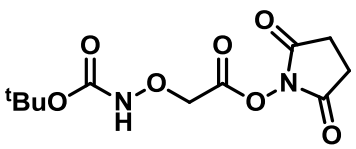

This compound was synthesised in accordance with a literature procedure.[262] To a solution of *N*-boc-aminooxyacetic acid (1.0 g, 5.2 mmol) in DMF (20 mL), *N*-hydroxy-succinimide (750 mg, 6.5 mmol) was added, followed by a solution of *N,N*-dicyclohexyl-carbodiimidazole

(1.35 g, 6.54 mmol) in DMF (60 mL). The reaction mixture was stirred at room temperature under nitrogen and monitored by TLC (ethyl acetate) until no starting material remained. The solvents were removed *in vacuo* and the resulting solid was extracted with ethyl acetate, filtered, washed with brine, dried over magnesium sulfate, filtered, and concentrated *in vacuo*. The resulting beige precipitate was purified by recrystallisation (DCM/heptane) to afford a white powder (1.4 g, 92%); δ_H (400 MHz, $CDCl_3$) 1.48 (s, 9H), 2.88 (t, 4H), 4.79 (s, 2H), 7.67 (s, 1H); δ_C (400 MHz, $CDCl_3$) 26.1, 28.7, 71.4, 83.2, 156., 165.6, 169.2; *m/*z ESI-MS+ 260.12, $C_{11}H_{16}N_2O_7$ requires 288.10 (100%).

***Tert*-butyl 2,2-dimethyl-4,8-dioxo-3.6-dioxa-5,9-diazaundecan-11-oate (7)**

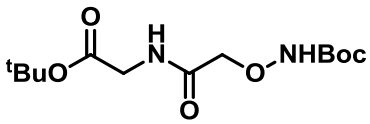

This novel compound was synthesised by modifying an existing procedure.[263] To a solution of glycine *tert*-butyl ester hydrochlorate (150 mg, 0.89 mmol) in DMF (10 mL) was added *N*-*tert*-butoxycarbonylaminooxyacetic acid-2,5-dioxypyrrolidin-1-yl ester (390 mg, 1.3 mmol) followed by diisopropylethylamine (1.17 mL, 6.71 mmol). The reaction was stirred under nitrogen for 4 h after which the DMF and diisopropylethylamine were removed *in vacuo*. The resulting yellow oil was dissolved in chloroform, washed with 0.5 M hydrochloric acid (4 × 10 mL), semi-saturated sodium bicarbonate (3 × 10 mL) then brine (15 mL), dried over magnesium sulfate and filtered. The yellow oil was passed over a short plug (SiO_2: ethyl acetate) and the resulting yellow oil was thoroughly dried *in vacuo* (190 mg, 70%); δ_H (400 MHz, DMSO-d_6) 1.40 (s, 9H, O-^{t}*Bu*), 1.41 (s, 9H, Boc-^{t}*Bu*), 3.80-3.78 (d, 2H Gly-CH_2), 4.20 (s, 2H), 8.30 (t, 1H, N*H*), 10.26 (s, 1H, O-N*H*); δ_C (400 MHz, $CDCl_3$) 28.1, 28.2, 41.5, 75.9, 82.0, 82.9, 157.6, 168.6, 169.3; *m/z* ESI-MS− 303.16, $[C_{13}H_{23}N_2O_6]^-$ requires 303.16 (100%).

2-(2-(amino-oxy) acetamido) acetic acid (8)

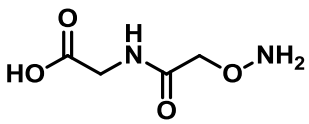

This novel compound was synthesised according to a literature procedure.[264] *Tert*-butyl 2,2-dimethyl-4,8-dioxo-3.6-dioxa-5,9-diazaundecan-11-oate (190 mg, 0.62 mmol) was treated with trifluoroacetic acid:water (95:5, 5 mL) for 4 hours. The trifluoroacetic acid was

evaporated under a stream of nitrogen and the product precipitated with ice-cold ether (15 mL) before collection by centrifugation. The resulting white pellet was washed with ice cold ether (15 mL) and re-centrifuged, before lyophilising from deuterated water (2 mL) yielding a pale green oil (93 mg, 94%); δ_H (400 MHz, DMSO-d_6) 8.39 (t, 1H, N*H*), 4.33 (s, 2H), 3.83 (s, 2H); δ_C (400 MHz, MeOH-d_4) 40.8, 71.7, 167.7, 171.2; *m/z* ESI-MS− 147.06, $[C_4H_7N_2O_4]^-$ requires 147.04 (100%).

AO-Linear RGD (10)

This compound was synthesised according to a literature procedure.[265] Manual solid-phase peptide synthesis (0.1 mmol, *Method I*) was used; *m/z* MALDI-ToF+ 412.02, $[C_{14}H_{27}N_8O_7]^+$ requires 412.20 (100%).

AO-(KLAKLAK)$_2$ (14)

This product was prepared by automated solid-phase peptide synthesis on a 0.1 mmol scale. The final coupling was carried out by adding **6** (60 mg, 0.25 mmol) to the suspension of resin pre-swelled in DMF. After 3 hours, the TNBS test indicated completion of the reaction. The beads were washed with DMF, then DCM and dried overnight. Cleavage from the solid support and removal of the acid labile protecting groups was performed using TFA:TIPS:H_2O (95:2.5:2.5) for 4 hours at room temperature. After filtration, the product was precipitated with cold ether and centrifuged to afford a while solid which was lyophilised from water (50 mg, 31%); *m/z* MALDI-ToF+ 1596.11, $[C_{74}H_{143}N_{22}O_{16}]^+$ requires 1596.26 (100%).

Linear R(Pbf)GD(O^{t}Bu)fK(Alloc)

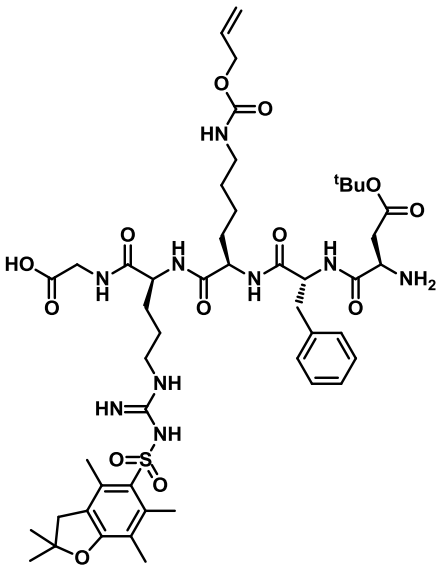

This product was prepared by adapting a reported procedure using manual solid-phase peptide synthesis *Method I* (SASRIN, 0.4 mM).[266] Cleavage of the peptide from the resin was achieved using HFIP:DCM (6 mL/g resin:14 mL/g resin). Solvents were removed *in vacuo* to afford a white powder (300 mg, 75%) which was used without further purification. *m/z* ESI-MS+ 1014.51, $C_{48}H_{72}N_9O_{13}S^+$ requires 1014.50 (100%); RP-HPLC R_f = 14.5 min (*Method A*).

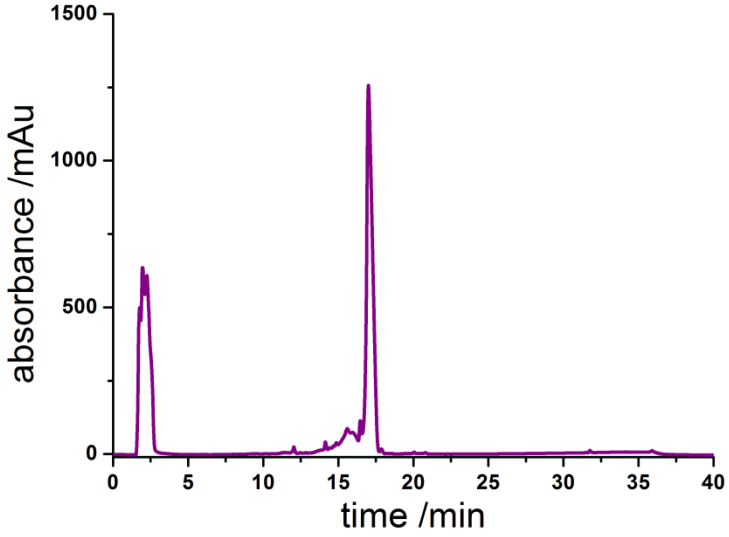

Figure 111: *RP-HPLC spectrum (250 nm) of the cleaved peptide.*

Cyclic R(Pbf)GD(O^{t}Bu)fK(Alloc)

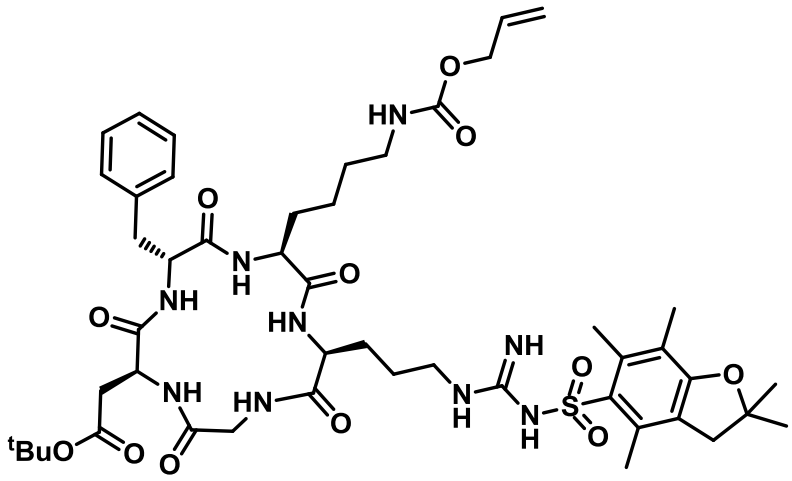

This compound was prepared by adapting a reported procedure.[267] Linear R(Pbf)GD(O^{t}Bu)fK(Alloc) (300 mg, 0.30 mmol) was dissolved in DMF* (600 mL) ([peptide] 0.5 mM). To this solution HBTU (170 mg, 0.45 mmol) was added, followed by DIPEA (310 µL, 1.8 mol), dropwise. The reaction mixture was stirred at room temperature overnight under N_2. The solvents were removed *in vacuo* and the product purified by recrystallisation (DCM:diethyl ether) affording a pale yellow solid (300 mg, 72%); δ_H (500 MHz, DMSO-d_6,) 8.42 (t, 1H, Gly-N*H*), 8.11 (d, 1H, Lys-NH_2), 8.06-7.99 (m, 2H, Lys-N*H* and Arg-N*H*), 7.54 (d, 1H, Asp-N*H*), 7.30-7.10 (m, 6H, Phe-*Ph* and Arg-Guanidine-N*H*), 6.68 (br, 1H, Guanidine-N*H*), 6.37 (br, 1H, Guanidine-N*H*), 5.47-6.35 (m, 1H, Alloc-*H*), 5.28 (dd, 1H, Alloc-*H*), 5.17 (dd, 1H, Alloc-*H*), 4.61 (q, 1H, Phe-*H*), 4.41 (m, 4H, Alloc-CH_2 and Asp-CH_2), 4.06 (m, 1H, Gly-CH_2), 3.21 (d, 1H, Gly-CH_2), 3.02 (m, 2H, Lys-CH_2), 2.98-2.83 (m, 6H, Arg-CH_2 and Lys-CH_2), 2.83-2.79 (m, 2H, Arg-CH_2), 2.01 (s, 3H, Arg-Pbf-CH_3), 1.60-1.54 (m, 2H, Lys-CH_2), 1.41 (s, 9H, Asp-O^t*Bu*), 1.38 (s, 12H, Arg-Pbf-CH_3), 1.25 (m, 2H, Lys-CH_2), 1.00 (m, 2H, Lys-CH_2); *m/z* ESI-MS+ 1010.56; RP-HPLC R_f = 21.7 min (*Method A*).

* *The cyclisation was initially performed using DMF which had been stirred over and distilled from calcium hydride. A subsequent reaction in which two batches of linear RGDfK were reacted in parallel, one dissolved in freshly-distilled DMF and another with DMF from a newly-opened Winchester bottle, gave almost identical yields.*

Linear Protected AO-RGDfK

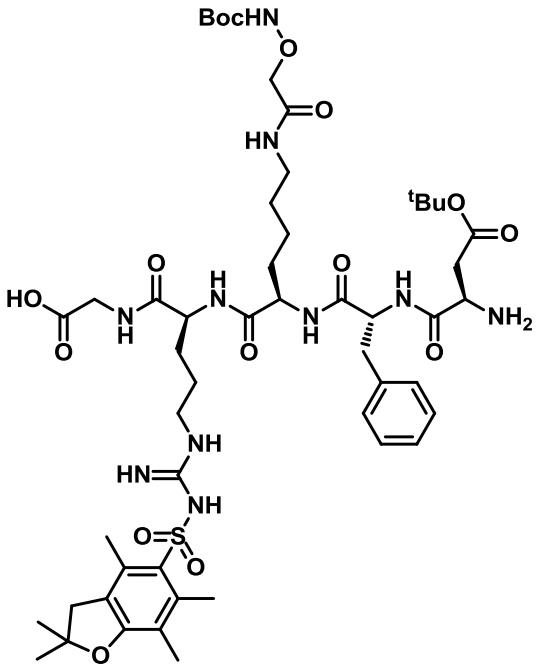

This product was prepared by adapting a reported procedure using manual solid-phase peptide synthesis *Method I* (SASRIN, 0.4 mM).[266] Cleavage of the peptide from the resin was achieved using DCM/1% TFA until the resin turned purple (4 × 4 mL × 3 min). Solvents were removed *in vacuo* to afford a white powder (150 mg, 68%). The product was used without further purification; *m/z* ESI MS+ 1103.53, $[C_{51}H_{79}N_{10}O_{15}S]^+$ requires 1103.54 (100%); RP-HPLC R_f = 15.9 min (*Method A*).

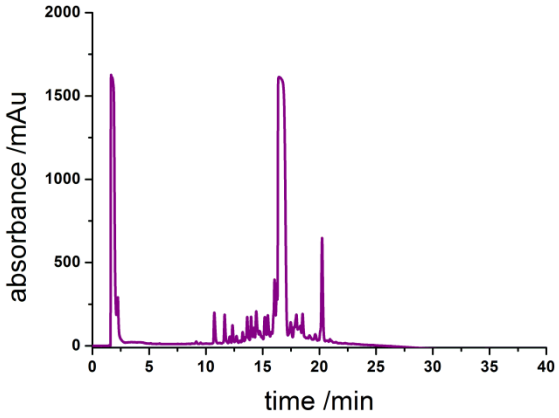

Figure 112: *RP-HPLC spectrum (250 nm) of the cleaved peptide.*

Cyclic R(Pbf)GD(O^{t}Bu)fK

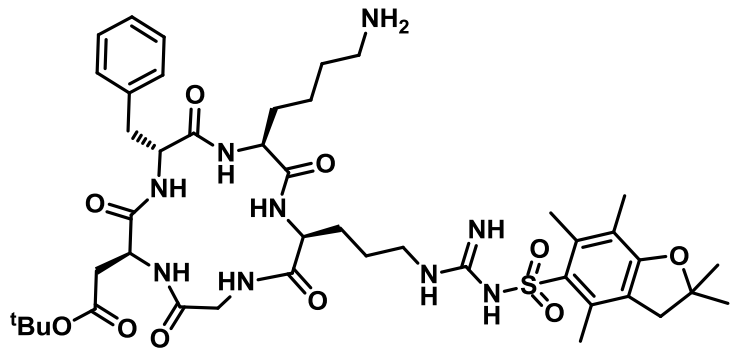

This compound was prepared by adapting an existing procedure.[266] Fully protected cyclic RDGfK (20 mg, 0.02 mmol) was dissolved in anhydrous DMF (5 mL). To this solution, phenylsilane (40 µL, 0.4 mmol) was added. The combined solution was freeze-thaw degassed three times before purging with nitrogen and adding tetrakistriphenylphosphine palladium(0) (4.6 mg, 20 mol%). The reaction was stirred under nitrogen at room temperature. After 30 mins, the solvent and excess phenylsilane were removed *in vacuo* yielding a brown solid (8 mg, 44%); δ_H (500 MHz, DMSO-d_6,) 8.42 (t, 1H, Gly-N*H*), 8.11 (d, 1H, Lys-NH_2), 8.06-7.99 (m, 2H, Lys-N*H* and Arg-N*H*), 7.54 (d, 1H, Asp-N*H*), 7.30-7.10 (m, 6H, Phe-*Ph* and Arg-Guanidine-N*H*), 6.68 (br, 1H, Guanidine-N*H*), 6.37 (br, 1H, Guanidine-N*H*), 4.61 (q, 1H, Phe-*H*), 4.41 (m, 4H, Asp-CH_2), 4.06 (m, 1H, Gly-CH_2), 3.21 (d, 1H, Gly-CH_2), 3.02 (m, 2H, Lys-CH_2), 2.98-2.83 (m, 6H, Arg-CH_2 and Lys-CH_2), 2.83-2.79 (m, 2H, Arg-CH_2), 2.01 (s, 3H, Arg-Pbf-CH_3), 1.60-1.54 (m, 2H, Lys-CH_2), 1.41 (s, 9H, Asp-O^t*Bu*), 1.38 (s, 12H, Arg-Pbf-CH_3), 1.25 (m, 2H, Lys-CH_2), 1.00 (m, 2H, Lys-CH_2); *m/*z ESI-MS+ 912.46, $[C_{44}H_{66}N_9O_{10}S]^+$ requires 912.47 (100%) ; RP-HPLC R_f 15.2 min (*Method A*).

Cyclic AO-R(Pbf)GD(O^{t}Bu)fK (13)

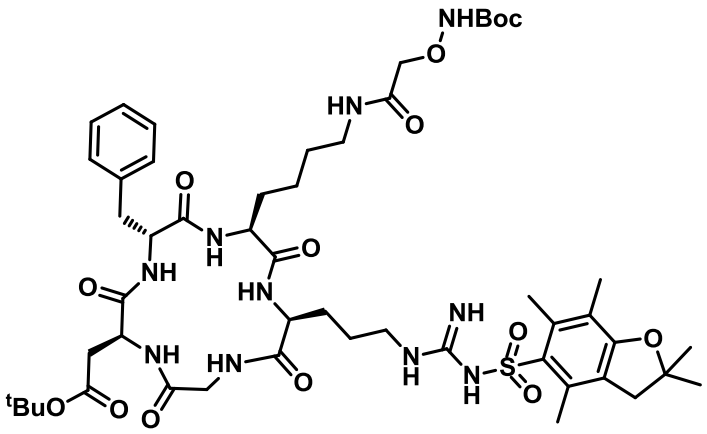

This compound was prepared by adapting an existing procedure.[266] Crude cyclic R(Pbf)GD(O^{t}Bu)fK was re-dissolved in anhydrous DMF (4 mL) and *N*-tert-butoxy-carbonyl-amino-oxy-acetic acid-2,5-dioxypyrrolidin-1-yl ester (13 mg, 0.040 mmol) was added. The reaction mixture was stirred at room temperature overnight. After removing the solvent, the orange solid was taken up in acetonitrile:water 3:1 and filtered. The product was isolated by semi-preparative RP-HPLC (*Method A*) and lyophilised overnight yielding a white solid (13 mg, 64%); δ_H (500MHz, DMSO-d_6) 1.00 (m, 2H, Lys-CH_2), 1.25 (m, 2H, Lys-CH_2), 1.38 (s, 12H, Arg-Pbf-CH_3), 1.41 (s, 18H, Asp-O^t*Bu* and AO-CH_3), 1.60-1.54 (m, 2H, Lys-CH_2), 2.01 (s, 3H, Arg-Pbf-CH_3), 2.83-2.79 (m, 2H, Arg-CH_2), 2.98-2.83 (m, 6H, Arg-CH_2 and Lys-CH_2), 3.02 (m, 2H, Lys-CH_2), 3.21 (d, 1H, Gly-CH_2), 4.06 (m, 1H, Gly-CH_2), 4.41 (m, 4H, AO-CH_2 and Asp-CH_2), 4.61 (q, 1H, Phe-*H*), 6.37 (br, 1H, Guanidine-N*H*), 6.68 (br, 1H, Guanidine-N*H*), 7.30-7.10 (m, 6H, Phe-*Ph* and Arg-Guanidine-N*H*), 7.54 (d, 1H, Asp-N*H*), 8.06-7.99 (m, 2H, Lys-N*H* and Arg-N*H*), 8.11 (d, 1H, Lys-NH_2), 8.42 (t, 1H, Gly-N*H*); *m/z* ESI-MS− 1083.55, $[C_{51}H_{75}N_{10}O_{14}S]^+$ requires 1084.53 (100%); RP-HPLC R_f 19.2 min (*Method A*).

Cyclic AO-RGDfK (12)

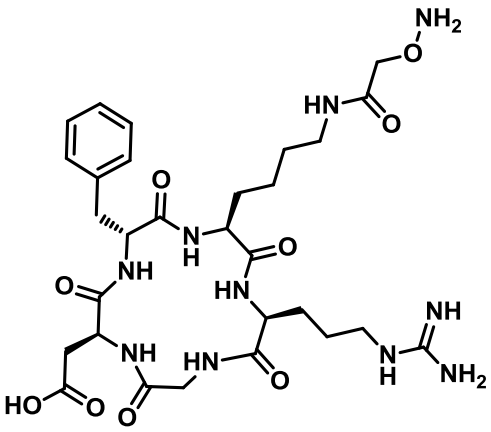

This compound was prepared by adapting an existing procedure.[266] Cyclic AO-R(Pbf)GD(O^{t}Bu)fK (21 mg, 19 mmol) was treated with TFA:TIPS:H_2O (5 mL, 95:2.5:2.5) for 4 hours. Following this the cleavage cocktail was reduced to a small volume by nitrogen bubbling and the product precipitated by the addition of ice-cold diethyl ether (15 mL). The product was collected by centrifugation, dissolved in water and lyophilised to give a white fluffy solid (10 mg, 78%); δ_H (500MHz, DMSO-*d*$_6$) 1.02 (m, 2H, Lys-C*H*$_2$) 1.28-1.56 (m, 8H), 1.69-1.73 (m, 1H), 2.36-2.39 (dd, 1H), 2.67-2.73 (m, 1H), 2.80-2.84 (m, 1H), 2.89-2.93 (m, 1H), 3.00-3.09 (m, 4H), 3.22-3.26 (m, 1H), 3.90-3.94 (m, 1H, Gly-C*H*$_2$), 4.00-4.06 (m, 1H, AO-C*H*$_2$ and Asp-C*H*$_2$), 4.13-4.18 (m, 3H), 4.43 (q, 1H), 4.63 (q, 1H, Phe-*H*), 7.14-7.20 (m, 4H), 7.24-7.27 (m, 2H), 7.52 (t, 1H), 7.60 (d, 1H), 7.98 (d, 1H), 8.00 (t, 1H) 8.01 (d, 1H), 8.10 (d, 1H), 8.40-8.42 (t, 1H); RP-HPLC (*Method A*) t_R 5.1 mins; *m/z* ESI-MS+ 677.39, $[C_{29}H_{45}N_{10}O_9]^+$ requires 677.34 (100%).

Peptide-Conjugated Porphyrin Dimers

Bis-AO-RGD Porphyrin Dimer (11)

Bis-benzaldehyde porphyrin dimer (22 mg, 0.81 μmol) and crude AO-RGD (13 mg, 0.030 mmol) were dissolved in DMSO (0.2 mL). Progress and purification were performed by RP-HPLC to afford a green glass (23 mg, 69%); *m/z* MALDI-ToF+ 2803.41, $[C_{142}H_{150}N_{24}O_{30}Zn_2]^+$ requires 2802.95 (100%).

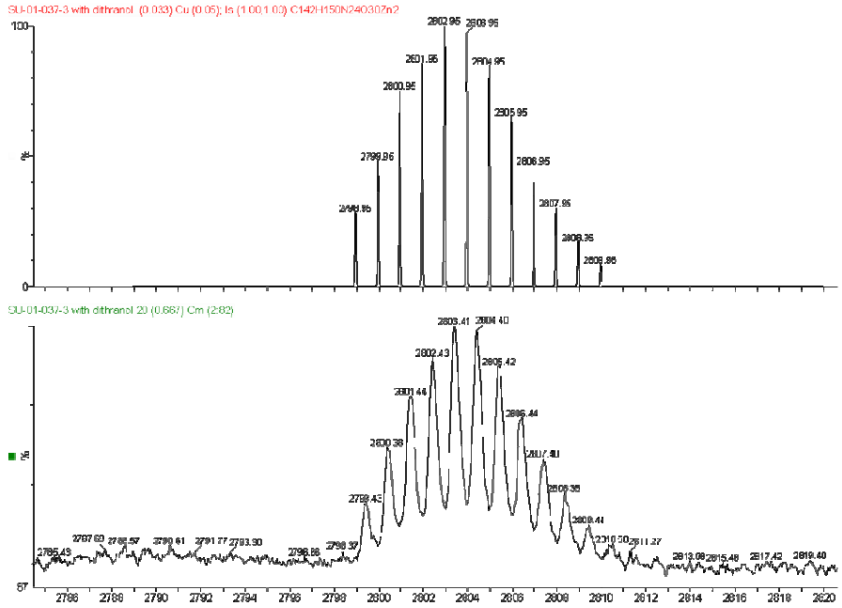

Figure 113: *Theoretical and experimental MALDI-ToF spectra of compound **11**. Data reproduced from Dr Ulrich's post-doctoral report.*

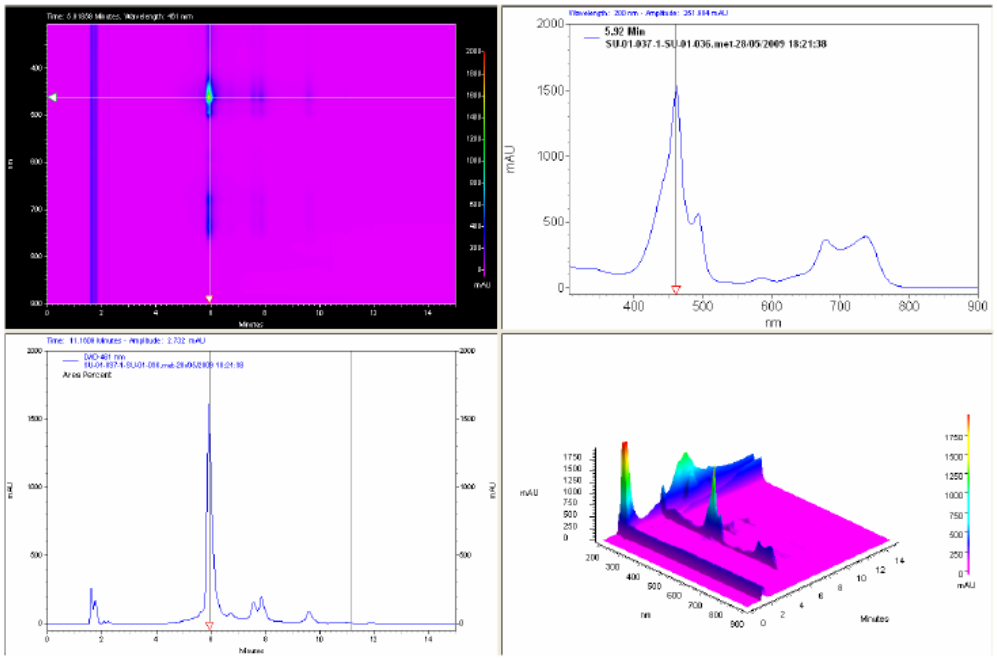

Figure 114: *RP-HPLC analysis of 11 showing the HPLC trace (bottom left) and 1D, 2D, and 3D UV/Vis spectra (top right, top left and bottom right respectively). Data reproduced from Dr Ulrich's post-doctoral report.*

Bis-AO-(KLAKLAK)$_2$ Porphyrin Dimer (15)

Bis-benzaldehyde porphyrin dimer (6.0 mg, 3.0 µmol) and AO-(KLAKLAK)$_2$ (15.8 mg, 6.60 µmol) were dissolved in DMSO (0.2 mL). Progress monitoring and purification were performed using RP-HPLC to give a green glass (8 mg, 52%).

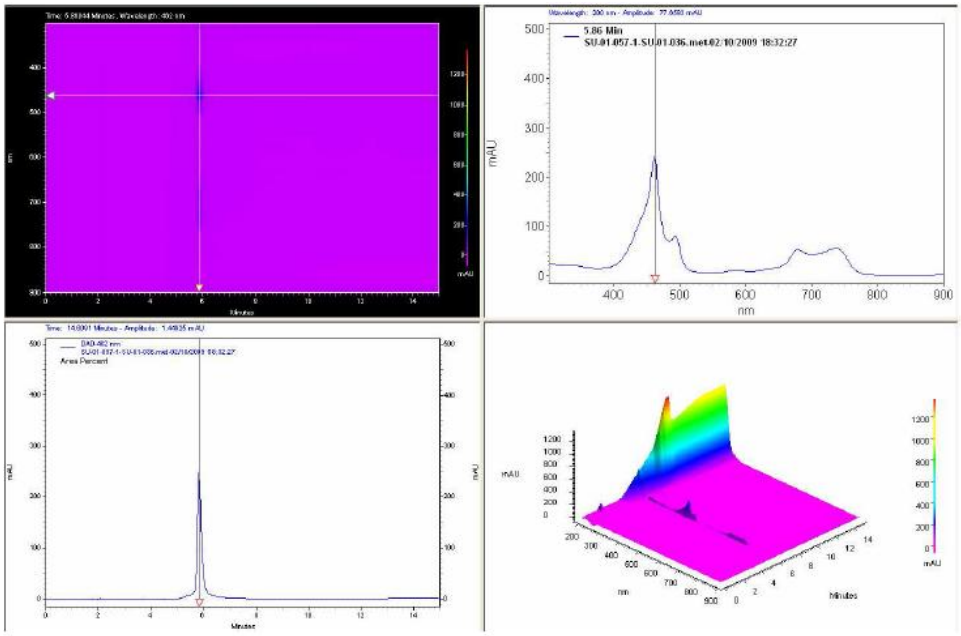

Figure 115: *RP-HPLC analysis of 11 showing the HPLC trace (bottom left) and 1D, 2D, and 3D UV/Vis spectra (top right, top left and bottom right respectively). Data reproduced from Dr Ulrich's post-doctoral report.*

Bis-AO-Glycine Porphyrin Dimer (9)

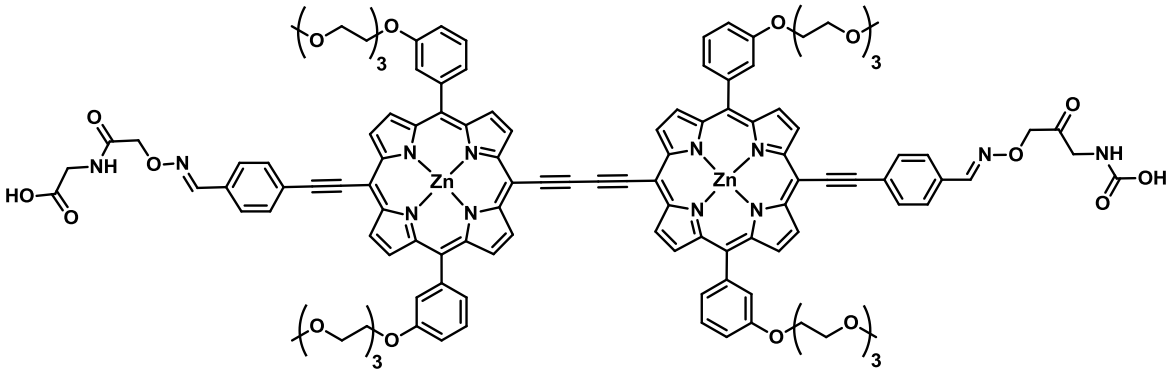

This novel compound was synthesised by adapting a reported procedure.[245] To bis-benzaldehyde porphyrin dimer (10 mg, 5.0 µmol) was added AO-Gly (300 µL of a 100 mM solution in DMSO, 2.5 mmol), acetic acid (30 µL) and aniline (3 µL). The solution was stirred at 40 °C and the reaction monitored by RP-HPLC (*Method D)*. After 4 h, the reaction

had stopped and the product (Rf: 8 min) was isolated by semi-preparative RP-HPLC (*Method D*). The THF and methanol were removed *in vacuo* followed by lyophilisation to give the pure product as a dark green powder (6 mg, 53%); δ_H (500 MHz, THF-d_4) 3.22 (s, 12H), 3.40-3.42 (m, 8H), 3.54-3.55 (m, 8H), 3.60-3.61 (m, 8H), 3.68-3.69 (m, 8H), 3.92-3.93 (t, 8H), 3.98-3.99 (d, 4H, *Gly-CH*$_2$), 4.36-4.38 (t, 8H), 4.66 (s, 4H, *AO-CH*$_2$), 7.27 (t, 2H, *Gly-NH*), 7.40-7.42 (d, 4H), 7.66-7.70 (t, 4H), 7.66-7.67 (d, 4H), 7.70 (s, 4H), 7.79-7.80 (d, *J* = 8.2 Hz 4H), 8.10-8.11 (d, *J* = 8.2 Hz, 4H), 8.41 (s, 2H, *Imine-H*), 8.93-8.94 (d, *J* = 4.6 Hz, 4H, *β-H)*, 9.00-9.01 (d, *J* = 4.6 Hz, 4H, *β-H)*, 9.75-9.76 (d, *J* = 4.6 Hz, 4H, *β-H)*, 9.87-9.88 (d, *J* = 4.6 Hz, 4H, *β-H)*, 10.84 (s, *OH*); *m/z* MALDI-ToF+ 2256.14, $C_{122}H_{114}O_{12}N_{24}Zn_2$ requires 2261.67 (100%); RP-HPLC (*Method D*) RP-HPLC R_f : 8 min.

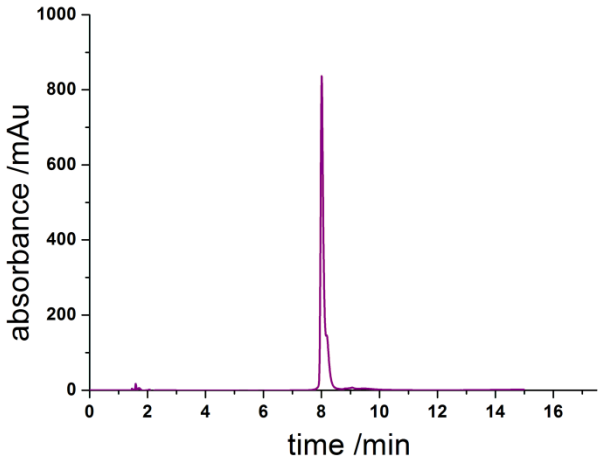

Figure 116: *RP-HPLC spectrum of* ***9*** *after purification by semi-preparative HPLC.*

Bis-Cyclic RGDfK Porphyrin Dimer

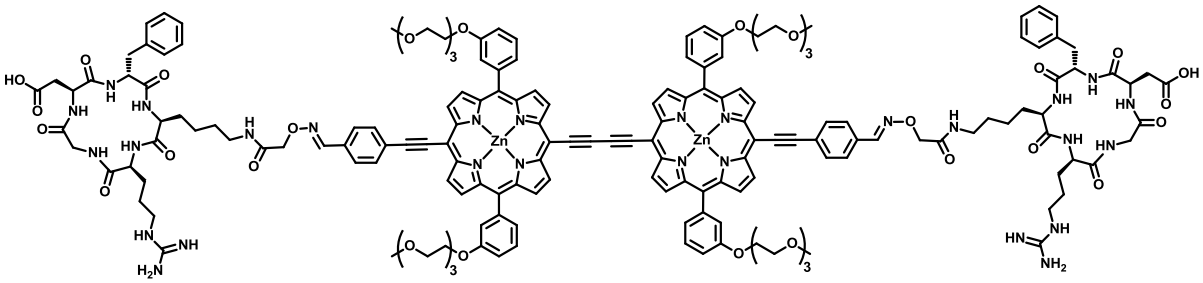

This novel compound was synthesised by adapting a reported procedure.[245] Bis-benzaldehyde appended porphyrin dimer (4.0 mg, 2.1 mmol) and cyclic RGDfK (3.2 mg, 4.0 mmol) were dissolved in 1:1 DMSO:NH_4OAc buffer (pH 4.5) (400 µL) and stirred at 35 ºC for 2 h. The

reaction progress was monitored by RP-HPLC (*Method B*). Purification was performed by semi-preparative RP-HPLC using the same method. RP-HPLC R_f: 6.3 min (*Method B*).

Overall Conclusions

This thesis documents the design and synthesis of dyes with exceptional two-photon absorption cross-sections, which have been modified both for specific biological applications and to improve their biological compatibility.

While the pharmacokinetics and sub-cellular localisation of a known two-photon PDT photosensitiser were demonstrated to be improvable by conjugation with short peptides, a coincident increase in the toxicity of the photosensitiser was observed. The use of a more rapid and efficient synthetic strategy would be necessary to further investigate the breadth of this problem.

A new project, based on two-photon uncaging of biologically active molecules by means of a photoinduced electron transfer, was developed. The principal of uncaging GABA *via* one-photon PeT was demonstrated *in vitro*. Analysis of the electron transfer kinetics showed that there is significant scope to improve the system, and it is hoped that order-of-magnitude increases in the two-photon uncaging cross-section will be observed in the future.

Appendix 1

Caged-Fluoroacetic Acid for Controlled Cytotoxicity

The caging of a highly cytotoxic species provides an alternative approach to PDT to achieve localised cell death. In addition, highly localised toxicity could be used in neurophysiology to deactivate individual neurons.

Fluoroacetic acid is highly cytotoxic molecule that, as a simple carboxylic acid, can be easily protected with many of the known caging groups. There are no examples of caged fluoroacetic acid in the literature, which is possibly due to its high toxicity (lethal oral dose 2-10 mg/kg in humans) and there being no antidote to its action.[268]

The reason for the compound's high toxicity is related to its metabolism. Upon entering the mammalian body, monofluoroacetic acid is converted to fluorocitrate. This inhibits coenzyme A, a critical enzyme in the early stages of the citric acid (Krebs) cycle and results in the deactivation of mitochondria. This deprives the cell of its main energy source and quickly leads to death by apoptosis. On an organism scale this results in the halting of oxidative metabolism, leading to lactic acidosis and the prevention of fatty acid oxidation, which leads to further acidosis. In addition, glutamate production is impaired, leading to reduced brain function. Death is usually the result of ventricular arrhythmia or hypertension several hours after a lethal dose is ingested.

Preliminary investigations into the possibility of caging fluoroacetic acid were conducted by derivatising a simple *para*-methoxyphenacyl group. The ease of derivatisation of phenacyl groups with carboxylic acids made the synthesis of a reference phenacyl-caged fluoroacetate very simple, an advantage when handling toxic compounds. For comparison, *para*-methoxyphenacyl acetate was also synthesised (**Scheme 1**).

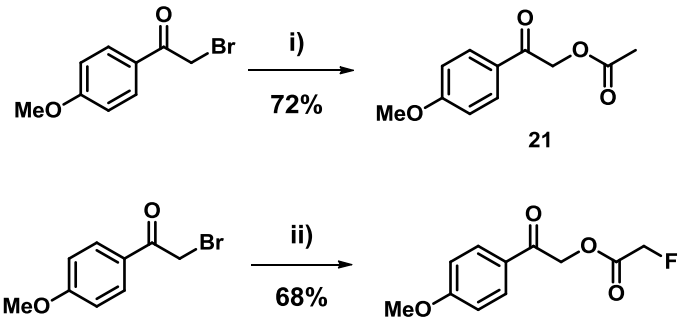

Scheme 1: *(i) Sodium acetate, ethanol, 100 °C, 2 h (ii) sodium fluoroacetate, NaI, DMF, 90 °C, 2 h.*

An important parameter for the biological application of caging groups is the stability of the bond between the caged compound and the caging group to hydrolysis. Some background hydrolysis under physiological conditions is inevitable, so measurement of the hydrolytic half-life was performed by incubating a 1 mM solution of the caged compound in PBS D_2O solution (pH 7.4) at 38 °C and monitoring hydrolysis by NMR.

Unfortunately, fluoroacetate esters were found to be particularly susceptible to hydrolysis. The half-life of phenacyl-caged fluoroacetate was found to be around 2 hours compared to 23 hours for phenacyl-caged acetate. This is a significant difference and, more importantly, a half-life of 2 hours is too short to be used in a potential biological application as there will be a significant amount of background hydrolysis and therefore systemic toxicity.

In addition to the phenacyl-caged acetate, a dimethoxy-*ortho*-nitrobenzyl-caged fluoroacetate was synthesised according to **Scheme 2**. This compound, which could potentially be used for two-photon uncaging, was synthesised with the intention of comparison with a PeT system.

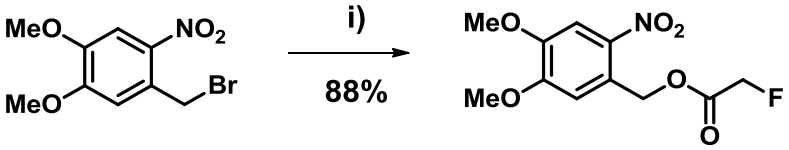

Scheme 2: *(i) Sodium fluoroacetate, NaI, DMF, 90 °C, 2 h.*

The synthesis is again simple and high yielding. Incubation of this compound in D_2O at 38 °C showed 50% hydrolysis after 6 hours. This is longer than the phenacyl derivative, but still quite a short time period. For example, an experiment lasting one hour would expect around 10% background uncaging.

Due to their hydrolytic susceptibility and the unreliability of a supply from commercial sources, no further investigation into caged-fluoroacetate was undertaken.

Bibliography

1. Boyd, R. W., *Nonlinear optics*, Elsevier, California, 2008, pp 1-65.
2. Williams, D. J., Organic polymers and nonpolymeric materials with good nonlinear optical properties, *Angew. Chem.*, 1984, **96**, 637-651.
3. Goeppert-Mayer, M., Uber elementarakte mit zwei quantensprüngen, *Ann. Phys.*, 1931, **9**, 273-295.
4. Dirac, P A. M., *The Principles of Quantum Mechanics*, Clarendon Press, Oxford, 1930.
5. Kaiser, W. and Garrett, C. G. B., Two-photon excitation in CaF_2:Eu^{2+}, *Phys. Rev. Lett.*, (1961), **7**, 229-231
6. Barzoukas, M. and Blanchard-Desce, M., Molecular engineering of push-pull dipolar and quadrupolar molecules for two-photon absorption: a multivalence-bond states approach, *J. Chem. Phys.*, 2000, **113**, 3951-3959.
7. Cronstrand, P. Norman, P., Luo, Y., Agren, H., Few-states models for three-photon absorption, *J. Chem. Phys.*, 2004, **121**, 2020-2029.
8. Birge, R. R., An introduction to two-photon spectroscopy, *NATO ASI Ser., Ser. C*, 1984, **139**, 457-471.
9. Birge, R. R., Pierce, B. M., Semi-classical time-dependent theory of two-photon spectroscopy. The effect of dephasing in the virtual level on the two-photon excitation spectrum of isotachysterol, *Int. J. Quantum Chem.*, 1986, **29**, 639-656.
10. Kasha, M., Characterization of electronic transitions in complex molecules, *Faraday Soc. Discuss.*, 1950, **9**, 14-19.
11. Helmchen, F. and Denk, W., Deep tissue two-photon microscopy, *Nat. Methods*, 2005, **2**, 932-940.
12. Chung, S.-J., Zheng, S., Odani, T., Beverina, L., Fu, J., Padilha, L. A., Biesso, A., Hales, J. M., Zhan, X., Schmidt, K., Ye, A., Zojer, E., Barlow, S., Hagan, D. J., van Stryland, E. W., Yi, Y., Shuai, Z., Pagani, G. A., Brédas, J.-L., Perry, J. W. and Marder, S. R., Extended squaraine dyes with large two-photon absorption cross-sections, *J. Am. Chem. Soc.*, 2006, **128**, 14444-14445.
13. Drobizhev, M., Stepanenko, Y., Karotki, A., Rebane, A., Taylor, P. N. and Anderson, H. L., Understanding strong two-photon absorption in π-conjugated porphyrin dimers *via* double-resonance enhancement in a three-level model, *J. Am. Chem. Soc.*, 2004, **126**, 15352-15353.
14. Friedrich, D. M. and McClain, W. M., Two-photon molecular electronic spectroscopy, *Annu. Rev. Phys. Chem.*, 1980, **31**, 559-577.
15. Birge, R. R., Parsons, B., Song, Q. W. and Tallent, J. R., *Molecular Electronics*, Blackwell Science, London, 1997.
16. Pawlicki, M., Collins, H. A., Denning, R. G. and Anderson, H. L., Two-photon absorption and the design of two-photon dyes, *Angew. Chemie. Int. Ed.*, 2009, **48**, 3244-3266.
17. Rebane, A., Drobizhev, M., Makarov, N. S., Beuerman, E., Haley, J. E., Krein, D. M., Burke, A. R., Flikkema, J. L. and Cooper, T. M., Relation between two-photon absorption and dipolar properties in a series of fluorenyl-based chromophores with electron donating or electron withdrawing substituents, *J. Phys. Chem. A.*, 2011, **115**, 4255-4262.

18. Heflin, J. R., Wong, K. Y., Zamani-Khamiri, O. and Garito, A. F., Nonlinear optical properties of linear chains and electron-correlation effects, *Phys. Rev. B.*, 1988, **38**, 1573-1576.
19. Kim, H. M. and Cho, B. R., Two-photon materials with large two-photon cross-sections. Structure-property relationship, *Chem. Commun.*, 2009, 153-164.
20. Van Stryland, E. W., and Hagab, D. J., *Encyclopaedia of optical engineering*, ed. Driggers, R. G. and Dekker, M., New York, 2003, pp. 1475-1481.
21. Bahae-Sheik, M., Said, A. A., Wei, T. H., Hagan, D. J. and van Stryland, E. W., Sensitive measurement of optical nonlinearities using a single beam, *IEEE J. Quantum Electron.*, 1990, **26**, 760-769.
22. Bass, M., van Stryland, E. W. and Stewart, A. F., Laser calorimetric measurement of two-photon absorption, *Appl. Phys. Lett.*, 1979, **34**, 142-144.
23. Xu, C., Webb, W. W., Measurement of two-photon excitation cross-sections of molecular fluorophores with data from 690 to 1050 nm, *J. Opt. Soc. Am. B: Opt. Phys.*, 1996, **13**, 481-491.
24. Patel, C. K. N. and Tam, A. C., Optoacoustic spectroscopy of liquids, *Appl. Phys. Lett.*, 1979, **34**, 467-470.
25. Kershaw, S., in *Characterization techniques and tabulations for organic nonlinear optical materials*, eds. Kuzyk, M. G. and Dirk, C. W., Marcel Dekker, New York, 1998, pp. 515-654.
26. Arnbjerg, J., Johnsen, M., Frederiksen, P. K., Braslavsky, S. E. and Ogilby, P. R., Two-photon photosensitized production of singlet oxygen: optical and optoacoustic characterization of absolute two-photon absorption cross sections for standard sensitizers in different solvents, *J. Phys. Chem. A.*, 2006, **110**, 7375-7385.
27. Albota, M., Beljonne, D., Brédas, J.-L., Ehrlich, J. E., Fu, J.-Y., Heikel, A. A., Hess, S. E., Kogej, T., Levin, M. D., Marder, S. R., McCord-Maughon, D., Perry. J. W., Röckel, H., Rumi, M., Subramaniam, G., Webb, W. W., Wu, X.-L., Xu, C., Design of organic molecules with large two-photon absorption cross sections, *Science*, 1998, **281**, 1653-1656.
28. Binev, I. G., Kuzmanova, R. B., Kaneti, J., Juchnovski, I. N., Determination of constants of anionic substituents based on nitrile infrared frequencies and intensities, *J. Chem. Soc. Perkin Trans.2*, 1982, 1533-1536.
29. Ventelon, L., Moreaux, L., Mertz, J. and Blanchard-Desce, M., New quadrupolar fluorophores with high two-photon excited fluorescence, *Chem. Commun.*, 1999, 2055-2056.
30. Ventelon, L., Charier, S., Moreaux, L., Mertz, J. and Blanchard-Desce, M., Nanoscale push-pull dihydrophenanthrene derivatives as novel fluorophores for two-photon-excited fluorescence, *Angew. Chem., Int. Ed.*, 2001, **40**, 2098-2101.
31. Werts, M. H., Gmouh, S., Mongin, O., Pons, T. and Blanchard-Desce, M., Strong modulation of two-photon-excited fluorescence of quadrupolar dyes by (de)protonation, *J. Am. Chem. Soc.*, 2004, **126**, 16294-16295.
32. Mongin, O., Porrès, L., Charlot, M., Katan, C. and Blanchard-Desce, Synthesis, fluorescence, and two-photon absorption of a series of elongated rodlike and banana-shaped quadrupolar fluorophores: A comprehensive study of structure-property relationships, *Chem. Eur. J.*, 2007, **13**, 1481-1498.
33. Ahn, T. K., Kim, K. S., Kim, D. Y., Noh, S. B., Aratani, M., Ikeda, C., Osuka, A. and Kim, D., Relationship between two-photon absorption and the π-conjugation pathway in

porphyrin arrays through dihedral angle control, *J. Am. Chem. Soc.*, 2006, **128**, 1700-1704.
34. Frixa, C., Mahon, M. F., Thompson, A. S., Threadgill, M. D., Direct Cu(I)-catalysed coupling of a carborane to a *meso*-tetraphenylporphyrin, *Tetrahedron Lett.*, 2002, **43**, 1557-1559.
35. Kim, K. S., Noh, S. B., Katsuda, T., Ito, S., Osuka, A. and Kim, D., Charge transfer induced enhancement of near-IR two-photon absorption of 5,15-bis(azulenylethynyl) zinc(II) porphyrins, *Chem. Commun.*, 2007, 2479-2481.
36. Balaz, M., Collins, H. A., Dahlstedt, E. and Anderson, H. L., Synthesis of hydrophilic conjugated porphyrin dimers for one-photon and two-photon photodynamic therapy at NIR wavelengths, *Org. Biomol. Chem.*, 2009, **7**, 847-888.
37. Hisaki, I., Hiroto, S., Noh, S. B., Kim, D., Shinokubo, H. and Osuka, A., Synthesis of doubly β-to-β 1,3-butadiyne-bridged diporphyrins: enforced planar structures and large two-photon absorption cross sections, *Angew. Chem. Int. Ed.*, 2007, **46**, 5125-5128.
38. Sakadzic, S, Roussakis, E., Yaseen, M. A., Mendeville, E. T., Srinivasan, V. J., Arai, K., Ruvinskaya, S., Devor, A., Lo, E. H., Vinogradov, S. A., Two-photon high-resolution measurement of partial pressure of oxygen in cerebral vasculature and tissue, *Nat. Meth.*, 2010, **7**, 755-759.
39. Spangler, C. W., Rebane, A., Starkey, J., Drobizhev, M., Targeted two-photon PDT photo-sensitizers for the treatment of subcutaneous tumors, *Proc. SPIE*, 2009, **7380**, Pt 2 Photodynamic Therapy.
40. Dy, J. T., Maeda, R., Nagatsuka, Y., Ogawa, K., Kamada, K., Ohta, K, Kobuke, Y., A photochromic porphyrin-perinaphthothioindigo conjugate and its two-photon absorption properties, *Chem. Commun.*, 2007, 5170-5172.
41. Kuebler, S. M., Rumi, M. in *Encyclopedia of Modern Optics Vol. III*, Elsevier, Oxford, 2005, pp. 189-206.
42. Lee, J.-W., Singer, J. P. and Thomas, E. L., Micro-/nanostructured mechanical materials, *Adv. Mater.*, 2012, **24**, 4782-4810.
43. Scrimgeour, J., Sharp, D. N., Blanford, C. F., Roche, O. M., Denning, R. G. and Turberfield, A. J., Three-dimensional optical lithography for photonic microstructures, *Adv. Mater.*, 2006, **18**, 1557-1560.
44. LaFratta, C. N., Fourkas, J. T., Baldacchini, T. and Farrer, R. A., Multiphoton fabrication, *Angew. Chem. Int. Ed.*, 2007, **46**, 6238-6258.
45. Wang, X.-Q., Chen, J.-Y., Mi, L. and Wang, P.-N., A comparison of tissue penetrations between single and two-photon-excitations, *Appl. Phys. Lett.*, 2009, **95**, 143705.
46. Ritz, J. P., Roggan, A., Isbert, C., Müller, G., Buhr, H. J. and Germer, C. T., Optical properties of native and coagulated procine liver tissue between 400 and 2400 nm, *Lasers Surg. Med.*, 2001, **29**, 205-212.
47. Mayer, G. and Heckel, A., Biologically active molecules with a "light switch", *Angew. Chemie. Int. Ed.*, 2006, **45**, 4900-4921.
48. Van Ryssen, M. P., Avlontis, N., Giniatullin, R. McDougall, C., Carr, J. L., Stanton-Humphreys, M. N., Borgström, E. L. A., Brown, C. T. A., Fayuk, D., Surin, A., Niitykoski, M., Khiroug, L. and Conway, S. J., Synthesis, photolysis studies and *in vitro* photorelease of caged TRPV1 agonists and antagonists, *Org. Biomol. Chem.*, 2009, **7**, 4659-4707.
49. Cambridge, S. B., Geissler, D., Calegari, F., Anastassiadis, K, Hasan, M. T., Stewart, A. F., Huttner, W. B., Hagan, V. and Bonhoeffer, T., Doxycycline-dependent photoactivated gene expression in eukaryotic systems, *Nat. Meth.*, 2009, **6**, 527-533.

50. Barth, A. and Corrie, J. E. T., Characterization of a new caged proton capable of inducing large pH jumps, *Biophys. J.*, 2002, **83**, 2864-2871.
51. Silankas, A., Foss, M., Wende, W., Urbanke, C., Lagunavicius, A., Pingoud, A. and Siksnys, V, Photocaged variants of the MunI and PvuII restriction enzymes, *Biochemistry*, 2011, **50**, 2800-2807.
52. Marriott, G., Caged protein conjugates and light-directed generation of protein activity: preparation, photoactivation, and spectroscopic characterization of caged G-actin conjugates, *Biochemistry*, 1994, **33**, 9092-9097.
53. Noguchi, J., Nagaoka, A, Watanabe, S., Ellis-Davies, G. C. R., Kitamura, K., Kano, M., Matsuzaki, M. and Kasai, H., *In vivo*, two-photon uncaging of glutamate revealing the structure-function relationships of dendritic spines in the neocortex of adult mice, *J. Physiol.*, 2011, **589**, 2447-2457.
54. Sanchez, J. A. and Vergara, J., Modulation of Ca^{2+} transients by photorelease of caged nucleotides in frog skeletal muscle fibers, *Am. J. Physiol.*, 1994, **266**, 1291-1300.
55. Ando, H., Furuta, T., Tsien, R. Y. and Okamoto, H., Photo-mediated gene activation using caged RNA/DNA in zebrafish embryos, *Nature Genetics*, 2001, **28**, 317-325.
56. Dieters, A., Principles and applications of the photochemical control of cellular processes, *Chem. Bio. Chem.*, 2010, **11**, 47-53.
57. Ellis-Davies, G. C. R., Caged compounds: photorelease technology for control of cellular chemistry and physiology, *Nat. Meth.*, 2007, **4**, 619-628.
58. Barltrop, J. A. & Schofield, P., Photosensitive protecting groups, *Tetrahedron Lett.*, 1962, **3**, 697-699.
59. Kaplan, J. H., Forbush III, B. and Hoffman, J. F., Rapid photolytic release of 5'-triphosphate from a protected analog: utilization by the sodium:potassium pump of human red blood cell ghosts, *Biochem.*, 1978, **17**, 1929-1935.
60. Pillai, V. N. R., Photoremovable protecting groups in organic synthesis, *Synthesis*, 1980, **1**, 1-26.
61. Lester, H. A. & Nerbonne, J. M., Physiological and pharmacological manipulations with light flashes, *Ann. Rev. Biophys. Bioeng.*,1982, **11**, 151-175.
62. Pelliccioli, A. P. and Wirz, J., Photoremovable protecting groups: reaction mechanisms and applications, *Photochem. Photobiol. Sci.*, 2002, **1**, 441-458.
63. Furuta, T. Wang, S. S.-H., Dantzker, J. L., Dore, T. M., Bybee, W. J., Callaway, E. M., Denk, W. and Tsien, R. Y., Brominated 7-hydroxycoumarin-4-ylmethyls: Photolabile protecting groups with biologically useful cross-sections for two photon photolysis, *Proc. Natl. Acad. Sci. U.S.A.*, 1999, **96**, 1193-1200.
64. Warther, D., Gug, S., Specht, A., Bolze, F., Nicoud, J.-F., Mourot, A. and Goeldner, M., Two-photon uncaging: New prospects in neuroscience and cellular biology, *Bioorg. Med. Chem.*, 2010, **18**, 7753-7758.
65. Zhao, Y. R., Zheng, Q., Dakin, K., Xu, K., Martinez, M. L., Li, W.-H., New Caged Coumarin fluorophores with extraordinary uncaging cross-sections suitable for biological imaging applications, *J. Am. Chem. Soc.*, 2004, **126**, 4653-4663.
66. Specht, A., Thomann, J.-S., Alarcon, K., Wittayanan, W., Ogden, D., Furuta, T., Kurakawa, Y., Goeldner, M., New photoremovable protecting groups for carboxylic acids with high photolytic efficiencies at near-UV irradiation. Application to the controlled photorelease of L-glutamate, *Chem. Bio. Chem.*, 2006, **7**, 1690-1695.
67. Hagen, V., Dekowski, B., Nache, V., Schmidt, R., Geissler, D., Lorenz, D., Eichorst, J., Keller, S., Kaneko, H., Benndorf, K., Wiesner, B., Coumarinylmethyl esters for ultrafast

release of high concentrations of cyclic nucleotides upon one- and two-photon photolysis, *Angew. Chemie*, 2005, **44**, 7887-7891.
68. Aujard, I., Benbrahim, C., Gouget, M., Ruel, O., Baudin, J.-B., Neveu, P., Jullien, L., *o*-nitrobenzyl protecting groups with red-shifted absorption: syntheses and uncaging cross-sections for one- and two-photon excitation, *Chem. Eur. J.*, 2006, **12**, 6865-6879.
69. Furuta, T., Takeuchi, H., Isozaki, M., Takahashi, Y., Kanehara, M., Sugimoto, M., Watanabe, T., Noguchi, K, Dore, T. M., Kurahashi, T., Iwamura, M., Tsien, R. Y., Bhc-cNMPS as either water-soluble or membrane permeant photoreleasable cyclic nucleotides for both one- and two-photon excitation, *Chem. Bio. Chem.*, 2004, **5**, 1119-1128.
70. Fedoryak, O. D., Sul, J.-Y., Haydon, P. G., Ellis-Davies, G. C. R., Synthesis of a caged glutamate for efficient one- and two-photon photorelease in living cells, *Chem. Commun.*, 2005, **29**, 3664-3666.
71. Ellis-Davies, G. C. R., Matsuzaki, M., Paukert, M., Kasai, H, Bergles, D. E., 4-carboxymethoxy-5,7-dinitroindolinyl-Glu: An improved caged glutamate for expeditious ultraviolet and two-photon photolysis in brain slices, *J. Neurosci*, 2007, **27**, 6601-6604.
72. Ellis-Davies, G. C. R., PCT Int. Appl., WO2008094922A1, 20080807, 2008.
73. Trigo, F. F., Papageorgiou, G., Corrie, J. E. T. and Ogden, D., Laser photolysis of DPNI-GABA, a tool for investigating the properties and distribution of GABA receptors and for silencing neurons *in situ*, *J. Neurosci.*, 2009, **181**, 159-169.
74. Hagen, V., Dekowski, B., Kotzur, N., Lechler, R., Wiesner, B., Briand, B. and Beyermann, M., {7-[bis(carboxymethyl)amino]coumarin-4-yl}methylcarbonyl derivatives for photorelease of carboxylic acids, alcohols/phenols, thioalcohols/thiophenols, and amines, *Chem. Eur. J.*, 2008, **14**, 1621-1627.
75. Hagen, V., Dekowski, B., Nache, V. Schmidt, R., Geissler, D., Lorenz, D., Eichorst, J., Keller, S., Kaneko, H., Benndorf, K. and Wiesner, B., *Angew. Chemie. Int. Ed.*, 2005, **44**, 7887-7891.
76. Donato, L., Mourot, A., Davenport, C. M., Herbivo, C., Warther, D., Léonard, J. Bolze, F., Nicoud, J.-F., Kramer, R. H., Goeldner, M. and Specht, A, Water-soluble, donor-acceptor biphenyl derivatives in the 2-(*o*-nitrophenyl)propyl series: highly efficient two-photon uncaging of the neurotransmitter γ-aminobutyric acid at λ = 800 nm, *Angew. Chemie Int. Ed.*, 2012, **51**, 1840-1843.
77. Specht, A., Bolze, F., Donato, L., Herbivo, C., Charon, S., Warther, D., Gug, S., Nicoud, J.-F. and Goeldner, M., The donor-acceptor biphenyl platform: A versatile chromophore for the engineering of highly efficient two-photon sensitive photoremovable protecting groups, *Photochem. Photobiol. Sci.*, 2012, **11**, 578-586.
78. Knibbe, H., Röllig, K., Schäfer, F. P., Weller, A., Charge-transfer complex and solvent-shared ion pair in fluorescence quenching, *J. Phys. Chem.*, 1967, **47**, 1184-1185.
79. Marcus, R. A., On the theory of oxidation-reduction reactions involving electron transfer. I, *J. Chem. Phys.*, 1956, **24**, 966-978.
80. Marcus, R. A., On the theory of oxidation-reduction reactions involving electron transfer. V. Comparison and properties of electrochemical and chemical rate constants, *J. Chem. Phys.*, 1963, **67**, 853-857.
81. Marcus, R. A., Chemical and electrochemical electron-transfer theory, *Annu. Rev. Phys. Chem.*, 1964, **15**, 155-196.
82. Closs, G. L. and Miller, J. R., Intramolecular long-distance electron transfer in organic molecules, *Science*, 1988, **240**, 440-447.

83. Miller, J. R., Beitz, J. V., Huddleston, R. K., Effect of free energy on rates of electron transfer between molecules, *J. Am. Chem. Soc.*, 1984, **106**, 5057-5068.
84. Miller, J. R., Calcaterra, L. T., Closs, G. L., Intramolecular long-distance electron transfer in radical anions. The effects of free energy and solvent on the reaction rates, *J. Am. Chem. Soc.*, 1984, **106**, 3047-3049.
85. Gould, I. R., Ege, D., Moser, J. E., Farid, S., Efficiencies of photoinduced electron-transfer reactions: role of the Marcus inverted region in return electron transfer within geminate radical-ion pairs, *J. Am. Chem. Soc.*, 1990, **112**, 4290-4301.
86. Gould, I. R. and Farid, S., Dynamics of bimolecular photoinduced electron-transfer reactions, *Acc. Chem. Res.*, 1996, **29**, 522-528.
87. Gould, I. R., Ege, D., Moser, J. E. and Farid, S., Efficiencies of photoinduced electron-transfer reactions: Role of the Marcus inverted region in return electron transfer with geminate radical-ion pairs, *J. Am. Chem. Soc.*, **112**, 1990, 4290-4301.
88. Banerjee, A. and Falvey, D. E., Protecting groups that can be removed though photochemical electron transfer: Mechanistic and product studies on photosensitized release of carboxylates from phenacyl esters, *J. Org. Chem.*, 1997, **62**, 6245-6251.
89. Kwangoo, L. and Falvey, D. E., Photochemically removable protecting groups based on covalently linked electron donor-acceptor systems, *J. Am. Chem. Soc.*, 2000, **122**, 9361-9366.
90. Wang, J. PhD Thesis, Georgia Institute of Technology, 2007.
91. Klán, P., Šolomek, T., Bochet, C. G., Blanc, A., Givens, R., Rubina, M., Popik, V., Kostikov, A. and Wirz, J., Photoremovable protecting groups in chemistry and biology: Reaction mechanisms and efficacy, *Chem. Rev.*, 2013, **113**, 119-191.
92. Greene, T. W., *Protective Groups in Organic Synthesis*, Wiley, New York, 1980.
93. Sheehan, J. C. and Umezawa, K., Phenacyl photosensitive blocking groups, *J. Org. Chem.*, 1973, **38**, 3771-3774.
94. Park, C. H. and Givens, R. S., New photoactivated protecting groups. 6. *P*-hydroxyphenacyl: A phototrigger for chemical and biochemical probes, *J. Am. Chem. Soc.*, 1997, **119**, 2453-2463.
95. Banerjee, A. and Falvey, D. E., Direct photolysis of phenacyl protecting groups studied by laser flash photolysis: An excited state hydrogen atom abstraction pathway leads to formation of carboxylic acids and acetophenone, *J. Am. Chem. Soc*, 1998, **120**, 2965-2966.
96. Demeter, A., Bérces, T., Study of the long-lived intermediate formed in the photoreduction of benzophenone by isopropyl alcohol, *J. Photochem. Photobiol. A.*, 1989, **46**, 27-40; Chilton, J., Giering, L., Steel, C., The effect of transient photoproducts in benzophenon-hydrogen donor systems, *J. Am. Chem. Soc.*, 1976, **98**, 1865-1870.
97. Anderson, J. C., Reese, C. B, A photo-induced rearrangement involving aryl participation, *Tetrahedron Lett.*, 1962, **3**, 1-4.
98. Banerjee, A. and Falvey, D. E., Protecting groups that can be removed through photochemical electron transfer: Mechanistic and product studies on photosensitized release of carboxylates from phenacyl esters, *J. Org. Chem.*, 1997, **62**, 6245-6251.
99. Camble, R., Garner, R. And Young, G. T., Novel facilitation of peptide synthesis, *Nature*, 1968, **217**, 247-248.
100. Camble, R., Garner, R. And Young, G. T., Amino-acids and peptides. Part XXX. Facilitation of peptide synthesis by the use of 4-picolyl esters for carboxy-group protection, *J. Chem. Soc. C.*, 1969, 1911-1916.

101. Sundararajan, C. and Falvey, D. E., C-O bond fragmentation of 4-picolyl- and *N*-methyl-4-picolinium esters triggered by photochemical electron transfer, *J. Org. Chem.*, 2004, **69**, 5547-5554.
102. Sundararajan, C. and Falvey, D. E., Photorelease of carboxylic acids, amino acids, and phosphates from *N*-alkylpicolinium esters using photosensitization by high wavelength laser dyes, *J. Am. Chem. Soc.*, 2005, **127**, 8000-8001.
103. Kaplan, J. H. Forbush III, B. And Hoffman, J. F., Rapid photolytic release of adenosine 5'-triphosphate from a protected analog: utilization by the sodium:potassium pump of human red blood cell ghosts, *Biochemistry*, 1978, **17**, 1929-1935.
104. Barltrop, J. A., Plant, P. J. and Schofield, P. Photosensitive protecting groups, *Chem. Commun.*, 1966, 822.
105. Pirrung, M. C., Dore, T. M., Zhu, Y. and Rana, V. S., Sensitized two-photon photochemical deprotection, *Chem. Commun*, 2010, **46**, 5313-5316.
106. Smirnova, J., Dominik, W., Pfleiderer, W. and Steiner, U. E., Synthesis of caged nucleosides with photoremovable protecting groups linked to intramolecular antennae, *Helv. Chim. Acta.*, 2005, **88**, 891-904.
107. Wöll, D. Laimgruber, S., Galetskaya, M., Smirnova, J., Pfleiderer, Heinz, B., Gilch, P. and Steiner, U. E., On the mechanism of intramolecular sensitization of photocleavage of the 2-(2-nitrohenyl)propoxycarbonyl (NPPOC) protecting group, *J. Am. Chem. Soc.*, 2007, **129**, 12148-12158.
108. Wöll, D., Smirnova, J., Galetskaya, M., Prykota, T., Bühler, J. Stengele, K. P., Pfleiderer, W. and Steiner, U. E., Intramolecular sensitization of photocleavage of the Photolabile 2-(2-nitrophenyl)propoxycarbonyl (NPPOC) protecting group: photoproducts and photokinetics of the release of nucleosides, *Chemistry*, 2008, **14**, 6490-6497.
109. http://www.macalester.edu/psychology/whathap/UBNRP/neuropathy/Ion%20Channels.html, accessed April 2013.
110. Cull-Candy, S., Brickley, S., Farrant. M., *Curr. Opin. Neurobiol.*, 2001, **11**, 327-335
111. Li, G. and Niu, L., How fast does the $GluR1Q_{flip}$ channel open?, *J Biol. Chem.*, 2004, **279**, 3990-3997.
112. Li, G., Sheng, Z., Huang, Z. And Niu, L., Kinetic mechanism of channel opening of the $GluRD_{flip}$ AMPA receptor, *Biochemistry*, 2005, **44**, 5835-5841.
113. Papageorgiou, G., Ogden, G. C., Barth, A and Corrie, J. E. T., Photorelease of carboxylic acids from 1-acyl-7-nitroindolines in aqueous solution: rapid and efficient photorelease of L-glutamate, *J. Am. Chem. Soc.*, 1999, **121**, 6503-6504.
114. Smith, M. A., Ellis-Davies, G. C. R. And Magee, J. C., Mechanism of the distance-dependent scaling of Schaffer collateral synapses in rat CA1 pyramidal neurons, *J. Physiol.*, 2003, **548**, 245-258.
115. Noguchi, J., Nagaoka, A., Watanabe, S., Ellis-Davies, G. C. R., Kitamura, K., Kano. M., Masuzaki, M. and Kasai, H., *In vivo* two-photon uncaging of glutamate revealing the structure-function relationships of dendritic spines in the neocortex of adult mice, *J. Physiol.*, 2011, **589**, 2447-2457.
116. Trigo, F. F., Papageorgiou, G., Corrie, J. E. T., Ogden, D., Laser photolysis of DPNI-GABA, a tool for investigating the properties and distribution of GABA receptors and for silencing neurons *in situ*, *J. Neu. Meth.*, 2009, **181**, 159-169.
117 Dellal, S. S., Luo, R. and Otis, T. S., $GABA_A$ receptors increase excitability and conduction velocity of cerebellar parallel fiber axons, *J. Neurophysiol.*, 2012, **107**, 2958-2970.

118. Trigo, F. F., Bouhours, B., Rostaing, P., Papageorgiou, G., Corrie, J. E. T., Triller, A., Ogden, D. and Marty, A., Presynaptic miniature GABAergic currents in developing interneurons, *Neuron*, 2010, **66**, 235-247.
119. Matsuzaki, M., Hayama, T., Kasai, H. and Ellis-Davies, G. C. R., Two-photon uncaging of γ-aminobutyric acid in intact brain tissue, *Nat. Chem. Bio.*, 2010, **6**, 255-257.
120. Trigo, F. F., Papageorgiou, G, Corrie, J. E. T. and Ogden, D., Laser photolysis of DPNI-GABA, a tool for investigating the properties and distribution of GABA receptors and for silencing neurons *in situ*, *J. Neurosci. Meth.*, 2009, **181**, 159-169.
121. Nikolenko, V., Yuste, R. Zayat, L., Baraldo, L. M. and Etchenique, R., Two-photon uncaging of neurochemicals using inorganic metal complexes, *Chem. Commun.*, 2005, 1752-1754.
122. Papageorgiou, G. and Corrie, J. E. T., Synthesis of an anionically substituted nitroindoline-caged GABA reagent that has reduced affinity for GABA receptors, *Tetrahedron*, 2007, **63**, 9668-9676.
123. Mendive, C. B., Hansmann, D., Bredow and Bahnemann, D., New insights into the mechanism of TiO2 photocatalysis: thermal processes beyond the electron-hole creation, *J. Phys. Chem. C*, 2011, **115**, 19676-19685.
124. Papageorgiou, G. and Corrie, J. E. T., Synthesis of an anionically substituted nitroindoline-caged GABA reagent that has reduced affinity for GABA receptors, *Tetrahedron*, 2007, **63**, 9668-9676.
125. Montalti, M., Credi, A., Prodi, L. and Gandolfi, M. T., *Handbook of Photochemistry, Third Edition*, Taylor & Francis CRC Press, Florida, 2006, pp 601-604.
126. Borak, J. B. and Falvey, D. E., A new photolabile protecting group for release of carboxylic acids by visible-light-induced direct and mediated electron transfer, *J. Org. Chem.*, 2009, **74**, 3894-3899.
127 .Wu, F.-I., Dodda, R., Jakka, K., Huang, J.-H., Hsu, C.-S., Shu, C.-F, Enhancing the thermal and spectral stabilities of polyfluorene-based blue-light-emitting materials by incorporating pendent spiro-cycloalkyl groups, *Polymer*, 2004, **45**, 4257-4263.
128. Khan, S., Castellano, F., Spudich, J. L., McCray, J. A., Goody, R. S., Reid, G. P., Trentham, D. R., Excitatory signalling in bacteria probed by caged chemoeffectors, *Biophys. J.*, 1993, **65**, 2368-2382.
129. Khan, S., Amoyaw, K., Spudich, J. L., Reid, G. P., Trentham, D. R., Bacterial chemoreceptor signalling probed by flash photorelease of a caged serine, *Biophys. J.*, 1992, **62**, 67-68.
130. Wolosker, H., Dumin, E., Balan, L. and Foltyn, V. N., D-amino acids in the brain: D-serine in neurotransmission and neurodegeneration, *The FEBS Journal*, 2008, **275**, 3514-3526.
131. Mothet, J. P., Preant, A.T., Wolosker, H., Brady Jr, R. O., Linden, D. J., Ferris, C. D., Rogawski, M. A. and Snyder, S. H., D-Serine is an endogenous ligand for the glycine site of the *N*-methyl-D-aspartate receptor, *Proc. Natl Acad. Sci. U.S.A.*, 2000, **97**, 4926-4931; Panatier, A., Theodosis, D. T., Mothet, J. P., Touquet, B., Pollegioni, L., Poulain, D.A. and Oliet, S. H., Glia-derived D-serine controls NMDA receptor activity and synaptic memory, *Cell*, 2006, **125**, 775-784;Wolosker, H., NMDA receptor regulation by D-serine: new findings and perspectives, *Mol. Neurobiol.*, **36**, 152-164.
132. Palma-Cerda, F., Auger, C., Crawford, D. J., Hodgson, A. C. C., Reynolds, S. J., Cowell, J. K., Swift, K. A. D., Cais, O, Vyklicky, L., Corrie, J. E. T., Ogden, D., New caged neurotransmitter analogs selective for glutamate receptor sub-types based on

methoxynitroindoline and nitrophenylethoxycarbonyl caging groups, *Neuropharmacology*, 2012, **63**, 624-634.
133. **(1*S*, 3*R*)-3,5-*ACPD***: Ma, D., Ma., J. and Dai, L., Stereospecific synthesis of (1*S*, 3*R*)-1-aminocyclopentane-1,3-dicarboxylic acid, a selective agonist of metabotropic glutamate receptors, *Tetrahedron: Asymmetry*, 1997, **8**, 825-827; **(*S*)-AMPA**: Hansen, J. J., Krogagaard-Larsen, P. J., Isoxazole amino-acids as glutamic acid agonists. Synthesis of some analogues and homologues of ibotenic acid, *J. Chem. Soc. Perkin Trans. 1*, 1980, 1826-1833; **(+)-α-Kainic acid**: Trost, B. M. and Rudd, M. T., An asymmetric total synthesis of (+)-α-Kainic acid, *Org. Lett.*, 2003, **5**, 1467-1470; **NMDA**: Watkins, J. C., The synthesis of some acidic amino acids possessing neuropharmacological activity, *J. Medical and Pharmaceutical Chemistry*, 1962, **5**, 1187-1199.
134. Morrill, C. and Grubbs, R. H., Synthesis of functionalized vinyl boronates *via* Ruthenium-catalyzed olefin cross-metathesis and subsequent conversion to vinyl halides, *J. Org. Chem.*, 2003, **68**, 6031-6034.
135. Traber, B. Priv.-Doz, J. J. W., Rominger, F., Oeser, T., Gleiter, R., Goebel, M., Wortmann, R., Hexasubstituted donor-acceptor benzenes as nonlinear optically active molecules with multiple charge-transfer transitions, *Chem. Eur. J.*, 2004, **10**, 1227-1238.
136. Lightfoot A. P., Twiddle, S. J. R. and Whiting A., A stereoselective synthesis of 1,6-diphenyl-1,3,2-dioxaborinane as a two-carbon alkenyl building block, *Org. Biomol. Chem.*, 2005, **3**, 3167-3172.
137. Michels, J. J., O'Connell, M. J., Taylor, P. N., Wilson, J. S., Cacialli, F., and Anderson, H. L., Synthesis of conjugated polyrotaxanes, *Chem. Eur. J.*, 2003, **9**, 6167-6176.
138. Rafiee, E., Mahdavia, H., Joshaghani, M., Iodination of alcohols over Keggin-type heteropoly compounds: A simple, selective and expedient method for the synthesis of alkyl iodides, *South African Journal of Chemistry*, 2010, **63**, 135-140.
139. Nielsen, C. B., Johnsen, M., Arnbjerg, J., Pittelkow, M., McIlroy, S. P., Ogilby, P. R. and Jørgsen, Synthesis and characterization of water-soluble phenylene-vinylene-based singlet oxygen sensitizers for two-photon excitation, *J. Org. Chem.*, 2005, **70**, 7065-7079.
140. Abe, H., Makida, H, Inouye, M., Development of a convergent synthetic method for saccharide-linked ethynylpyridine foldamers by Huisgen reaction, *Tetrahedron*, 2012, **68**, 4353-4361.
141. Donohoe, T. J., Ironmonger, A., Kershaw, N. M., Synthesis of (-)-(Z)-deoxypukalide, *Angew. Chem. Int. Ed.*, 2008, **47**, 7314-7316.
142. Terasaka, T., Kinoshita, T., Kuno, M., Seki, N., Tanaka, K. And Nakanishi, I., Structure-based design, synthesis, and structure-activity relationship studies of novel non-nucleoside adenosine deaminase inhibitors, *J. Med. Chem.*, 2004, **47**, 3730-3743.
143. Saravanamurugan, S., Fehrmann, R. and Riisager, A., Synthesis and characterization of ammonium-pyridinium-, and pyrrolidinium-based sulfonamido functionalized ionic liquids, *Synth. Comm.*, 2012, **42**, 3383-3394.
144. Yoshida, M., Higuchi, M. and Shishido, K., Stereoselective construction of substituted chromans by palladium-catalyzed cyclization of propargylic carbonates with 2-(2-hydroxyphenyl)acetates, *Org. Lett.*, 2009, **11**, 4752-4755.
145. Li, Z. and Bittman, R., Synthesis and spectral properties of cholesterol- and FTY720-containing boron dipyrromethane dyes, *J. Org. Chem.*, 2007, **72**, 8376-8382.
146. Kaila, N., Janz, K., DeBernardo, S., Bedard, P. W., Camphausen, R., T., Tam, S., Tsao, D. H. H., Keith Jr, J. C., Nickerson-Nutter, C., Shilling, A., Young-Sciame, R. and

Wang, Q., Synthesis and biological evaluation of quinoline salicylic acids as P-Selectin antagonists, *J. Med. Chem*., 2007, **50**, 21-39.
147. Kaila, N., Janz, K., DeBernardo, S., Bedard, P. W., Camphausen, R., T., Tam, S., Tsao, D. H. H., Keith Jr, J. C., Nickerson-Nutter, C., Shilling, A., Young-Sciame, R. and Wang, Q., Synthesis and biological evaluation of quinoline salicylic acids as P-Selectin antagonists, *J. Med. Chem*., 2007, **50**, 21-39.
148. Sandararajan, C. and Falvey, D. E., C-O bond fragmentation of 4-picolyl- and *N*-methyl- 4-picolinium esters triggered by photochemical electron transfer, *J. Org. Chem.*, 2004, **69**, 5547-5554.
149. Dougherty, T. J., Photodynamic therapy, *Photochem. Photobiol.*, 1993, **58**, 895-900.
150. Traumer, K. B. And Hasan, T., Photodynamic treatment of rheumatoid and inflammatory arthritis, *Photochem. Photobiol.*, 1996, **64**, 740-750.
151. Pass, H. I., Photodynamic therapy in oncology: Mechanisms and clinical use, *J. Natl. Cancer. Inst.*, 1993, **85**, 443-456.
152. Augustin, A. J., Scholl, S., Kirchof, J., Treatment of neovascular age-related macular degeneration: Current therapies, *Clinical Opthalmology*, 2007, **3**, 175-182.
153. Spikes, J. D. in *Primary Photoprocesses in Biology and Medicine*, ed. Berghausen, R. V., Jori, G., Land, E. J. & Truscott, T. H., Plenum Press, New York, 1985, 209-227.
154. Raab, O., Uber die Wirkung fluoresezierender Stoffe auf Infusorian, *Zeitung Biol.*, 1900, **39**, 524-526.
155. Meyer-Betz, F. Untersuchungen uber die biologische photodynamische Wirkung des Hematoporphyrins und anderer derivative des Blut und Galenafarbstoffs, *Dtsch. Arch. Klin.*, 1913, **112**, 476-503.
156. Lipson, R. L. and Baldes, E. J., Photodynamic properties of a particular hematoporphyrin derivative, *AMA Archives of Dermatology*, 1960, **82**, 508-516.
157. Lipson, R. L., Baldes, E. J. and Olsen, A. M., Use of a derivative of hematoporphyrin in tumour detection, *J. Natl. Cancer. Inst.*, 1961, **26**, 1-12.
158. Schwartz, S. K., Abolon, K. and Vermund, H., Some relationships of porphyrins, X-rays and tumours, *Univ. Minn. Med. Bull.*, 1955, **27**, 7-8.
159. Lipson, R. L., Baldes, E. J. and Olsen, A. M., Hematoporphyrin derivative: a new aid for endoscopic detection of malignant disease, *J. Thorac. Cardiovasc. Surg.*, 1961, **42**, 623-629.
160. Diamond, I., Mcdonagh, A. F., Wilson, C. B., Granelli, S. G., Nielsen, S., Jaenicke, R., Photodynamic therapy of malignant tumours, *Lancet*, 1972, **2**, 1175-1177.
161. Dougherty, T. J., Grindley, G. B., Fiel, R., Weishaupt, K. R. and Boyle, D. G., Photoradiation therapy II. Cure of animal tumours with hematoporphyrin and light, *J. Natl. Cancer Inst.*, 1975, **55**, 115-121.
162. Dougherty, T. J., Lawrence, G., aufman, J. H., Boyle, D., Weishaupt, R. And Goldfarb, A., Photoradiation in the treatment of recurrent breast carcinoma, *J. Natl. Cancer Inst.*, 1979, **62**, 231-237.
163. Kelly, J. F., Snell, M. E. and Berenbaum, M. C., Photodynamic destruction of human bladder carcinoma, *Br. J. Cancer*, 1975, **31**, 237-244.
164. Kelly, J. F. and Snell, M. E., Hematoporphyrin derivative: a possible aid in the diagnosis and therapy of carcinoma of the bladder, *J. Urol.*, 1976, **115**, 150-151.
165. Dougherty, T. J. *et al*, Photoradiation therapy for the treatment of malignant tumours, *Cancer Res.*, 1978, **38**, 2628-2635.
166. Ortner, M-A. and Dorta, G., Technology insight: Photodynamic therapy for cholangiocarcinoma, *Nat. Clin. Pract. Gastroenterol. Hepatol.*, 2006, **3**, 459-467.

167. Conio, M., Cameron, A. J., Chak, A., Blanchi, S., Filiberti, R., Endoscopic treatment of high-grade dysplasia and early cancer in Barrett's oesophagus, *Lancet. Oncol.*, 2005, **6**, 311-321.
168. Dennis, E. J., Dolmans, G. J., Fukumura, D. and Jain, R. K., Photodynamic therapy for cancer, *Nat. Rev. Cancer*, 2003, **3**, 380-387.
169. Castano, A. P., Mroz, P. and Hamblin, M. R., Photodynamic therapy and anti-tumour immunity, *Nat. Rev. Cancer*, 2006, **6**, 535-545.
170. Oleinick, N. L., Morris, R. L. and Belichenko, T., The role of apoptosis in response to photodynamic therapy: what, where, why and how, *Photochem. Photobiol. Sci.*, 2002, **1**, 1-21.
171. Gorner, C. J. and Razum, N. J., Acute skin response in albino mice following porphyrin photosensitisation under oxic and anoxic conditions, *Photochem. Photobiol.*, 1984, **40**, 435-439.
172. Hatz, S., Lambert, J. D. C. and Ogilby, P. R., Measuring the lifetime of singlet oxygen in a single cell: addressing the issue of cell viability, *Photochem. Photobiol. Sci*, 2007, **6**, 1106-1116.
173. Peng, Q., Moan, J. and Nesland, J. M., Correlation of subcellular and intratumoral photosensitizer localization with ultrastructural features after photodynamic therapy, *Ultrastructural Pathology*, 1996, **2**, 109-129.
174. Kessel, D. and Reiners, J. J., Apoptosis and autophagy after mitochondrial or endoplasmic reticulum photodamage, *Photochem. Photobiol.*, 2007, **5**, 1024-1028.
175. Chen, Q., Chen, H. and Hetzel, F., Tumour oxygenation changes post-photodynamic therapy, *Photochem. Photobiol.*, 1996, **63**, 128-131.
176. Shumaker, B. P. and Hetzel, F. W., Clinical laser photodynamic therapy in the treatment of bladder carcinoma, *Photochem. Photobiol.*, 1987, **46**, 899-901.
177. Henderson, B. W. and Dougherty, T. J., How does photodynamic therapy work?, *Photochem. Photobiol.*, 1992, **55**, 145-157.
178. Hopper, C., Photodynamic therapy: A clinical reality in the treatment of cancer, *Lancet. Oncol.*, 2000, **1**, 212-219.
179. Dolmans, D. E. J. D. J., Fukumura, D. and Jain, R. K., Photodynamic therapy for cancer, *Nat. Rev. Cancer.*, 2003, **3**, 380-387.
180. Gossner, L., Stolte, M., Sroka, R., Rick, K., May, A., Hahn, E. G. and Ell, C., Photodynamic ablation of high-grade dysplasia and early cancer in Barrett's esophagus by means of 5-aminolevulinic acid, *Gastroenterology*, 1998, **114**, 448-455.
181. Neville Julie, A., Welch, E. and Leffell David, E. Management of nonmelanoma skin cancer in 2007, *Nat. Clin. Pract. Oncol.*, 2007, **4**, 462-469
182. Ormrod, D. and Jarvis, B., Topical aminolevulinic acid HCl photodynamic therapy, *Am. J. Clin. Dermatol.*, 2000, **1**, 133-139.
183. Szeimies, R. M., Karrer, S., Radakovic-Fijan, S., Tanew, A., Calzavara-Pinton, P. G., Zane, C., Sidoroff, A., Hempel, M., Ulrich, J., Proebstle, T., Meffert, H., Mulder, M., Saloman, D., Dittmar, H. C., Bauer, J. W., Kernland, K. And Braathen, L., Photodynamic therapy using topical methyl 5-levulinic acid compared with cryotherapy for actinic keratosis: a prospective, randomized study, *J. Am. Acad. Dermatol.*, 2002, **47**, 258-262.
184. Kennedy, J. C. and Pottier, R. H., Protoporphyrin IX: A clinically useful photosensitizer for photodynamic therapy, *J. Photochem. Photobiol. B*, 1992, **14**, 275-292.
185. Houle, J-M and Strong, A., Clinical pharmacokinetics of verteporfin, *Journal of Clinical Pharmacology*, 2002, **42**, 547-557.

186. Kevin, K. B., Mark, S. B., Neil. M. B., Susan, B. B., Donato, G., Lewis, H., Jennifer, I. L., Menchini, U., Joan, W. M., Jordi, M. M., Michael, J. P., Pournaras, C., Reaves, A., Rosenfeld, P., Andrew, P. S., Schmidt-Erfurth, U., Sickenberg, M., Lawrence. J. S., Jason, S. S., Strong, H. A., Virgili, G. and George, A. W., Verteporfin therapy for subfoveal chloroidal neovascularization in age-related macular degeneration: four-year year results of an open-label extension of 2 randomized trials—VIP report no. 3, *Opthalmology*, 2003, **110**, 1283-1285.
187. Bandello, F., Blinder, K., Brellser, N. M., Brown, A. L., Miller, J. W., Potter, M. J., Pornaras, C., Reaves, A., Rosenfeld, P. J., Slakter, J. S., Soubrane, G., Strong, H. A. and Stur, M., Verteporfin in photodynamic therapy: report no. 5. *Opthalmology*, 2004, **111**, 2144.
188. Weissleder, R., A clearer vision for *in vivo* imaging, *Nat. Biotech.*, 2001, **19**, 316-317.
189. Fujishima, I., Sakai, T., Tanaka, H., Ryu, K., Uemura, Y., Fujishima, K., Horiuchi, N., Daikuzono, N. and Sekiguchi, Y., Photodynamic therapy using pheophorbide *a* and Nd:YAG laser, *Neurol. Med. Chir.*, 1991, **31**, 257-263.
190. Yamashita, Y., Moriyasu, F., Ono, S., Kimura, T., Kajimura, K., Someda, H., Hamato, N., Nabeshima, M., Sakai, M. and Okuma, M., Photodynamic therapy on phephorbide-*a* and Q-switched Nd:YAG laser on human hepatocellular carcinoma, *Gastroenterologia Japonica*, 1991, **26**, 623-627.
191. Fisher, W. G., Partridge Jr, W. P., Dees, C. and Wachter, E. A., Simultaneous two-photon activation of Type-I photodynamic therapy agents, *Photochem. Photobiol.*, 1997, **66**, 141-155.
192. Khurana, M., Collins, H. A., Karotki, A., Anderson, H. L., Cramb, D. T. and Wilson, B. C., Quantitative *in vitro* demonstration of two-photon photodynamic therapy using Photofrin and Visudyne, *Photochem. Photobiol.*, 2007, **83**, 1441-1448.
193. Dahlstedt, E., Collins, H. A., Balaz, M., Kuimova, M. K., Khurana, M., Wilson, B. C., Phillips, D. and Anderson, H. L., One- and two-photon phototoxicity of conjugated porphyrin dimers with high two-photon absorption cross-sections, *Org. Biomol. Chem.*, 2009, **7**, 897-904.
194. Khurana, M., Ulrich, S., Kim, A., Moriyama, Y., Netchev, G., Akens, M. K., Anderson, H. L. and Wilson, B. C., Biodistribution and pharmacokinetic studies of porphyrin dimer photosensitiser (Oxidime) by fluorescence imaging and spectroscopy in mice bearing xenograft tumours, *Photochem. Photobiol.*, 2012, **88**, 1531-1538.
195. Lipinski, C. A., Lombardo, F., Dominy, B. W., Feeney, P. J., Experimental and computational approaches to estimate solubility and permeability in drug discovery and development setting, *Adv. Drug. Delivery Rev.*, 1997, **23**, 3-25.
196. Fischer, P. M., Krausz, E., Lane, D. P., Cellular delivery of impermeable effector molecules in the form of conjugates with peptides capable of mediating membrane translocation, *Bioconjugate Chem.*, 2001, **12**, 825-841.
197. Steven, V. and Graham, D. Oligonucleotide conjugation to cell-penetrating (TAT) peptide by Diels-Alder cycloaddition, *Org. Biomol. Chem.*, 2008, **6**, 3781-3787.
198. Wada, S-I., Hitoria, Y., Yokoe, S., Nakagawa, O and Urata, H., Cellular uptake of covalent conjugates of oligonucleotides with membrane-modifying peptide, peptaibol, *Bioorg. Med. Chem.*, 2012, **20**, 3219-3222.
199. Malhotra, M., Tomaro-Duchesneau, C. and Prakash, S., Synthesis of TAT peptide-tagged PEGylated chitosan nanoparticles for siRNA delivery targeting neurodegenerative diseases, *Biomaterials*, 2013, **34**, 1270-1280.

200. Ojea-Jiménez, I., García-Fernández, L., Lorenzo, J. and Puntes, V. F., Facile preparation of cationic gold nanoparticle-gold conjugates for cell penetration and nuclear targeting, *ACS Nano*, 2012, **6**, 7692-7702.
201. Hsu, T. and Mitragotri, S. Delivery of siRNA and other macromolecules into skin and other cells using a peptide enhancer, *Proc. Natl. Acad. Sci. U. S. A*, 2011, **108**, 15816-15821.
202. Rouselle, C. *et al*, New advances in the transport of doxorubicin through the blood-brain barrier by a peptide-vector mediated strategy, *Mol. Pharmacol.*, 2000, **57**, 679-686.
203. Watts, Z. I., Easton, C. J., Peculiar stability of amino acids and peptides from a radical perspective, *J. Am. Chem. Soc*, 2009, **131**, 11323-11325.
204. Vivès, E., Schmidt, J., Pèlegrin, A., Cell-penetrating and cell-targeting peptides in drug delivery, *Biochim. Biophys. Acta*, 2008, **1786**, 126-138.
205. Frankel, A. D., Pabo, C. O., Cellular uptake of the Tat protein from human immunodeficiency virus, *Cell*, 1988, **55**, 1189-1193.
206. Wright, L. R., Rothbard, J. B., Wender, P. A., Guanidinium rich peptide transporters and drug delivery, *Curr. Protein Pept. Sci.*, 2003, **4**, 105-124.
207. Goun, E. A., Pillow, T. H., Jones, L. R., Rothbard, J. B. and Wender, P. A., Molecular transporters: synthesis of oligoguanidinium transporters and their application to drug delivery and real-time imaging, *Chem. Bio. Chem.*, 2006, **7**, 1497-1515.
208. Richard, J. P., Melikov, K., Vives, E., Ramos, C., Verbeure, B., Gait, M. J., Chernomordik, L. V., Lebleu, B., Cell-penetrating peptides. A reevaluation of the mechanism of cellular uptake, 2003, **278**, 585-590.
209. Sternberg, E. D., Dolphin, D. and Brückner, Porphyrin-based photosensitisers for use in photodynamic therapy, *Tetrahedron*, 1998, 54, 4151-4202.
210. Tirand, L., Frochot, C., Vandresse, R., Thomas, N., Trinquet, E., Pinel, S., Viriot, M.-L., Guillemin, F., Barberi-Heyob, M., A peptide competing with $VEGF_{165}$ binding on neuropilin-1 mediates targeting of a chlorine-type photosensitizer and potentiates its photodynamic activity in human endothelial cells, *J. Controlled Release*, 2006, **111**, 153-164.
211. Bisland, S. K., Singh, D., Gariépy, J., Potentiation of chlorin e6 photodynamic activity *in vitro* with peptide-based intracellular vehicles, *Bioconjugate Chem.*, 1990, **10**, 982-992.
212. Sibrian-Vasquez, M., Jensen, T. J. and Vicente, M. G. H., Synthesis, characterization, and metabolic stability of porphyrin-peptide conjugates bearing bifunctional signalling sequences, *J. Med. Chem.*, 2008, **51**, 2915-2923.
213. Hanahan, D. and Weinberg, R.A., The hallmarks of cancer, *Cell*, 2000, **1**, 57-70.
214. Hahn, W. C. and Weinberg, R. A., Modelling the molecular circuitry of cancer, *Nat. Rev. Cancer*, 2002, **2**, 331-341.
215. Levine, A. J. and Puzio-Kuter, A. M. The control of the metabolic switch in cancers by oncogenes and tumour suppression genes, *Science*, 2010, **330**, 1340-1344.
216. Tasselli, L. and Chua, K. F., Metabolism in the driver's seat. *Nature*, 2012, **492**, 362-363.
217. Carmeliet, P. Angiogenesis in life, disease and medicine, *Nature*, 2005, **438**, 932-936.
218. Avraamides, C. J., Garmy-Susini, B. and Varner, J. A., Integrins in angiogenesis and lymphangiogenesis, *Nat. Rev. Cancer*, 2008, **8**, 604-617.
219. Fingar, V. H., Kik, P. K., Haydon, P. S., Carrito, P. B., Abang, E., Wieman, T. J., Analysis of acute vascular damage after photodynamic therapy using benzoporphyrin derivative (BPD), *Br. J. Cancer.*, 1999, **79**, 1702-1708.

220. Star, W. M., Marijnissen, H. P. A., van den Berg-Blok, A. E., Versteeg, J. A. C., Franken, K. A. P., Reinhold, H. S., Destruction of rat mammary tumor and normal tissue microcirculation by hematoporphyrin derivative photoradiation observed *in vivo* in sandwich observation chambers, *Cancer Res.*, 1986, **46**, 2532-2540.
221. Plow, E. F., Haas, T. A., Zhang, L., Loftus, J. and Smith, J. W., Ligand binding to integrins, *J. Biol. Chem.*, 2000, **275**, 21785-21788.
222. Pierschbacher, M. D. and Ruoslahti, E., Cell attachment activity can be duplicated by small synthetic fragments of the molecule, *Nature*, 1984, **309**, 30-33.
223. Xiong, J. P., Stehle, T., Zhang, R., Joachimiak, A., Frech, M., Goodman, S. L., Arnaout, M. A., Crystal structure of the extracellular segment of integrin $\alpha_v\beta_3$ in complex with an Arg-Gly-Asp ligand, *Science*, 2002, **296**, 151-155.
224. Haubner, R., Gratias, R., Diefenbach, B., Goodman, S. L., Joncyk, A., Kessler, H., Structural and functional aspects of RGD-containing cyclic pentapeptides as highly potent and selective $\alpha_v\beta_3$ antagonists, *J. Am. Chem. Soc.*, 1996, **118**, 7461-7472.
225. Pierschbacher, M. D. and Ruoslahti, E., Influence of stereochemistry of the sequence Arg-Gly-Asp-Xaa on binding-specificity in cell-adhesion, *J. Biol. Chem.*, 1987, **262**, 17294-17298.
226. Haas, T. A. and Plow, E. F., Integrin-ligand interactions: a year in review, *Curr. Opin. Cell Biol.*, 1994, **6**, 656-662.
227. Danhier, F., Le Breton, A., Préat, V., RGD-based strategies to target alpha(v) beta(3) integrin in cancer therapy and diagnosis, *Mol. Pharmaceutics*, 2012, **9**, 2961-2973.
228. Ferrara, N. and Kerbel, R. S., Angiogenesis as a therapeutic target, *Nature*, 2005, **438**, 967-974.
229. Strömblad, S., Becker, J. C., Yebra, M., Brooks, P. C., Cheresh, D. A., Suppression of p53 activity and $p21^{WAF1/CIP1}$ expression by vascular cell integrin $\alpha_v\beta_3$ during angiogenesis, *J. Clin. Invest.*, 1996, **98**, 426-433.
230. Stupack, D. G., Puente, X. S., Boutsabouloy, S., Storgard and C. M., Cheresh, D. A., Apoptosis of adherent cells by recruitment of caspase 8 to unligated integrins, *J. Cell Biol.*, 2001, **155**, 459-470.
231. Temming, K., Schifflers, R. M., Molema, G. and Kok, R. J., RGD-based strategies for selective delivery of therapeutics and imaging agents to the tumour vasculature, *Drug Resistance Updates*, 2005, **8**, 381-402.
232. Conway, C. L., Walker, I., Bell, A., Roberts, D. J. H., Brown, S. B. and Vernon, D. I., *In vivo* and *in vitro* characterisation of a protoporphyrin IX-cyclic RGD peptide conjugate for use in photodynamic therapy, *Photochem. Photobiol. Soc.*, 2008, **7**, 290-298.
233. Campbell, N. A., Biology: Exploring life, 2006, Pearson Prentice Hall, Boston Massachusetts.
234. Warburg, O., On the origin of cancer cells, *Science*, 1956, **123**, 309-314.
235. Someja, S., Xu, J., Kondo, K., Ding, D., Salvi, R. J., Yamasoba, T., Rabinovich, P. S., Weindruch, R., Leeuwenburgh, C., Tanokura, M. and Prolla, T. A., Age-related hearing loss in C57Bl/6J mice is mediated by Bak-dependent mitochondrial apoptosis, *Proc. Natl. Acad. Sci. U. S. A.*, 2009, **106**, 19432-19437.
236. Yousif, L. F., Stewart, K. M. and Kelley, S. O., Targeting mitochondria with organelle-specific compounds: strategies and applications, *Chem. Bio. Chem.*, 2009, **10**, 1939-1950.
237. Juzeniene, A., Peng, Q., Moan, J., Milestones in the development of photodynamic therapy and fluorescence diagnosis, *Photochem. Photobiol. Sci.*, 2007, **12**, 1234-1245.
238. Hermanson, G. T., Bioconjugate Techniques, Academic Press Inc., San Diego, 1996.

239. Dirksen, A. and Dawson, P. E., Expanding the scope of chemoselective peptide ligations in chemical biology, *Curr. Opin. Chem. Bio.*, 2008, **12**, 760-766.
240. Shao, J. and Tam, J. P., Unprotected peptides as building-blocks for the synthesis of peptide dendrimers with oxime, hydrazone and thiazolidine linkages, *J. Am. Chem. Soc.*, 1995, **117**, 3893-3899.
241. Villien, M., Deroo, S., Gicquel, E., Defranq, E., Moucheron, C., Mesmaeker, A. K. D., Dumy, P., The oxime bond formation as an efficient tool for the conjugation of ruthenium complexes to oligonucleotides and peptides, *Tetrahedron*, 2007, **63**, 11299-11306.
242. Forget, D., Boturyn, D., Renaudet, O., Defranq, E., Dumy, P., Highly efficient synthesis of peptide- and carbohydrate-oligonucleotide conjugates using chemoselective oxime and thiazolidine formation, *Nucleosides Nucleotides & Nucleic Acids*, 2003, **22**, 1427-1429.
243. Misicka, A. in Neuropeptides in Neuroprotection and Neuroregeneration, Ed. Fred J. Nyberg, CRC Group Taylor & Francis, Florida, 2012, pp 209-229.
244. Merrifield, R. B., Solid phase peptide synthesis. I. The synthesis of a tetrapeptide, *J. Am. Chem. Soc.*, 1963, **85**, 2149-2154.
245. El-Faham, A. and Albericio, F., Peptide coupling reagents, more than a letter soup, *Chem. Rev.*, 2011, **111**, 6557-6602.
246. Dirksen, A., Hackeng, T. M. and Dawson, P. E., Nucleophilic catalysis of oxime ligation, *Angew. Chemie. Int. Ed.*, 2006, **45**, 7581-7584.
247. Cordes, E. H. and Jencks, W. P., Nucleophilic catalysis of semicarbazone formation by anilines, *J. Am. Chem. Soc.*, 1968, **84**, 826-831.
248. Dessolin, M., Guillerez, M.-G., Thieriet, N., Guibé and Loffet, A., New allyl group acceptors for palladium catalyzed removal of allylic protection and transacylation of allyl carbamates, *Tetrahedron Letters*, 1995, **36**, 5741-5744.
249. Boturyn, D. and Dumy, P., A convenient access to $\alpha_v\beta_3$/ $\alpha_v\beta_5$ integrin ligand conjugates: regioselective solid-phase functionalisation of an RGD based peptide, *Tetrahedron Lett.*, 2001, **42**, 2787-2790.
250. Orski, S. V., Poloukhtine, A. A., Selvanathan, A., Mao, L., Popik, V. L. and Locklin, J., High density orthogonal surface immobilisation *via* photoactivated copper-free click chemistry, *J. Am. Chem. Soc.*, 2010, **132**, 11024-11026.
251. Liu, L-H., Lerner, M. M. and Yan. M., Derivatization of pristine graphene with well-defined chemical functionalities, *Nano Lett.*, 2010, **10**, 3754-3756.
252. Barltrop, J. A. and Owen, T. C., 5-(3-carboxymethoxyphenyl)-2-(4,5-dimethylthiazolyl)-3-(4-sulfophenyl)tetrazolium, inner salt (MTS) and related analogs of 3-(4,5-dimethylthizolyl)-2,5-diphenyltetrazolium bromide, *Biorg. Med. Chem. Lett.*, 1991, **1**, 611-614.
253. Johnson, L. V., Walsh, M. L. and Chen, L. B., Localization of mitochondria in living cells with rhodamine 123, *Proc. Natl Acad. Sci. USA*, 1980, **77**, 990-994.
254. Bagheri, M., Beyermann, M. and Dathe, M., Mode of action of cationic antimicrobial peptides defines the tethering position and the efficacy of biocidal surfaces, *Bioconjugate Chem.*, 2012, **23**, 66-74.
255. Garcia, G., Hammerer, F., Poyer, F., Achelle, S., Teulade-Fichou, M.-P. and Maillard, P., Carbohydrate-conjugated porphyrin dimers: Synthesis and photobiological evaluation for a potential application in one-photon and two-photon photodynamic therapy, *Bioorg. Med. Chem.*, 2013, **21**, 153-165.

256. Wong, C.-H. and Zimmerman, S. C., Orthogonality in organic, polymer, and supramolecular chemistry: from Merrifield to click chemistry, *Chem. Commun.*, 2013, **49**, 1679-1695.
257. Gil, M. V., Arévalo, M. J., López, Click chemistry – what's in a name? Triazole synthesis and beyond, *Synthesis*, 2007, **11**, 1589-1620.
258. Colombo, M. and Bianchi, A., Click chemistry for the synthesis of RGD-containing integrin ligands, *Molecules*, 2010, **15**, 178-197.
259. Umezawa, N., Matsumoto, N., Iwama, S., Kato, N., Higuchi, T., Facile synthesis of peptide-porphyrin conjugates: Towards artificial catalase, *Bioorg. Med. Chem.*, 2010, **18**, 6340-6350.
260. Hancock, W. S. and Battersby, J. E., *Anal. Biochem.*, 1976, **71**, 260-264
261. Cristina, G., Boccalon, M. and Pasquato, L., Straightforward synthesis of fluorinated amphiphilic thiols, *Eur. J. Org. Chem.*, 2008, **19**, 3308-3313.
262. Duléry, V., Renaudet, O. and Dumy, P., Ethoxyethylidene protecting group prevent *N*-overacylation in aminooxy peptide synthesis, *Tetrahedron*, 2007, **63**, 11952-11958.
263. Beaumont, S, Ilardi, E. A., Monroe, L. R. and Zakarian, A., Valence tautomerism in titanium enolates: catalytic radical haloalkylation and application in the total synthesis of neodysidenin, *J. Am. Chem. Soc.*, 2010, **132**, 1482-1483.
264. Applied Biosciences Technical Bulletin, Cleavage, Deprotection and Isolation of Peptides after Fmoc synthesis
265 Namavari, M., Cheng, Z., Zhang, R., De, A., Levi, J., Hoerner, J. K.., Yaghoubi, S. S., Syud, F. A., A novel method for direct site-specific radiolabeling of peptides using [F-18]FDG, *Bioconjugate Chem.*, 2009, **20**, 432-436.
266. Dai, X., Su, Z., Liu, J. O., An improved synthesis of a selective $\alpha_v\beta_3$, *Tetrahedron Lett.*, 2000, 41, 6295-6298.
267. Boturyn, D. and Dumy, P., A convenient access to $\alpha_v\beta_3/\alpha_v\beta_5$ integrin ligand conjugates: regioselective solid-phase functionalisation of an RGD based peptide, *Tetrahedron Lett*, 2001, **42**, 2787-2790.
268. Proudfoot, A. T., Bradberry, S. M., Vale, J. A., Sodium fluoroacetate poisoning, *Toxicological Reviews*, 2006, **25**, 213-219.